#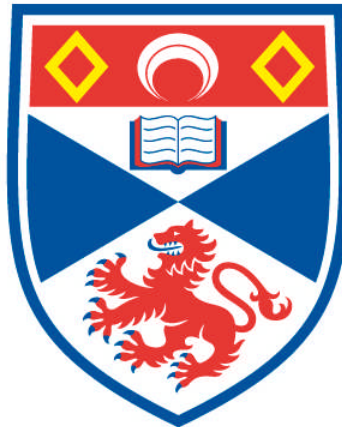 DEVELOPMENT OF A NOVEL CELL-BASED SCREENING PLATFORM TO IDENTIFY INHIBITORS OF VIRAL INTERFERON ANTAGONISTS FROM CLINICALLY IMPORTANT VIRUSES

## Andri Vasou

## A Thesis Submitted for the Degree of PhD
## at the
## University of St Andrews

## 2016

**Full metadata for this item is available in
Research@StAndrews:FullText
at:
http://research-repository.st-andrews.ac.uk/**

**Please use this identifier to cite or link to this item:
http://hdl.handle.net/10023/8266**

# Development of a Novel Cell-Based Screening Platform to Identify Inhibitors of Viral Interferon Antagonists from Clinically Important Viruses

## Andri Vasou
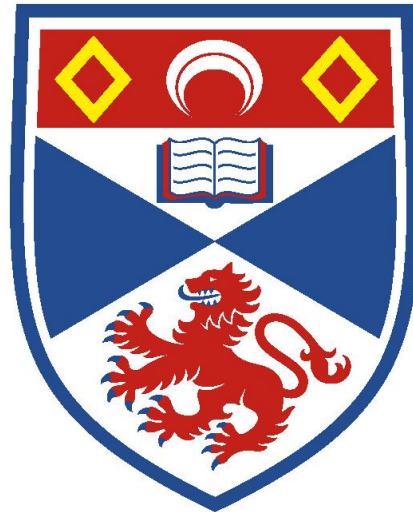
University of
St Andrews

**A thesis submitted for the degree of PhD**
**at the**
**University of St Andrews**

**January 2016**

# Abstract

All viruses encode for at least one viral interferon (IFN) antagonist, which is used to subvert the cellular IFN response, a powerful antiviral innate immune response. Numerous *in vitro* and *in vivo* studies have demonstrated that IFN antagonism is crucial for virus survival, suggesting that viral IFN antagonists could represent promising therapeutic targets. This study focuses on Respiratory Syncytial Virus (RSV), an important human pathogen for which there is no vaccine or virus-specific antiviral drug. RSV encodes two IFN antagonists NS1 and NS2, which play a critical role in RSV replication and pathogenicity. We developed a high-throughput screening (HTS) assay to target NS2 via our A549.pr(ISRE)GFP-RSV/NS2 cell-line, which contains a GFP gene under the control of an IFN-stimulated response element (ISRE) to monitor IFN-signalling pathway. NS2 inhibits the IFN-signalling pathway and hence GFP expression in the A549.pr(ISRE)GFP-RSV/NS2 cell-line by mediating STAT2 degradation. Using a HTS approach, we screened 16,000 compounds to identify small molecules that inhibit NS2 function and therefore relinquish the NS2 imposed block to IFN-signalling, leading to restoration of GFP expression. A total of twenty-eight hits were identified; elimination of false positives left eight hits, four of which (AV-14, -16, -18, -19) are the most promising. These four hit compounds have $EC_{50}$ values in the single μM range and three of them (AV-14, -16, -18) represent a chemically related series with an indole structure. We demonstrated that the hit compounds specifically inhibit the STAT2 degradation function of NS2, not the function of NS1 or unrelated viral IFN antagonists. At the current time, compounds do not restrict RSV replication *in vitro*, hence hit optimization is required to improve their potency. Nonetheless, these compounds could be used as chemical tools to determine the unknown mechanism by which NS2 mediates STAT2 degradation and tackle fundamental questions about RSV biology.

**DECLARATIONS**

I, **Andri Vasou**, hereby certify that this thesis (which is approximately 56,870 words) has been written by me, that it is the record of work carried out by me, and that it has not been submitted in any previous application for a higher degree.

Date ……................... Signature of candidate ………................................

I was admitted as a research student in September 2011 as a candidate for the degree of **Doctor of Philosophy (PhD) in Molecular Virology**; the higher study for which this is a record and was carried out at the University of St. Andrews between 2012 and 2015.

Date ……................... Signature of candidate ………................................

We hereby certify that the candidate has fulfilled the conditions of the Resolution and Regulations appropriate for the degree of Doctor of Philosophy at the University of St. Andrews, and that the candidate is qualified to submit this thesis in application for that degree.

Date ……................... Signature of supervisor ………................................

**Dr. C.S. Adamson**

Date ……................... Signature of supervisor ………................................

**Prof. R.E. Randall**

In submitting this thesis to the University of St Andrews I understand that I am giving permission for it to be made available for use in accordance with the regulations of the University Library for the time being in force, subject to any copyright vested in the work not being affected thereby.  I also understand that the title and the abstract will be published, and that a copy of the work may be made and supplied to any *bona fide* library or research worker, that my thesis will be electronically accessible for personal or research use unless exempt by award of an embargo as requested below, and that the library has the right to migrate my thesis into new electronic forms as required to ensure continued access to the thesis.

The following is an agreed request by candidate and the supervisors regarding the electronic publication of this thesis:

Access to printed copy and electronic publication of thesis through the University of St Andrews.

Date ……................... Signature of candidate ………..................................

Date ……................... Signature of supervisor ………..................................

**Dr. C.S. Adamson**

Date ……................... Signature of supervisor ………..................................

**Prof. R.E. Randall**

# *Acknowledgments*

I am very grateful to my supervisor Dr Catherine Adamson for giving me the opportunity to study for a PhD at the University of St Andrews, and also for her advice, encouragement and support throughout this study. Also, I would like to express my warmest gratitude to my second supervisor Professor Richard Randall for his continuous optimism and his guidance, which has been essential for this work. I am in indebted to all of my colleagues for making the lab such a pleasant environment to work in, and especially Dr Lena Andrejeva and Mr Dan Young for their invaluable help and advice. I am also sincerely thankful to my friends for our 'inspirational' lunch-break chats, and for all the great moments we shared together in the bubble.

I owe an eternal gratitude to my parents, Christa and Panikkos, for their undivided love and endless support that always gets me through everything; I really owe you for where I am today! Many thanks to my lovely sisters, Nicole and Yiota, for being my helpline; our phone chats always helped me stay positive and keep fighting. Special thanks to my boyfriend, Harry, for his love and understanding, for supporting my dreams, and for staying by my side till the end.

I dedicate this thesis to my beloved uncle, whose faith in me has always been my inspiration; I will never let you down!

**Table of Contents**

# List of Figures

# List of tables

# Abbreviations

| | |
|---|---|
| **% [v/v]** | Percentage concentration (volume per volume) |
| **% [w/v]** | Percentage concentration (weight per volume) |
| **°C** | Degrees Celsius (temperature). |
| **2', 5'-OAS** | 2', 5'- oligoadenylate synthetase |
| **aa** | Amino-acid |
| **AECs** | Airway epithelial cells |
| **ALRI** | Acute lower respiratory tract illness |
| **ATP** | Adenosine triphosphate |
| **AVG** | Average |
| **BRSV** | Bovine RSV |
| **CARD** | Caspase recruitment domain. |
| **Cardiff** | CARD adaptor inducing IFN-β |
| **CCL2/5** | Chemokine (C-C motif) ligand 2/5 |
| **CD4/8** | Cluster of differentiation 4/8 |
| **cGAS** | Cyclic guanosine monophosphate–adenosine monophosphate (GMP-AMP) synthetase |
| **COPD** | Chronic obstructive pulmonary disease |
| **CPE** | Cytopathic effect. |
| **CTD** | C-terminal domain |
| **DAPI** | 4', 6-diamidino-2-phenylindole |
| **DCs** | Dendritic cells |
| **DDU** | Dundee drug discovery unit |
| **DDX41** | DEAD box protein 41 |
| **DMEM** | Dulbecco's modified Eagle's medium. |
| **DMSO** | Dimethyl sulphoxide. |
| **dNTP** | Deoxyribonucleotide triphosphate. |
| **dsRNA** | Double-stranded RNA |
| **ECL** | Enhanced chemiluminescence |
| **EDTA** | Ethylene diamine tetra-acetic acid. |
| **elF-2a** | Eukaryotic initiation factor 2a |
| **F** | Fusion protein |

| | |
|---|---|
| **FBS** | Foetal bovine serum |
| **FI** | Formalin-inactivated |
| **FITC** | Fluorescein isothiocyanate |
| **G** | Glycoprotein |
| **GAGs** | Glycosaminoglycans |
| **GAS** | IFN-γ-activated site |
| **GFP** | Green fluorescent protein |
| **h** | Hours (Time) |
| **HCV** | Hepatitis C virus |
| **HIV** | Human immunodeficiency virus |
| **HRP** | Horse-radish peroxidase |
| **HTS** | High-throughput screening |
| **IFI16** | Gamma-interferon-inducible protein 16 |
| **IFITMs** | IFN-induced transmembrane proteins |
| **IFITs** | IFN-induced proteins with tetratricopeptide repeats |
| **IFN** | Interferon |
| **IFNAR** | Type I IFN receptor |
| **IKK** | IκB kinase |
| **IL** | Interleukin. |
| **IPS-1** | IFN-β promoter stimulator protein 1 |
| **IRF** | IFN regulatory factor |
| **ISGF3** | Interferon-stimulated gene factor 3 |
| **ISGs** | IFN-stimulated genes |
| **ISRE** | IFN-stimulated response element |
| **IκB** | Inhibitor of NF-κB |
| **JAK** | Janus activated kinase |
| **kb** | Kilo-base |
| **kDa** | Kilo-Dalton |
| **L** | Large protein (polymerase) |
| **LPS** | Lipopolysaccharide |
| **M** | Molar concentration (moles per liter). |

| | |
|---|---|
| **M** | Matrix protein |
| **MAP1B** | Microtubule-associated protein 1B |
| **MAVS** | Mitochondrial antiviral-signalling protein |
| **MCS** | Multiple cloning site |
| **Mda-5** | Melanoma differentiation-associated gene-5 |
| **MHC** | Major histocompatibility complex |
| **min** | Minutes (time) |
| **miRNAs** | Micro-RNAs |
| **MOI** | Multiplicity of infection |
| **mRNA** | Messenger RNA |
| **MW** | Molecular weight |
| **MyD88** | Myeloid differentiation factor 88 |
| **NEDD8** | Natural precursor cell expressed, developmentally down-regulated 8 |
| **NEMO** | NF-κB essential modulator |
| **NF-κB** | Nuclear factor kappa B |
| **NIK** | NF-κB-inducing kinase |
| **NLRs** | Nucleotide oligomerisation domain (NOD)-like receptors |
| **NLS** | Nuclear localisation signal |
| **NS** | Non-structural proteins |
| **ns** | Non-significant |
| **nt** | Nucleotides |
| **OASL** | 2'-5'-oligoadenylate synthetase-like |
| **ORF** | Open reading frame |
| **P** | Phosphoprotein |
| **PAMPs** | Pathogen-associated molecular patterns |
| **PAC** | Puromycin N-acetyl-transferase |
| **PBS** | Phosphate-buffered saline |
| **PCR** | Polymerase chain reaction |
| **PDRs** | Positive regulatory domains |
| **PEG** | Polyethylene glycol |
| **PFU** | Plaque forming units |

| | |
|---|---|
| **PI** | Protease inhibitor |
| **PI3K** | Phosphatidylinositol 3-kinase |
| **PIV2/3** | Parainfluenza virus 2/3 |
| **PIV5** | Parainfluenza virus 5 (formerly known as SV5; simian virus 5) |
| **PKR** | Double-stranded RNA activated protein kinase |
| **PML** | Promyelocytic leukemia protein |
| **PRRs** | Pattern-recognition receptors |
| **PVDF** | Polyvinylidene difluoride |
| **QC** | Quality control |
| **RABV** | Rabies virus |
| **RANTES** | Regulated on activation, normal T cell expressed and secreted |
| **RIG-I** | Retinoic acid-inducible gene I |
| **RIP1** | Receptor interacting protein 1 |
| **RLRs** | Retinoic acid-inducible gene I (RIG-I)-like receptors |
| **RNP** | Ribonucleoprotein complex. |
| **rpm** | Rounds per minute |
| **RSV** | Respiratory syncytial Virus |
| **RT** | RT |
| **SD** | Standard deviation |
| **SDS** | Sodium dodecyl sulfate |
| **SDS-PAGE** | Sodium dodecyl sulphate polyacrylamide gel electrophoresis. |
| **SeV** | Sendai virus |
| **SH** | Small hydrophobic protein |
| **SH2** | Src homology 2 |
| **siNT** | Non-targeting siRNA |
| **siRNA** | Short-interfering RNA. |
| **SOCS** | Suppressor of cytokine signalling |
| **ssRNA** | Single-stranded RNA |
| **STAT** | Signal transducers and activators of transcription |
| **TAK1** | TGF-β activating kinase 1 |
| **TBK1** | TRAF family member-associated NF kappa-B activator - (TANK)-binding kinase 1 |

| | |
|---|---|
| **TBK1** | TRAF family member-associated NF-κb activator (TANK)-binding kinase 1) |
| **Th2** | Type 2 T-helper cells |
| **TLRs** | Toll-like receptors |
| **TNFα** | Tumor necrosis factor α |
| **Tom70** | Translocase of outer membrane 70 kDa subunit |
| **TRAF** | Tumor-Necrosis Factor (TNF) receptor associated factors |
| **TRAF3** | TNF-receptor associated factor 3 |
| **TRIF** | Toll-interleukin (IL)-1-resistannce (TIR) domain-containing adaptor inducing IFN-β |
| **TRIMs** | Tripartite motifs |
| **TRIP** | TRAF-interacting protein |
| **Tyk2** | Tyrosine kinase 2 |
| **VISA** | Virus-induced signalling adapter |
| **wt** | Wild type |
| **x g** | Times g (gravity) |
| **μg** | Micrograms |
| **μl** | Microliters |

# Chapter 1: Introduction

## 1.1 Introduction to the interferon system

The early innate immune response to viral infections is characterized by the rapid production of interferons (IFNs), a group of widely expressed cytokines, which play key roles in mediating the antiviral response. Although IFNs are best known for their role in innate immunity, they also have other functions related to immunomodulation, proliferation (anti-growth) and the regulation of the adaptive immune response (González-Navajas *et al.,* 2012; Caraglia *et al.,* 2013; Hertzog 2012). Despite the fact that the majority of viruses have well-established mechanisms to circumvent the IFN system, the IFN response remains critical in slowing the progress of virus infections and thus, giving time for the development of an adaptive immune response.

The IFN family consists of three main classes of related cytokines; type I, II and III IFNs. Type I IFNs are a diverse group of molecules, which was firstly described almost sixty years ago (Isaacs & Lindenmann 1957). These include IFN-α and IFN-β that are directly induced in response to viral infection, whereas other members of type I IFNs (IFN-ω, -ε, -κ, -δ) have a less defined role in antiviral response (Hertzog & Williams 2013). In humans, IFN-β is encoded by a single *IFNB* gene, whereas fourteen distinct genes encode for different subtypes of IFN-α (Ivashkiv & Donlin 2014). The type II IFN has a single member, IFN-γ, which despite having pleiotropic functions related to innate and adaptive responses, it is not secreted directly after viral infection, and therefore it has limited direct antiviral effects (Schroder *et al.,* 2004). Type III IFNs, which is also known as the IFN-λ family, was discovered more recently, and consists of

four molecules (IFN-λ1, IFN-λ2, IFN-λ3 and IFN-λ4) (Kotenko *et al.,* 2003; Egli *et al.,* 2014). Similar to type I IFNs, these molecules are secreted directly in response to viral infection and their induction appears to be regulated by common mechanisms as the IFN-α genes (Onoguchi *et al,* 2007; Lazear *et al.,* 2015). Although type I and III IFNs share common regulatory pathways, several aspects of IFN-λ biology are different. For instance, the IFN-λ signalling controls frequent or persistent low-level infections at epithelial barriers, without creating severe inflammation, whereas IFN-α/β mediates a more inflammatory and systemic response, as it signals in almost all nucleated cells (Lazear *et al.,* 2015; Wack *et al.,* 2015). The type I IFNs, primarily the IFN-α/β response is the most powerful host defense against virus infections. Therefore, this study focuses on the IFN-α/β response, and particularly IFN-β, because the mechanism behind the virus-induced expression of IFN-β is better understood. The type I IFN response is divided into two pathways: the IFN-induction pathway and the IFN-signalling pathway, which are described in detail below.

## 1.1.1 Type I IFN-induction pathway

The type I IFNs are produced mainly by innate immune cells, such as macrophages and dendritic cells (DCs), however, non-immune cells, such as fibroblasts and epithelial cells, are also capable of producing IFNs, more predominantly IFN-β (Ivashkiv & Donlin 2014). The activation of the type I IFN-induction pathway requires the recognition of pathogen-associated molecular patterns (PAMPs), which are molecules generated by viruses during their replication cycle. These viral components are usually parts of the viral genome, such as single-stranded RNA (ssRNA), double-stranded RNA (dsRNA), genomic DNA, or viral proteins (reviewed in Iwasaki 2012).

The PAMPs can be recognized as 'non-self' signatures by pattern-recognition receptors (PRRs) that trigger the activation of the downstream IFN-induction pathways. Two main classes of PRRs have been described; (i) cytoplasmic sensors, including the retinoic acid-inducible gene I (RIG-I)-like receptors (RLRs), the nucleotide oligomerization domain (NOD)-like receptors (NLRs), and an increasing range of newly described cytosolic nucleic acid sensors (e.g. cGAS), and (ii) membrane bound receptors, such as Toll-like receptors (TLRs) (Broz & Monack 2013). This study focuses on Respiratory Syncytial Virus (RSV), which is a negative sense single stranded RNA (-ssRNA) virus. Cytoplasmic and endosomal recognition of RNA viruses is predominantly mediated by RLR and TLR receptors, thus the rest of this section will focus on the RLR- and TLR-dependent activation of the IFN-β induction pathway, which is summarized in Figure 1.1.

## 1.1.1/1 RLR-dependent activation of type I IFNs

Two well-characterized RLRs are the retinoic acid inducible gene I (RIG-I) and the melanoma differentiation-associated gene-5 (mda-5). These are two widely expressed RNA helicases that can sense virus-derived nucleic acids generated in cytoplasm (reviewed in Goubau *et al.,* 2013). Specifically, RIG-I is capable of recognizing blunt short double-stranded 5'-triphosphorylated RNA, whereas mda-5 is found to recognize long dsRNA (Kato *et al.,* 2008). Following binding to their appropriate ligands, both RIG-I and mda-5 undergo conformational changes that expose their caspase recruitment domains (CARDs), which can subsequently interact with the mitochondrial antiviral-signalling protein (MAVS) adaptor, also known as Cardif/VISA/IPS-1 (Figure 1.1) (Kawai *et al.,* 2005).
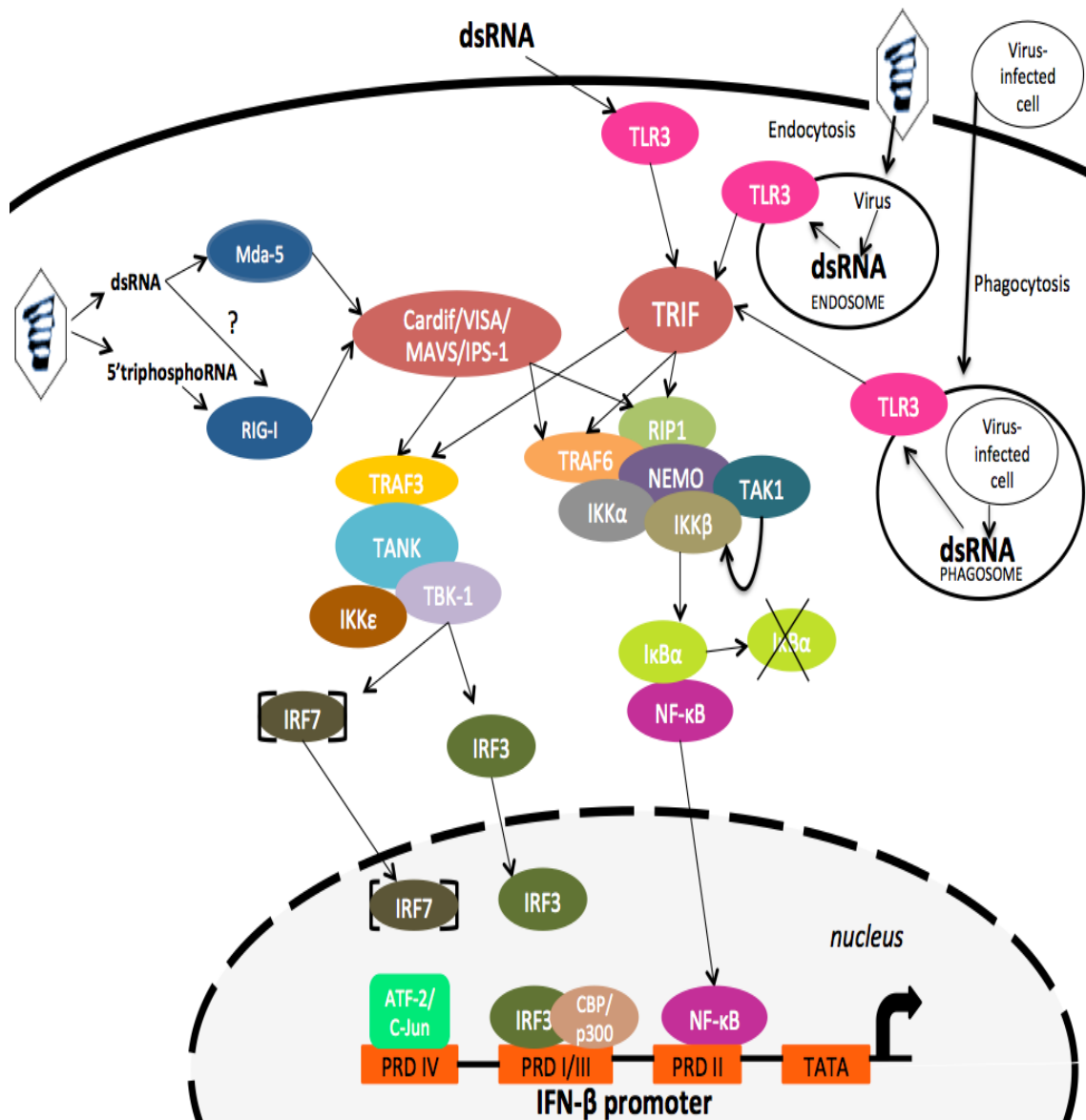
**Figure 1.1 IFN-induction pathway** The RLR- and TLR3-dependent activation of the type I IFN (IFN-β) induction pathway is illustrated. Cytoplasmic dsRNA and 5'-triphospoRNA are recognized by mda-5 and RIG-I, respectively. The TLR3-dependent signalling is activated in response to extracellular dsRNA and dsRNA present in phagosomes or endosomes. Both pathways lead to the phosphorylation and nuclear translocation of IRF3 and NF-κB transcription factors, where they bind the IFN-β promoter and initiate transcription of IFN-β. Modified from Randall and Goodbourn (2008).

The engagement with the adaptor activates a number of downstream kinases, which are essential for activating IFN regulatory factor-3 (IRF3) and the nuclear factor kappa B (NF-κB), respectively (Figure 1.1). The RLR-mediated activation of IRF3 requires recruitment of an E3 ubiquitin ligase, the TNF-receptor associated factor 3 (TRAF3), which associates with the adaptor protein MAVS (Paz *et al.,* 2011). Downstream of TRAF3, TBK1 (TRAF family member-associated NF-κB activator (TANK)-binding kinase 1) and the inducible IκB kinase (IKKε), are activated in an uncharacterized manner, and directly phosphorylate IRF3 (Goubau *et al.,* 2013). Following its phosphorylation, IRF3 dimerizes, and translocates into the nucleus, where it combines with its co-activator CBP/P300 to induce transcription of the IFN-β promoter (Figure 1.1) (Perry *et al.,* 2005). The activation of the IFN-β promoter can be also amplified by a positive feedback loop, in which the early produced IFN-α/β trigger the transcription of IRF7; IRF7 is successively activated by TBK1 and IKKε in a similar manner to IRF3 (Trinchieri 2010).

Activation of NF-κB obligates its dissociation from its inhibitor IκB molecules. This involves activation of IκB molecules by two kinases, IKKα and IKKβ, which subsequently allows the polyubiquitination of the IκB molecules and their destruction by the proteasome (Zandi *et al.,* 1997). The IKKα and IKKβ molecules bind to a regulatory subunit, the NF-κB essential modulator (NEMO) to form the IKK-complex, which is a core element of the NF-κB cascade (Randall & Goodbourn 2008). The IKK-complex interacts with upstream signalling molecules, including RING type E3 ligases (e.g. TRAF6) and kinases (e.g. RIP1), which act as an activation platform (Figure 1.1) (Hoesel & Schmid 2013). Although, the exact mechanism by which IKKα and IKKβ become activated remains obscure, it is clear that their activation requires

phosphorylation on two serine residues; Ser177 and Ser181 for IKKβ, and Ser176 and Ser180 for IKKα (Israël 2010). It was shown that phosphorylation of IKKβ is mediated by the TGF-β activating kinase 1 (TAK1), which in turn phosphorylates IκBα (Wang et al. 2001). Notably, phosphorylation of IKKα is not necessary for activating the canonical pathway, though it is required for activation of the alternative NF-κB pathway (Israël 2010). Activation of the IκB molecules and their subsequent proteasomal degradation leads to the liberation of NF-κB, which makes the nuclear localization signal (NLS) of the p65 subunit of NF-κB accessible (Hoesel & Schmid 2013). Subsequently, NF-κB translocates to the nucleus where it serves as an enhanceosome component for the activation of the IFN-β promoter (Figure 1.1).

The *IFNB* gene promoter contains four positive regulatory domains (PRDs I to IV), which serve as binding sites for the transcription factors described above (Figure 1.1). In particular, IRF3/IRF7 associates with PRD I/III, ATF-2/c-Jun heterodimers interact with PRD IV, and NF-κB binds to PRD II (Basagoudanavar *et al.,* 2011). Optimal induction of the *IFNB* gene requires binding of the transcription factors IRF3 and NF-κB together with the ATF-2/c-Jun dimers to the IFN-β promoter (Randall & Goodbourn 2008) (Figure 1.1).

## 1.1.1/2 TLR-dependent activation of type I IFNs

The TLR family also plays an instructive role in innate immune responses against viral infections, as members of the TLR family (e.g. TLR2. TLR3, TLR6, TLR7 and TLR9) trigger intracellular signalling pathways that lead to production of IFN-β (Iwasaki 2012). More precisely, TLR3 receptors can recognize extracellular dsRNA, dsRNA delivered through the endosomes and dsRNA presented in phagosomes (Figure

1.1) (Alexopoulou *et al.,* 2001; Schulz et al. 2005). Although most of TLRs signal through an adaptor called myeloid differentiation factor 88 (MyD88), activation of the TLR3-dependent pathway requires TRIF (Toll-interleukin (IL)-1-resistannce (TIR) domain-containing adaptor inducing IFN-β) (Goubau *et al.,* 2013; Takeda & Akira 2004). Engagement of TLR3 by dsRNA leads to TLR3 dimerization and its tyrosine phosphorylation that causes TRIF recruitment. TRIF recruitment leads to activation of both IRF3 and NF-κB 'arms' of the type I IFN induction pathway, in almost the same way that MAVS adaptor does during the RIG-I/mda-5 activation pathway (Figure 1.1) (Goubau *et al.,* 2013).

In addition to the TLR3-dependent pathway, TLR7 and TLR9 receptors can also trigger activation of the IFN-β induction pathway (Iwasaki 2012). The TLR7- and TLR9-dependent pathways are activated by ssRNA and DNA, respectively, which is delivered through the endosomes (Heil *et al.,* 2004; Tabeta *et al.,* 2004). In brief, TRL7 and TLR9 recruit the MyD88 adaptor, which causes the phosphorylation and the translocation of both IRF7 and NF-κB to the nucleus, where they can bind and activate the IFN-β promoter (Randall & Goodbourn 2008; Takeuchi & Akira 2009). Unlike the TLRs discussed above, the TLR4 receptor responds entirely to an extracellular signal and it activates the IFN-induction pathway primarily in response to bacteria pathogens and lipopolysaccharide (LPS) (Kawai & Akira 2006). The TLR4 receptor signals through both the TRIF-dependent pathway (like TLR3) and the MyD88-dependent pathway (like TLR7 and TLR9) to activate IRF3 and NF-κB, respectively (Yamamoto *et al.,* 2002). Whilst the role of TLR4 activation against virus infection remains unclear, there is evidence that RSV and VSV envelope proteins (F and G, respectively) can induce type I IFNs through a TLR4-dependent pathway (Marr & Turvey 2012; Georgel

*et al.,* 2007). Moreover, TLR2 is expressed on the surface of immune cells in association with TLR1 or TLR6 and signals though both MyD88 and Tirap (toll-interleukin 1 receptor domain containing adaptor protein) (Takeda & Akira 2004). TLR2 and TLR6 complexes are known for their ability to activate early innate immunity in response to bacterial motifs, as well as viruses, including Hepatitis C virus and Dengue virus (Chang *et al.,* 2007; Chen *et al.,* 2015).

Recognition of 'foreign' cytoplasmic DNA in some mammalian cells, especially macrophages and DCs can also trigger the activation of the IFN-induction pathway (Ishii *et al.,* 2006). More recently, numerous cytoplasmic viral DNA sensors have been identified, including cGAMP synthase (cGAS) (Sun *et al.,* 2013), DDX41 helicase (Zhang *et al.,* 2011) and IFIT16 (Unterholzner *et al.,* 2010). These sensors induce type I IFNs through a central signalling cascade involving a molecule called stimulator of IFN genes (STING), which serves as a scaffold for the phosphorylation of IRF3 by the kinase TBK1 (Tanaka & Chen 2012). In addition to virus stimuli, type I IFNs can be induced by host factors and cytokines such as tumor necrosis factor (TNF), which signal via IRF1 rather than via IRF3 and IRF7 (Yarilina *et al.,* 2008). In conclusion, type I IFNs are rapidly induced in response to virus stimuli through a number of different pathways, which are predominantly activated by RLR and TLR sensor molecules either in the cytoplasm or endosomes. Regardless the mechanism behind the activation of the IFN-β promoter, following its induction, IFN-β is secreted from infected cells, and binds to its receptor on the surface of infected or uninfected cells, in order to mediate activation of the IFN-signalling pathway, which is reviewed in the following subsection.

## 1.1.2 Type I IFN-signalling pathway

<u>1.1.2/1 Signalling responses to IFN-α/β</u>

The biological activities of IFN-α/β are initiated after the activation of the JAK (Janus activated kinase) /STAT (signal transducers and activators of transcription) signalling pathway, which is also known as the type I IFN-signalling pathway (Figure 1.2). All the type I IFNs signal through a common heterodimeric receptor, which is composed by two distinct subunits, namely IFNAR1 and IFNAR2 (Kim *et al.,* 1997). Each of these receptor subunits interacts with a member of the Janus activated kinase (JAK) family; the IFNAR1 subunit is constitutively associated with tyrosine kinase 2 (Tyk2), whereas IFNAR2 is associated with JAK1 (Ivashkiv & Donlin 2014). In addition to JAK1, STAT1 and STAT2 also bind to the cytoplasmic domain of the IFNAR2 subunit in untreated cells, however, STAT1 can only bind when STAT2 is present (Li *et al.,* 1997). Furthermore, it is also demonstrated that STAT1 and STAT2 weakly associate with each other in the cytoplasm prior to cytokine stimulation (Stancato *et al.,* 1996).

The ligand-induced dimerization of the receptor causes a conformational change, such that JAK1 phosphorylates and activates Tyk2, which then cross-phosphorylates JAK1 to activate it further (Gauzzi *et al.,* 1996). Tyk2 phosphorylates tyrosine 466 on IFNAR1 and tyrosine 690 on STAT2, whereas STAT1 is phosphorylated by JAK1 on tyrosine 701 (Stark *et al.,* 1998). In particular, when Y466 of IFNAR1 is phosphorylated, it creates a docking site, where the Src homology 2 (SH2) domain of STAT2 can bind to, allowing the tyrosine phosphorylation of STATs (Yan *et al.,* 1996). Transcriptional activation by STAT1, whether activated by type I or

II IFN, also requires phosphorylation on serine 727, which is catalyzed by several cellular kinases (Uddin *et al.,* 2002).
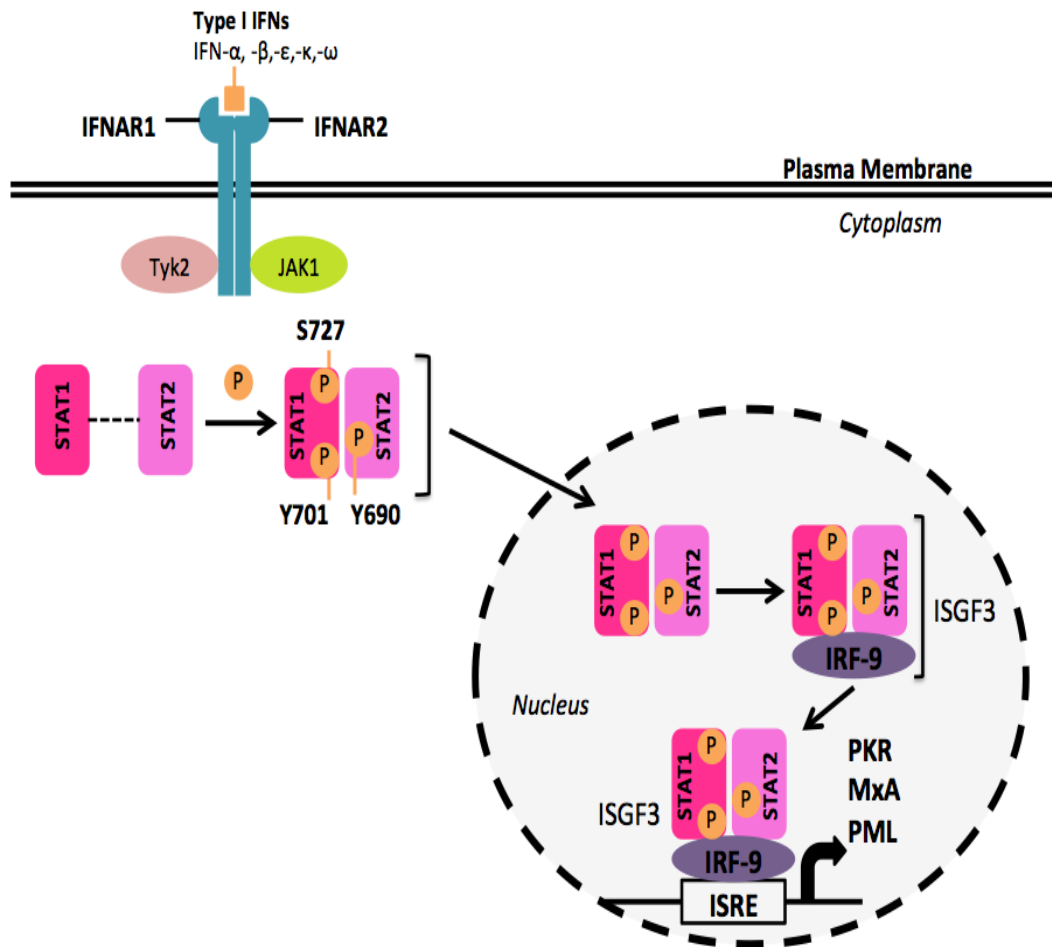
**Figure 1.2 The IFN-signalling pathway**. The JAK/STAT pathway is activated after the binding of IFN-α/β to IFNAR receptor. Phosphorylated STAT1 and STAT2 localize into the nucleus, where they bind IRF9 to form the ISGF3 complex. The ISGF3 transcription factor binds to the ISRE sequences, which are present in the promoters of ISGs (e.g. MxA) to initiate their transcription, and establish an antiviral state in the virus-infected cell. Modified from Platanias (2005).

The phosphorylation of both STATs is followed by their dissociation from the receptor, which allows the phosphorylated STAT1–STAT2 heterodimer to translocate into the nucleus (Stark *et al.,* 1998; Yan *et al.,* 1996). In the nucleus, the STAT1–STAT2 heterodimers interact with the DNA binding protein IRF9 to form the STAT1–STAT2–IRF9 complex, which is known as the interferon-stimulated factor gene 3 (ISGF3) (Figure 1.2) (Ivashkiv & Donlin 2014). ISGF3 is the major transcription factor formed in response to type I IFNs, as it stimulates the activation of the IFN-stimulated response element (ISRE), which initiates transcription of hundreds of genes, the IFN-stimulated genes (ISGs), many of which have antiviral activity (Schoggins & Rice 2011) .

The antiviral mechanisms of some ISGs have been studied extensively and reviewed comprehensively, including the ds-RNA dependent protein kinase (PKR) (Nakayama et al. 2010), the 2'5'-oligoadenylate synthetase (OAS) (Silverman 2007), the Mx family of genes (Haller & Kochs 2011), IFN-induced proteins with tetratricopeptide repeats (IFITs) and IFN-induced transmembrane proteins (IFITMs). (Lenschow 2010; Diamond & Farzan 2013), the promyelocytic leukemia (PML) nuclear bodies (Everett & Chelbi-Alix 2007), the tripartite motif (TRIMs) family (Yap & Stoye 2012), and viperin (Helbig & Beard 2014). One remarkable property of ISG-mediated antiviral activity is the magnitude with which a single IFN effector can restrict virus replication. For instance, IFIT1/ISG56 is primarily responsible for the IFN-induced inhibition of parainfluenza type 5 virus (PIV5) by selectively inhibiting the translation of PIV5 mRNAs (Andrejeva *et al.,* 2013). Nonetheless, it is known that ISGs have a plethora of other functions. Some of them, including PKR, are involved in the establishment of a pro-apoptotic state in target cells (Maher *et al.,* 2007; Nakayama *et*

*al.,* 2010), whereas others, such as the cyclin-dependent kinase (CDK) inhibitor p21 (also known as pWAF, CIP) are profoundly cytostatic, triggering a growth arrest at the $G_1/S$ transition point in many cell types (Ferrantini *et al.,* 2007). Moreover, other ISGs have a major role in promoting the transition from innate to adaptive immune responses, and one key example is the class I major histocompatibility complex (MHC) (Le Bon & Tough 2002).

## 1.1.2/2 Crosstalk between IFN-signalling pathways

Whilst the activation of the STAT1–STAT2–IRF9 heterodimer is the canonical mode of ISRE activation, IFNAR activation induces the formation of other STAT complexes; it activates STAT1 and STAT3 homodimers and heterodimers in most cell types and STAT4, STAT5 and STAT6 in certain cell types (Torpey *et al.,* 2004; Gomez & Reich 2003; Gupta *et al.,* 1999; van Boxel-Dezaire *et al.,* 2006). These complexes can either bind to the ISRE or to another type of element, known as an IFN-γ-activated site (GAS) element, which can be also present in the promoter of ISGs (Brierley *et al.,* 2006). Signalling in response to type III IFNs (IFN-λ family) follows a very similar pattern to that in response to type I IFNs, as it also leads to the formation of the STAT1–STAT2–IRF9 heterodimer, despite signalling through a different receptor (IFNLR) (Lazear *et al.,* 2015). In contrast, type II IFN (IFN-γ) signals through the IFNGR receptor, and leads to the formation of STAT1-STAT1 homodimers, which bind to GAS elements in the nucleus and activate transcription of ISGs (Randall & Goodbourn 2008). Although not a part of the canonical type I signalling responses, STAT1 homodimers could be also activated through the IFN-α/β signalling, indicating that crosstalk exists between the two pathways (Decker *et al.,* 1991). Interestingly,

IKKε is important for regulating the balance between type I and type II IFN response, as the IKKε-mediated phosphorylation of STAT1 suppresses STAT1 homodimer formation, and thereby facilitates ISGF3 formation, augmenting type I antiviral responses (Ng *et al.,* 2011). In addition, many ISGs show either sustained induction in response to IFNs or biphasic induction kinetics, which are usually related to IRF1. In particular, IRF1 binds to most, if not all ISREs, and it is induced by both IFN-α/β and IFN-γ, but it is more responsive to IFN-γ (Randall & Goodbourn 2008). Although, IRF1 plays a central role in the regulation of ISGs expression, it still remains unclear how IRF1 regulates gene expression between type I and II IFNs. Interestingly, each of these IFNs induces a unique and partially overlapping set of ISGs, whereas some other ISGs, such as PKR and OAS, can be activated directly by viral dsRNA in the absence of IFN (Lemaire *et al.,* 2008; Ibsen *et al.,* 2015). Taken together, the induction of ISGs is mediated through various mechanisms that could be intersecting and often self-reinforcing.

In conclusion, type I IFN-signalling pathway is an extremely powerful antiviral defense mechanism, which mediates an autocrine loop and induces the expression of ISGs in response to virus replication. ISGs establish an antiviral state within infected cells or neighboring uninfected cells, which provides protection from virus infections in the absence of adaptive immunity.

## 1.2 Viral IFN antagonism

The survival of almost all mammalian viruses, regardless of genome type and complexity, is based on their ability to outrun innate immunity before the development of adaptive immune responses (Versteeg & Garcia-Sastre 2010). Viruses have evolved an astounding variety of IFN antagonistic strategies targeting virtually all parts of the IFN system, often in a highly specific manner (Weber & Haller 2007). Over 170 different viral IFN antagonists from 93 distinct viruses have been described to date, and nearly 50% of them antagonize multiple steps of the cellular IFN system (Versteeg & Garcia-Sastre 2010). Although every viral IFN antagonist is unique in its own right, they counteract the cellular IFN response by using common strategies, including: (i) global inhibition of cellular gene expression, (ii) sequestration, cleavage or degradation of IFN effector molecules, and (iii) acquisition of replication strategies that are insensitive to IFNs (Randall & Goodbourn 2008; Versteeg & Garcia-Sastre 2010).

### 1.2.1 The pleiotropic nature of viral IFN antagonists

The multifunctionality of viral IFN antagonists is reliant to the nature of virus genome. For instance, the relatively limited genome capacity of RNA viruses favors high degree of multifunctionality and restricts the variability of accessory proteins. Hence, RNA viruses do not have genes that exclusively encode for IFN antagonists, as in the case of large DNA viruses, but instead IFN antagonists are highly multifunctional and sometimes conserved within related RNA viruses (Versteeg & Garcia-Sastre 2010). A key example of a multifunctional IFN antagonist is the NS1 protein of Influenza A and B viruses (Family *Orthomyxoviridae*), which despite its small size (26 kDa) antagonizes the host immune responses in a species-specific manner using a plethora of

different strategies (Kochs *et al.,* 2007; Hale *et al.,* 2008). Although multifunctionality is a common characteristic for RNA viruses, small DNA viruses also encode for multifunctional proteins. For instance, the E6 and E7 proteins of Human Papilloma Virus (HPV) are well known for their oncogenic properties, but they also have a numerous functions against the cellular IFN response (Cordano *et al.,* 2008). In contrast, some other DNA viruses have larger genomes and sometimes encode for proteins with functions limited to IFN antagonism. For example, poxviruses encode for proteins called 'viroceptors', which can be either secreted or localized to the surfaces of infected cells and compete with the cellular IFN receptor for its ligand (Seet *et al.,* 2003).

The nature of the virus genome and the genomic replication tactics differ between families, hence the IFN inhibitory strategies vary with some of them having a higher prevalence in certain virus classes (Katze *et al.,* 2002). More precisely, negative-sense single-stranded RNA (-ssRNA) viruses are more susceptible to detection by the IFN sensory molecules, compared to +ssRNA or DNA viruses. Therefore, interfering with the RLR-mediated pathways is a common feature between -ssRNA viruses, and it has been extensively reported in a number of different -ssRNA families, such as *Paramyxoviridae* and *Orthomyxoviridae* (Andrejeva *et al.,* 2004; Gack *et al.,* 2009). Defending the host cell innate immunity is crucial for successful viral infections, therefore viruses have evolved a plethora of mechanisms to circumvent the cellular IFN response and establish infections, which are often highly pathogenic and virulent.

## 1.2.2 The plethora of IFN evasion tactics evolved by Paramyxoviruses

The current study focuses on RSV, which is the prototype species of Genus *Pneumovirus*; Subfamily *Pneumovirinae*; Family *Paramyxoviridae*; Order *Mononegavirales* (Collins *et al.,* 2013). The *Paramyxoviridae* family has two subfamilies: (i) *Paramyxovirinae* subfamily, which includes important human and animal pathogens such as mumps, measles virus, the human parainflluenza viruses (HPIVs), and (ii) *Pneumovirinae* subfamily, which consists of two genera, the *Pneumoviruses* and the *Metapneumoviruses*. The Genus *Pneumonovirus* consists of RSV and its animal relatives, such as the bovine RSV (BRSV), ovine RSV (ORSV) and pneumonia virus of mice (PVM), and the Genus *Metapneumovirus* consists of human and avian metapneumonovirus (Collins *et al.,* 2013). RSV is considered to be one of the most complex members of *Paramyxoviridae* family, because it encodes additional proteins, namely NS1, NS2, SH, M2-1, M2-2, that are not present in any other virus of the family (Chambers & Takimoto 2009).

### 1.2.2/1 Viral IFN antagonists of *Paramyxovirinae*

Viral IFN antagonism has been extensively studied within the *Paramyxoviridae* family, which is the largest virus family with pleiotropic and also conserved IFN antagonists. The paramyxoviruses that belong to the P*aramyxovirinae* subfamily encode accessory proteins (V/C/W), which abrogate various facets of the cellular type I IFN response (Audsley & Moseley 2013). The V, C and W proteins are encoded by the same gene that encodes for the P protein; V/W proteins are produced through RNA editing, and an overlapping open reading frame (ORF) encodes for the C protein (Chambers &

Takimoto 2009). Therefore, P/V/W proteins share N-terminal sequences, but they have different C-termini, which usually have unique functions.

Although paramyxoviruses exhibit a commonality in their viral IFN antagonists, the manner with which they inhibit the cellular IFN response varies within the subfamily and it is highly dependent on the accessory proteins expressed by each virus (Parks & Alexander-Miller 2013). Specifically, the majority of paramyxoviruses utilize the same strategy to subvert the IFN-induction pathway, which involves the highly conserved cysteine-rich C-terminal domain (CTD) of their V proteins. This domain binds to mda-5, and prevents downstream activation of the IFN-β promoter (Andrejeva *et al.,* 2004). Furthermore, most paramyxoviruses are resistant to the antiviral responses induced by IFNs, as their V proteins also have the ability to inhibit STATs (Goodbourn & Randall 2009). Although almost all V proteins act against the JAK/STAT pathway, they inhibit STATs using different molecular mechanisms, ranging from cytoplasmic sequestration to proteasomal degradation (Figure 1.3) (Audsley & Moseley 2013). For instance, PIV5 V protein targets STAT1 for proteasome-mediated degradation (Didcock *et al.,* 1999), whereas Nipah virus V protein sequesters STAT1 and STAT2 in the cytoplasm and prevents their nuclear localization, which impedes them from binding to the ISRE sequences (Rodriguez *et al.,* 2002).

In addition to the inhibition strategies imposed by V proteins, the C and W proteins also have imperative functions against the cellular IFN response. For example, the V protein of Sendai virus (SeV) has no effect on the IFN-signalling pathway (Gotoh *et al.,* 1999) but instead SeV encodes for a set of four C proteins, the larger of which is mainly responsible for STAT1 inhibition though degradation (Garcin *et al.,* 2002). The PIV3 C protein also targets STAT1 but not through degradation, as it was shown to

inhibit its phosphorylation (Malur *et al.,* 2005). Furthermore, other paramyxoviruses encode for W proteins, which are also potent antagonist of the IFN-signalling pathway. For instance, Nipah virus W protein sequesters STAT1 in the nucleus, and thereby blocks transcription of the IFN-induced effector molecules (Shaw *et al.,* 2005).
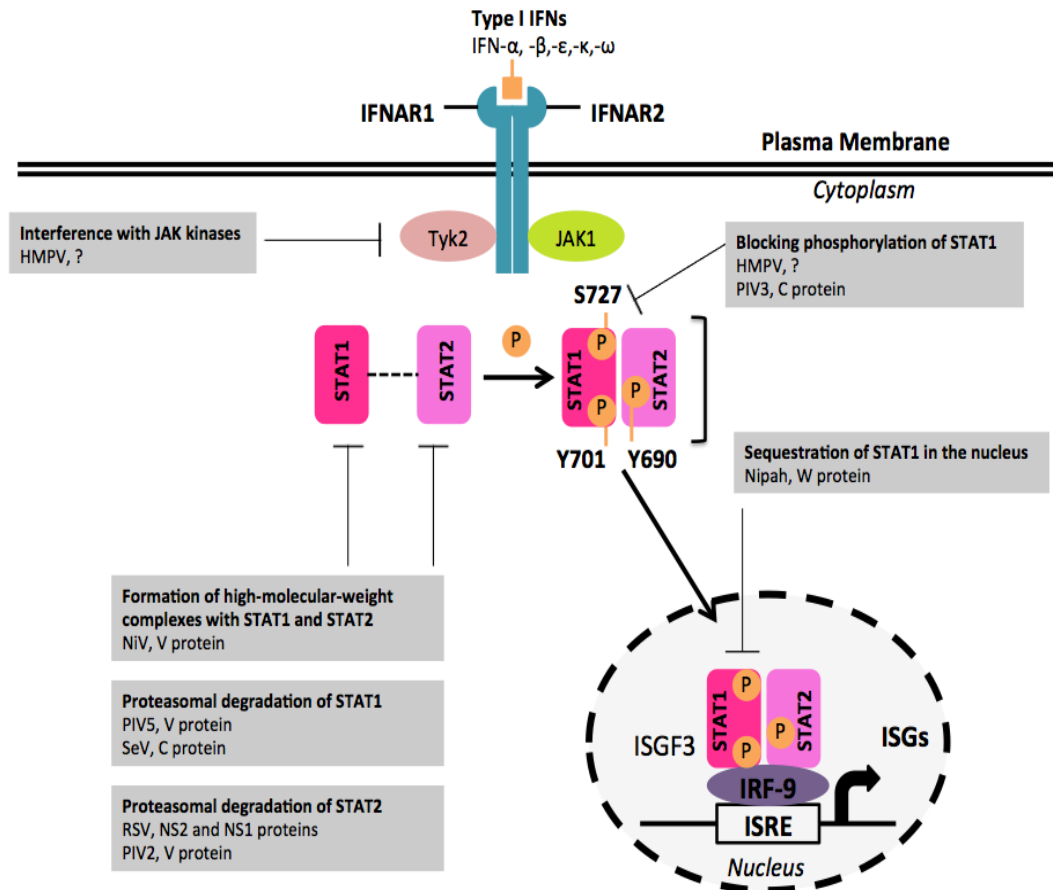


**Figure 1.3 Paramyxovirus inhibition of the IFN-signalling pathway.** A remarkable variety of different type I IFN evasion strategies have been reported within family *Paramyxoviridae*. Paramyxoviruses encode viral IFN antagonists (V, C, W, NS1 and NS2), which circumvent all different steps of the IFN-signalling pathway, including phosphorylation, nuclear translocation of STATs and ISGF3-mediated activation of the ISRE sequences of ISGs. hMPV interacts with JAK kinases and inhibits phosphorylation of STAT1, however it remains unknown, which viral protein(s) is responsible for these functions.

## 1.2.2/1 Viral IFN antagonists of *Pneumovirinae*

Adding to the variation observed within the *Paramyxoviridae* family, the paramyxoviruses that belong to the *Pneumovirinae* subfamily do not express any of the V, C or W accessory proteins, and instead some encode for two non-structural proteins (NS), NS1 and NS2, which impose similar functions to V, C or W proteins (Figure 1.3). RSV NS1 and NS2 proteins work either independently or co-operatively to inhibit the early innate immunity by circumventing multiple steps of the IFN induction and signalling pathways (Barik 2013), as will be discussed in detail in Section 1.4. Although RSV does not express any of the accessory proteins found in other paramyxoviruses, it antagonizes the IFN-signalling pathway using similar strategies. RSV NS1 and NS2 mediate proteasomal degradation of STAT2 (Spann *et al.,* 2004; Lo *et al.,* 2005; Goswami *et al.,* 2013), a function also observed by the V protein of PIV2 (P*aramyxovirinae* subfamily) (Parisien *et al.,* 2001). In contrast, BRSV NS1 and NS2 have not been reported to antagonize STAT2, though NS1 and NS2 proteins of both human and bovine RSV use a common strategy to suppress the IFN-induction pathway, which involves inhibition of IRF3 (Schlender *et al.,* 2000; Spann *et al.,* 2004). Furthermore, human metapneumovirus (hMPV) (Genus *Metapneumovirus*) lacks NS1 and NS2, nonetheless hMPV modulates cellular innate immune response by down regulating Jak1 and Tyk2, and subsequently inhibiting STAT1 phosphorylation using a yet unknown mechanism (Dinwiddie & Harrod 2008; Junping Ren *et al.,* 2011).

In conclusion, paramyxoviruses outrun the cellular IFN response using an astonishing array of strategies that are attributed to their multifunctional and in some cases conserved IFN antagonists. Escaping early innate immunity is crucial for virus infection, therefore targeting IFN antagonism/antagonists appears to be a promising

strategy for developing new therapeutic approaches. This study focuses on RSV, and particularly on its two IFN antagonists, NS1 and NS2. Hence, the following section introduces RSV, and discuses the intricate strategies of its two IFN antagonists NS1 and NS2 against the cellular IFN response.

# 1.3 Introduction to Respiratory Syncytial Virus (RSV)

## 1.3.1 RSV epidemiology and pathogenicity

RSV was first isolated from nasal secretions of young chimpanzees in 1955, and was initially named 'chimpanzee coryza agent' (Blount et al. 1956). A year after, it was also isolated from two human infants, one with bronchiolitis and one with pneumonia (Chanock et al. 1956). Since then, RSV is recognized as the leading cause of acute lower respiratory tract illness (ALRI) in infants and young children worldwide (Hall *et al.,* 2009). RSV is also a significant cause of morbidity and mortality among immunocompromised individuals and the elderly (Falsey *et al.,* 2000). The clinical severity of RSV infections can vary from mild upper respiratory tract infection to severe bronchiolitis; approximately 40% of all primary RSV infections in infancy result in ALRI (Simoes *et al.,* 2003; Paes *et al.,* 2011). Interestingly, RSV re-infections occur throughout life and they do not depend on antigenic differences. First or second infections mostly lead to ALRI but there is a substantial reduction in disease severity in following infections that presumably reflects increasing protective immunity (Collins & Melero 2011). It still remains controversial whether there is a relationship between the clinical severity and RSV subtype (A and B) (Wright & Piedimonte 2011), which can circulate independently from each other or also co-circulate during one epidemic (Kneyber *et al.,* 1998; Anderson *et al.,* 1985).

It has been estimated that, in 2005, RSV caused 34 million cases of ALRI in children younger than five years old globally, 3.4 million of which required hospitalization (Nair *et al.,* 2010). Moreover, 66,000 to 199,000 children younger than 5 years old died from RSV-associated ALRI in 2005, with 99% of these deaths occurring in developing countries (Nair *et al.,* 2010). RSV morbidity and mortality rates are

considerably higher in premature-born infants (<35 weeks gestational age) and in infants with chronic lung disease (such as bronchopulmonary dysplasia and cystic fibrosis) or hemodynamically significant congenital heart disease (CHD) (Venkatesh & Weisman 2006; Wright & Piedimonte 2011). Similar to other respiratory viruses, RSV can also trigger exacerbations of asthma and chronic obstructive pulmonary disease (COPD), which are two common inflammatory diseases of the airways, however the link between RSV and these diseases is not well understood yet (Kurai *et al.,* 2013; Mehta *et al.,* 2013).

*In vivo*, RSV is largely restricted to the superficial cells of the respiratory epithelium and shedding occurs at the apical membrane of airway epithelial cells (AECs), suggesting that polarized epithelium is the preferred cellular target (Zhang *et al.,* 2002). RSV infection causes airway obstruction due to peribroncheal mononuclear cell infiltration, mucus secretion, and sometimes syncytia formation in the lungs (Van Drunen Littel-Van Den Hurk & Watkiss 2012). *In vitro* models suggested that RSV is not inherently a highly cytopathic virus, as during an infection of several weeks, RSV triggered little visible damage to lung tissue but it caused impairment of the ciliary beating (Zhang *et al.,* 2002). This suggests that the RSV-induced effects on ciliary function presumably facilitate the airway obstruction that is characteristic of RSV disease. Severe RSV infections are also associated with the activation of inflammatory cytokines and activated granulocytes in the airways of infants and children with ARLI (Collins & Melero 2011). Neutrophils are the most abundant immune cell activated during severe RSV infection in infants (Abu-Harb *et al.,* 1999), however activation of the DC8+ T lymphocytes (Graham *et al.,* 1991) and Th2 biased stimulation of the CD4+ T lymphocytes have been also suggested to mediate RSV disease (Adkins *et al.,* 2004;

Collins & Melero 2011). Although immune and inflammatory responses can enhance RSV disease, viral load is also correlated with RSV disease severity in infants (DeVincenzo *et al.,* 2010; Houben *et al.,* 2010). The mechanisms behind RSV pathogenicity are not fully understood, however viral (e.g. viral load), environmental (e.g. smoking) and host factors (e.g. prematurity), all contribute to the severity of RSV disease (Van Drunen Littel-Van Den Hurk & Watkiss 2012).

## 1.3.2 RSV current treatment

Despite extensive efforts, development of an anti-RSV vaccine has proven to be particularly challenging and complicated, especially after the disastrous vaccination trials with a formalin-inactivated RSV vaccine (FI-RSV) in 1969 (Kim *et al.,* 1969). FI-RSV not only failed to provide immunity to RSV but 80% of the immunized children required hospitalization when naturally infected with the wild-type virus, because natural exposure resulted in immune-mediated enhancement of disease (Collins & Melero 2011; Kim *et al.,* 1969). Since then, prophylactic options are limited to passive immunization with a humanized RSV-neutralizing, fusion (F)-specific monoclonal antibody, the Palivizumab (Synagis[TM]; MedImmune), which provides 55% reduction in RSV-associated hospitalization (Anon 2006). A second generation monoclonal antibody, the motavizumab (MedImmune), was shown to bind to RSV F protein 70-fold better than palivizumab, and it exhibits about a 20-fold improvement in neutralization of RSV *in vitro* (Wu *et al.,* 2007). Despite its better efficacy *in vitro*, there was questionable evidence that motavizumab had additional benefit in comparison to palivizumab *in vivo*, and administration of motavizumab significantly increased adverse

effects in infants, therefore the US FDA committee never approved its use in the clinic (Wright & Piedimonte 2011).

For therapeutic intervention, the nucleoside analogue ribavirin is the only drug licensed for RSV treatment in humans, but its use is limited due to the lack of proven efficacy, the difficulty of administration (usually aerosolic), and concerns of toxicity (Anon 2006; Collins & Melero 2011). A number of different therapeutic agents such as bronchodilators, corticosteroids, β-agonists, epinephrine and montelukast (used for the maintenance treatment of asthma) have been suggested for RSV treatment, but clinical trials have not demonstrated conclusive clinical benefit, (Wright & Piedimonte 2011; Krilov 2011). In conclusion, current treatment of acute RSV infections mainly involves supportive care, which highlights the lack of effective therapeutic options, and the need for new antiviral drugs for RSV treatment.

## 1.3.3 Overview of RSV genome and replication cycle

RSV virions are pleomorphic spherical or filamentous particles, which consist of a nucleocapsid packaged in a lipid envelope derived from the host cell plasma membrane (Figure 1.4/A) (Collins *et al.,* 2013). RSV entry requires attachment to cellular glycosaminoglycans (GAGs), which is followed by fusion with the plasma membrane, allowing the release of the viral genome in the cytoplasm (Figure 1.5) (Hallak *et al.,* 2000). RSV envelope contains three proteins: the fusion (F), the glycoprotein (G) and the small hydrophobic protein (SH) (Figure 1.4/A). The F protein directs viral penetration and syncytium formation. Similar to its counterparts in *Paramyxoviridae*, the RSV F protein is synthesized as a precursor $F_0$ and it is activated by furin-like host protease to yield two disulfide-linked subunits, $F_1$ and $F_2$ (González-Reyes *et al.,* 2001).

A

B



| | N protein | | P protein | | L protein | | Single stranded RNA |
|---|---|---|---|---|---|---|---|
| | G protein | | F protein | | SH protein | | Matrix protein |

| 3' Le | NS1 | NS2 | N | P | M | SH | G | F | M2 | L | Tr 5' |
|---|---|---|---|---|---|---|---|---|---|---|---|
| aa | 139 | 124 | 391 | 241 | 256 | 64 | 296 | 574 | 194/90 | 2165 | |
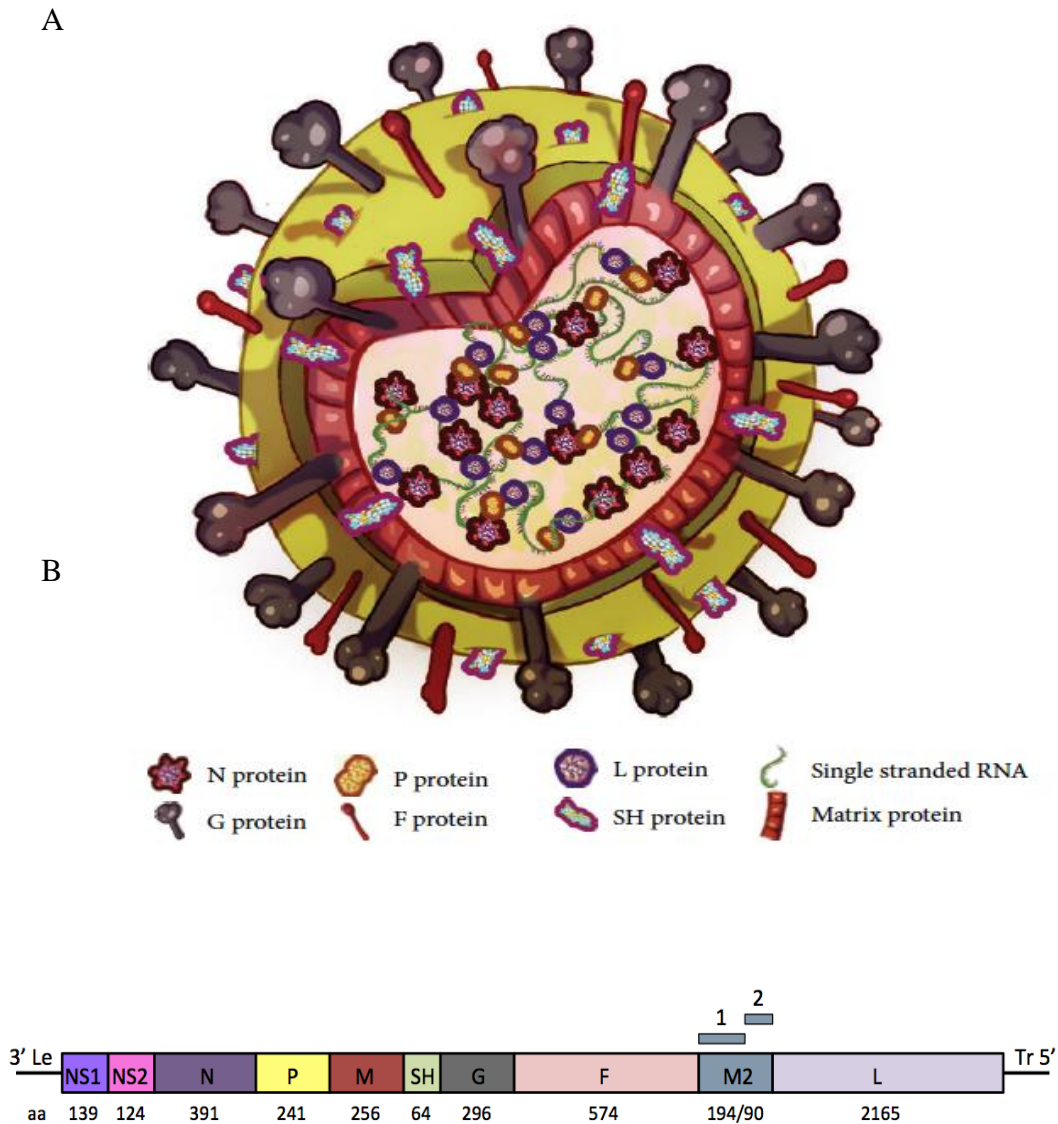
**Figure 1.4 Structure and genome organization of RSV (A) RSV virion particle** (approximately 200nm). RSV envelope consists of F, G, and SH. M is present between the outer envelope and the inner RNP. From Bawage *et al.,* (2013) **(B) RSV gene map.** The map shows the negative sense RNA genome of RSV, which has a 3' end leader (Le) and a 5'end trailer (Tr) region. The overlapping M2-1 and M2-2 ORFs are shown over the gene. The numbers below the map indicate the size of each RSV protein in amino acids (aa). The viral proteins are as follows: NS1, nonstructural protein 1; NS2, nonstructural protein 2; N, nucleoprotein; P, phosphoprotein; M, matrix protein; SH, small hydrophobic glycoprotein; G, attachment glycoprotein; F, fusion glycoprotein; M2-1, product of the first ORF in the M2 mRNA; M2-2; product of the second ORF in the M2 RNA; L, large polymerase protein.

F cleavage liberates a hydrophobic stretch of amino acids called the fusion peptide, which is inserted into the target cell membrane and leads to the creation of a stable helical bundle that forms as the viral and cell membranes are apposed (Collins *et al.,* 1984; McLellan *et al.,* 2011). The G protein plays a major but not exclusive role in attachment and it was found to bind cell-surface GAGs, including heparan sulfate (Hallak et al. 2007). The F and G proteins are the only virus neutralization antigens and are the two major protective antigens (Collins & Crowe 2007). In contrast to F and G, the SH protein has no apparent contribution to viral entry. Instead, SH is a short transmembrane glycoprotein with similar structural features to viporins, which are a small class of proteins that can modify membrane permeability, and can affect budding and apoptosis (Gonzalez & Carrasco 2003; Collins *et al.,* 2013).

RSV has a non-segmented, negative-sense RNA genome of 15.2 kb long, which encodes 10 transcription units in the order 3'-NS1-NS2-N-P-M-SH-G-F-M2-L-5' (Figure 1.4/B) (Collins 1991). The RSV genome replicates in cytoplasmic inclusion bodies, where the negative-sense viral genomic RNA serves as a template for the production of mRNAs by viral RNA-dependent RNA polymerase complexes (Figure 1.5) (Harrison *et al.,* 2010). Similar to the rest of *Mononegavirales,* subgenomic RSV mRNAs are produced in a polar gradient, in which transcription decreases along the gene order, as the polymerase detaches from the genome template at various gene junctions (Figure 1.5) (Collins *et al.,* 2013). Each mRNA encodes for a single polypeptide, except M2 mRNA that has an upstream and a downstream ORFs, which partially overlap and encode for the M2-1 and M2-2 proteins, respectively (Figure 1.4/B). Later in the infectious cycle, the viral polymerase ignores transcription signals and produces positive-sense replicative intermediate called the antigenome, which

serves as a template for the production of progeny negative-sense genomes (Figure 1.5) (Collins & Melero 2011).

The phosphoprotein (P) protein is also important for virus replication as it is an essential co-factor of the viral polymerase (Collins & Crowe 2007). It also acts as an adaptor that binds to N and M2-1 proteins to mediate interactions in the nucleocapsid and polymerase complex (Asenjo *et al.,* 2006; Khattar *et al.,* 2001; García-Barreno *et al.,* 1996). M2-1 protein is an essential transcription processivity factor that is important for the efficient synthesis of full-length mRNAs (Fearns & Collins 1999), and it is also a transcriptional anti-terminator factor that enhances the ability of the viral polymerase to read-through intergenic junctions (Hardy & Wertz 1998). The other product of M2 gene, the M2-2 protein is not essential for viral viability, but it appears to be important in modulating the balance between transcription and RNA replication (Bermingham & Collins 1999). The matrix (M) protein lines the inner envelope surface and is important in virion morphogenesis and virus assembly as it is required for the transport of nucleocapsids from viral inclusion bodies to plasma membrane (Mitra *et al.,* 2012). Although RSV genome replication takes place entirely in the cytoplasm, M protein was also found in the nucleus, where it interacts with the host cell transcription machinery (Figure 1.5) (Ghildyal *et al.,* 2003).

RSV assembly and budding occur at the plasma membrane and the minimum protein requirements for infectious virus particles are the F, M, N and P proteins (Teng & Collins 1998). RSV buds preferentially from the apical surface of infected polarized epithelial cells by hijacking the cellular apical recycling endosome (Figure 1.5) (Brock *et al.,* 2003). In addition to structural proteins and proteins involved in genome replication, RSV encodes for two NS proteins, NS1 and NS2, which are the two major
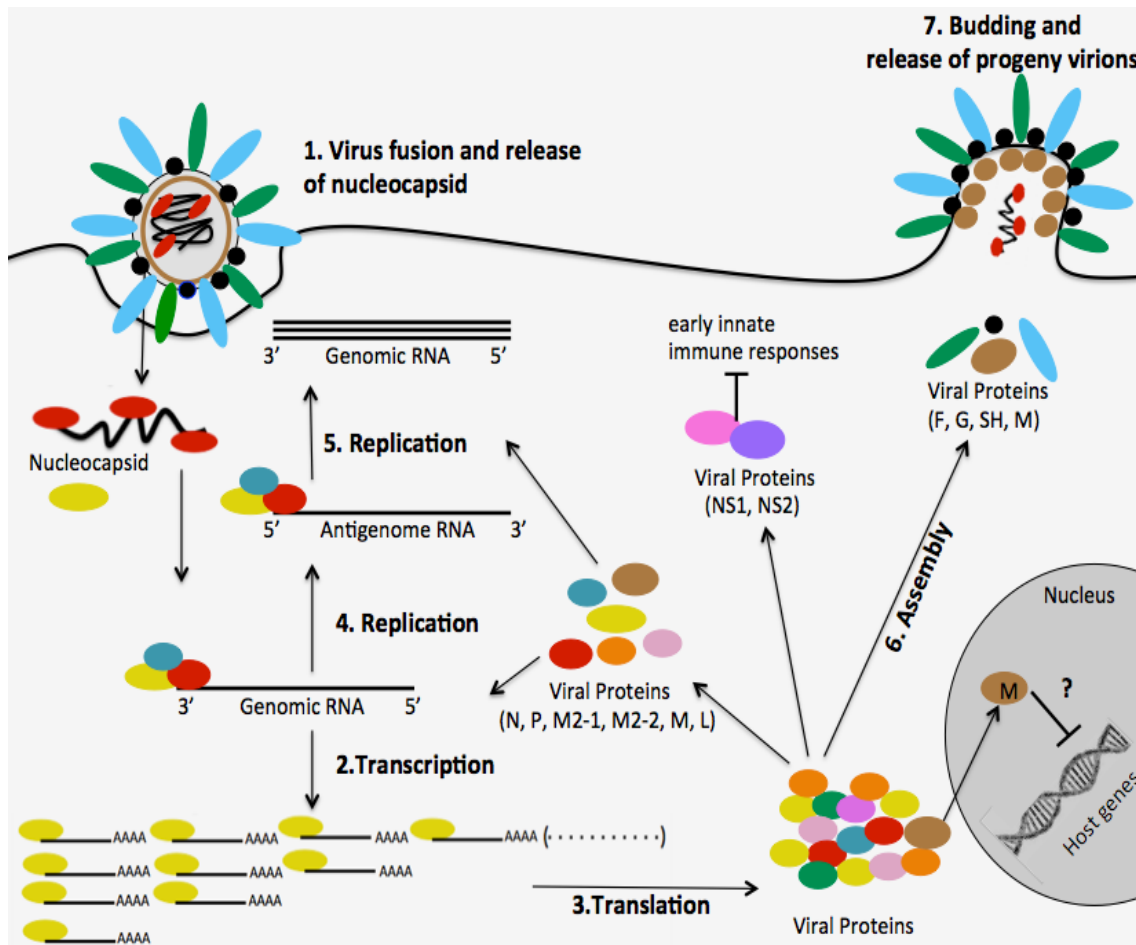
**Figure 1.5 RSV replication cycle** (**1**) RSV enters by direct fusion at the plasma membrane, releasing the encapsidated genome RNA and RNA-dependent RNA polymerase (yellow) into the cytoplasm, where viral mRNA synthesis occurs mainly at inclusion bodies. (**2**) Minimal unit for RNA transcription and replication requires L, N and P proteins of the RNP complex, and likely M2-1, M2-2 and M. (**3**) The polymerase uses the genome as a template to produce capped and polyadenylated mRNAs, which are transcribed in a polar gradient, and then translated into viral proteins. Early during infection NS1 and NS2 antagonize the innate immune response to allow virus replication in the cytoplasm. (**4-5**) The polymerase uses the genomic RNA to produce a positive sense antigenome RNA, which serves as a template for the production of progeny negative-sense genomes **6-7.** The M protein migrates to the nucleus, possibly to block the transcription of host genes, and later it is suggested that it returns to the cytoplasm, and recruits the nucleocapsid at the assembly point. The encapsidated genomes are assembled with other viral proteins (F, G, SH, N, P and M) and bud from the plasma membrane to produce progeny virus particles from the apical surface. (F; light blue, G; green, SH; black, N; red, L; yellow, P; blue, M; brown, M2-1; orange, M2-2; light pink, NS1; pink, NS2; purple)

IFN antagonists encoded by RSV. These proteins are the main focus of this study, as we are interested in targeting them to identify small molecules that suppress their function against the cellular IFN system. RSV NS1 and NS2 proteins and their functions are described below.

## 1.3.3/1 RSV NS1 and NS2 proteins

RSV NS1 and NS2 are two small proteins (139 and 124 amino acid residues long, respectively), which are expressed early after RSV infection (Collins & Crowe 2007). Although NS proteins have several functions associated with virus replication and viral pathogenesis, they are primarily known because of their ability to antagonize the cellular IFN response, which allows a more robust virus replication (Barik 2013). Since RSV genome transcription has a polar gradient, NS1 and NS2 are the most abundant RSV proteins, as they are the most promoter-proximal genes (Figure 1.5 and 1.6) (Collins *et al.,* 2013).

NS1 and NS2 proteins are unique to RSV, without sequence homologs in any other virus or eukaryotic genomes, except their NS1 and NS2 counterparts of other RSV stains, such as BRSV (Bossert *et al.,* 2003; Schlender *et al.,* 2000). The molecular structure of RSV NS1 and NS2 has not been solved yet, therefore there is limited knowledge regarding NS1 and NS2 functional domains (Figure 1.6). NS1 and NS2 exhibit no discernible sequence similarity with each other, since the longest common peptide sequence between them is the DNLP tetrapeptide at their C-terminus (Figure 1.6), the function of which is not completely understood yet. It has been previously shown that NS1 and NS2 protein co-precipitate, suggesting that they have the ability to heterodimerize and form complexes (Swedan *et al.,* 2009). The DNLP tetrapeptide is

not essential for heterodimer formation, however it is indispensable for other interactions that are related to IFN antagonism (Swedan *et al.,* 2011), which are addressed in the following section. Evidence suggests that both NS1 and NS2 form homodimers, which might allow them to accomplish more complex and dynamic regulation of host signalling cascades (Swedan *et al.,* 2009; Swedan *et al.,* 2011). Unfortunately, the lack of structural information, together with the unstable nature of these proteins, impedes us from revealing NS1 and NS2 interactions, which would allow us to further elucidate their functions in IFN antagonism and understand their extended roles in RSV replication.
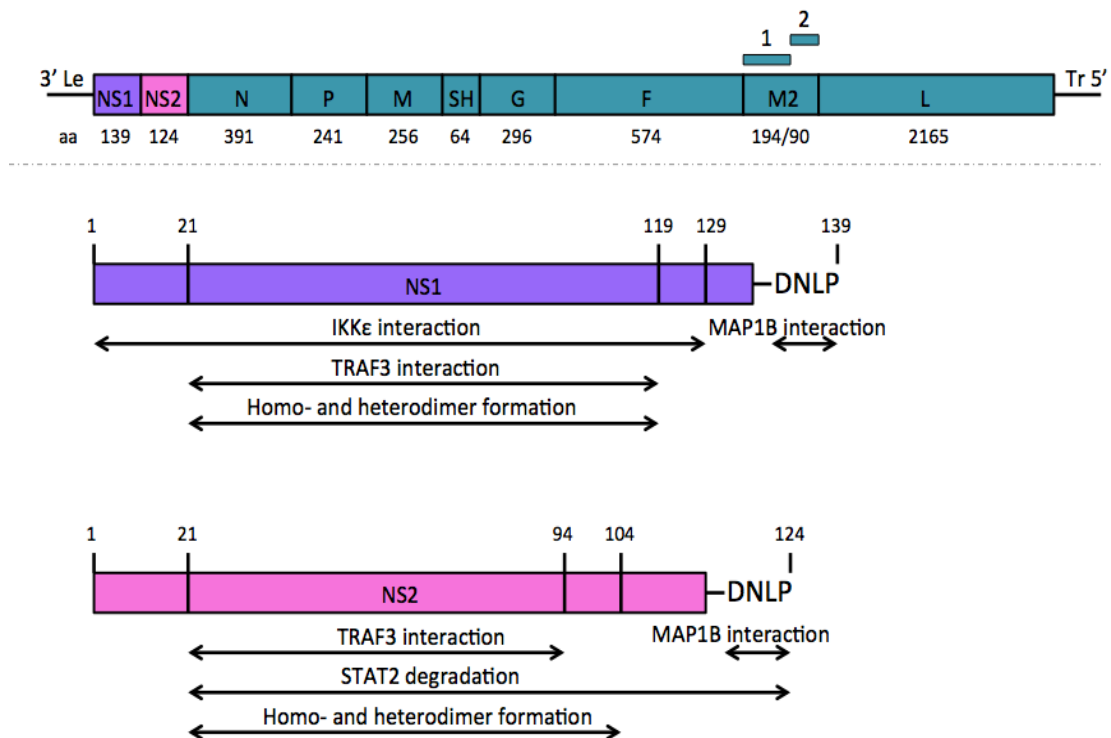


**Figure 1.6 Main functional domains of RSV NS1 and NS2 proteins.** The boundaries of each domain are drawn based on the published work of Swedan *et al.,* (2011), and they indicate the domain required for each interaction. The C-terminal tetrapeptide DNLP is the only common sequence between NS1 and NS2. RSV genome is described in Figure 1.3.

.

Of the eleven RSV proteins, NS1 and NS2 exhibit an intermediate to high degree of sequence conservation (65-82% amino-acid identity) between the two human RSV antigenic subgroups A and B (RSVA and RSVB) and ovine or bovine RSV, as they were found to be more highly conserved than the SH or G proteins but were less well conserved than any of the other proteins (Alansari & Potgieter 1994; Pastey & Samal 1995). Sequence comparisons between human RSVA and RSVB have shown that NS1 and NS2 were highly conserved at the amino-acid level, as they shared 92% and 87% sequence similarity, respectively (Johnson & Collins 1989). An evolutionary analysis of human RSVA and RSVB genomes collected from 1998 to 2010 showed that for all coding sequences (CDSs), there was more variation in RSVA than RSVB sequences, however the number of non-synonymous mutations was higher in some of the RSVB CDSs (Rebuffo-Scheer *et al.,* 2011). Although NS1 and NS2 CDSs had a high number of non-synonymous mutations, the CDSs with the highest non-synonymous mutations were those for the G, M2-2, and SH. Specifically, the average of the non-synonymous versus synonymous mutation ratio (dN/dS) for RSVB NS1 and NS2 CDSs was 0.092 and 0.052, whereas G, M2-2, and SH CDSs had higher dS/dN ratio, which was equal to 0.376, 0.155, 0.173, respectively (Rebuffo-Scheer *et al.,* 2011). Moreover, a recent study have investigated the local evolutionary patterns of RSVA and RSVB in Kilifi, Kenya, over a 10-year period, and showed that NS1 had a lower evolutionary rate (substitution/site/year) than NS2, the CDS of which was the second more variable after the G CDS (Agoti *et al.,* 2015). NS2 showed an elevated level of evolutionary rate, consistent with a protein interacting with polymorphic host target proteins, including host-immune factors (Spann *et al.,* 2005; Swedan *et al.,* 2011) and perhaps cytoskeleton (Liesman *et al.,* 2014).

# 1.4 RSV evasion strategies against the type I IFN system

## 1.4.1 PRRs activation in response to RSV infection

Cytopathic effects of RSV in human airways have been observed in histological studies of lung tissue from fatal cases of RSV infection, indicating that the primary target cells for RSV replication are human bronchial, bronchiolar and alveolar epithelial cells (Welliver *et al.,* 2007; Lay *et al.,* 2013). Consequently, the first site of encounter between RSV and the host is the respiratory epithelium, which induces early innate immune response at the site of infection (Lay *et al.,* 2013).

The precise innate immune responses to RSV infection are not well understood, though evidence suggests that RSV activates different types of PRRs. Specifically, RSV infections rapidly induce RIG-I, a RLR receptor, the activation of which is associated with induction of type I but also type III IFNs (Bitko *et al.,* 2008). Consistent with this finding, other studies have shown that RSV is a potent inducer of IFN-α/β and IFN-λ during *in vitro* infections of AECs and A549 basal epithelial cells (Spann *et al.,* 2004; Ramaswamy *et al.,* 2006). Interestingly, RSV infection of nasal epithelial cells (NECs) was shown to trigger the induction of only IFN-λ, suggesting that IFN-λ, but not IFN-α/β, is perhaps the first line of defense against RSV infection in the upper respiratory tract (Okabayashi *et al.,* 2011). However, the crosstalk between the two pathways makes it difficult to uncover the series of innate immune events that are activated in response to RSV in the respiratory epithelium.

Among all TLRs, TLR3 receptors are the most abundant in AECs, however TLR3s can only recognize dsRNA in endocytic compartments and currently, there is no evidence to support that RSV generates TLR3-activating dsRNA species during its replication. In contrast, RSV infection in mice was found to trigger activation of TLR2

and TLR6 receptors in leukocytes, which activate innate immunity against RSV by promoting TNF, interleukin-6 (IL-6), CCL2 (Chemokine (C-C motif) ligand 5), and CCL5 (also known as RANTES) (Murawski *et al.,* 2009). An interesting study showed that purified RSV F protein binds to TLR4 and/or its co-receptor CD14 (Marr & Turvey 2012). However, the significance of this observation remains unresolved, since RSV infection does not block the LPS-induced activation of TLR4, indicating that TLR4 receptor complex does not seem to play a biological role in RSV pathogenesis (Marr & Turvey 2012). Taken together, these studies provide evidence that TLR-dependent signalling is important for activating early innate responses to RSV, however the role of TRLs in controlling RSV infections needs to be further explored.

A member of the NLR family, the nucleotide-binding oligomerization domain containing 2 (NOD2) was also shown to be rapidly induced after RSV infection but the relative importance of the pathway in regards to RSV detection in comparison to the RLR and TLR pathway still remains to be explicated (Vissers *et al.,* 2012; Barik 2013). Hence, the rest of this section will focus on RSV evasion strategies against the RLR- and TLR-mediated activation of type I IFNs, which have well defined roles in controlling virus infections.

## 1.4.2 The importance of RSV NS1 and NS2 for IFN antagonism

The success of RSV in establishing infections in AECs relies on its capacity to suppress the innate and acquired immune responses. As discussed earlier in Section 1.2, one of the main differences between RSV and other members of *Paramyxoviridae* family is that RSV does not express any of the V/C/W proteins, which confer IFN resistance to other paramyxoviruses, but instead RSV expresses two putative NS

proteins; NS1 and NS2 (Parks & Alexander-Miller 2013). Recombinant RSVs (rRSVs) in which the NS1 and/or NS2 genes have been deleted singly or in combination (RSV.ΔNS1, RSV.ΔNS2 and RSV.ΔNS1/2) are IFN-sensitive and replicate inefficiently *in vitro*, indicating important defects in virus-host interplay (Jin *et al.,* 2000; Schlender *et al.,* 2000; Spann *et al.,* 2003; Spann *et al.,* 2004). Specifically, the replication of the RSV.ΔNS1/2 in A549 cells was severely reduced (>100-fold reduced) compared to wild type RSV (wtRSV), whereas RSV.ΔNS1 and RSV.ΔNS2 were moderately attenuated (20- to 45-fold reduced) (Spann *et al.,* 2004). These viruses also form pinpoint plaques in HEp-2 cells; plaques were up to 95% reduced in size for the RSV.ΔNS1/2 mutant, and 90% and 80% for RSV.ΔNS1 and RSV.ΔNS2, respectively (Spann *et al.,* 2003; Jin *et al.,* 2000). In IFN-incompetent cells, the replication of the RSV.ΔNS2 was comparable to wtRSV, whereas the RSV.ΔNS1 and RSV.ΔNS1/2 mutants replicated less efficiently (20-fold decrease) (Teng & Collins 1998; Spann *et al.,* 2004; Jin *et al.,* 2000; Young *et al.,* 2003). This indicates that the replication deficiency of these viruses is primarily due to enhanced IFN responses, emphasizing the importance of NS1 and NS2 for IFN antagonism.

The replication kinetics of RSV.ΔNS1 and RSV.ΔNS2 have also been studied *in vivo*. Studies on the recombinant virus that lacks NS1 showed that the replication of RSV.ΔNS1 was more than 2000-fold reduced in the upper respiratory tract and more than 17,000-fold reduced in the lower, when compared to the wtRSV infection in chimpanzees (Teng *et al.,* 2000). Likewise, the replication levels of the recombinant virus that lacks NS2 were also quantified in chimpanzees; RSV.ΔNS2 was found to replicate to moderate levels in the upper respiratory tract but it showed 10,000-fold reduction in replication in the lower respiratory tract compared to the wtRSV

(Whitehead *et al.,* 1999). In conclusion, *in vivo* studies suggest that the functions of NS1 and NS2 are more important for the establishment of lower respiratory tract infections, which are more pathogenic and often lead to severe respiratory defects. The restriction of viral replication observed for the RSV NS deletion viruses is presumably due to augmented IFN responses, which allow the development of a more powerful innate and adaptive immunity to RSV infection (Karron *et al.,* 2013).

## 1.4.3 RSV NS1 and NS2 functions against type I IFNs

### 1.4.3/1 NS1 and NS2 functions against the IFN-induction pathway

The vast majority of RSV anti-IFN properties are attributed to NS1 and NS2, which have joint, as well as, independent functions against the cellular IFN response. The molecular mechanisms by which NS1 and NS2 suppress IFN-induction pathway are currently under intense investigation and the existing experimental data is still inconclusive. NS1 and NS2 have been reported to interact with multiple steps of the RLR-mediated pathway but all of these interactions have yet to be elucidated (Figure 1.7). The first studies to report NS-mediated IFN antagonism were performed using BRSV (Schlender *et al.,* 2000; Bossert *et al.,* 2003). BRSV NS1 and NS2 have been found to interact with the IFN-induction pathway by blocking phosphorylation of IRF3 (Bossert *et al.,* 2003). Given that human and bovine RSV share 71% similarity, regarding the amino acid sequences of their individual proteins, it is not surprising that NS1 and NS2 of human RSV have been reported to have a similar function against the IFN-induction pathway. Specifically, it has been shown that NS2 inhibits the nuclear accumulation of both IRF3 and NF-κB (Ling *et al.,* 2009; Spann *et al.,* 2004). However, the level of inhibition was significantly greater when both NS1 and NS2 were present,

suggesting that NS1 and NS2 act cooperatively to suppress activation and nuclear localization of both IRF3 and NF-κB (Spann *et al.,* 2005). A more recent study suggested a different mechanism for IRF3 inhibition, according to which NS1 interferes with the interaction of IRF3 with its cofactor CBP, and subsequently inhibits IRF3 binding to the IFN-β promoter to suppress IFN-β induction (Ren *et al.,* 2011).

In addition to the interactions with IRF3 and NF-κB, evidence suggests that NS1 and NS2 mediate a decrease in the expression levels of TRAF3, whereas NS1 also mediates a decrease in IKKε and IRF7 (Figure 1.7) (Swedan *et al.,* 2009; Goswami *et al.,* 2013). It is suggested that NS1 and NS2 reduce TRAF3 levels through a novel non-proteasomal mechanism, for which their common C-terminal tetrapeptides are not required, however the C terminus of NS1 is involved in lowering IKKε levels by a nonproteasomal mechanism (Figure 1.7) (Swedan *et al.,* 2011; Swedan *et al.,* 2009).

Interestingly, NS2 appears to antagonize the early activation of the RIG-I signalling cascade by binding to the N-terminal CARD of RIG-I, and thus inhibiting its interaction with the downstream component MAVS (Figure 1.7) (Ling *et al.,* 2009). It is also speculated that the inhibition of the RIG-I pathway is caused by an interaction between NS1 and NS2 with MAVS in mitochondria. Specifically, intracellular localization studies have shown that NS2 and NS1-NS2 complexes localize in mitochondria, whereas singular expression of NS1 results in nuclear localization, suggesting that NS1-NS2 complex might directly interact with mitochondrial MAVS to block RIG-I mediated signalling (Swedan *et al.,* 2011). In addition to the interaction of NS2 with RIG-I, NS1 was shown to degrade RIG-1 when constitutively expressed in A549 cells (Goswami *et al.,* 2013), however the prevalence of these interactions during RSV infection remains to be elucidated. In conclusion, RSV NS1 and NS2 have

evolved a plethora of mechanisms with which they circumvent key steps of the IFN-induction signalling cascade, including early events like RIG-I activation, and latter events like IRF3 and NF-κB nuclear translocation.
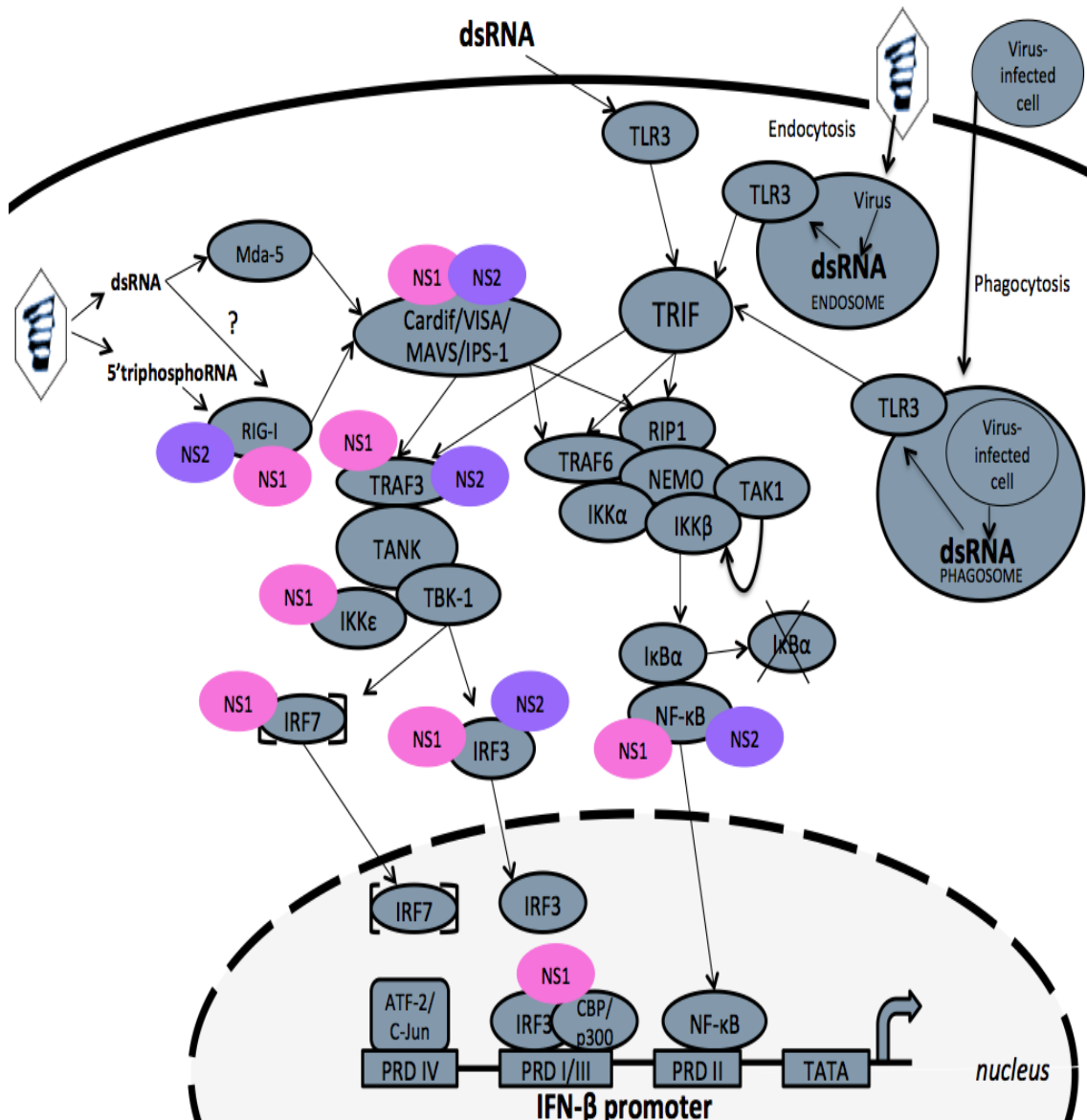


**Figure 1.7 RSV NS1 and NS2 interactions with the IFN-induction pathway.** RSV NS1 and NS2 have been reported to interact with several effector molecules of the IFN-induction pathway to suppress the activation of the IFN-β promoter, and block the IFN response to RSV infection. There are a noteworthy number of interactions in the literature, most of which seem to target the RIG-I dependent IFN induction pathway.

## 1.4.3/2 NS1 and NS2 functions against the IFN-signalling pathway

RSV NS1 and NS2 proteins also counteract the IFN-signalling pathway and subsequently suppress the activation of the ISRE elements, which are present within the promoters of ISGs (Ramaswamy *et al.,* 2004). The majority of studies that focus on the RSV-mediated IFN antagonism unanimously suggest that RSV infections and expression of recombinant NS1 and NS2 in epithelial cells causes an evident decrease in STAT2 levels, which outruns the downstream events of the IFN-α/β response. However, there is controversy regarding the molecular mechanism that RSV uses to mediate a decrease in STAT2 levels. In particular, the majority of evidence supports that STAT2 decrease is mainly driven by NS2 with NS1 having some effect (Spann *et al.,* 2004; Lo *et al.,* 2005; Swedan *et al.,* 2011; Goswami *et al.,* 2013), whereas other evidence suggests that STAT2 degradation requires only NS2 (Ramaswamy *et al.,* 2006). In contrast, Elliott *et al.,* (2007) proposed a NS2-independent mechanism and suggested that NS1 has an E3 ligase activity that is crucial for STAT2 degradation. It is possible that the exact stoichiometry of the NS1, NS2 and NS1-NS2 heterodimer varies between these studies and that may account for some of the differences reporter in the literature, which are discussed in detail below.

One of the earliest studies to support NS-mediated STAT2 antagonism was published by Lo *et al.,* (2005), who showed that constitutive expression of NS2 is related to a significant reduction in STAT2, whereas NS1 expression had a less significant impact on STAT2 levels. Interestingly, co-expression of NS1 and NS2 suppressed STAT2 below baseline levels, suggesting that NS1 and NS2 work together to achieve robust inhibition of STAT2 (Lo *et al.,* 2005). Furthermore, it was shown that NS2 interacts with the host microtubule-associated protein 1B (MAP1B) through its C-

terminus DNLP tetrapeptide (Figure 1.5), and this interaction was found to be essential

for the STAT2-decreasing activity of NS2 (Swedan *et al.,* 2011). In fact, it is suggested

that MAPIB could be part of the NS1-NS2 complex, hence it might be important for the

synergistic functions of NS1 and NS2 (Swedan *et al.,* 2011).

Shedding more light on the mechanism behind STAT2 decrease, other studies

demonstrated that STAT2 antagonism is caused by a NS2-mediated proteasomal

degradation (Ramaswamy *et al.,* 2006; Ramaswamy *et al.,* 2004). In general,

proteasome-mediated degradation of proteins usually occurs after protein ubiquitylation.

The process of protein ubiquitylation is catalyzed by coordinated enzymatic reactions

that are mediated by enzymes known as E1 (ubiquitin-activating enzyme), E2

(ubiquitin-conjugating enzyme) and E3 (ubiquitin ligase) (Da Fonseca *et al.,* 2012;

Jiang & Chen 2011). E3 ligases are responsible for targeting ubiquitylation to specific

substrate proteins, by covalently attaching ubiquitin to lysine side chains of the

substrate protein (Jiang & Chen 2011). Some of the E3 ubiquitin ligases belong to the

suppressor of cytokine signalling (SOCS) family of proteins, which are involved in

inhibiting the JAK/STAT pathway (Yoshimura *et al.,* 2007). Interestingly, RSV-

induced STAT2 degradation was prevented by knocking down expression of

endogenous E3 ligase components like Cul2 and Rbx1 (Elliott *et al.,* 2007). The same

study has also shown that NS1 associates with Cul2, suggesting that NS1 can assemble

ubiquitin ligase enzymes to target STAT2 to the proteasome (Elliott *et al.,* 2007).

Notably, internal sequences of NS1 and NS2 shared distant homology to the consensus

sequence for elongin C and cullin 2 binding motif (BC box), which occurs in E3 ligases

such as SOCS, proposing that this motif might be responsible for the E3 ligase activity

of NS1 and NS2 that permits STAT2 degradation (Elliott *et al.,* 2007; Swedan *et al.,*

2009). However, the role of this motif still remains unclear, since mutations within the BC box motif did not inhibit STAT2 degradation or any other function of either NS1 or NS2 protein (Swedan *et al.,* 2011). Interestingly, a more recent study have demonstrated that RSV NS1 protein upregulates SOCS1 mRNA independently of the RLR signalling pathway, suggesting that SOCS1 might be important for the degradation activity of NS1 against STAT2 or other innate immune proteins (Xu *et al.,* 2014).

The first model to describe the NS-degradasome has recently been proposed by Goswami *et al.,* (2013), who suggested that NS proteins assemble a heterogeneous degradation complex (~300 − 750 kDa in size), which translocates to mitochondria upon RSV infection. Their controversial findings suggest that optimal RSV suppression of cellular interferon response requires mitochondrial MAVS to be part of the NS-degradasome, hence MAVS facilitates the NS-mediated RIG-1 inhibition, and STAT2 degradation (Goswami *et al.,* 2013). To date, no other studies have been reported that either support or refute this observation, however a few studies have reported association of RSV NS1 and NS2 with mitochondria. Specifically, proteomic analyses of the RSV NS1 interactome indicated that NS1 is associated with a number of mitochondrial proteins (Wu *et al.,* 2012). Consistent with these findings, Boyapalle *et al.,* (2012) have demonstrated that RSV NS1 directly binds to mitochondrial MAVS, however the domains of interaction have not been mapped. Interestingly, another recent study has shown that during RSV infection proteins involved in innate antiviral immune response (e.g.Tom70) accumulate on mitochondria, supporting the hypothesis that mitochondria are likely to be hijacked by NS1 and NS2 for the assemblage of the NS-degradasome (Munday *et al.,* 2015). The role of mitochondria in RSV infection remains

to be further elucidated, however current evidence unanimously suggests that they have important implications for RSV biology, and perhaps IFN antagonism.

Although the function of RSV NS1 and NS2 against STAT2 is well documented, the precise mechanism behind STAT2 degradation is undetermined. Our up-to-date knowledge suggests that STAT2 degradation is a synergistic event that requires both NS1 and NS2, and remarkably, this function still remains the only documented interaction of RSV NS1 and NS2 with the type I IFN signalling cascade.

## 1.4.3/3 NS1 and NS2 interactions with antiviral ISGs

Current investigations suggest that RSV NS1 and NS2 can also directly suppress ISGs. For instance, NS1 and NS2 were shown to antagonize the RSV-mediated upregulation of the let-7i and miR-30b miRNAs, which have an antiviral effect and are induced by an IFN- or NF-κB-dependent mechanism, respectively (Thornburg *et al.,* 2012). More recently, another study have shown that NS1 can suppress the function of an IFN-induced antiviral protein, namely 2'-5'-oligoadenylate synthetase-like (OASL) by mediating proteasomal degradation of specific OASL isoforms (Dhar *et al.,* 2015). RSV infection also activates several ISGs of the IFIT family, namely ISG56, ISG54 and ISG60 (Hastie *et al.,* 2012; Janssen *et al.,* 2007), however it is still unclear whether RSV interferes directly with these IFITs, the antiviral role of which is also not clear yet.

## 1.4.4 NS-independent functions of RSV against type I IFN system

In addition to the RSV NS1 and NS2 functions against the cellular IFN response, other RSV proteins have been reported to interact directly or indirectly with

several factors of the cellular IFN pathway. RSV G contains a conserved CX3C chemokine-like motif, which binds to the CX3C receptor (CX3CR1) on various immune cells and airway epithelial cells, and thereby inhibits innate immune responses to RSV infection (Chirkova *et al.,* 2013). RSV G protein was also shown to modulate the expression of two SOCS proteins, SOCS1 and SOCS3, to inhibit type I IFNs and ISG15 expression very early, as well as late in infection (Oshansky *et al.,* 2009). The RSV N protein also has a role in antagonizing host innate immunity by interacting with dsRNA-regulated protein kinase PKR, which induces early innate immunity responses to RSV infection (Minor *et al.,* 2010). Specifically, it has been reported that N binds to PKR, and prevents it from phosphorylating eIF-2a and inhibiting protein synthesis (Groskreutz *et al.,* 2010). Another interesting study has shown that the N protein co-localizes with mda-5 and MAVS, suggesting that N protein localizes these molecules within the viral inclusion bodies to attenuate the downstream signalling cascade that activates the IFN-β promoter (Lifland *et al.,* 2012). In summary, although RSV IFN evasion strategies are primarily executed by NS1 and NS2, a few recent studies have illustrated that other RSV proteins might also contribute to IFN antagonism perhaps at different stages during the replication process.

## 1.5 RSV NS1 and NS2 functions beyond IFN antagonism

One of the earliest studies to evaluate the effect of NS1 and NS2 on virus replication was Jin *et al.,* (2000), who quantified the replication kinetics of recombinant RSV viruses lacking NS1 and NS2 (RSV.ΔNS1 and RSV.ΔNS2, respectively). As discussed earlier, RSV.ΔNS2 grew poorly only on IFN-competent cells, whereas RSV.ΔNS1 was equally attenuated in cells that were either proficient or incompetent to IFN, indicating that NS1 protein has functions in virus replication beyond IFN antagonism (Jin *et al.,* 2000). A similar study showed that replacement of RSV NS1 and NS2 by PIV5 V protein partially restored some of the IFN-inhibitory functions but did not fully restore virus replication, also suggesting that RSV NS1 and NS2 have other functions related to virus replication (Tran *et al.,* 2007). Consistent with these findings, RSV NS1 protein was found to be a potent inhibitor of RSV polymerase-mediated transcription and RNA replication in a minireplicon assay, indicating that NS1 could play a role as a negative regulatory protein (Atreya *et al.,* 1998). Beside the expected interactions of RSV P protein with itself and N protein, it has been demonstrated that P can also bind to NS1, indicating a direct role of NS1 in the replication complex (Hengst & Kiefer 2000). It has been also shown that NS1 co-precipitates with M protein during virus infection, however no interaction was detected between NS2 and RSV structural proteins (Evans *et al.,* 1996).

Furthermore, previous studies have demonstrated that RSV induces a G1-phase arrest in the cell-cycle (Gibbs *et al.,* 2009; Smith *et al.,* 2011). Interestingly, recombinant RSV lacking NS1 lost its ability to modulate the cell cycle, indicating that RSV NS1 is indispensable for this function (Wu *et al.,* 2012). More specifically, NS1 was found to interact with complexes, which contain proteins that are involved in the

regulation of cell cycle, such as ATR (ataxia telangiectasia- and Rad3-related protein) and MED29 (mediator complex subunit 29), suggesting that these interactions are important for the NS1 function against the cell cycle (Wu *et al.,* 2012).

NS1 and NS2 also appear to have a crucial role in suppressing premature apoptosis, allowing the virus time to replicate. Specifically, they were found to activate anti-apoptotic genes through a phosphatidylinositol 3-kinase (PI3K)- and NF-κB-dependent but IFN-independent mechanisms (Bitko *et al.,* 2008). Likewise, bioinformatic and proteomic analyses of the NS1 interactome indicated that NS1 interacts with a number of cellular proteins, most of which were related to the inhibition of apoptosis and also the regulation of transcription of host cell mRNAs (Wu *et al.,* 2012). Despite that there is less known about the role of RSV NS2 in virus replication apart from IFN antagonism, an interesting study has recently shown that NS2 is a contributing factor for the exacerbation RSV airway disease by promoting cell shedding of the airway epithelial cells, which facilitates viral release but also contributes to the obstruction of the distal airways (Liesman *et al.,* 2014).

In conclusion, NS1 and NS2 have a plethora of anti-IFN functions but also have functions beyond IFN antagonism, which are related to virus replication and pathogenicity. All evidence suggests that NS1 and NS2 can work synergistically, sharing subunits, activities and cellular locales to inhibit IFN response but in addition, being different proteins allows them to perform specific individual roles related to virus replication and virus pathogenicity (Barik 2013). This highlights the multifunctional nature of NS1 and NS2, and also intensifies the importance of NS1 and NS2 for RSV infection.

## 1.6 Advances in RSV antivirals

With the lack of effective antiviral treatments, supportive therapy remains the mainstay of care for patients hospitalised with RSV infection and it is often combined with oxygen and mechanical ventilation as well as pharmacotherapy with ribavirin, intravenous immunoglobulin (Palivizumab), bronchodilators and corticosteroids (Wright & Piedimonte 2011; Chu & Englund 2013). The currently available antiviral approaches have debatable cost-effectiveness, therefore treatment of RSV is usually reserved for patients with ALRI, or to prevent progression from upper respiratory to lower respiratory tract infection in high-risk individuals, such as preterm infants, the elderly and those suffering from cardiovascular diseases and immunosuppression (Chu & Englund 2013).

The lack of RSV vaccine and virus-specific antivirals highlights the clinical need for new anti-RSV therapies. There is an extensive ongoing research that aims the development of better RSV therapeutics, and although a number of promising new antiviral agents are under development by multiple pharmaceutical and biotechnology companies, none of them has been approved for clinical use yet. These include small molecule fusion inhibitors, attachment inhibitors, inhibitors of RNA synthesis, and small interfering RNA particles (siRNA) (Table 1.1). Screening compound libraries in cellular antiviral assays led to the discovery of small-molecule RSV inhibitors that target the F protein, few of which are currently in clinical trials (Meanwell *et al.,* 2011). One of the F inhibitors, TMC-353121, and an inhibitor of the polymerase, YM-53404, are still at the preclinical stage of development (Sudo et al. 2005; Roymans et al. 2010; Chu & Englund 2013). The effectiveness of the recently discovered oral RSV F inhibitor GS-5806 also generates a level of optimism, showing that small molecule

antiviral agents can control RSV infection *in vivo* (Wright 2014; DeVincenzo *et al.,* 2014). Clinical trials demonstrated that RSV infected individuals had lower virus load and lower total mucus weight, when administrated 50 mg of GS-5806 (DeVincenzo *et al.,* 2014). The evaluation of the GS-5806 is at an early stage, hence the usefulness and the effectiveness of this drug still needs to be confirmed against natural RSV infections in infants. In addition to chemical compounds, other types of molecules have been shown to inhibit RSV infectivity *in vitro*, including peptides and small-interfering RNAs (siRNAs) (Krilov 2011). In particular, cocktails of intranasal antiviral siRNAs have been proposed for RSV therapy but their efficacy remains unverified (Barik & Lu 2015).

**Table 1.1 RSV drug candidates**

| Drug Name | Viral Antigen Target | Stage of Development | Reference |
|---|---|---|---|
| Small molecule inhibitors | | | |
| BMS-433771 | F protein | Animal models | (Cianci *et al.,* 2004; Meanwell *et al.,* 2011) |
| TMC-353121 | F protein | Preclinical | (Roymans *et al.,* 2010) |
| BTA-9881 | F protein | Phase I | (Chu & Englund 2013) |
| MDT-637 | F protein | Phase I | (Chu & Englund 2013) |
| GS-5806 | F protein | Phase II | (DeVincenzo *et al.,* 2014) |
| YM-53404 | L protein | Preclinical | (Sudo *et al.,* 2005) |
| RSV-604 | N protein | Phase II | (Chapman *et al.,* 2007) |
| Other inhibitors | | | |
| siRNAs | NS1 protein | Animal models | (Zhang *et al.,* 2005) |
| siRNAs | P protein | Animal models | (Bitko *et al.,* 2005) |
| siRNAs | N protein | Phase II | (DeVincenzo *et al.,* 2010) |

The majority of RSV drug candidates target RSV F protein and traditional drug targets (e.g. virus-encoded enzymes), and there are no drug candidates in the literature that target either NS1 or NS2 proteins. More than ten years ago, a study showed that siRNA nanoparticles targeting NS1 resulted in attenuated RSV infection and infection-induced pulmonary pathology in mice (Zhang *et al.,* 2005), however the efficacy of the intranasal siNS1 was never tested in clinical studies.

It is widely accepted that the major obstacle in antiviral therapies (especially against RNA viruses) is the generation of drug-resistant virus strains; it has been estimated that virus' mutation rates (substitutions per nucleotide per cell infection (s/n/c)) range from $10^{-8}$ to $10^{-6}$ s/n/c for DNA viruses to $10^{-6}$ to $10^{-4}$ s/n/c for RNA viruses, which is much higher than the $10^{-10}$ s/n/c observed for bacterial and lower eukaryotes (Sanjuán *et al.,* 2010; Gago *et al.,* 2009). Therefore, it is very doubtful that a single molecule could ever prevent RSV infection without the acquisition of drug resistance virus strains. The existing antiviral therapies against other RNA viruses, including HIV and HCV, indicate that combinational therapy using different mechanistic classes of antiviral drugs can be the future for the establishment of an effective anti-RSV therapy. Current investigations are heavily leaning towards the identification of entry inhibitors, nonetheless NS1 and NS2 inhibitors have the potential to be valuable antiviral drugs for RSV control and prevention.

## 1.7 The importance of HTS in drug discovery

Over the past two decades, HTS has emerged and matured as a platform of early drug discovery in both the pharmaceutical industry and the academia (Zang *et al.,* 2012). In early 1990s, biochemical HTS assays became a central area of drug discovery, however recent efforts have been dedicated to the development of cell-based HTS platforms, which provide better predictability of clinical efficacy, and thus reduce the number of animal tests and accelerate the drug discovery process (Carnero 2006).

Considering that the first article on HTS was published in 1991, and that it takes on average 13.5 years from target identification to drug approval (Paul *et al.,* 2010), it is still early to evaluate the success of HTS in drug discovery. Nonetheless, it has been estimated that among 58 drugs that were approved between 1991 and 2008, 19 were attributed to HTS (Perola 2010). The first two approved drugs with origins in HTS hits were tyrosine-kinases with anti-cancer properties, namely Gefitinib (Iressa; AstraZeneca) and Erlotinib (Tarceva; Roche), which received approval by FDA in 2003 and 2004, respectively (Fry *et al.,* 1994). Another successful example of cell-based HTS in drug discovery is the commercialization of Eltrombopag (Promacta/Revolade; GlaxoSmithKline), a thrombopoietin (TPO) receptor agonist, which was approved by the FDA in 2008, for treating chronic idiopathic thrombocytopenic purpura (Duffy *et al.,* 2001). The approved drugs with origins in HTS hits have a wide range of targets and act against different diseases, including cancer, diabetes and other diseases, like pulmonary hypertension and hypernatremia (Zang *et al.,* 2012; Macarron *et al.,* 2011).

HTS assays have been widely utilized for the identification of antiviral therapeutics. In particular, the discoveries made from HTS have considerably contributed to HIV treatment, since three of the anti-retroviral agents that are currently

used in the highly active antiretroviral therapy (HAART) were originally identified using HTS assays (Macarron *et al.,* 2011). HAART is the most effective currently available antiviral therapy, and it consists of several classes of drugs that act on different stages of the HIV life cycle. HTS led to the discovery of an HIV-1 entry inhibitor, namely Maraviroc (Selzentry; Pfizer) (MacArthur & Novak 2008), a protease inhibitor, called Tipranavir (Aptivus; Boehringer Ingelheim) (Temesgen & Feinberg 2007) and Etravirine (Intelence; Tibotec Pharmaceuticals), which is a reverse transcriptase inhibitor (De Corte 2005).

In conclusion, HTS represents an effective method for discovering novel antiviral agents or repurposing existing molecules. The success of a HTS approach requires carefulness and precision and relies on several screening steps such as reagent preparation, assay development and most importantly, target identification and screening library.

## 1.8 Research Objectives

The overall aim of this study was to develop a modular screening platform, which would allow viral IFN antagonists to be subjected to HTS for the identification of novel small molecules that inhibit their function(s). This project sought to determine whether a novel class of virus-specific antiviral drugs that work by inhibiting viral IFN antagonists' function could be developed. Small molecules that inhibit targeted viral IFN antagonists would allow us to validate this vital class of viral proteins as therapeutic targets, and could also represent useful research tools for revealing the pleiotropic functions of viral IFN antagonists. The current study aims to (i) develop a cell-based HTS assay that allows identification of small molecules that inhibit viral IFN antagonists, (ii) utilize this screening approach to target RSV IFN antagonists NS1 or NS2 to identify small molecules that inhibit their function(s) against the cellular IFN response, (iii) validate the ability of hit compounds to inhibit RSV NS1 or NS2 function(s), (iv) investigate the specificity of the hit compounds to reveal their mechanism of action, (v) characterize hit compounds in regards to their ability to restrict RSV replication *in vitro.*

# Chapter 2: Materials and Methods

## 2.1 Cells, viruses and antibodies

### 2.1.1 Mammalian cell-lines

293T:      Human embryonic kidney cell-line (provided by Professor Richard Iggo, University of Bordeaux)

A549:      Human carcinomic alveolar basal epithelial cell-line (European Collection of Cell Cultures (ECACC))

HEp2:      Hela derivatives, human cervix carcinoma epithelial cell-line (ECACC)

Fibroblasts: Human dermal fibroblasts (provided by Professor Sophie Hambleton, University of Newcastle)

In addition to the basic cell-lines mentioned above, the following A549 and Hep2 derivatives (generated by others) were also used in this study:

A549.pr(IFN-β)GFP: A549 cell-line stably expressing the green fluorescence (GFP) gene under the control of the IFN-β promoter (Chen *et al.,* 2010). This cell-line has inducible resistance to puromycin as expression of puromycin N-acetyl-transferase (PAC) is also under the control of the IFN-β promoter.

A549.pr(IFN-β)GFP-BVDV/Npro: A549.pr(IFN-β)GFP cell-line stably expressing the N-terminal protease (Npro) of Bovine Viral Diarrhea Virus (BVDV) with an N-terminal V5 tag (Chen *et al.,* 2010). This cell-line encodes for encodes for PAC.

A549.pr(IFN-β)GFP-HCV/NS3.4A(1b): A549.pr(IFN-β)GFP cell-line stably expressing the NS3.4A protease of HCV genotype 1b with a C-terminal V5 tag (produced by Dr Catherine Adamson). This cell-line encodes for encodes for PAC.

A549.pr(ISRE)GFP : A549 cells producing GFP under the control of the ISRE (MxA) element (produced by Dr Claudia Haas and Mrs Zoe Gage). This cell-line has inducible resistance to puromycin as expression of PAC is also under the control of the ISRE promoter.

Hep2-BVDV/Npro: Hep2 cells stably expressing BVDV N pro (Carlos *et al.,* 2007). This cell-line encodes for encodes for PAC.

Hep2-PIV2/V: Hep2 cells stably expressing PIV2 V protein (produced by Mr Dan Young). This cell-line encodes for encodes for PAC.

In addition to the cell-lines mentioned above, the following permanent cell-lines were generated (Section 2.3) and used as part of this study:

***A549.pr(IFN-β)GFP derivatives:***

A549.pr(IFN-β)GFP-RSV/hNS1: A549.pr(IFN-β)GFP cell-line stably expressing 'humanized' codon-optimized NS1 (hNS1) protein of RSV with an N-terminal V5 tag. This cell-line encodes for blasticidin-S deaminase, which confers resistance to blasticidin.

A549.pr(IFN-β)GFP-RSV/hNS2: A549.pr(IFN-β)GFP cell-line stably expressing hNS2 protein of RSV with an N-terminal myc-tag. This cell-line encodes for encodes for PAC.

A549.pr(IFN-β)GFP-RSV/hNS1.hNS2: A549.pr(IFN-β)GFP cell-line stably expressing hNS1 and hNS2 proteins of RSV with an N-terminal V5 tag or myc-tag, respectively. This cell-line encodes for encodes for both blasticidin-S deaminase and PAC.

*A549.pr(ISRE)GFP derivatives:*

A549.pr(ISRE)GFP-RSV/hNS1: A549.pr(ISRE)GFP cell-line stably expressing hNS1 protein of RSV with an N-terminal V5 tag. This cell-line encodes for blasticidin-S deaminase.

A549.pr(ISRE)GFP-RSV/hNS2: A549.pr(IFN-β)GFP cell-line stably expressing hNS2 protein of RSV with an N-terminal myc-tag. This cell-line encodes for encodes for PAC.

A549.pr(IFN-β)GFP-RSV/hNS1.hNS2: A549.pr(IFN-β)GFP cell-line stably expressing hNS1 and hNS2 proteins of RSV with an N-terminal V5 tag or myc-tag, respectively. This cell-line encodes for encodes for both blasticidin-S deaminase and PAC.

A549.pr(ISRE)GFP-RBV/P: A549.pr(ISRE)GFP cell-line stably expressing P protein of Rabies virus(RBV) with an N-terminal V5 tag. This cell-line encodes for encodes for PAC.

A549.pr(ISRE)GFP-PIV5/V: A549.pr(ISRE)GFP cell-line stably expressing V protein of PIV5. This cell-line encodes for encodes for PAC.

## 2.1.2 Viruses

PIV5 VΔC (vM2): A strain of PIV5, which has the C-terminal of its V protein deleted, therefore it cannot circumvent the IFN induction (He *et al.,* 2002). The PIV5 VΔC (vM2) stock is a defective-interfering (DI) rich preparation of the PIV5 VΔC strain, which was generated by Mr Dan Young (Chen *et al.,* 2010).

wtRSV: A wild-type A2 strain of RSV, which was kindly provided by Professor Peter Collins (NIAID, USA). The full-length cDNA sequence of the wtRSV(A2) was published by Collins *et al.,* (1987) (GeneBank Accession No. M74568).

RSV.ΔNS1 and RSV.ΔNS2: Recombinant RSV A2 viruses that have the NS1 or the NS2 gene deleted, respectively (Collins & Murphy 2002). These viruses were also provided by Professor Peter Collins (NIAID, USA).

rRSV: A recombinant 'wild-type' Long strain RSV virus (Rameix-Welti *et al.,* 2014), which was kindly provided by Jean-François Eléouët (Unité de Virologie et Immunologie Moleculaires, France).

## 2.1.3 Antibodies

All the primary and secondary antibodies used in this study are listed on Table 2.1, except the mouse anti-RSV fusion antibody (1:250) (AbD Serotec), which was used for visualising RSV plaques with immunostaining.

**Table 2.1 List of antibodies.** Primary and secondary antibodies used for western blotting (WB) and/or immunostaining (IF)

| Antibody | Company | Ab dilution for WB | Time WB/IF | Ab dilution for IF |
|---|---|---|---|---|
| **Primary Antibodies** | | | | |
| mouse anti-V5 (336/SV5-Pk1) | AbD Serotec® | 1:2000 | 1 h/ 1h | 1:400 |
| mouse anti-myc (4A6) | Merck Millipore, | 1:1000 | O/N/1 hour | 1:200 |
| rabbit anti-Mx1/2/3 (H-285) | Santa Cruz Biotechnology | 1:750 | O/N/1h | 1:50 |
| rabbit anti-STAT2 (C-20) | Santa Cruz Biotechnology | 1:1000 | O/N/1h | 1:200 |
| mouse anti-β-actin | Sigma-Aldrich | 1:10000 | 1 h/- | - |
| goat anti-RSV | Abcam® | 1:1500 | O/N/- | 1:200 |
| **Secondary Antibodies** | | | | |
| rabbit anti mouse (HRP[1])-conjugated | Sigma-Aldrich | 1:2000 | 1 h/- | - |
| goat anti rabbit (HRP[1])-conjugated | Sigma-Aldrich, | 1:2000 | 1 h/- | - |
| donkey anti goat (HRP[1])-conjugated | Santa Cruz Biotechnology | 1:2000 | 1 h/- | - |
| IRDye®80°°W goat anti-mouse | LI-COR | 1:10000 | 1 h/- | - |
| IRDye®680RD donkey anti-goat | LI-COR, | 1:10000 | 1 h/- | - |
| IRDye®680RD goat anti-rabbit | LI-COR | 1:10000 | 1 h/- | - |
| goat anti-mouse TR[2] | AbD Serotec® | - | - /1h | 1:400 |
| donkey anti-goat TR[2] | Santa Cruz Biotechnology | - | - /1h | 1:400 |
| goat anti-rabbit TR[2] | AbD Serotec®, | - | - /1h | 1:400 |
| goat anti-mouse FITC[3] | Southern Biotech | - | - /1h | 1:400 |
| donkey anti-goat FITC[3] | Abcam® | - | - /1h | 1:400 |
| goat anti-rabbit FITC[3] | Sigma-Aldrich | | - /1h | 1:400 |

[1] Horseradish peroxidase (HRP),
[2] Texas Red (TR),
[3] Fluorescein isothiocyanate (FITC)

## 2.2 Cell culture

### 2.2.1 Cell maintenance

Cell monolayers were cultured in 25cm$^2$, 75cm$^2$ or 175 cm$^2$ tissue culture flasks (Greiner Bio-One) in Dulbecco's modified Eagle's medium (DMEM) supplemented with 10% [v/v] fetal bovine serum (FBS; ThermoScientific) and 1% [v/v] penicillin and streptomycin (pen/strep), and incubated at 37°C/5% $CO_2$. Cells were routinely trypsinised (Trypsin/ ethylenediaminetetraacetic acid (EDTA)) when approximately 90% confluent.

### 2.2.2 Cryopreserving and resuscitation of cells.

Cells were tested for mycoplasma, using the PCR Mycoplasma Test Kit II, following manufacture's instructions (PromoKine) and only mycoplasma-negative cells were stored in our liquid nitrogen collection. Cells were trypsinized, resuspended in 10% [v/v] FBS/DMEM, and pelleted at 1500 rpm for 5 min at room temperature (RT). Cells were then resuspended in freezing medium (DMEM supplemented with 30% [v/v] FBS and 10% [v/v] DMSO), aliquoted into cryovials and frozen at -80°C, before long-term storage in liquid nitrogen. For resuscitation of cells, cryovials were rapidly thawed at 37°C, before centrifugation at 1500 rpm for 5 min at RT. Cells were then resuspended and grown in normal growth medium at 37°C/5% $CO_2$. The following day, medium was replaced in order to remove traces of DMSO. The appropriate antibiotic selection markers (e.g. puromycin or blasticidin) were added once cells formed 50% healthy monolayers.

# 2.3 Generation of A549.pr(IFN-β)GFP and A549.pr(ISRE)GFP derivatives that stably express viral IFN antagonists

## 2.3.1 Gene Sequences

Codon-optimized, 'humanized' versions of the RSV/Long genes for NS1 (hNS1) and NS2 (hNS2) were published by Lo et al., 2005 (GenBank accession no. AY904040.1 and AY904041.1, respectively). The rabies virus P (RV/P) gene sequence derived from the challenge virus standard (CVS) strain 11 (GenBank accession no. ADJ29909.1). The published sequences were synthesized by Dundee Cell Products, and therefore the desired peptide tags were added to the sequences (Appendix 1). The RSV/hNS1 and RV/P sequence had a N-terminus V5-tag (GKPIPNPLLGLDST) (Randall *et al.,* 1987), whereas hNS2 had a N-terminus myc-tag (EQKLISEEDL). The PIV5/V sequence derived from PIV5 W3 strain (GenBank accession no. JQ743318.1).

## 2.3.2 Generation of lentivirus transfer vectors

For the development of reporter cell-lines that express viral IFN antagonists, we used second-generation lentivirus system, which consists of three lentiviral plasmids. The transfer vectors supply the minimum cis-acting genetic sequences (e,g LTRs, packaging (ψ) site, the rev response element (RRE), the central polypurine tract (cPPT) and SFFV promoter) necessary for the vector to transduce the target cell and deliver a gene of interest. In order to create an infectious lentivirus, two packaging plasmids are required; i) the CMV-R plasmid, which encodes the gag structural proteins and pol and (ii) the VSV-G plasmid, which encodes the envelope glycoprotein of vesicular stomatis virus (VSG) for the generation of pseudotyped virus particles that can be transduced to

a broad range of host cell types.

Two lentiviral transfer vectors were used for the generation of the A549 reporter cell-line derivatives. These were the pdl'SV5V'IB vector, which encodes for blasticidin-S deaminase to confer resistance to blasticidin, and the pdlNotI'IRES.puro vector, which encodes for puromycin N-acetyl-transferase (PAC), and hence confers resistance to puromycin (Appendix 2). RSV hNS2 and Rabies P genes were cloned directly into the pdlNotI'IRES.puro vector, because they were synthesized with compatible restriction sites at their 5' and 3' ends (BamH1 and NotI, respectively). This led to the generation of the pdl.RSV.hNS2/NotI'IRES.puro and pdl.RBV.P/NotI'IRES.puro lentiviral transfer vectors. In order to clone RSV hNS1 into the pdl'SV5V'IB vector, the right restrictions sites were added at the 5' and 3' ends of the gene sequence (BamH1 and NdeI, respectively) using polymerase chain reaction (PCR). The gene was cloned into an intermediate cloning vector, the pGEM®-T Easy vector (Promega), and then sub-cloned into the pdl'SV5V'IB vector to generate the pdl'RSV/hNS1'IB transfer vector. The lentiviral vector which encodes for PIV5/V (pdl.PIV5/V.puro) was previously generated by Dr Marian Killip, and it was used for the generation of the A549.pr(ISRE)GFP-PIV5/V reporter cell-line.

## 2.3.2/1 Polymerase Chain Reaction (PCR)

All PCR reactions were carried out using the KOD hot start DNA polymerase (Merck Millipore). PCR reactions were carried out in 200 µl PCR tubes; the reaction mix had a total volume of 50 µl, and typically comprised of the following: 5 µl 10X polymerase buffer (1X final conc.), 3 µl 25 mM $MgSO_4$ (1.5 mM final conc.), 5 µl 2 mM dNTPs (0.2 mM final conc.), 1.5 µl of 10 mM appropriate forward and reverse

primers (0.3 µM final conc.), 1 µl of plasmid DNA template (10 ng final conc.), and 1

µl KOD hot start DNA polymerase (0.02 U/ µl final conc.). Table 2.2 shows the primers

designed for this study. PCR reactions were carried out in a thermocycler (Biometra®,

T-gradient), using the cycling conditions shown in Table 2.3.

**Table 2.2 Primer sequences.**
For generating the pdl'SV5V'IB.RSV.hNS1.blast vector

| Primer Name | Sequence (5' to 3' end) |
|---|---|
| Forward: BamH1_RSV.hNS1 | GGCGGATCCATGGGAAAGCCGATCCCAAAC |
| Reverse: NotI_RSV.hNS1 | GGC**CATATG**CTTAAGGGGTTG |

**Note:**
BamH1 restriction site**, NdeI restriction site**

**Table 2.3 Cycling conditions for KOD Hot Start DNA polymerase**

| Step | | Duration | Temperature |
|---|---|---|---|
| 1. Polymerase activation | | 2 min | 95°C |
| 2. Denature | | 20 s | 95°C |
| 3. Annealing | | 10 s | lowest Tm °C - 5°C |
| 4. Extension | if target size <500 bp | 10 s / kb | 70°C |
| | if target size 500-1000 bp | 15 s / kb | 70°C |

2.3.2/2 DNA gel electrophoresis

PCR reactions were analysed on a 0.7 % [w/v] agarose gel (Sigma-Aldrich) in

TBE buffer (1M Tris base, 1M Boric acid and 0.02 M EDTA). The samples were mixed

with the appropriate volume of DNA loading buffer (Promega), prior to DNA

electrophoresis. Samples were run at 90V in TBE buffer (containing 1 μg/ml ethidium bromide), until bands were clearly resolved. Along with the samples, known DNA size markers were also run (1kb and 100 bp ladders; Promega). Resolved DNA bands of interest were excised under UV light, and purified using the QIAquick PCR purification kit (following manufacturer's instructions; QIAGEN®).

## 2.3.2/3 Cloning into pGEM®-T Easy vector

Before cloning into the lentiviral transfer vector, the amplified inserts were cloned into the commercially available pGEM®-T Easy vector (Promega). The pGEM®-T Easy vector has T-overhangs at the insertion site, therefore cloning into the pGEM®-T Easy vector requires the generation of poly-A tailed inserts. For the A-tailing reaction, 7 μl of purified PCR product were incubated with 1 μl of GoTaq® DNA polymerase (5 units) (Promega), 1 μl of 10X polymerase buffer (1X final conc.) and 1 μl of dATPs (0.2 mM final conc.). The total 10-μl reaction was incubated at 70°C for 30 minutes. The poly-A tailed inserts were ligated into pGEM®-T Easy vector using T4 DNA ligase (Promega). A standard ligation reaction comprised of 1 μl pGEM®-T Easy vector (50 ng), 5 μl of 2X rapid ligation buffer, 1 μl of T4 DNA ligase (3 Weiss Units/ μl) and lastly, 3 μl of the purified PCR product. The ligation reactions were performed overnight at 4°C.

The following day, the ligation mixture was transformed into 100 μl of ultra-competent *E. coli* cells (JM109) prepared using the Z-Competent™ *E. coli* Transformation Kit (following manufacture's instructions: ZYMO Research). Transformants were plated on ampicillin/X-Gal plates overnight at 37°C to allow blue-white colony screening. Briefly, the pGEM®-T Easy vector contains the lacZ gene,

which encodes for β-galactosidase enzyme, an enzyme occurring in *E.coli* that cleaves lactose into glucose and galactose. In principle, functional β-galactosidase enzyme is produced due to α-complementation, a process that is disrupted in clones containing recombinant DNA. Functional β-galactosidase induces the hydration of X-gal (Thermo Fisher Scientific), which then produces an insoluble blue pigment called 5,5'-dibromo-4,4'-dichloro-indigo, therefore successfully transformed clones that carry the gene of interest are the ones that form white colonies (Whitehouse 2014).

Transformed white colonies were inoculated into 5 ml of Luria-Bertani (LB) broth supplemented with 5 μl ampicillin (50 mg/ml) (Sigma) and incubated overnight at 37°C in an orbital shaker (225 rpm). The plasmids were extracted with QIAprep Spin Miniprep Kit (following manufacture's instructions; QIAGEN®). Successfully cloned plasmids were confirmed with dye-terminator sequencing analysis performed by Dundee Sequencing Services.

## 2.3.2/4 UV spectrophotometry

The concentration of purified plasmid DNA was quantified by measuring Absorbance at 260 nm (A260) using NanoDrop 1000 UV spectrophotometer (ThermoScientific). The purity of DNA preparation (i.e. protein or ethanol contamination) was indicated by the A260/A280 ratio (ratios > 1.8 were considered acceptable)

## 2.3.2/5 Cloning into lentiviral transfer vectors

The pdl'RSV/hNS1'IB lentiviral transfer vector was generated by extracting the RSV/hNS1 gene from pGEM®-T Easy vector and ligating it into the pdl'SV5V'IB

vector using the BamH1-NdeI restriction sites. The pdl.RSV.hNS2/NotI'IRES.puro and pdl.RBV.P/NotI'IRES.puro vectors were generated by cloning the RSV hNS2 and Rabies P gene sequences into the pdlNotI'IRESpuro vector using the BamH1-NotI restriction sites, which are present on the vector's multiple cloning site (MCS). Typical restriction digest reactions were carried out following manufacturer's instructions (Promega). The reactions were run on a 0.7 % [w/v] agarose gel, and the DNA bands that corresponded to the vector and insert molecular weight were excised from the gel, and purified using QIAquick Gel extraction kit (following manufacturer's instructions; QIAGEN®). The concentration of the purified DNA fragments was measured using UV spectrophotometry. Ligations were carried out using T4 DNA ligase (Promega). A standard ligation reaction contained 100 ng of vector DNA, 1 μl of T4 DNA ligase, 1 μl 10X ligase buffer, and the appropriate concentration of insert DNA was calculated using the following formula;

*ng of insert = [((ng of vector) x (kb size of insert)) / (kb size of vector)] x ( molar ratio of (insert/ vector))*

Deionized water was added to a final reaction volume of 10 μl. The reactions were incubated overnight at 4°C, and plasmid DNA was amplified, purified and sequenced, as previously described. For higher DNA concentrations, the lentivirus transfer vectors were extracted with the QIAGEN Plasmid *Plus* Maxi Kit (following manufacturer's instructions; QIAGEN®), before using them for generating lentiviruses.

## 2.3.3 Lentivirus-mediated generation of A549.pr(IFN-β)GFP and A549.pr(ISRE)GFP derivatives that stably express viral IFN antagonists

### 2.3.3/1 Transfection of 293T cells for lentivirus production

To generate lentivirus stocks, Lipofectamine® 2000 (Invitrogen) was used to transfect T75 flasks of 70% confluent Human Embryonic Kidney 293T cells with 10 μg of transfer vector, together with 6 μg of the CMV-R and 6 μg of the VSV-G packaging plasmids (following manufacturer'sinstructions; Invitrogen). The cells were incubated at 37°C for 5 hours with the transfection mix, and then the transfection mix was replaced with 10 ml of DMEM (10% [v/v] FBS). At 48h post-transfection the supernatant was collected, then clarified by centrifugation (3000 rpm, 15 mins) and filtration (45 μm filters). Lentivirus stocks were stored in 1 ml aliquots at -80°C.

### 2.3.3/2 Lentiviral transductions of A549 reporter cells

The lentivirus stocks were used to generate reporter cell-lines expressing the gene of interest.  Therefore, T25 flasks of 50% confluent A549 reporter cells were transduced with 1 ml of lentivirus, 1ml of DMEM (serum free, antibiotic free) and polybrene (final conc. 8 μg/ml). The cells were incubated at 37°C for 2.5 hours, before adding 2 ml of DMEM (10% [v/v] FBS), and incubating at 37°C for 2 days. Selections with the appropriate antibiotic followed; selection with puromycin (2 μg/ml) lasts 2 days, whereas selections with blasticidin (10 μg/ml) lasts 4-6 days. The generated A549 reporter cell-line derivatives were maintained under antibiotic selection until used for further experiments.

# 2.4 Characterization of reporter cell-line derivatives that stably express viral IFN antagonists

## 2.4.1 SDS-PAGE gel electrophoresis

One of the approaches used to evaluate the expression of the viral IFN antagonists in the reporter cell lines was western blot analysis. Before western blot analysis, proteins were separated by SDS-PAGE (sodium dodecyl sulfate (SDS) polyacrylamide gel electrophoresis (PAGE)). Specifically, cells were grown in 6-well plates until 90-100 % confluent monolayer, washed twice in phosphate buffered saline (PBS), and then lysed in 200 μl of disruption buffer (10M Urea, 20% [w/v] SDS, 15% [v/v], β-mercaptoethanol, 0.004 [w/v] bromophenol blue). Afterwards, cell lysates were sonicated in short 5 second pulses for 3-5 cycles and then heated for 10 minutes at 95°C to ensure the proteins are denatured. The samples were loaded on 12% hand-cast polyacrylamide gels (30% Protogel), the recipe of which is shown in Table 2.4. Gels were run with 1X TGS running buffer (25mM Tris, 192mM glycine, 0.1% [w/v] SDS pH 8.3) at 110V for approximately 2 hours in Bio-Rad electrophoresis tanks.

**Table 2.4 SDS-PAGE resolving and casting gel recipes**

| Reagent | 12 % Resolving Gel | 4% Stacking Gel |
|---|---|---|
| 30% Acrylamide (ProtoGel) | 10 ml | 1.3 ml |
| Resolving Gel Buffer (0.375 M Tris-HCl, 0.1% SDS, pH 8.8) OR Stacking buffer (0.125 M Tris-HCl, 0.1% SDS, pH 6.8 | 6.25 ml | 2.5 ml |
| 10% [w/v] Ammonium persulfate (APS) | 250 μl | 100 μl |
| TEMED (Tetramethylethylenediamine) | 25 μl | 10 μl |
| Water | 8.475 ml | 6.09 ml |
| Total Volume (for four gels) | 25 ml | 10 ml |

## 2.4.2 Western blot analysis

After SDS-PAGE electrophoresis, the proteins were transferred to polyvinylidene difluoride (PVDF) membranes using the Bio-Rad Trans-blot Turbo Transfer system with 1X NuPage transfer buffer (500 mM Bicine, 500 mM, Bis-Tris, 20.5 mM EDTA). PVDF membranes were activated in 100% methanol prior to transfer. Following transfer, membranes were blocked for 1 hour at RT in PBS containing 5% [w/v] skimmed milk powder and 0.1% [v/v] Tween-20. The membranes were subsequently incubated with the appropriate primary antibody, which are all listed in Table 2.5. All the antibodies were diluted in blocking buffer. Afterwards, the membranes were washed 6 times for 5 minutes in PBS plus 0.1% [v/v] Tween-20 to remove any unbound primary antibody. For chemiluminescence, the membranes were incubated with secondary antibodies conjugated to horseradish peroxidase (HRP). Following a second round of washing with PBS 0.1% [v/v] Tween-20, enhanced chemilumescent (ECL) Pierce™ western blotting substrate (LifeTechnologies) was added to the membranes for 5 minutes for the detection of horseradish peroxidase (HRP) enzyme activity. Finally, the membranes were exposed to X-ray film and developed using the KODAK X-OMAT 1000 processor. When Odyssey CLx has been used instead of chemiluminescence, the HRP-conjugated secondary antibodies were replaced with the LiCOR's IRDye secondary antibodies. Membranes were imaged and bands quantified using the Odyssey CLx Imaging Suite (Image Studio) program.

## 2.4.3 Immunofluorescence

The expression of the viral IFN antagonist has been also evaluated by immunofluorescence. For immunofluorescence, the cells were grown on circular glass coverslips (1 mm thick). Firstly, cells were rinsed thrice with 1 ml PBS (2% [v/v] FBS)

and then fixed with 1 ml of 5% [v/v] formaldehyde/PBS for 30 minutes. Then, the fixed cells were washed thrice with 1 ml PBS supplemented with 2% [v/v] FBS. The permeabilisation of the cell membranes was achieved by incubating the cover slips in 1 ml of 0.1 % [v/v] Triton X/PBS for 20 minutes. Following another round of washing with 2% [v/v] FBS/PBS, 30 µl of primary antibody dilution in 2% [v/v] FBS/PBS was added onto the coverslips and left in darkness, at RT, for 1 hour. Following primary antibody incubation, the slides were washed thrice with 2% [v/v] FBS/PBS and then 30 µl of secondary antibody dilution in 2% [v/v] FBS/PBS was added onto the cover slips and left in darkness, at RT, for 1 hour. DAPI (4', 6-diamidino-2-phenylindole) dye was added to the cells together with the secondary antibody diluted 1:1000. The slides were again washed twice with 2% [v/v] FBS/PBS and finally, drops of citifluor mounting buffer (Citifluor Ltd) were placed onto microscope glass slides and coverslips were gently inverted above them. The slides were observed with a Nikon Microphot-FXA immunofluorescence microscope and kept at 4°C after observation. All immunofluorescent pictures have been taken at 20X magnification, unless otherwise indicated.

## 2.4.4 Induction of the IFN-β promoter or ISRE element

In order to activate the IFN-β promoter, the A549.pr(IFN-β)GFP cell-line and its derivatives were infected with PIV5.VΔC (vM2) virus ($2x10^8$ Pfu/ml) at a MOI of 7 (diluted 1:100 in DMEM (10% [v/v] FBS)) . Then, the cells were incubated for 24 hours at 37°C, before measuring GFP expression. To activate the ISRE element, the A549.pr(ISRE)GFP cell-line and its derivatives were treated with $10^4$ U/ml of purified IFN-α (Roferon, NHS) in DMEM (10%[v/v] FBS), and incubated for 48 hours at 37°C, before measuring GFP expression

The GFP expression was either observed with fluorescent microscopy or quantified using TECAN infinite® 200 plate reader. For visualizing GFP expression, cells were grown on coverslips until confluent monolayers, and then the appropriate inducer was added (PIV5-VΔC or IFN-α). The induced cells were fixed with 5% [v/v] formaldehyde/PBS, and GFP expression was observed with a Nikon Microphot-FXA immunofluorescence microscope. All fluorescent pictures have been taken at 20X magnification, unless otherwise indicated. Furthermore, our cell-based reporter assay is adapted to a 96-well plate format, which allowed automated detection of GFP expression using the TECAN plate reader. In order to measure GFP fluorescent units, $3\times10^4$ cells were seeded in 100 µl DMEM (10 % [v/v] FBS) per well. The next day confluent monolayers were treated with the appropriate inducer, so that there were at least 3 repeats for each treatment. To measure GFP the excitation was set at 488 nm and emission at 518 nm, and the data was analyzed using the Magellan data analysis software.

## 2.5 siRNA transfections for knocking out gene expression

In order to knock out hNS2 expression in the A549.pr(ISRE)GFP-RSV/hNS2 cell-line, siRNAs were designed against the mRNA sequence of RSV hNS2 protein (Table 2.5). For this experiments, we used a non-targeting siRNA (siNT), as a negative control (ON-TARGETplus Non-targeting siRNA, Dharmacon). The siRNAs were shipped as dried pellets of 20 nmol. The dried pellets were resuspended in 1ml of 1X siRNA buffer (ThermoScientific). The final concentration of the master stock was 20 µM (pmol/µl), which was used to generate 100 nM working stocks in 1X siRNA buffer.

**Table 2.5 siRNAs designed for knocking out expression of RSV hNS2** (Dharmacon/Thermo Fisher Scientific)

| Name | | siRNA sequence |
|------|------|------|
| **sihNS2** | Sense | 5' GCACCAAGUACAAGAAGUAUU 3 |
| | Antisense | 5' UACUUCUUGUACUUGGUGCUU 3' |

## 2.5.1 siRNA transfections using Lipofectamine® RNAiMax

For siRNA transfections we used Lipofectamine® RNAiMax (Life Technologies). The RNA-lipid complexes were prepared first, and then the appropriate concentration of cells was added to the complexes. The following protocol is optimized for siRNA transfections in a 12-well plate. To generate the RNA-lipid complexes, 100 μl of 100 nM siRNA (10 nM final conc.) was added to 100 μl of 1:100 lipofectamine RNAiMax (1:1000 final dilution) in serum free Opti-MEM® (Life Technologies). The plate containing the mixture was centrifuged for 1 min at 1000 rpm at RT to ensure solutions are at the bottom of each well and well mixed. The mixture was incubated for 30 min at RT to allow time for RNA-lipid complexes to form. Afterwards, 800 μl of $6x10^4$ cell/ml were added to the RNA-lipid complexes, and mixed well by pipetting up and down several times. The plates were incubated at 37°C/5% $CO_2$ for 1-3 days, and the level of knock down was observed with western blot analysis.

## 2.5.2 IFN treatment following siRNA transfections

To assess restoration of GFP expression upon NS2 siRNA knockdown, cells were transfected with sihNS2, and then treated with IFN-α. The transfection procedure was the same as described above, however the assay volumes were adjusted to a 96-well plate. In particular, 10 μl of 500 nM siRNA was added to 10 μl of 1:100 lipofectamine®

RNAiMax in serum free Opti-MEM® (Life Technologies). In addition, we used higher

concentration of cells, $3x10^5$ cell/ml instead of $6x10^4$ cell/ml to have the same cell

density as our standard assay. Following siRNA transfections cells were incubated for

24 hours at 37°C/5% $CO_2$, and then treated with 10 µl of 1:10 (final conc. 9090.90

U/ml) IFN-α (Roferon, NHS) for further 48 hours. The GFP expression levels were

measured using TECAN plate reader, as described earlier, and fluorescent images were

taken using IncuCyte cell imager at 10X maginification.

## 2.6 Preparation of RSV stocks

### 2.6.1 Virus propagation – Supernatant

Multiple T175 cm$^2$ flasks were infected for each virus stock and combined

together at the final step for concentrating the virus. T175 cm$^2$ flasks with 80-90%

confluent Hep2-BVDV/Npro cells were infected with 20 ml of virus inoculum, which

contained low MOI virus (MOI 0.01) diluted in 2% [v/v] FBS/DMEM containing

pen/strep. The flasks were tightly closed and left rocking at 37°C without replacing the

inoculum with fresh media. Flasks were checked under the microscope every day for

cytopathic effect (CPE), and usually viruses were harvested three days after infection.

For wtRSV, extensive cell death and syncytia were formed three days after infection.

Similarly, RSV.ΔNS1 and RSV.ΔNS2 caused extensive cell death by the third day but

the size of the syncytia was much smaller, when compared to the wild type (Figure 2.1).

The procedure for harvesting the supernatant and concentrating the virus was

conducted strictly at 4°C or on ice. Firstly, the 20 ml of media was collected from each

flask and the attached cells were scraped into 10 ml of PBS. The scraped cells

underwent two rounds of sonication (30 seconds each) using an ultrasonic bath

sonicator to release the virus particles that were attached to the cell surface, and therefore have not been released to the media. The sonicated cells were added to the harvested virus and centrifuged at 1200 rpm for 7 min to spin out the cell debris. The pelleted cell debris was discarded and the clarified supernatant was concentrated using polyethylene glycol (PEG) 6000.
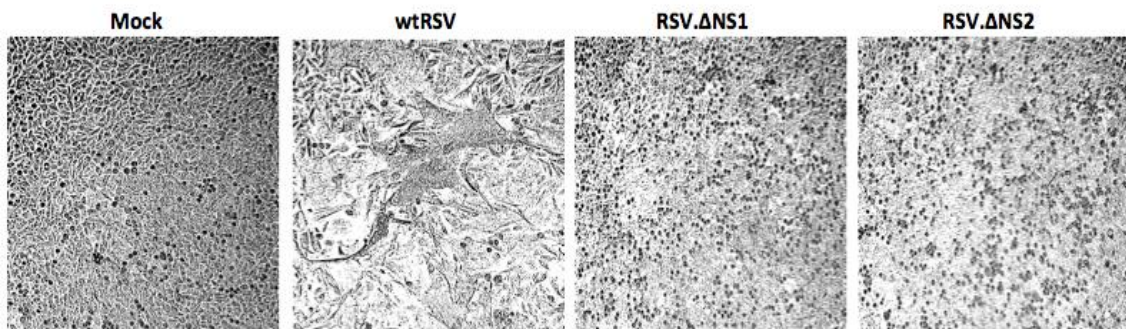


**Figure 2.1 CPE of RSV infections three days after infection**. wtRSV infection causes fusion of cells to from large syncytia, whereas RSV.ΔNS1 and RSV.ΔNS2 infections mostly result in cell death and rounded up cells.

## 2.6.2 Virus propagation – PEG-6000 concentration

To concentrate the virus, 50% [w/v] PEG-6000 was added to the supernatant to a final concentration of 10% [w/v] and stirred at 4°C for 1 hour. Then, the supernatant (+PEG-6000) was centrifuged at 4000xg for 30 min, and the pelleted virus was suspended in serum-free media (1ml per each flask). The concentrated virus sample was vortexed to ensure virions were evenly distributed throughout aliquot period. Virus stocks were aliquoted in 100 μl aliquots, which were snap-frozen with liquid nitrogen and stored immediately in -80°C freezer. The titers of the stocks were determined with plaque assays.

## 2.7 RSV plaque assays

Hep2 naïve or Hep2-BVDV/Npro cells were seeded at a density of $2 \times 10^5$ cells/ml in 12-well plates, 24 hours prior to infection to achieve 90-100% confluent monolayers. The RSV virus stocks were serially diluted (30 μl of virus stock in 270 μl serum-free DMEM) in dilutions ranging from $10^{-1}$ to $10^{-7}$. The dilution series were prepared in duplicate in 96-well plates. Growth media was removed and 100 μl of each virus dilution was added to the cells, starting from the highest to the lowest dilution. Plates were incubated for 1 hour at 37°C/5% $CO_2$, and gently shaken every ten minutes to ensure coverage. Then, the virus inoculum was aspirated and 1 ml of methylcellulose overlay was added to each well (0.5% [v/v] methylcellulose, 2% [v/v] FBS DMEM containing pen/strep). Plates were incubated at 37°C/5% $CO_2$ with as little movement as possible for 4-7 days or until syncytia were visible. The cells were fixed by adding 1 ml of 10% [v/v] formaldehyde/PBS at the top of the overlay. After 1 hour incubation at RT, the fixative was poured off and replaced with PBS. At this step, plates were stored at 4°C, if they were not directly used for immunostaining.

## 2.7.1 HRP-based Immunostaining

Prior immunostaining, cells were washed with PBS three times to remove all traces of overlay and fixative. Then, 250 μl of blocking buffer (5% [w/v] dried skimmed milk in PBS) was applied on each well and the plate was incubated with rocking for 30 min to 1 hour at RT or overnight at 4°C. Blocking buffer was removed and 200 μl of a mouse anti RSV fusion antibody (AbD Serotec) diluted 1:250 in blocking buffer was added to each well, and the plate was incubated with rocking for 1 hour at RT. Then, primary antibody was removed and wells were washed three times with PBS before

adding 200 μl per well of anti-mouse HRP antibody (Sigma-Aldrich) diluted 1:1000 in blocking buffer. Plates were incubated with rocking for 1 hourat RT, and then secondary antibody was removed and PBS washes were repeated. The secondary antibody was detected with the 4 CN peroxidase substrate system (KPL), which was prepared just before use by combining equal volumes of 4 CN Peroxidase Substrate and Peroxidase Substrate Solution B (1:1 solution). Then, 200 μl of the peroxidase substrate solution was added in each well, and the plate was incubated with rocking at RT until purple plaques become visible, usually 10 min after substrate addition. Plaques were counted using microscope to ensure accurate counting of the plaques. Then, virus titers (PFU/ml) were calculated using the following formula:

*Virus titer (Pfu/ml) = (number of plaques) / ((dilution factor) x (volume of diluted virus added to the well))*

## 2.8 RSV infections

Monolayers of cells were infected with virus suspended in 2% [v/v] FBS/DMEM at an appropriate MOI. Monolayers were washed prior to infection in PBS to remove all traces of serum. During the adsorption period, low-volume virus inoculum (50 μl/ well, for a 24-well plate) was added to the cells for 1h on a rocking platform at 37°C, and then 2% [v/v] FBS/DMEM was added to a maximum volume of 400 μl/well (for a 24-well plate), without removing the inoculum. Cells were incubated at 37°C/5% $CO_2$ until harvested.

# 2.9 Performance of a HTS approach to target RSV NS2

## 2.9.1 Assay Development

The quality and robustness of our assay has been validated at a 96-well plate format, and then it was further miniaturized to a 384-well plate format (Figure 2.2), using in-house screening equipment. The protocol of the 96-well and 384-well plate assay is shown in Table 2.6. These experiments did not require addition of any chemical compounds; hence the low signal controls were as indicated in Figure 2.2, whereas the rest of the wells were all treated with interferon for 48 hours to assess the variation in GFP signal along the plate. For the 96-well plate assay, $3x10^5$ cells/ml were seeded in 100 μl DMEM (10 % [v/v] FBS) per well, in clear 96-well microplates (Greiner Bio-one), using a microplate dispenser (WellMate, Thermo Scientific). The next day, 10 μl of 1:10 IFN-α (Roferon, NHS) diluted in 10 % [v/v] FBS/DMEM (final dilution 1:110) was added to the columns 2-11 using the WellMate cell dispenser. Plates were spun down at 1200 rpm at RT for 30 seconds, and then incubated at 37°C/5% $CO_2$ for 48 hours. On the last day of the assay, the cells were fixed with 100 μl of 10 % [v/v] formaldehyde/PBS (5 % [v/v] final conc.) for 20 minutes, washed under running water, and dried on paper towels. Then, 100 μl PBS added in each well, and GFP fluorescent units were measured using the TECAN plate reader. Once GFP readings were taken, all the wells were stained with 50 μl 0.15% [w/v] crystal violet for 30 minutes, and the absorbance (A650 nm) was measured using TECAN plate reader. The dispensing of formaldehyde, PBS and crystal violet was carried out using the WellMate cell dispenser.
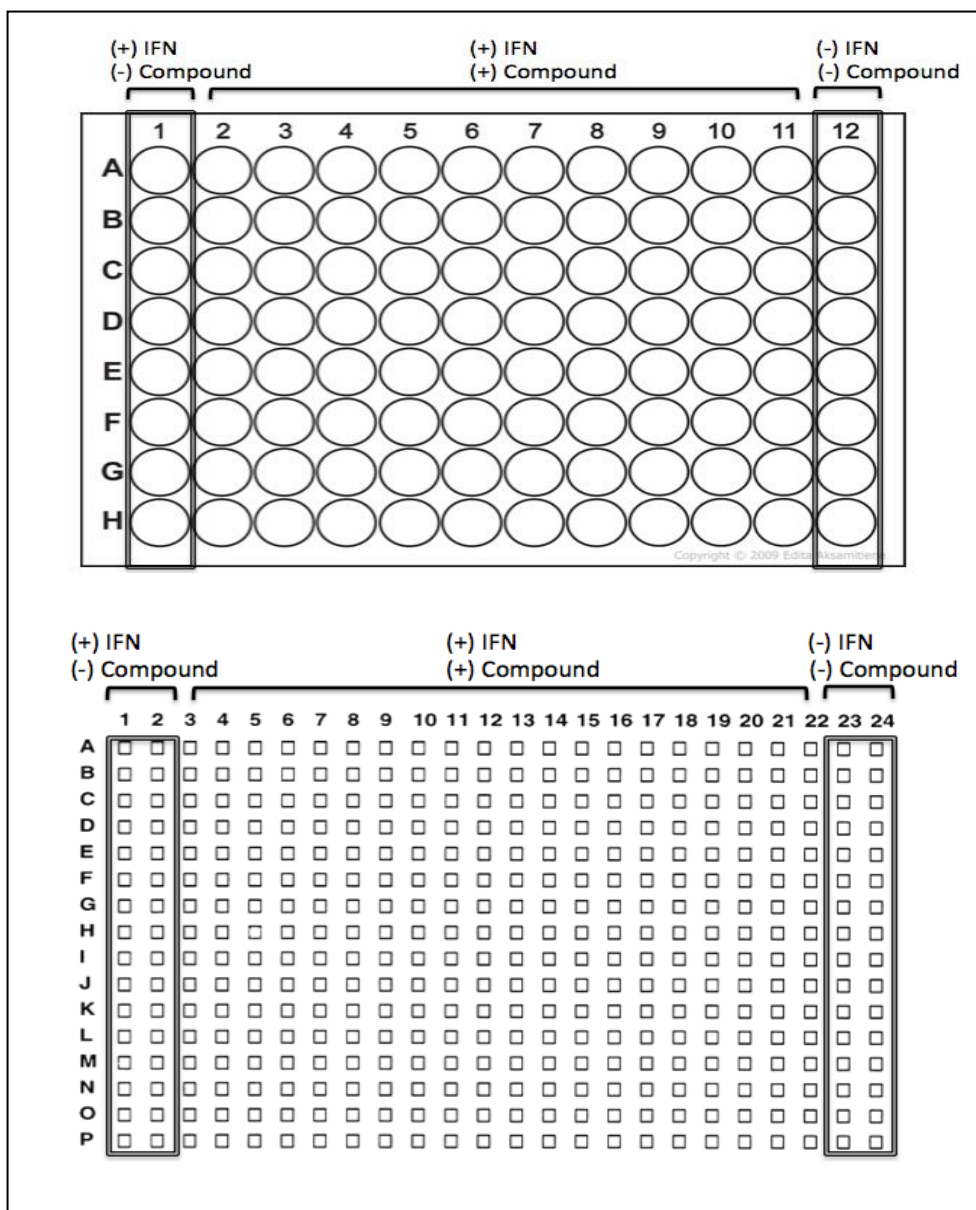
**Figure 2.2 Schematic presentation of the 96-well (top plate) and 384-well (bottom plate) format of our HTS assay.** Columns 1 (96-well plate)/Columns 1 and 2 (384-well plate): (+) IFN controls, these wells were treated with IFN only (high signal controls). Columns 2-11(96-well plate) / Columns 3-22 (384-well plate): Testing wells, these wells were treated with 11.42 µM of compound for 2 hours and then treated with IFN for 48 hours. Column 12 (96-well plate) / Columns 23 and 24 (384-well plate): Low signal controls, these wells had no treatment.

The exact same procedure was followed for the 384-well plate assay, however the concentration and volumes of the reagents were adjusted to a lower density format, as shown on Table 2.6.

**Table 2.6 Protocol of 96-well and 384-well plate formats of the A549 reporter assay**

| Day | Description | 96-well format | 384-well format |
|---|---|---|---|
| **Day 1** | Cell plating | $3 \times 10^4$ cells/well Total Volume in each well: 100 μl | $1.12 \times 10^4$ cells/well Total Volume in each well: 50 μl |
| **Day 2** | IFN treatment for 48 hours (Roferon A/NHS, $1\times10^6$ units /ml) | 10 μl of 1:10 dilution / well (final conc. 9090.90 U/ml ~$10^4$ U/ml ) | 20 μl of 1:40 dilution / well (final conc. 7142.85 U/ml) |
| **Day 4** | Fix plates for 20 min | 100 μl of 10% [v/v] formaldehyde/PBS fixing buffer | 23 μl of 20% [v/v] formaldehyde/PBS fixing buffer |
| | Wash and read plates | Washes with water, read in 100 μl PBS | Washes with water, read in 20 μl PBS |
| | Crystal Violet Staining for 20 min to assess cell viability | 50 μl 0.15% [v/v] crystal violet stain | 15 μl 0.15% [v/v] crystal violet stain |

## 2.9.1/1 Statistical Validation/ Data analysis

The performance of our HTS assay was quantified with three statistical parameters: (i) the signal to background ratio (S/B), which it is also known as fold increase in signal, (ii) the signal variability as indicated by the percentage of coefficient of variation (%CV), (iii) the $Z'$ factor, which is a measure of statistical effect size that takes into consideration both signal window and signal variability of negative and positive controls. Statistical parameters were calculated using the following formulas;

i)      *Fold increase (S/B) = μ (experimental FU value) / μ (background FU value), where FU stands for fluorescent units, μ stands for mean*

*ii)     % CV = % (σ / µ),*

*where µ stands for mean, and σ for standard deviation.*

*iii)     Z' factor = 1 − [(3 (σ$_p$ + σ$_n$)) / | µ$_p$ − µ$_n$|],*

*where µ stands for mean, σ for standard deviation, p for positive control and n for*
*negative control.*

The quantitative assessment of assay quality was based on the Dundee's Drug
Discovery Unit (DDU) quality control (QC) guidelines, according to which an excellent
and robust cell-based HTS assay should have S/B ratio > 2.5, %CV < 10% and Z' factor
> 0.5. The Z' factor is a dimensionless statistical parameter that has a range of 0 to 1.
For an assay to be considered appropriately robust for compound screening, the Z'
factor has to be greater than 0.5 (Zhang 1999; Hughes *et al.,* 2011).

## 2.9.2 In-house HTS to identify inhibitors of RSV NS2 IFN antagonist

To identify small molecule inhibitors of the RSV NS2 protein, the
A549.pr(ISRE)GFP-RSV/hNS2 cell-line was subjected to HTS using an in-house
chemical library, the Maybridge 16,000 compound library, which was kindly provided
by Professor Nick Westwood (University of St Andrews, UK). The compound library
consisted of fifty 384-well plates, hence the screen was carried out into five batches of
ten plates to minimize handling error. The protocol of our screen is summarized in
Table 2.7. HTS requires large number of cells, therefore A549.pr(ISRE)GFP-
RSV/hNS2 cells were grown into T175 cm$^2$ tissue culture flasks. On the first day of the
assay, cells were split using 0.48 mM EDTA to avoid over-trypsinizing the interferon
receptors on cell surface.  Then, cells were seeded in barcoded black 384-well cell bind
plates (Greiner Bio-one) at a density of 1.12 x 10$^5$ cells/ml in 50 µl 10 % [v/v]

FBS/DMEM per well. Throughout the assay, plates were incubated in stacks of three in an incubator used only for HTS to minimize the probability of getting incubator related plate patterns, such as edge effects. The next day, 80 nl of compound was added to each well (final screening concentration 11.42 μM) using an automated liquid-handling robot (MiniTrak$^{TM}$). The compounds were added to columns 3-22 of each plate, whereas columns 1-2 and 23-24 were the no compound controls (Figure 2.2). Plates were incubated at 37°C/5% $CO_2$ for 2h and then, 20 μl of 1:40 IFN-α ((final conc. 7142 U/ml)) was added to the columns 1-22 using a microplate dispenser (WellMate, Thermo Scientific). To make sure that the reagents were well mixed, the plates were spun down at 1200 rpm for 30 seconds at RT, and then incubated at 37°C/5% $CO_2$ for 48 hours. Afterwards, cells were fixed with 20 μl of 20% [v/v] formaldehyde/PBS (5% [v/v] final conc.) using the WellMate dispenser. Plates were left at RT for 20 min and then, the fixative was removed and plates were washed under running water. Water residues were removed by drying plates on tissue paper. Then, 50 μl of PBS were added in every well using the WellMate dispenser. GFP expression levels were measured using the TECAN microplate reader, and analyzed using the Magellan data analysis software. Cell viability was assessed after staining the wells with 20 μl of 0.15 % [w/w] crystal violet for 30 min. Plates were washed with water, and let to dry on tissue paper, before measuring the crystal violet absorbance (A6500 nm) using the TECAN microplate reader.

**Table 2.7 Protocol of a 384-well format cell-based HTS assay**

| Step | Parameter | Value | Description |
|------|-----------|-------|-------------|
| 1 | Plate cells | 50 µl | A549.pr(ISRE)GFP-RSV/hNS2 |
|    | Incubation time | 18 h | 37°C / 5% $CO_2$ |
| 2 | Compound Addition | 80 nl | 1: 875 dilution |
|    | Centrifugation | 30 sec | 1200 rpm at RT |
|    | Incubation time | 2 hours | 37°C / 5% $CO_2$ |
| 3 | Interferon treatment | 20 nl | 1: 40 dilution |
|    | Centrifugation | 30 sec | 1200 rpm |
|    | Incubation time | 48 h | 37°C / 5% $CO_2$ |
| 4 | Fix plates | 23 µl | 40% Formaldehyde/PBS |
|    | Incubation time | 20 min | RT |
| 5 | Assay readout – GFP signal | 488 nm / 518 nm | TECAN plate reader |
| 6 | Cell viability assay | 15 µl | 0.15% Crystal violet stain |
|    | Incubation time | 20 min | RT |
|    | Assay readout – Absorbance | 650 nm | TECAN plate reader |

| Step | Notes |
|------|-------|
| 1 | Cell seeded at a density of $1.12 \times 10^5$ cells/ml in Greiner Bio-one black 384-well cell bind plate. |
| 2 | Library concentration was 10 mM and screen was conducted at 11.42 µM. Compounds were added to the columns 3-22, using the MiniTrak Robot. |
| 3 | IFN-α (Roferon, NHS) has a concentration of $10^6$ U/ml and it was added to the cells at a final dilution of 1:140, which is equal to 7142.85 U/ml. IFN-α (Roferon, NHS) was added to the columns 1-22. |
| 4, 5 | After fixing, plates were washed with water and GFP readings were taken in 20 µl of PBS. |
| 6 | Plates were left to dry overnight before $A_{650}$ readings were taken. |
| 1, 3,4,6 | All liquid transfers were carried out using the WellMate microplate dispenser |

## 2.9.2/1 Statistical validation of primary screen

The statistical validation of the HTS assay was performed using the three statistical parameters described in the Section 2.9.1/1, and hit selection was performed on the plates that passed the QC criteria. Hit compounds that had a percentage (%) effect in fluorescent signal 50% above the assay control were selected. In addition to the % effect, hits were designated as molecules that restored GFP expression $\geq 3$ standard deviations (SD) (Z-Score= 3) above the sample signal mean, which was calculated using the following formula;

$$Z\text{-}Score = (X\text{-}\mu)/\sigma$$

where X is the raw signal, $\mu$ is the mean GFP signal of all the compound-containing wells of one plate, and $\sigma$ is the standard deviation of all compound containing wells of one plate.

## 2.9.2/2 Hit validation

### 2.9.2/2.1 Dose-response analysis

After running a primary screen, the selected hits were tested at various concentrations and plotted against the GFP signal to test whether they form good dose-response curves. For those hits that had a sigmoidal function, the half maximal effective concentration ($EC_{50}$) was calculated using the Hill equation, which is a four-parameter logistic equation;

$$Y= B + [(T\text{-}B)\,/\,(1 +\ (EC_{50}\,/\,X)^h]$$

A standard dose-response curve is defined by four parameters, namely B: baseline response (bottom asymptote), T: maximum response (top asymptote), h: slope (hill slope or hill coefficient), and the $EC_{50}$ value, which is the drug concentration that

provokes a response halfway between baseline and maximum (Goktug *et al.,* 2013). In

this study, the $EC_{50}$ values were calculated using Prism Software (GraphPad).

## 2.9.2/2.2 Testing the stability of the compounds' activity

To assess the activity of hit compounds over time, 10 μM of compound or

0.05% [v/v] DMSO was added to T25 $cm^2$ flasks containing either 50-60% confluent

A549 naïve cells in 8 ml of 10 % [v/v] FBS/DMEM or plain growth media. A 400-μl

sample was collected from each flask every day for a week and stored at -80°C. On the

eighth day of the experiment, 100 μl of each sample was added into 96-well plates (3

wells for each condition) containing A549.pr(ISRE)GFP-RSV/hNS2 cells. The

compounds were incubated with the cells for 2 hours, and then cells were treated with

IFN-α (Roferon, NHS), as described in Section 2.4.4. The activity of the compounds

was assessed in regards to their ability to restore the GFP expression levels in the

A549.pr(ISRE)GFP-RSV/hNS2 cells. The GFP restoration mediated by fresh

compound (10 μM) was set as the maximum restoration activity for each compound.

After GFP fluorescent units were measured, the cell density in each well was observed

with crystal violet (A650 nm) and GFP expression was normalized based on cell

density.

## 2.9.2/2.3 Testing the compounds' toxicity

The compounds' toxicity was tested using AlamarBlue[TM] cell viability assay

(following manufacture's instructions; ThermoScientic). This assay quantitatively

measures the viability of mammalian cell-lines, based on their ability to metabolically

process the oxidized form of AlamarBlue reagent (non-fluorescent blue) to the reduced

form of AlamarBlue reagent (fluorescent red). The oxidized AlamarBlue reagent is 100% reduced in metabolically active healthy cells. The AlamarBlue assay was performed in a 96-well plate format. In particular, A549.naïve cells and A549.pr(ISRE)GFP-RSV/hNS2 cells were seeded at a density of $3x10^4$ cells/well (100μl total volume / well) leaving column 12 empty. Column 12 was left for the 100% reduced and the 0% reduced controls, which were added in triplicate at the end of the assay. The 100% reduced AlamarBlue control was prepared after autoclaving 10 % [v/v] AlamarBlue/ 10% [v/v] FBS/DMEM, whereas the 0% [v/v] reduced AlamarBlue control was non-autoclaved 10% [v/v] AlamarBlue/ 10% [v/v] FBS/DMEM. A negative control of only medium without cells was also added to determine background signal (column 11). To construct dose-response curves, compounds were serially diluted (2-fold dilutions starting at 50 μM) on the cells and incubated for 48 hours (columns 2-10). After incubation, oxidized AlamarBlue reagent was added at the top of each well to a final concentration of 10 % [v/v]. The AlamarBlue reagent was incubated with the cells for 4 hours at 37°C, and fluorescent units were measured with excitation wavelength at 545 nm and emission wavelength at 590 nm, using the TECAN plate reader. The % reduction of AlamarBlue was calculated using the following formula;

*% Reduction of AlamarBlue reagent = 100 X [(Experimental FU value – Negative control FU value) / (100% reduced positive control FU value - Negative control FU value)],*

*where FU stands for fluorescent units*

**2.9.2/2.4 Testing hit compounds activity in regards to their impact on RSV growth**

The compounds' impact on RSV growth was tested using plaque assays and growth curves. The plaque assays were carried out as described in Section 2.7. In order to assess the effect of the compounds on RSV plaque size and number, 10 μM of the tested compound was added into the 0.5% [v/v] methylcellulose overlay. In addition, RSV growth kinetics were performed in A549 naïve cells in the absence or the presence of the hit compounds, as described before by Stewart *et al.,* (2014). In particular, A549 naïve cells were seeded in T25 flasks, so that they were 80-90% confluent on the next day. Flasks were infected with 1 ml of RSV (A2 or Long strain) at a MOI of 0.01 in 2% [v/v] FBS/DMEM. The flasks were tightly closed, and gently shaken for 3 hours at 37°C to facilitate virus spread and attachment. Afterwards, the inoculum was removed, and the cells were washed 5 times with PBS to ensure that non-attached virus particles were removed. Once cells were washed, they were treated with 5 ml of 10% [v/v] FBS/DMEM containing 10 μl of the tested compounds or equivalent volume of DMSO (0.05% [v/v]). At various times post infection the amount of infectious virus in the culture medium was estimated (Pfu/ml) by plaque assays on Hep2-BVDV/Npro cells, as described in Section 2.7.

# Chapter 3: Development of a modular cell-based HTS assay to target viral IFN antagonists for drug discovery

## 3.1 Introduction

All viruses, studied to date, encode at least one viral IFN antagonist, which is used to counteract the cellular IFN system, a powerful antiviral innate immune response. Viral IFN antagonists circumvent the IFN response using an astonishing repertoire of functions. Numerous genetic studies, both in cell culture and animal models, have demonstrated that knockout of viral IFN antagonist function is a critical determinant of viral replication, virulence and pathogenicity. Inhibition of viral IFN antagonist function impedes a virus' ability to counteract the cellular IFN response, predisposing infection outcome in favor of the host and consequently viral clearance. Hence, this vital class of viral proteins represents a diverse plethora of novel therapeutics targets that are not generally targeted by traditional antiviral approaches.

### 3.1.1 Overview of assay concept

We have embarked on a project to develop a cell-based HTS platform that will allow us to identify inhibitors of specific targeted viral IFN antagonists of choice. Prior to this study, two A549 reporter cell-lines have been developed by members of the Randall/Adamson group, which represent the foundation of our screening platform. The A549 reporter cell-lines have a fluorescent reporter gene (GFP) under the control of the IFN-β promoter or the ISRE element, and are named; A549.pr(IFN-β)GFP (Chen *et al.,* 2010) and A549.pr(ISRE)GFP, respectively. Therefore, the A549.pr(IFN-β)GFP and

A549.pr(ISRE)GFP reporter cell-lines provide a straightforward method to monitor activation or inhibition of either the IFN-induction or IFN-signalling pathway by measuring GFP expression (Figure 3.1).
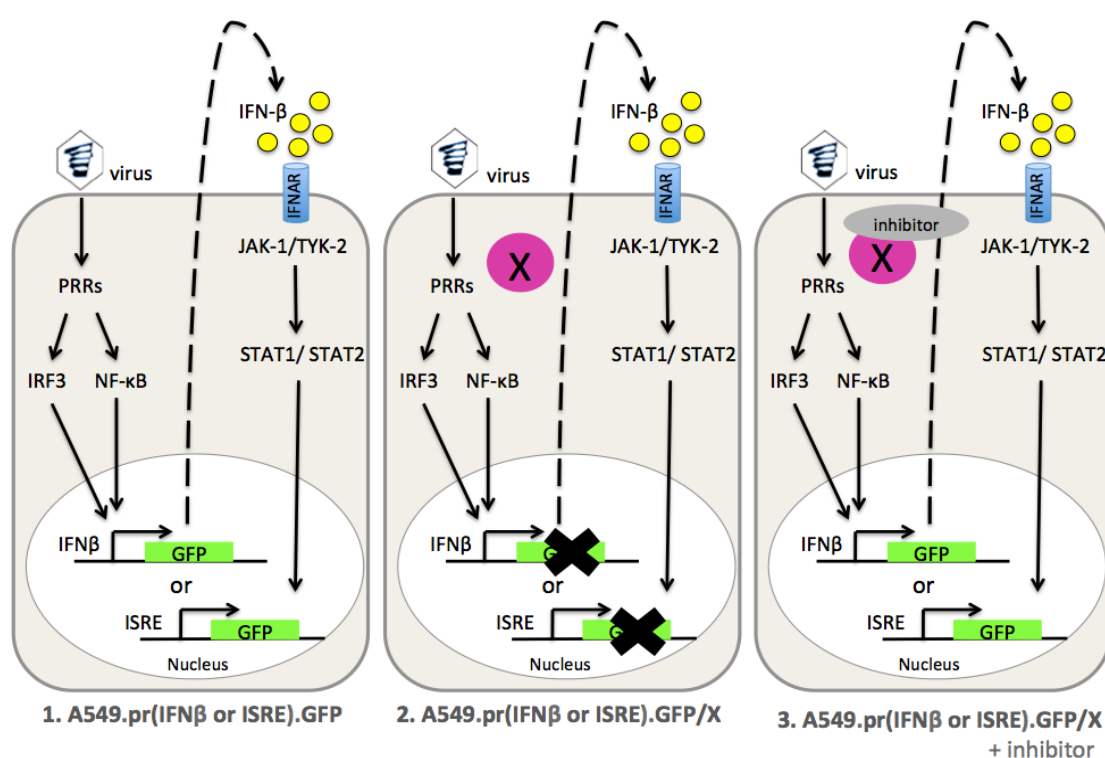


**Figure 3.1 Schematic overview of the assay concept in three basic steps.** Step 1: Development of GFP reporter cell-lines that allow monitoring of the IFN-induction or IFN-signalling pathways (A549.pr(IFN-β)GFP and A549.pr(ISRE)GFP). Step 2: Expression of a viral IFN antagonist (X) will suppress the cellular IFN induction and/or signalling, and hence block the GFP expression in the A549.pr(IFN-β)GFP and/or A549.pr(ISRE)GFP reporter cell-line. Step 3: A small molecule inhibitor will block the function of the viral IFN antagonist (X) against the cellular IFN induction or/and signalling and will eventually restore GFP expression in the reporter assay.

In this study, we further developed these reporter cell-lines by generating derivatives that expressed viral IFN antagonists of clinically important viruses for which there is a need for new antiviral drugs (Figure 3.1). We hypothesized that the ability of a reporter cell to produce GFP would be reduced when a viral IFN antagonist is expressed, because viral IFN antagonists block cells' ability to produce and/or respond

to IFNs. A small molecule that inhibits the viral IFN antagonist would suppress the antagonist's function against the cellular IFN system and would increase GFP expression in the reporter cell-line. Therefore, reporter cell-lines that express viral IFN antagonists would facilitate the identification of small molecules that inhibit viral IFN antagonists and subsequently restore GFP expression (Figure 3.1). Any small molecule inhibitors identified would allow us to validate viral IFN antagonists as suitable drug targets and could represent starting molecules for future antiviral drug development. Furthermore, inhibitors of viral IFN antagonists could also be utilized as research tools to better understand the function of these critical viral proteins and explore their role in virus replication.

## 3.2 Results

### 3.2.1 Verification of A549.pr(IFN-β)GFP and A549.pr(ISRE)GFP reporter cell-lines

In order to verify the A549.pr(IFN-β)GFP and A549.pr(ISRE)GFP reporter cell-lines, we quantified the ability of the reporter cell-lines to produce GFP fluorescent signal following addition of the appropriate inducer (Figure 3.2). The IFN-β promoter was activated using a genetically modified PIV5 virus, which expresses a truncated form (deletion of C terminus) of the V protein (PIV5.VΔC) and therefore has lost its ability to counteract the IFN-induction pathway (Chen *et al.,* 2010). As expected, PIV5.VΔC infection led to activation of the IFN-β promoter and subsequently induced GFP expression in the A549.pr(IFN-β)GFP cell-line, whereas the uninfected cells did not produce GFP, as observed by fluorescent microscopy (Figure 3.2/A). The average background fluorescent signal in the A549.pr(IFN-β)GFP cell-line was 7821 fluorescent

units, which was increased to 13929 following PIV5.VΔC infections, resutling in a fold

increase in GFP expression equal to 1.8 (Figure 3.2/B).
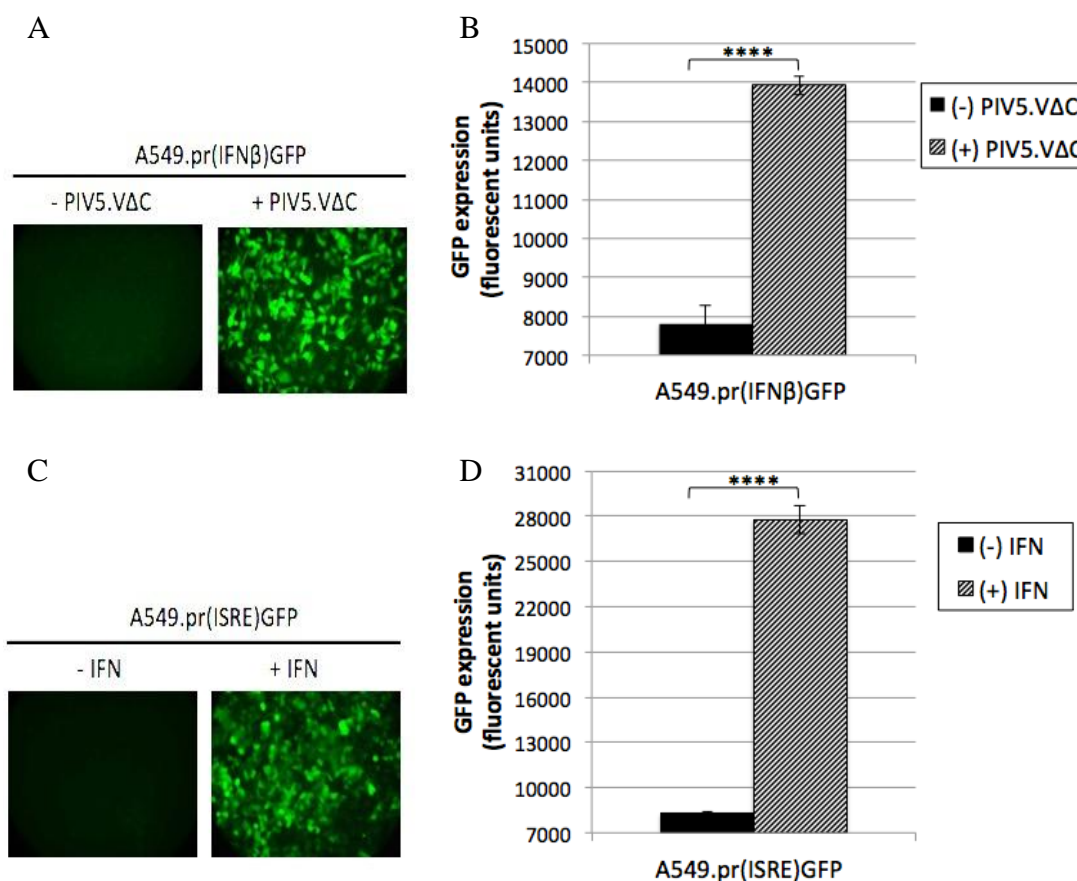


**Figure 3.2 Verification of A549.pr(IFN-β)GFP (A-B) and A549.pr(ISRE)GFP reporter cell-lines (C-D).** The A549.pr(IFN-β)GFP cell-line was infected with PIV5.VΔC virus (~MOI 7) for 24 hours for activating the IFN-β promoter. The A549.pr(ISRE)GFP was treated with purified IFN-α ($10^4$ U/ml) for 48 hours to activate the ISRE element. Following induction of the IFN-β promoter or ISRE element, GFP fluorescent units were observed with fluorescent microscopy (A and C) or quantified using TECAN plate reader (B and D). Graphs present mean values (n=8) with standard deviations (SD). Statistical analysis was performed using unpaired t-test, ****$p < 0.0001$ (Prism/GraphPad).

The IFN-signalling pathway was activated following 48-hour incubation with

IFN-α/β, which signals through the IFNAR receptor to activate the ISRE element.

Similar to the A549.pr(IFN-β)GFP cell-line, fluorescent microscopy showed that the

A549.pr(ISRE)GFP cell-line produced high GFP expression in response to IFN-α/β treatment, whereas the untreated cells did not produced GFP (Figure 3.2/C). Quantification of GFP fluorescent signal showed a significant increase in GFP expression when A549.pr(ISRE)GFP was treated with IFN-α/β (Figure 3.2/D). Specifically, the average background signal in A549.pr(ISRE)GFP was 8268 fluorescent units, and following IFN-α/β treatment the fluorescent signal was increased to 27796, corresponding to a fold increase in GFP expression equal to 3.4 (Figure 3.2/D). In conclusion, both A549.pr(IFN-β)GFP and A549.pr(ISRE)GFP produced high GFP expression following addition of the appropriate inducer, confirming that these reporter cell-lines represent a powerful method for monitoring activation of IFN-induction and IFN-signalling pathways.

## 3.2.2 Verification of assay controls; A549.pr(IFN-β)GFP and A549.pr(ISRE)GFP derivatives that constitutively express BVDV/Npro or PIV5/V

The aim of this study was to generate derivatives of A549 reporter cell-lines that express viral IFN antagonists of clinically important viruses and further utilized them for HTS to identify small molecule inhibitors that suppress their function. We reasoned that expression of viral IFN antagonists would reduce GFP expression in the A549.pr(IFN-β)GFP and A549.pr(ISRE)GFP cell-lines. To assess this, we used genetically modified reporter cell-lines that stably expressed viral IFN antagonists with well-documented anti-IFN properties. These were the BVDV Npro and the PIV5 V proteins, which were used as controls in our study. A variant of the A549.pr(IFN-β)GFP reporter cell line that stably expressed BVDV/Npro has been generated and verified

prior to this project by members of the Randall group (Chen *et al.,* 2010). In brief, BVDV/Npro is the N-terminal protease (Npro) encoded by the BVDV polyprotein, which targets IRF3 for proteasomal degradation (Hilton *et al.,* 2006). Thus, when BVDV/Npro is expressed, the activation of the IRF3 downstream immune effectors is blocked. Expression of BVDV/Npro was detected using the V5 epitope tag, which is fused to its N-terminus (Figure 3.3/A). The effect of BVDV/Npro on the activation of IFN-β promoter was measured with regards to GFP expression (Figure 3.3/B and 3.3/C). Specifically, A549.pr(IFN-β)GFP-BVDV/Npro reporter cell-line did not produce GFP following PIV5.VΔC infections, indicating that BVDV/Npro suppressed the PIV5.VΔC-induced activation of the IFN-β promoter in the A549.pr(IFN-β)GFP-BVDV/Npro reporter cell-line (Figure 3.3/B). Quantification of GFP fluorescent units showed that GFP production was dramatically inhibited (95% reduction) in A549.pr(IFN-β)GFP-BVDV/Npro compared to the naïve A549.pr(IFN-β)GFP reporter cell-line (Figure 3.3/C).

In order to generate a similar control variant of the IFN-signalling cell-line, we created a derivative of A549.pr(ISRE)GFP that constitutively expressed PIV5 V protein (Figure 3.3/B). Broadly, PIV5 V protein antagonizes the IFN-signalling by targeting STAT1 for proteasome-mediated degradation, and subsequently blocks the ISRE-induced transcription of ISGs (Didcock *et al.,* 1999). Similar to the BVDV/Npro-expressing cell-line, expression of PIV5 V completely blocked GFP expression in the A549.pr(ISRE)GFP-PIV5/V cell-line, as none of the cells produce GFP in response to IFN-α treatment (Figure 3.3/E). Quantification of the GFP fluorescent signal showed that PIV5 V completely blocked activation of the ISRE element in the A549.pr(ISRE)GFP-PIV5/V cell-line, resulting into complete inhibition of GFP

fluorescent signal (100% reduction) compared to the naïve A549.pr(ISRE)GFP reporter cell-line    (Figure 3.3/F). Overall, GFP fluorescent levels were totally blocked by BVDV/Npro and PIV5/V expression, indicating sufficient inhibition of both  IFN-induction and IFN-signalling pathways in our reporter assay.

To further characterize the A549.pr(ISRE)GFP-PIV5/V cell-line, the functionality of PIV5 V was tested based on its ability to reduce MxA expression (Figure 3.4). In brief, ISRE elements are present within the promoters of ISGs, and thereby ISRE activation regulates their transcription. The ISRE element used for generating the A549.pr(ISRE)GFP reporter cell-line is part of the promoter of MxA, which is an IFN-induced GTPase with reported antiviral activity against a wide range of viruses (Haller & Kochs 2011). Thus, MxA and GFP expression are under the control of the same promoter in the A549.pr(ISRE)GFP reporter cell-line. MxA expression was highly upregulated in the A549.pr(ISRE)GFP cell-line following IFN-α treatment, whereas, similar to GFP expression, MxA expression was completely blocked in the A549.pr(ISRE)GFP-PIV5/V cell-line (Figure 3.4). Taken together, this data suggests that we successfully developed a control variant of A549.pr(ISRE)GFP that stably expresses PIV5 V protein, which completely suppresses activation of the IFN-signalling, as determined by measuring GFP signal and MxA expression.
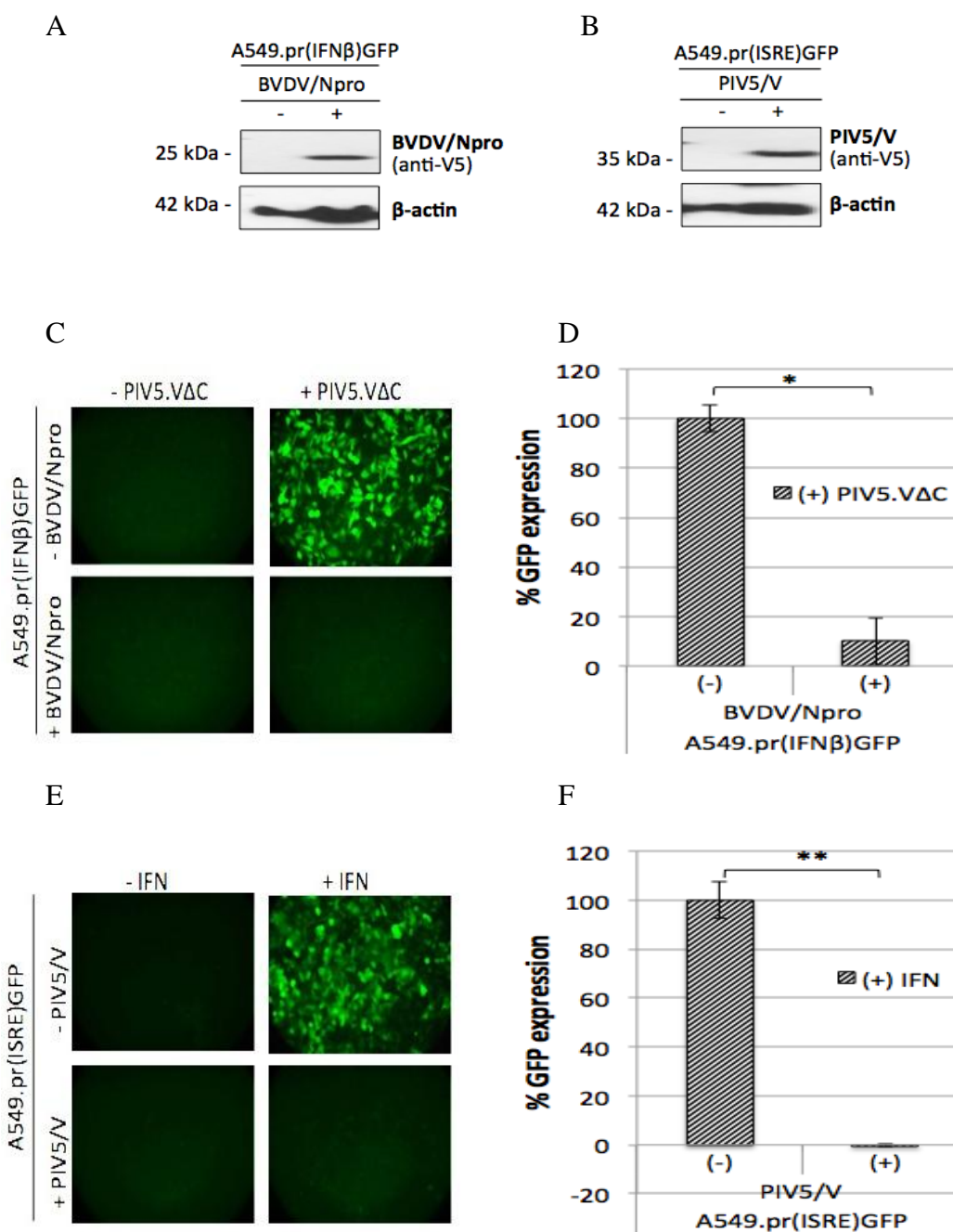
**Figure 3.3 Characterization of A549.pr(IFN-β)GFP and A549.pr(ISRE)GFP derivatives that constitutively express BVDV/Npro and PIV5/V. (A-B)** Western blot analysis shows expression of BVDV/Npro and PIV5/V in the A549.pr(IFN-β)GFP and A549.pr(ISRE)GFP reporter cell-lines, respectively. **(C-D)** GFP expression in A549.pr(IFN-β)GFP-BVDV/Npro cell-line following infections with PIV5.VΔC (1:100 dilution) for 24 hours was observed using fluorescent microscopy and quantified using TECAN plate reader. **(E-F)** GFP expression in the A549.pr(ISRE)GFP-PIV5/V cell-line following treatment with purified IFN-α ($10^4$ U/ml) for 48 hours was observed using fluorescent microscopy and quantified using TECAN. Graphs are presented as percentage (%) of GFP expression relative to A549.pr(IFN-β)GFP and A549.pr(ISRE)GFP, which were set as 100% controls, respectively. Bars represent mean values (n=4) and error bars show SD. Statistical analysis was performed using unpaired t-test, *p<0.05, **p<0.001 (Prism/GraphPad).
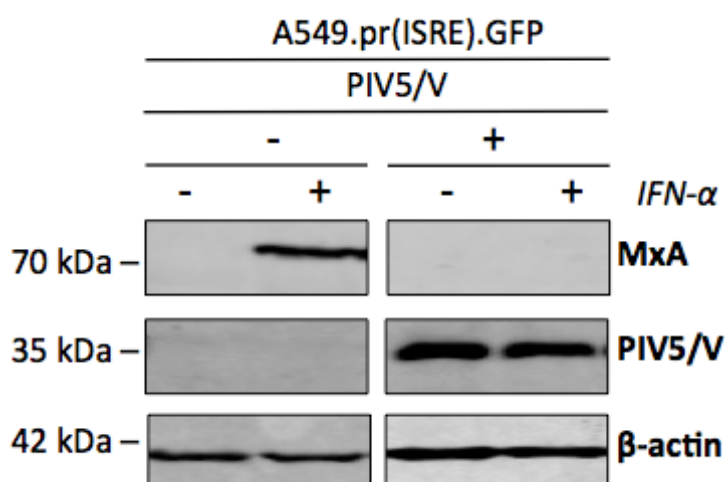
**Figure 3.4 Effect of PIV5 V on MxA expression upon activation of the IFN-signalling pathway.** MxA expression was observed using Odyssey CLx imager, following 16-hour treatment with purified IFN-α (2000 U/ml). Expression of PIV5 V protein was detected using anti-V5 antibody.

## 3.2.3 Proof-of-principle data demonstrating that our cell-based assay is suitable for identifying small molecules that inhibit the function of targeted viral IFN antagonist.

To generate proof-of-principle data, we exploited HCV NS3.4A protease inhibitors (PIs), the only clinically approved drug class that target a viral IFN antagonist. NS3.4A is essential for HCV replication as it mediates cleavage of the viral polyprotein; it also antagonizes the IFN-induction pathway by cleaving the signalling adaptors MAVS and TRIF at Cys-508 and Cys-372 residues, respectively (Meylan *et al.,* 2005; Lin *et al.,* 2006; Li *et al.,* 2005). In order to test our hypothesis that inhibitors of viral IFN antagonists can be identified via GFP restoration, we utilized an A549.pr(IFN-β)GFP derivative that constitutively expresses HCV NS3.4A protease of genotype 1b (A549.pr(IFN-β)GFP-HCV/NS3.4A(1b)), which was previously made by Dr Catherine Adamson (Figure 3.5).

A



B
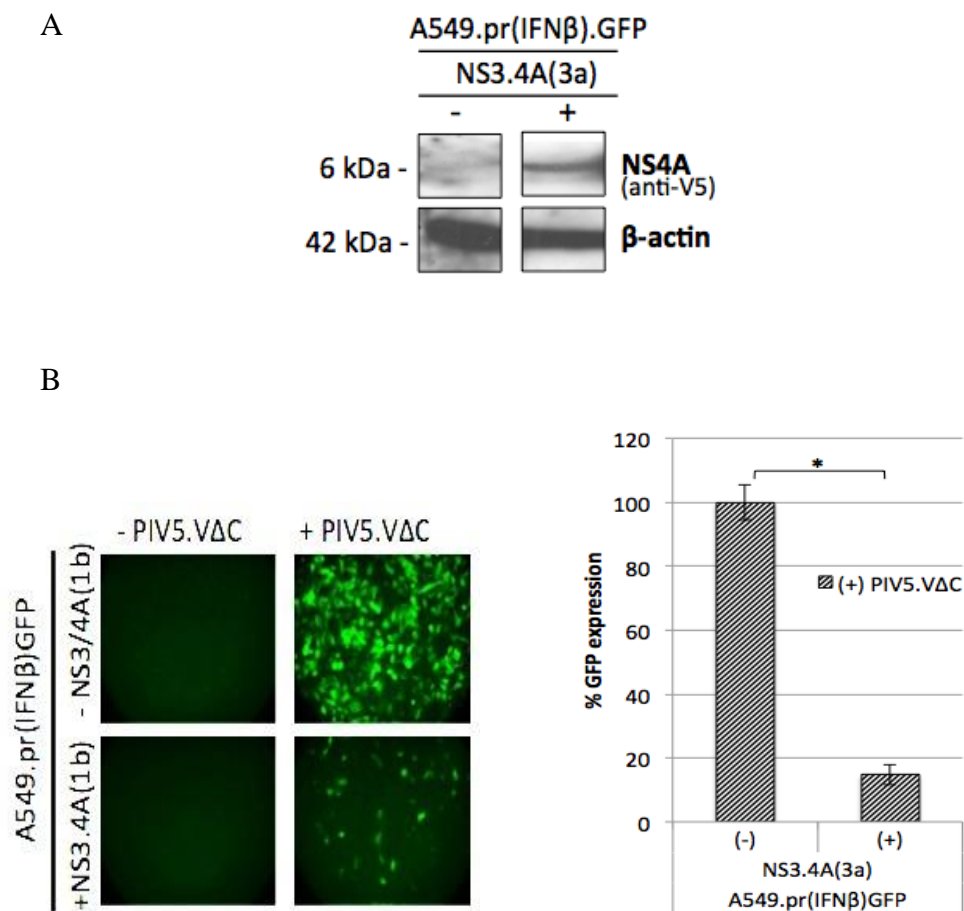


**Figure 3.5 Characterization of the A549.pr(IFN-β)GFP-HCV/NS3.4A(1b) reporter cell-line (A)** Western blot analysis shows expression of NS3.4A(1b). Expression of NS3.4A(1b) was detected with anti-V5 antibody and visualised with Advansta WesternBright ECL HRP substrate (Advansta). **(B)** GFP expression in the A549.pr(IFN-β)GFP-NS3/4A(1b). The cells were infected with the PIV5.VΔC virus (~MOI 7) for 24 hours and afterwards GFP expression was observed with fluorescent microscopy and quantified using the TECAN plate reader. The graph is presented as percentage (%) of GFP expression relative to A549.pr(IFN-β)GFP, which was set as 100% control. The bars show mean values (n=4) and error bars represent SD. Statistical analysis was performed using unpaired t-test, *p<0.05 (Prism/GraphPad).

Prior to using the A549.pr(IFN-β)GFP-HCV/NS3.4A(1b) cell-line to generate

proof-of-principle data, expression of NS3.4A(1b) was confirmed by western blot

analysis (Figure 3.5/A). The V5 epitope tag that is fused to the C-terminus of

NS3.4A(1b) was used for detection. Since the NS3.4A protease is a non-covalent

heterodimer, the anti-V5 antibody detected only the NS4A protein, which is a small protein around 6 kDa (Figure 3.5/A). In addition, we tested the level of GFP expression in the A549.pr(IFN-β)GFP-HCV/NS3.4A(1b) cell-line (Figure 3.5/B). Interestingly, only a few GFP positive cells were detected in the A549.pr(IFN-β)GFP-HCV/NS3.4A(1b) cells after infection with PIV5.VΔC (Figure 3.5/B). In agreement with fluorescent microscopy, quantification of GFP fluorescent units showed that GFP expression was reduced to 18% in the A549.pr(IFN-β)GFP- HCV/NS3.4A(1b) cell-line compared to A549.pr(IFN-β)GFP (Figure 3.5/B). This data indicates that NS3/4A protease effectively antagonizes the IFN-induction pathway, mediating a significant reduction in the activity of the IFN-β promoter, and subsequenly blocking GFP expression in our reporter assay.

To assess GFP restoration in A549.pr(IFN-β)GFP- HCV/NS3.4A(1b) cell-line, we utilized Danoprevir (ITMN-191/RG7227), which is a genome-specific inhibitor of HCV NS3.4A. Danoprevir was serially diluted against the A549.pr(IFN-β)GFP-HCV/NS3.4A(1b) reporter cell-line and the level of GFP expression was measured following PIV5.VΔC infection (Figure 3.6). As observed previously, A549.pr(IFN-β)GFP expressed high GFP expression after PIV5.VΔC infection, whereas GFP signal was considerably reduced in the A549.pr(IFN-β)GFP-HCV/NS3.4A(1b) cell-line, compared to A549.pr(IFN-β)GFP (Figure 3.6). Danoprevir had no effect on the level of GFP produced by the A549.pr(IFN-β)GFP cell-line after infection with PIV5.VΔC (Figure 3.6). In contrast, Danoprevir suppressed the ability of NS3.4A(1b) to antagonize the IFN-induction pathway, and increased GFP expression in the A549.pr(IFN-β)GFP-HCV/NS3.4A(1b) cell-line, in a concentration-specific manner (Figure 3.6). In particular, Danoprevir concentrations above 50 nM (log10= 1.69) gradually blocked the

activity of the IFN antagonist, resulting in a dose-specific increase in GFP fluorescent signal. Drug concentrations above 5 μM (log10= 3.69) caused up to 69.65% restoration of GFP expression, indicating that Danoprevir strongly inhibited the antagonistic function of NS3.4A(1b) against the IFN-induction pathway (Figure 3.6). Overall, we generated proof-of-principle data supporting our hypothesis that GFP restoration could provide the basis for the identification of small molecule inhibitors of targeted viral IFN antagonists.
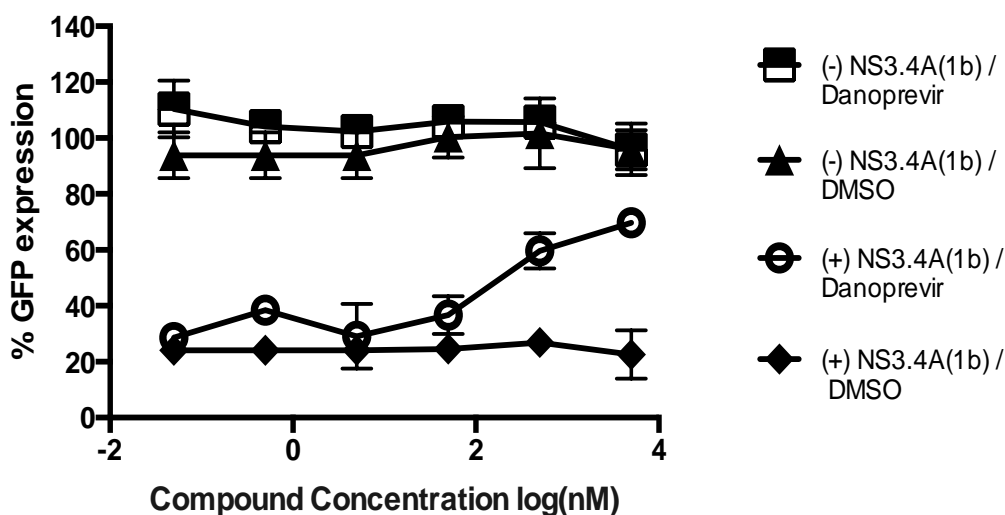


**Figure 3.6 Proof-of-principle data showing that a HCV/NS3.4A inhibitor (Danoprevir ) restored GFP expression in A549.pr(IFN-β)GFP-HCV/NS3.4A(1b) reporter cell-line in a dose-response manner.** Danoprevir or DMSO was serially diluted in the A549.pr(IFN-β)GFP and A549.pr(IFN-β)GFP-HCV/NS3/4A(1b) cell-lines and incubated for 2 hours at 37°C / 5% $CO_2$. Then, reporter cells were infected with PIV5.VΔC (inducer of the IFN-β promoter) at a MOI of 7 for 24 hours and GFP expression was measured using TECAN plate reader. Danoprevir was serially diluted in concentrations ranging from 0.05 nM (log10= -1.3) to 5 μM (log10= 3.69). Equivalent volumes of DMSO were added. The graph is presented as percentage (%) of GFP expression based on the DMSO/-PIV5.VΔC A549.pr(IFN-β)GFP control which was set as the 100% control. The bars show mean values (n=4) and error bars represent SD.

## 3.3 Summary

We successfully developed a cell-based reporter assay, which allows viral IFN antagonists to be subjected to HTS. Our assay is based on two validated A549 reporter cell-lines, the A549.pr(IFN-β)GFP and A549.pr(ISRE)GFP cell-lines, which produce GFP under the control of the IFN-β promoter or ISRE element, respectively. Hence these reporter cell-lines represent a straightforward method to monitor inhibition or activation of the IFN-induction and IFN-signalling pathways. The IFN-β promoter can be activated following infection with PIV5.VΔC, which is a potent inducer of the IFN-induction pathway; therefore the A549.pr(IFN-β)GFP reporter cell-line produces GFP (1.8 fold increase in GFP expression) in response to PIV5.VΔC infection. The ISRE element is activated following IFN-α treatment, which subsequenlty induces high GFP expression (3.4 fold increase) in the A549.pr(ISRE)GFP reporter cell-line. We also demonstrated that stable expression of BVDV Npro and PIV5 V reduced GFP expression to background levels in the A549.pr(IFN-β)GFP and A549.pr(ISRE)GFP cell-lines. GFP expression was inhibited up to 95% and 100% in the A549.pr(IFN-β)GFP-BVDV/Npro and A549.pr(ISRE)GFP-PIV5/V cell-lines, respectively, illustrating that the expression of viral IFN antagonists blocks the ability of the reporter cell-lines to produce GFP. Taken together, this data demonstrates that the A549.pr(IFN-β)GFP and A549.pr(ISRE)GFP cell-lines could provide the basis for developing a modular screening platform, which would allow viral IFN antagonists to be subjected to HTS.

In addition, we used a HCV NS3-4A PI to generated proof-of-principle data demonstrating that our cell-based assay is suitable for identifying small molecules that inhibit viral IFN antagonist function(s). Specifically, we utilized a A549.pr(IFN-β)GFP

derivative that constitutively expresses HCV NS3.4A(1b). HCV/NS3.4A(1b) inhibited PIV5.V$\Delta$C-induced GFP expression (80% reduction) in the A549.pr(IFN-$\beta$)GFP-NS3.4A(1b) reporter cell-line. When a HCV/ NS3.4A(1b) inhibitor (Danoprevir) was added to the A549.pr(IFN-$\beta$)GFP-NS3.4A(1b) reporter cell-line, GFP expression was increased in a dose-specific manner, indicating that the function of NS3.4A against MAVS/TRIF was effectively suppressed by the inhibitor. Overall, this data supports that restoration of GFP expression can be used as a measurable parameter to identify small molecules that inhibit the anti-IFN functions of targeted viral IFN antagonists in our reporter assay.

# Chapter 4: Targeting RSV-encoded IFN antagonists NS1 and NS2

## 4.1 Introduction

RSV is an important human pathogen with an unmet clinical need for new therapeutic strategies, which is highlighted by the lack of RSV vaccine and virus-specific antivirals. Recombinant RSV viruses that lack NS1 and/or NS2 exhibited attenuated replication in animal models (Whitehead *et al.,* 1999; Teng *et al.,* 2000), emphasizing the importance of NS1 and NS2 for RSV replication, which makes NS1 and NS2 potential attractive targets for drug discovery. RSV NS1 and NS2 suppress the cellular IFN response, by inhibiting multiple signalling factors of the IFN-induction and/or IFN-signalling pathway. Therefore, we sought to utilize our cell-based assay to target NS1 and NS2 for the identification of candidate small molecule inhibitors that suppress their function against the cellular IFN response. Small molecules that inhibit the function(s) of NS1 and/or NS2 could potentially represent good drug candidates, and they could also be used as novel chemical tools to address fundamental questions about RSV biology.

## 4.2 Results

### 4.2.1 Generation and characterization of reporter cell-line derivatives that constitutively express RSV IFN antagonists NS1 and NS2

In order to target NS1 and NS2 using HTS, we generated derivatives of the A549.pr(IFN-β)GFP and A549.pr(ISRE)GFP reporter cell-lines that expressed NS1 or

NS2. To achieve constitutive expression of NS1 and NS2, we used codon-optimized, 'humanized' versions of NS1 and NS2 (hNS1 and hNS2), which have been previously shown to have improved expression in A549 cells compared to the wild type sequences (Lo *et al.,* 2005). The hNS1 and hNS2 sequences were successfully cloned into our lentiviral system to generate two lentiviruses that encode hNS1 or hNS2. These lentiviruses were used to generate two derivatives of the IFN-induction reporter cell-line, namely A549.pr(IFN-β)GFP-RSV/hNS1 and A549.pr(IFN-β)GFP-RSV/hNS2 and two derivatives of the IFN-signalling reporter cell-line, namely A549.pr(ISRE)GFP-RSV/hNS1 and A549.pr(ISRE)GFP-RSV/hNS2.

Given that NS1 and NS2 can form a heterodimer, which is essential for their joint roles in suppressing various steps of IFN-induction and IFN-signalling(Lo *et al.,* 2005; Swedan *et al.,* 2011; Spann *et al.,* 2004), we also generated derivatives that expressed hNS1 and hNS2 together, in order to determine whether better inhibition of the IFN system is achieved when both IFN antagonists are present. The hNS1- and hNS2-encoding lentiviruses had two different resistance markers (blasticidin and puromycin, respectively), which allowed us to select for both genes in a single cell-line. Hence, sequential transductions with both lentiviruses in A549.pr(IFN-β)GFP and A549.pr(ISRE)GFP led to the generation of the A549.pr(IFN-β)GFP-hNS1.hNS2 and A549.pr(ISRE)GFP-hNS1.hNS2 cell-line, respectively.

The hNS1 and hNS2 proteins were tagged at their N-termini, which allowed us to detect hNS1 and hNS2 expression in the reporter cell-line derivatives. Specifically, hNS1 expression was higher in the A549.pr(IFN-β)GFP-RSN/hNS1 compared to the A549.pr(IFN-β)GFP-RSN/hNS1.hNS2 reporter cell-line, as indicated by western blot analysis (Figure 4.1/A). Although the western blot bands were not quantified, we could
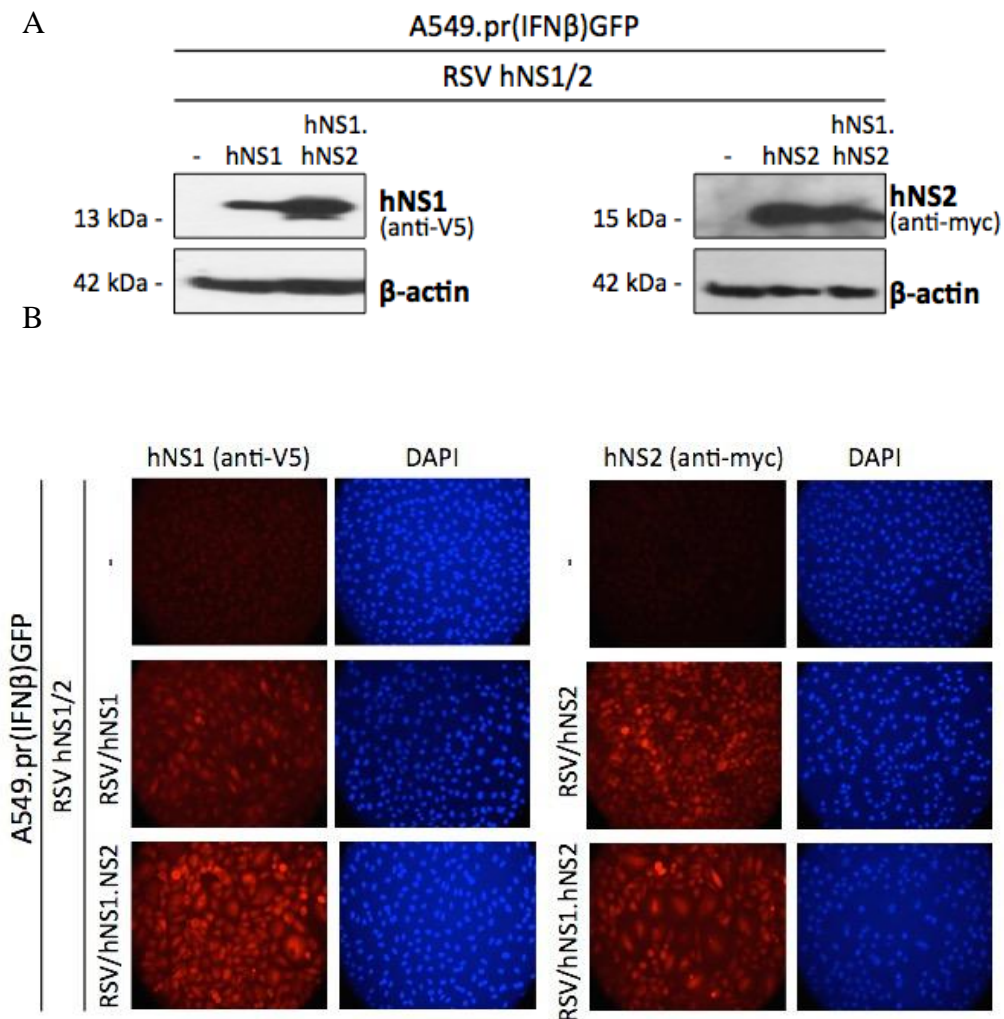
**Figure 4.1 Expression of RSV hNS1 and hNS2 in the A549.pr(IFN-β)GFP cell-line was determined by western blot analysis (A) and immunofluorescence microscopy (B)**. RSV hNS1 and RSV hNS2 expression was detected using an anti-V5 and anti-myc antibody, respectively. Enhanced chemiluminescence (ECL) with horseradish peroxidase (HRP) was used as detection method for western blotting.

still detect a clear difference in hNS1 expression (Figure 4.1/A). Similarly, immunofluorescence microscopy against RSV/hNS1 showed less fluorescent signal in the A549.pr(IFN-β)GFP-RSN/hNS1 compared to the A549.pr(IFN-β)GFP-RSN/hNS1.hNS2 cell-line (Figure 4.1/B). hNS1 expression also varied between the A549.pr(ISRE)GFP-RSN/hNS1 and the A549.pr(ISRE)GFP-RSN/hNS1.hNS2 reporter

cell-lines (Figure 4.2). Western blot analysis showed that hNS1 expression was almost three times higher in the A549.pr(ISRE)GFP-RSV/hNS1.hNS2 cell-line compared to the A549.pr(ISRE)GFP-RSV/hNS1 cell-line (Figure 4.2/A and 4.2/B). Likewise, immunofluorescence microscopy showed that hNS1 expression was slightly higher in the A549.pr(ISRE)GFP-RSN/hNS1.hNS2 cell-line compared to A549.pr(ISRE)GFP-RSN/hNS1 (Figure 4.2/D). Overall, the generation of reporter cell-line derivatives that constitutively expressed hNS1 appeared to be challenging, since hNS1 expression showed cytotoxicity effect, which considerably reduced the cells' growth rate. Interestingly, hNS1 expression appeared to be more sustainable in reporter cell-line derivatives that expressed both hNS1 and hNS2. Although hNS1.hNS2-expressing cell-lines expressed two IFN antagonists, they were growing faster than the hNS1-expressing cell-lines, suggesting that the functions of the hNS1-hNS2 heterodimer were perhaps less toxic to the reporter cells compared to hNS1 functions.

Unlike hNS1, constitutive expression of hNS2 did not show cytotoxicity, hence generating reporter cell-line derivatives that stably expressed hNS2 was less problematic. In both A549.pr(IFN-β)GFP and A549.pr(ISRE)GFP cell-lines, hNS2 expression was lower when expressed together with hNS1 compared to the cell-lines that expressed only hNS2, as indicated by western blot analysis (Figure 4.1/A and 4.2/A). Quantification of NS2 expression in the IFN-signalling cell-line showed that hNS2 expression was nearly five times higher in A549.pr(ISRE)GFP-RSV/hNS2 cell-line compared to the A549.pr(ISRE)GFP RSV/hNS1.hNS2 (Figure 4.2/C). The differences in NS2 expression were also evident by immunofluorescence microscopy in between
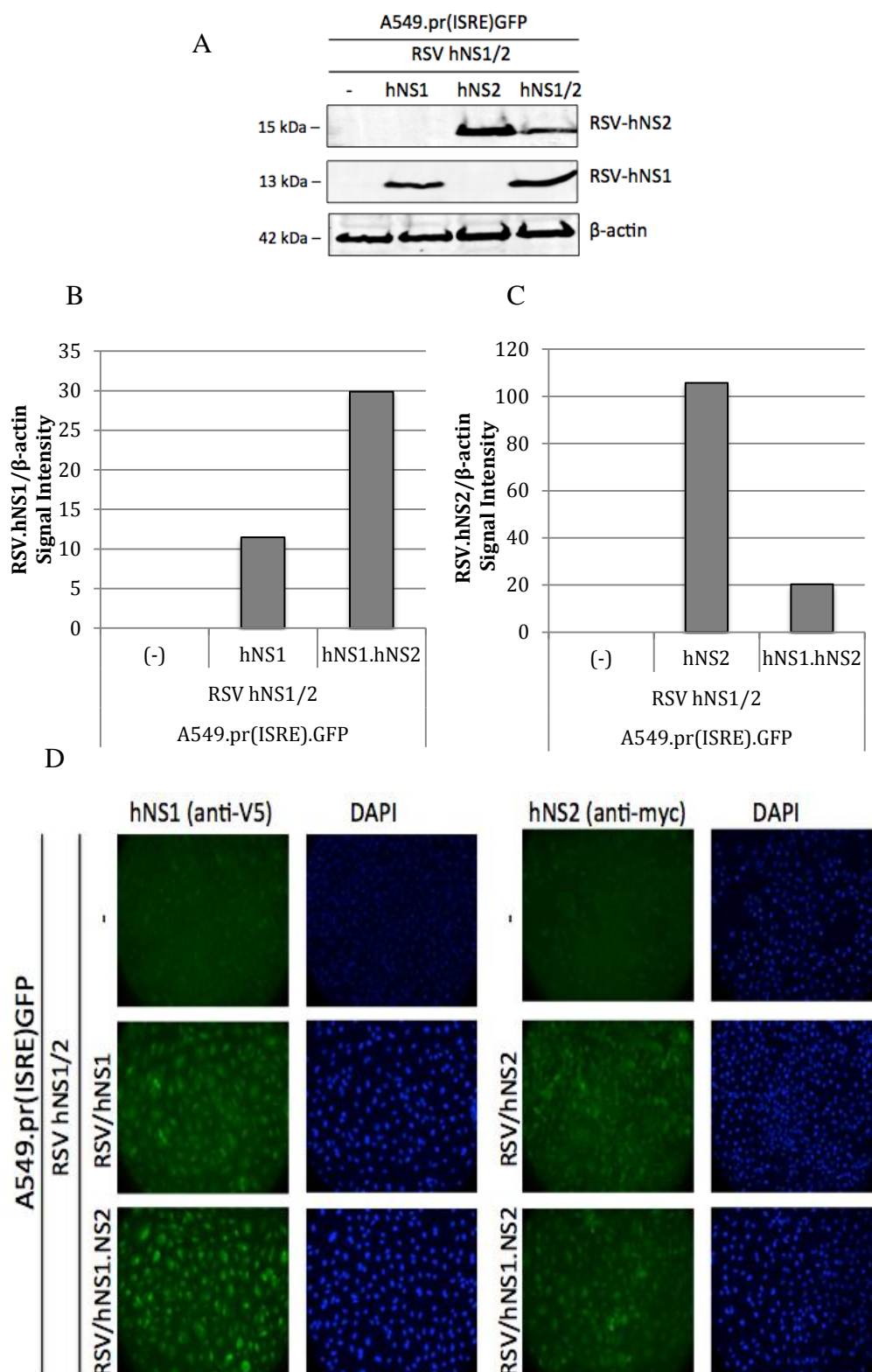
**Figure 4.2 Expression of hNS1 and hNS2 in the A549.pr(ISRE)GFP reporter cell-line. (A)** Expression of hNS1 and hNS2 was observed using infrared fluorescent western blot analysis using Odyssey LI-COR. **(B-C)** Bands were quantified using the Image Studio^TM software. The hNS1 and hNS2 signal intensities were quantified to relatively measure the protein expression levels, which were normalised to the β-actin signal intensity. **(D)** Expression of hNS1 and hNS2 was observed using immunofluorescence microscopy. RSV hNS1 and RSV hNS2 were detected using an anti-V5 and anti-myc antibody, respectively.

the different hNS2-expressing cell-lines (Figure 4.1/B and 4.2/E). The observed differences in the hNS2 expression were probably due to the fact that the A549.pr(ISRE)GFP-RSV/hNS2 served as the basis for creating the A549.pr(ISRE)GFP-RSV/hNS1.hNS2 cell-line, and perhaps the second round of antibiotic selection led to variation in hNS2 expression. Overall, regardless the differences in expression, we successfully generated derivatives of A549.pr(IFN-β)GFP and A549.pr(ISRE)GFP cell-lines that constitutively expressed hNS1 or/and hNS2, using lentivirus technology.

It is worth mentioning that the reporter cell-line derivatives generated in this study were not sub-cloned due to time constrains. Although screening against a homogeneous cell-line is more preferable, selecting for single clones increases the risk of screening against a dysfunctional or damaged population of cells. Therefore, for future applications beyond this study, we generated a FACS-based method, which allows the generation of a homogeneous population of cells in regards to expression of viral IFN antagonists, without selecting for single cell clones. In this method, the expression of the viral IFN antagonist is directly linked to a reporter gene that encodes for mcherry protein, as they are both expressed from the same ORF. This was achieved by creating a lentivirus transfer vector that contained the Thosea asigna virus (TaV) 2A peptide, which can separate different protein coding sequences in a single ORF, through a mechanism known as 'ribosomal-skipping' (Donnelly *et al.,* 2001). This method was tested using the RSV NS2 protein and successfully led to the development of a reporter cell-line derivative, A549.pr(ISRE)GFP-cherry-2A-RSV/hNS2, that expresses both mcherry and RSV hNS2 (Appendix 3). Using the 2A technology, we can generate reporter cell-line derivatives that express viral IFN antagonists and a fluorescent reporter protein, which allows FACS sorting based on fluorescent signal.

## 4.2.2/1 Testing the functionality of RSV hNS1 and hNS2 via ability to block GFP expression in the A549.pr(IFN-β)GFP and A549.pr(ISRE)GFP reporter cell lines.

GFP expression is directly linked to the activity of the IFN-β promoter and the ISRE/MxA element in our reporter assay. Hence, the ability of hNS1 and hNS2 to antagonize the IFN induction and signalling pathways was quantified by measuring the GFP expression in the derivative A549.pr(IFN-β)GFP and A549.pr(ISRE)GFP reporter cell-lines. In order to determine if hNS1 and NS2 proteins were functional in the A549.pr(IFN-β)GFP derivative reporter cell-lines, the IFN-induction pathway was induced via infection with PIV5.VΔC and the capacity of the cell-lines to produce GFP was quantified (Figure 4.3). As expected, PIV5.VΔC infections in the naïve A549.pr(IFN-β)GFP reporter resulted in high GFP expression (Figure 4.3). Unexpectedly, however, PIV5.VΔC infection in the derivative A549.pr(IFN-β)GFP reporter cell-lines expressing hNS1 and/or hNS2 led to significant cell death, especially in the cell-line expressing hNS1 and hNS2 together (Figure 4.3). Specifically, fluorescent microscopy showed that, for all three cell-lines, the majority of the cells that survived the PIV5.VΔC infections produced high or at least some level of GFP, indicating that hNS1 and hNS2 did not completely inhibit the activation of the IFN-β promoter (Figure 4.3). Interestingly, although all of the cells were positive for GFP, the hNS1-expressing cells produced lower GFP signal compared to the hNS2-expressing cells (Figure 4.3), suggesting that hNS1 is possibly a better antagonist of the IFN-induction pathway. Due to the differences observed in cell densities following PIV5.VΔC infections, quantification of GFP fluorescent units was misleading (data not shown). Overall, for undetermined reasons, PIV5.VΔC-induced CPE was dramatically

elevated in the hNS1- and hNS2-expressing A549.pr(IFN-β)GFP cell-lines. Although this is an interesting observation, it interfered with the validity of our assay and did not allow us proceed any further with these reporter cell-line derivatives.



**Figure 4.3 Induction of the IFN-β promoter in the RSV hNS1-, hNS2- and hNS1.hNS2-expressing A549.pr(IFN-β)GFP cell-lines, as indicated by GFP expression.** The IFN-induction pathway was activated following 24-hour infections with PIV5.VΔC (~ MOI 7), before observing GFP expression with fluorescent microscopy.

Likewise, in order to determine if hNS1 and NS2 proteins are functional in the A549.pr(ISRE)GFP derivative reporter cell-lines the IFN-signalling pathway was induced via treatment with IFN-α (Figure 4.4). Following induction, GFP expression was observed with fluorescent microscopy (Figure 4.4/A) and quantified using TECAN plate reader (Figure 4.4/B). As expected, IFN-α treatment led to the activation of the IFN-signalling, and therefore induced high GFP expression in the naive A549.pr(ISRE)GFP reporter cell-line (Figure 4.4/A). Expression of hNS1 had less

impact on GFP signal compared to hNS2, however hNS1 and hNS2 co-expression inhibited GFP expression to nearly background levels (Figure 4.4/A). Likewise, quantification of GFP fluorescent units indicated that hNS1 expression caused 51% reduction in GFP expression levels, whereas hNS2 expression led to 78% inhibition (Figure 4.4/B). Interestingly, co-expression of hNS1 and hNS2 almost completely blocked GFP signal mediating 91% inhibition (Figure 4.4/B). Overall, this data shows that the activity of the ISRE element (as indicated by GFP expression) is more affected by the presence of hNS2 rather than hNS1 but it is mostly inhibited when both hNS1 and hNS2 are present.

In order to confirm the validity of our assay, we sought to demonstrate that the MxA expression corresponds to the GFP expression in these reporter cell-lines. Therefore, the A549.pr(ISRE)GFP cell-line and its derivatives were treated with IFN-α, and MxA levels were observed with western blot analysis (Figure 4.5). As expected, the MxA expression was highly upregulated by IFN-α in the naive A549.pr(ISRE)GFP cell-line (Figure 4.5). Similar to GFP expression, hNS1 expression significantly reduced MxA levels (**, $P<0.01$) causing a 44% reduction compared to the naïve A549.pr(ISRE)GFP cell-line (Figure 4.5). hNS2 expression caused a more significant reduction in MxA levels (****, $p<0.0001$) compared to hNS1. Specifically, MxA levels were reduced to up to 19% after NS2 expression and were further reduced to 9% when NS2 was expressed together with hNS1 (Figure 4.5). The difference in MxA levels between the NS2- and NS1.hNS2-expressing cell-lines was not statistically significant (ns, $P>0.05$), indicating that NS2 expression has a more important role in inhibiting IFN-signalling pathway, which is in agreement with our previous observations based on GFP expression.
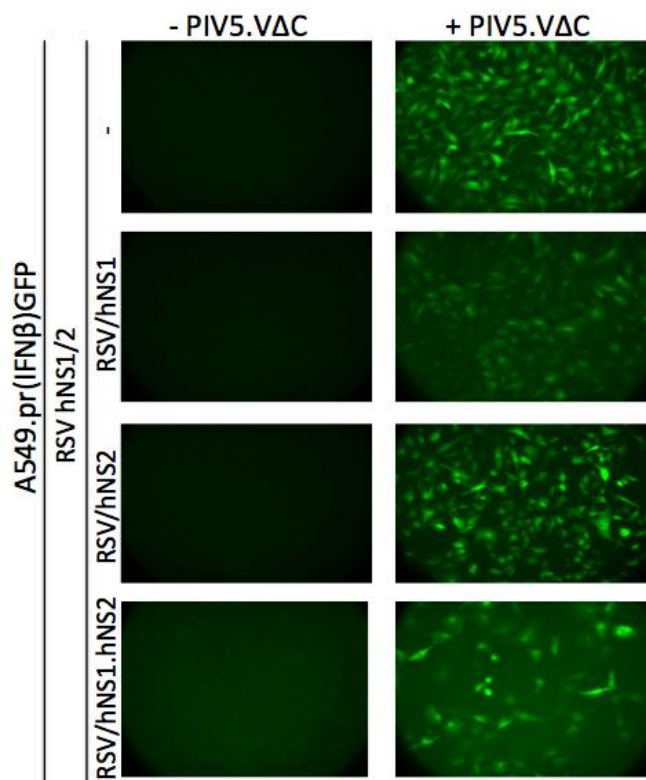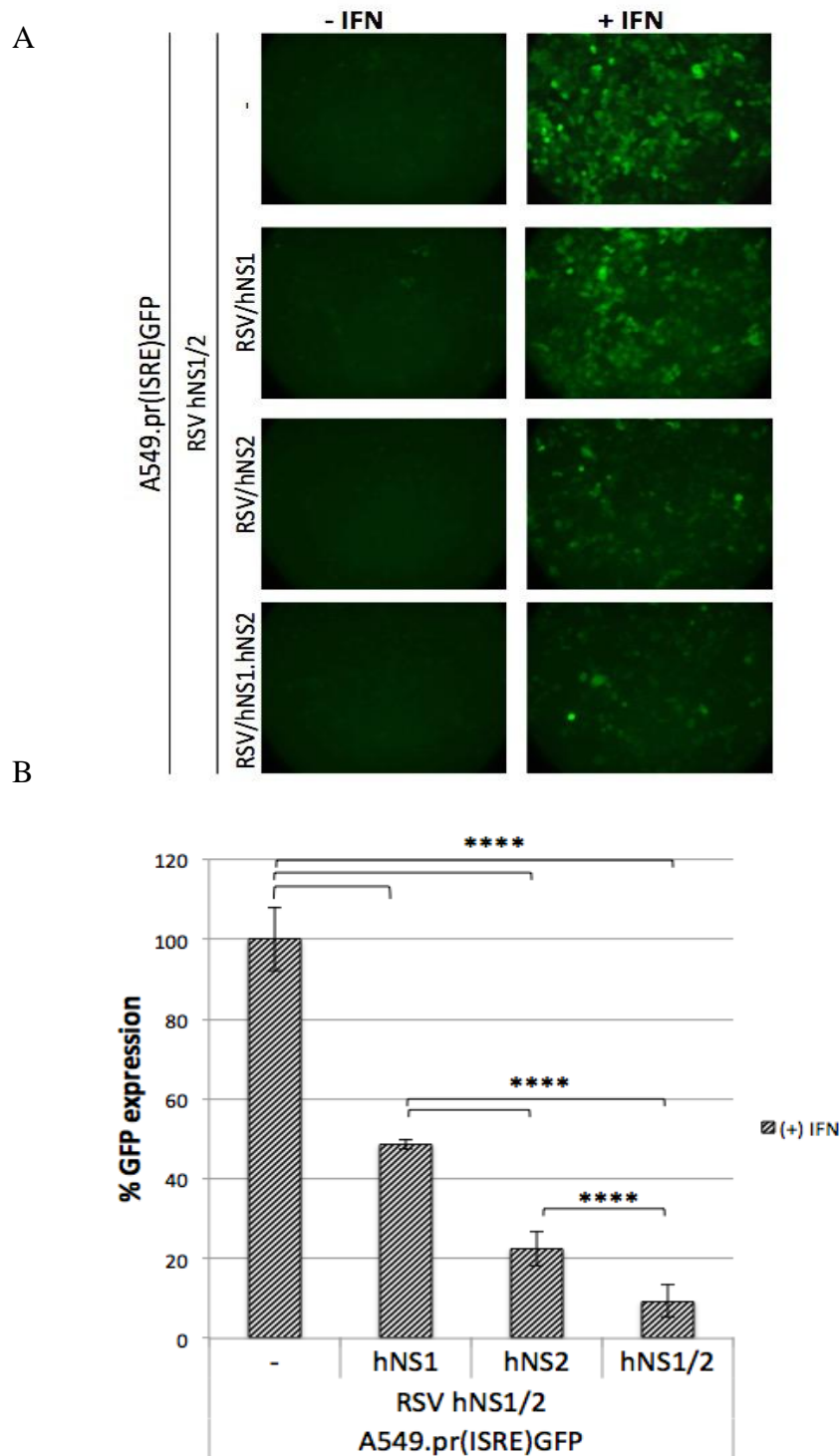
**Figure 4.4 Induction of the ISRE promoter in the RSV hNS1-, hNS2- and hNS1.hNS2-expressing A549.pr(ISRE)GFP cell-lines, as indicated by GFP expression.** GFP expression was observed with fluorescent microscopy (A) and quantified using TECAN plate reader (B). The IFN-signalling pathway was activated following 48-hour treatment with purified IFN-α ($10^4$ U/ml). Graph is presented as percentage (%) of GFP expression relative to naïve A549.pr(ISRE)GFP, which was set as 100% control. Statistical analysis was performed using one-way ANOVA test and Tukey's multiple comparisons test ($F_{(3,33)}=619.0$, ****$p<0.0001$) (Prism/GraphPad). Mean values (n=10), error bars=SD.
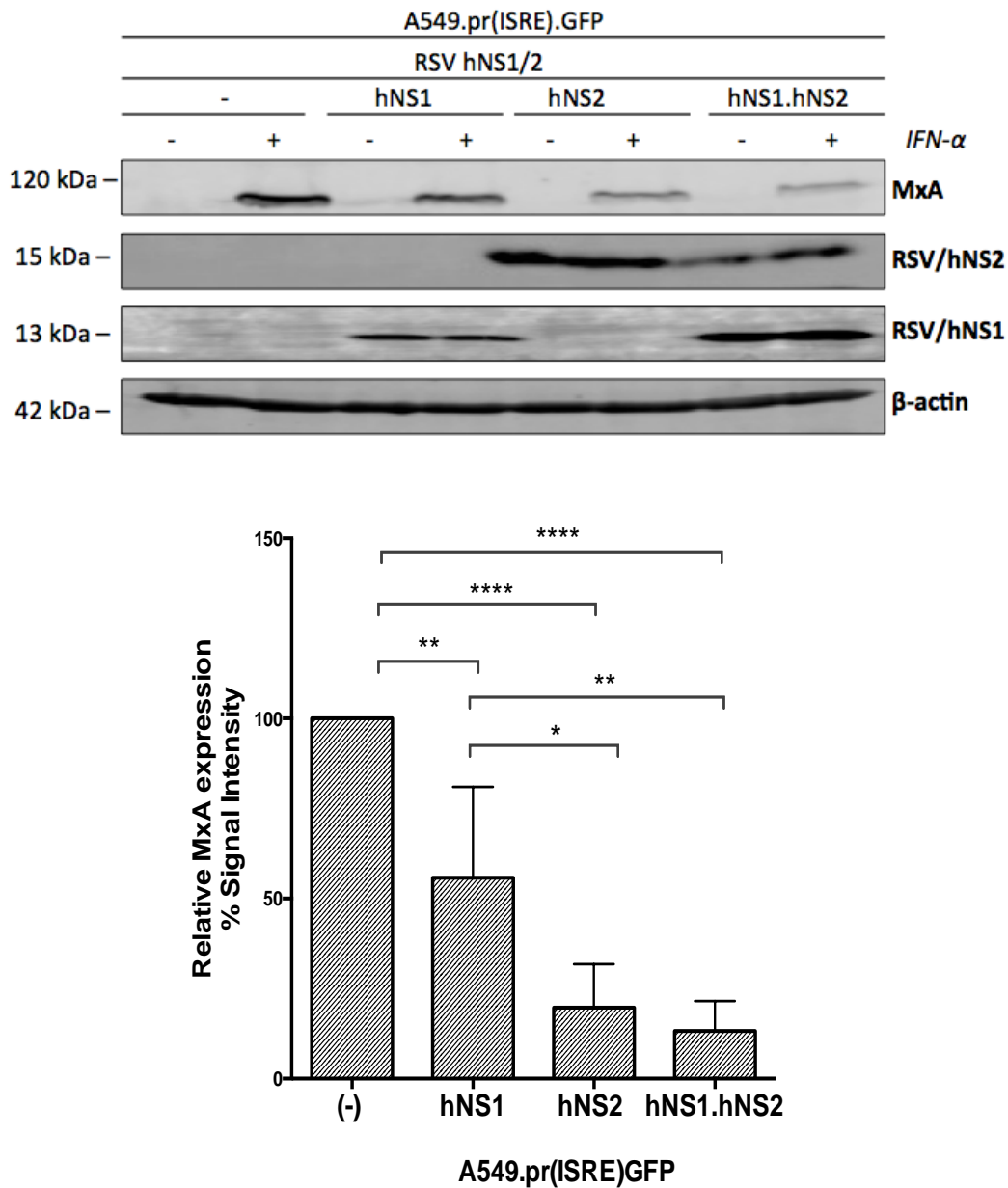
**Figure 4.5 Effect of hNS1 and hNS2 on MxA expression upon activation of the IFN-signalling pathway.** Following 16-hour treatment with purified IFN-α (2000 U/ml), MxA expression was observed using Odyssey CLx imager and quantified using ImageStudio software. The MxA signal intensity was normalized to β-actin levels, and presented as a % relative to the naïve A549.pr(ISRE)GFP reporter cell-line, which was set as 100%. Statistical analysis was performed using one-way ANOVA test and Tukey's multiple comparisons test ($F_{(3,12)}=29.86$, $p<0.0001$), ****$p<0.0001$, **$p<0.01$, *$p<0.05$ (Prism/GraphPad). Mean values (n=4), error bars=SD

Overall, in agreement with published work (Lo *et al.,* 2005; Swedan *et al.,* 2011; Ramaswamy *et al.,* 2006), our data demonstrated that RSV hNS2 counteracts type I IFN-signalling pathway more potently compared to RSV hNS1, whereas maximum inhibitory effect requires both hNS1 and hNS2.

## 4.2.2/2 Evaluating hNS1 and hNS2 functionality via STAT2 degradation in the A549.pr(ISRE)GFP reporter cell-line.

Previous studies have showed that RSV NS1 and NS2 cooperate to degrade STAT2 through the proteasome, nevertheless NS2 was found to be more important for this function (Lo *et al.,* 2005; Swedan *et al.,* 2009; Ramaswamy *et al.,* 2004; Elliott *et al.,* 2007). Therefore, in order to further assess the functionality of hNS1 and hNS2 in our reporter cell-lines, we measured STAT2 expression (Figure 4.6). In the naïve A549.pr(ISRE)GFP cell-line that does not express any viral IFN antagonists, we observed high levels of endogenous STAT2 (Figure 4.6). A 22% reduction in STAT2 levels was observed in the A549.pr(ISRE)GFP-hNS1 cell-line, which was not significantly different from the naïve control cell-line (ns, $p > 0.05$) (Figure 4.6). As anticipated, hNS2 expression had a greater effect on STAT2 levels and the reduction was significant compared to the naïve A549.pr(ISRE)GFP cell-line; hNS2 mediated a 73% decrease (\*\*, $p < 0.01$) when expressed on its own, and 87% decrease (\*\*\*, $p < 0.001$) when expressed together with hNS1 (Figure 4.6). This data is in agreement with other studies (Lo *et al.,* 2005; Swedan *et al.,* 2011; Goswami *et al.,* 2013) and strongly suggests that the STAT2 degradation is mostly driven by hNS2, however the presence of hNS1 is essential for establishing a robust inhibitory effect.
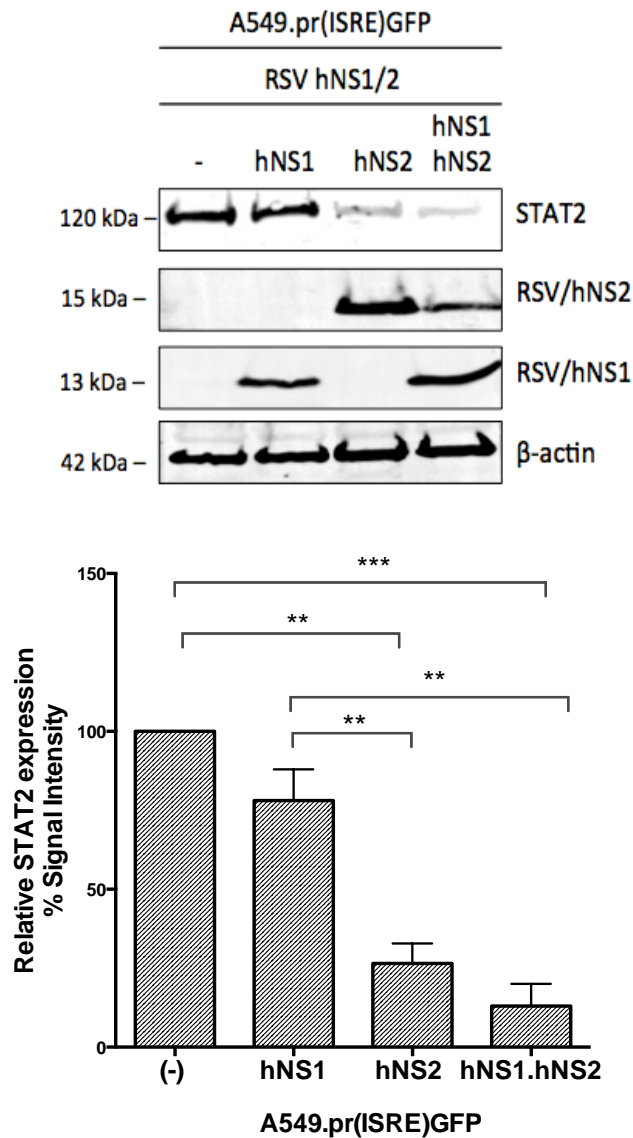
**Figure 4.6 Effect of hNS1 and hNS2 on STAT2 expression.** STAT2 expression was observed with near-infrared fluorescent western blot analysis (Odyssey CLx imager) and quantified using the Image Studio[TM] software. STAT2 quantification was carried out based on signal intensity, which was normalized to β-actin expression, and then presented as percentage (%), relative to naïve A549.pr(ISRE)GFP, which was set as 100%. Statistical analysis was performed using one-way ANOVA test and Tukey's multiple comparisons test ($F(3,4)=72.55$, $p=0.0006$), ***$p<0.001$, **$p<0.01$(Prism/GraphPad). Mean values (n=2), error bars=SD

## 4.2.3 Evaluating the role of NS1 and NS2 in STAT2 degradation in the context of RSV infection *in vitro*

Following these observations, we wanted to determine if our cell-lines reflect the function of NS1 and NS2 proteins in the context of viral infection, therefore we quantified STAT2 expression during *in vitro* RSV infection. To achieve this, A549 naïve cells were infected with wild type or recombinant RSV viruses that lack the NS1 or NS2 gene (RSV.ΔNS1 and RSV.ΔNS2, respectively) (Jin *et al.,* 2000), and STAT2 expression was measured in the absence or presence of IFN-α (Figure 4.7). Infection with wtRSV led to almost complete degradation of STAT2 (97% reduction) in the absence of IFN-α, and there was no increase in the STAT2 levels in the presence of IFN-α (Figure 4.7). In agreement with our previous data, the lack of NS1 did not affect RSV-mediated STAT2 degradation, as RSV.ΔNS1 infection significantly reduced STAT2 expression (86% reduction) almost to the same extent as wtRSV infection. In contrast, the RSV.ΔNS2 mutant mediated only a 30% reduction in STAT2 levels, indicating that the lack of NS2 had a significant effect (****, $p<0.0001$) on the STAT2 degradation function of RSV (Figure 4.7). This data is in agreement with published work (Ramaswamy *et al.,* 2006; Swedan *et al.,* 2011) and demonstrates that NS2 is indispensable for the RSV-mediated STAT2 degradation, which corresponds to the observations made in our reporter assay.

Despite wtRSV infection significantly reduced STAT2 expression levels compared to mock infected cells (****, $p<0.0001$), wtRSV upregulated MxA levels up to 50% in the absence of IFN-α, however no further increase was observed in the presence of IFN-α (Figure 4.7). This might be due to the fact that MxA is highly
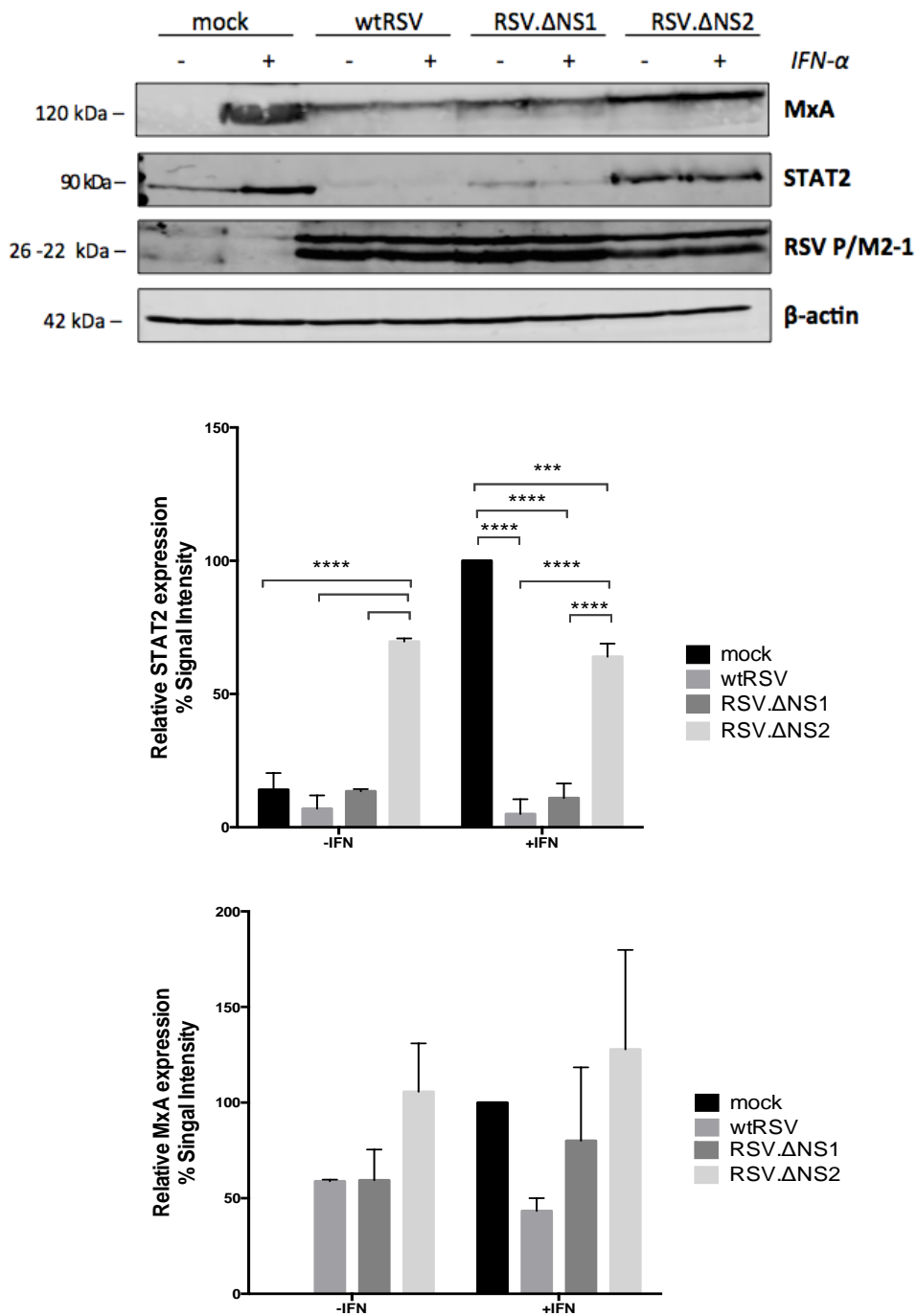
**Figure 4.7 Effect of wtRSV and recombinant RSV, RSV.ΔNS1 and RSV.ΔNS2, on MxA and STAT2 expression**. A549 naïve cells were infected with wtRSV (A2 strain), RSV.ΔNS1 or RSV.ΔNS2 for 24 hours at a MOI of 5, and the following day they were treated with purified IFN-α (2000 U/ml) for 16 hours. MxA and STAT2 levels were observed using Odyssey CLx imager and quantified using ImageStudio software. The quantification of the western blot bands was carried out based on signal intensity, which was normalized to β-actin expression, and then presented as a percentage (%) relative to the mock infected/ (+) IFN cells, which was set as the 100% control. Statistical analysis was performed using two-way ANOVA test and Tykey's multiple comparisons test (F (3,8)=201.3, p<0.0001) ****p<0.0001, ***p<0.001 (Prism/GraphPad). Mean values (n=2, 3), error bars=SD

upregulated by IFN-α, and leaky STAT2 expression might be enough to recruit transcription factors and trigger MxA expression. RSV.ΔNS1-induced MxA levels were very similar to wtRSV, however RSV.ΔNS2 induced higher MxA expression, similar to mock infected cells (Figure 4.7). Quantification of the MxA expression indicated considerable variation between different repeats, therefore the observed differences in MxA levels were not statistically significant (ns, p>0.05). However, the pattern of MxA expression pattern was consistent between different experiments; MxA was highly upregulated by RSV.ΔNS2 infections and less induced by RSV.ΔNS1 and wtRSV.

## 4.2.4 Proof-of-principle data demonstrated restoration of GFP in the A549.pr(ISRE)GFP-RSV/NS2 cell-line upon NS2 siRNA knockdown

The hNS1- and/or hNS2-expressing A549.pr(ISRE)GFP reporter cell-line derivatives were generated to allow us target NS1 and NS2 using a HTS approach. Our previous data showed NS1 and NS2 act synergistically to mediate STAT2 degradation, a function that is mainly driven by NS2, and thereby hNS2 inhibited GFP expression more effectively than hNS1 in our reporter assay. Hence, A549.pr(ISRE)GFP-RSV/hNS2 cell-line was further utilized for the identification of small molecules that inhibit NS2 function against the IFN-signalling pathway. Although the A549.pr(ISRE)GFP-hNS1.hNS2 cell-line had the lowest GFP expression, it was not considered for HTS, because screening against both NS1 and NS2 would complicate our assay and make the results inconclusive. For instance, an inhibitor would have to block the independent, as well as the joint functions of NS1 and NS2 to be selected as a candidate hit molecule.

In order to validate our hypothesis that small molecule inhibitors of RSV NS2 could be identified by conducting HTS using the A549.pr(ISRE)GFP-RSV/hNS2 cell-line, we sought to show that inhibition of hNS2 could lead to GFP restoration. Due to the lack of small molecules inhibitors of NS2, we used hNS2 siRNA knockdown to demonstrate restoration of GFP in the A549.pr(ISRE)GFP-RSV/hNS2. The capability of sihNS2 to knockdown hNS2 expression in the A549.pr(ISRE)GFP-RSV/hNS2 reporter cell-line was observed by western blot analysis (Figure 4.8). Our results showed that hNS2 expression was reduced to non-detectable levels, even after treatment with a low concentration of sihNS2 (10 nM) (Figure 4.8). Although sihNS2 treatment was effective, we observed that it had an effect on cells' growth rate, as the sihNS2-treated cells were growing slower than the control cells. The 96-well format of the GFP reporter assay is sensitive to cell densities, and in order to overcome this problem the cell seeding concentrations were adjusted accordingly for the next experiment.
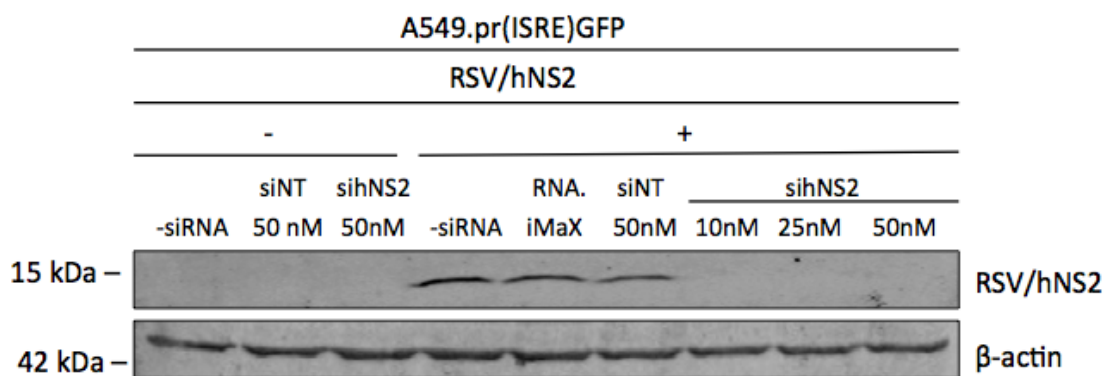


**Figure 4.8 sihNS2 treatment knockdowns RSV NS2 expression in the A549.pr(ISRE)GFP-RSV/hNS2 cell-line, as observed with western blot analysis.** The cell-lines were treated with 10 nM, 25 nM and 50 nM of sihNS2 for 24 hours. Three controls were used for this experiment; the -siRNA control contained only optiMEM, the RNAiMax control contained only the siRNA transfection reagent and the siNT control is a non-targeting siRNA, which was also used as a negative control (Dharmacon).

Once hNS2 knockout was confirmed, we tested whether sihNS2 treatment could restore GFP expression (Figure 4.9). In particular, A549.pr(ISRE)GFP and A549.pr(ISRE)GFP-RSV/hNS2 were treated with 50 nM sihNS2 for 24 hours, and then treated with IFN-α for 48 hours, before measuring and observing GFP expression (Figure 4.9/A and 4.9/B). The ability of the A549.pr(ISRE)GFP cell-line to produce GFP was not affected by sihNS2, as the level of GFP expression was similar to the three negative controls (-siRNA, RNAiMax and siNT) (Figure 4.9/A and 4.9/B). As expected, low GFP signal was observed in the A549.pr(ISRE)GFP-RSV/hNS2 for the all three negative controls (Figure 4.9/A and /B). Interestingly, treatment with 50 nM sihNS2 partially restored GFP expression in the A549.pr(ISRE)GFP-RSV/hNS2 cell-line (Figure 4.9/A and /B). Quantification of GFP showed that the A549.pr(ISRE)GFP-RSV/hNS2 produced 30% more GFP signal after sihNS2 treatment (Figure 4.9/A); the partially restored GFP expression was also confirmed by fluorescent microscopy (Figure 4.9/B).

To further explore this observation, we tested the STAT2 expression after sihNS2 treatment. In the A549.pr(ISRE)GFP cell-line, sihNS2 treatment had no effect on STAT2 expression, whereas higher STAT2 expression was observed in the A549.pr(ISRE)GFP-RSV/hNS2 cell-line, compared to the negative controls (Figure 4.9/C). In conclusion, our data suggests that siRNA NS2 knockdown was sufficient enough to reduce hNS2-mediated STAT2 degradation and subsequently increase GFP expression in the A549.pr(ISRE)GFP-RSV/hNS2 cell-line.

A



B



C
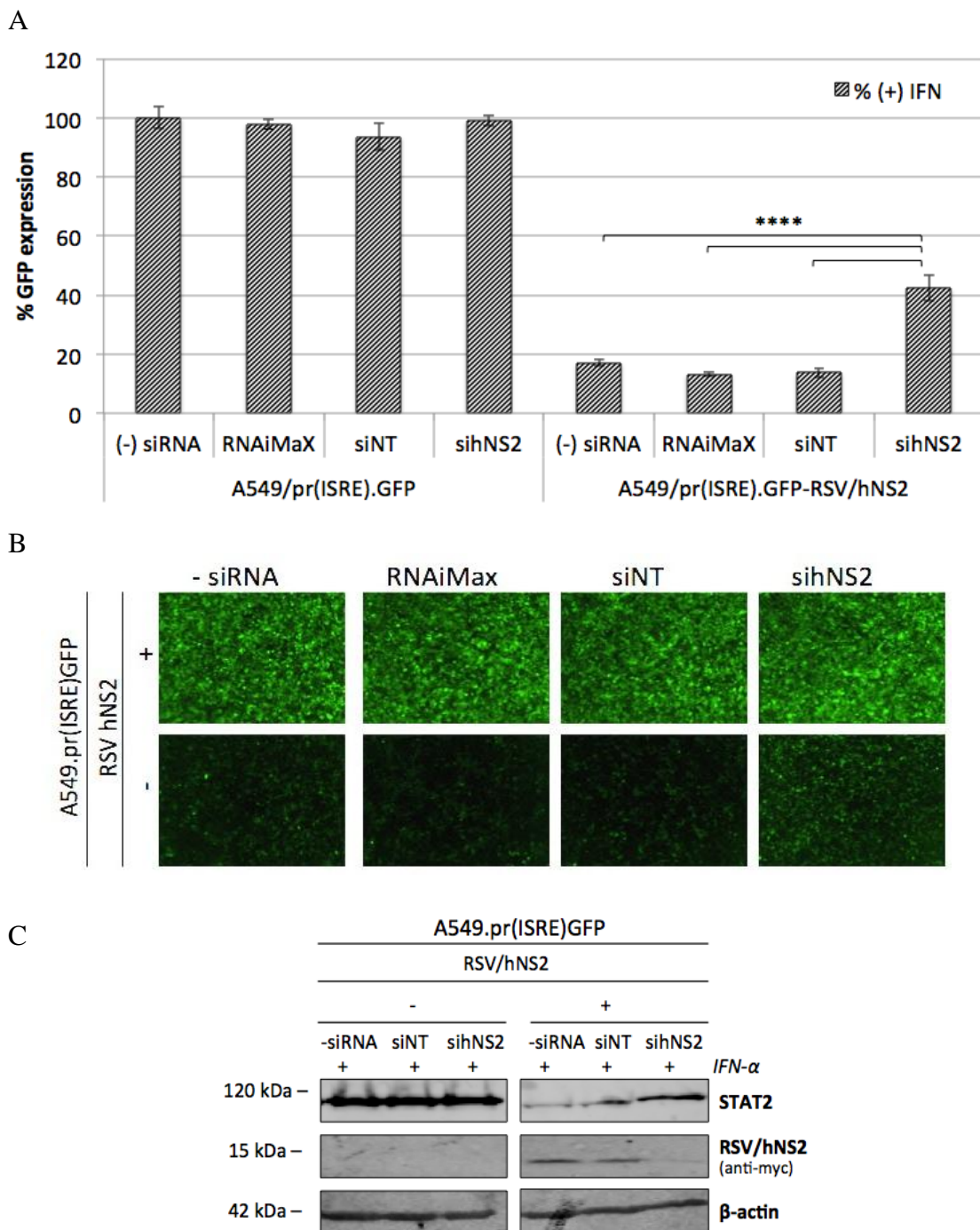


**Figure 4.9 Proof-of-principle data showing that GFP expression is restored in the A549.pr(ISRE)GFP-RSV/hNS2 cell-line following sihNS2 treatment.** Cells were seeded in a 96-well plate and transfected with 50 nM of siNT and sihNS2 for 24 hours, and then treated with IFN-α (10000 U/ml) for 48 hours. The -siRNA control contained optiMEM only, and a second control contained the siRNA transfection reagent only (RNAiMAx). **(A)** GFP expression was quantified using the TECAN plate reader. The graph is presented as percentage (%) of GFP expression relative to -siRNA/ +IFN A549.pr(ISRE)GFP control, which was set as 100%. Statistical analysis was performed using one-way ANOVA test and Tukey's multiple comparisons test (F $(3,16)$=179.5, ****$p<0.0001$) (Prism/GraphPad). Mean values ($n=5$), error bars =SD **(B)** Flluorescent images were taken using the Incucyte imager. **(C)** STAT2 expression as observed by western blot analyis. Cells were lysed with disruption buffer and STAT2 expression was observed with western blot analysis using Odyssey CLx imager.

## 4.3 Summary

In order to target RSV NS1 and NS2 using HTS, we developed derivatives of the A549.pr(IFN-β)GFP and A549.pr(ISRE)GFP reporter cell-lines that constitutively expressed hNS1 and hNS2, either separately or together. The expression of the proteins was successfully confirmed with immunodetection based on their N-terminal epitope tags. Expression of hNS1 was found to be toxic, however no apparent cytotoxicity was observed in the hNS2-expressing cell-lines.

NS1- and NS2-expressing reporter cell-lines were further characterized to determine the activity of the IFN-β promoter and ISRE element in these cell-lines by mesearing GFP expression. Infections with PIV5.VΔC were unexpectedly virulent in the NS-expressing A549.pr(IFN-β)GFP cell-lines, and therefore we were unable to draw conclucions about the functionality of NS1 and NS2 against the IFN-induction pathway. Hence, these reporter cell-lines were not taken any further, as they were not suitable for the development of a HTS approach. In contrast, expression of hNS1 or/and hNS2 in the A549.pr(ISRE)GFP reporter cell-lines allowed us to quantify the NS1 and NS2 antagonism against the IFN-signalling pathway. Previous studies have shown that RSV hNS1 and hNS2 can act synergistically or independently against the cellular IFN signalling (Ramaswamy *et al.,* 2004; Ramaswamy *et al.,* 2006; Swedan *et al.,* 2009; Swedan *et al.,* 2011). Likewise, our data demonstrated that expression of hNS2 inhibited GFP expression to a greater extent compared to hNS1, however maximal inhibitory effect was observed when hNS1 and hNS2 were co-expressed.

The most well documented function of NS1 and NS2 against the IFN-signalling pathway is their ability to mediate STAT2 degradation through the proteasome (Lo *et al.,* 2005; Swedan *et al.,* 2011; Spann *et al.,* 2004). Therefore, we quantified STAT2

expression, in order to assess the functionality of hNS1 and hNS2 in the reporter cell-lines. Our data illustrated that the STAT2 degradation function is mainly attributed to NS2, however the presence of NS1 is essential for more effective degradation. This observation was also confirmed in the context of virus infection, during which NS2 was found to be indispensable for the RSV-mediated STAT2 degradation.

In conclusion, A549.pr(ISRE)GFP reporter cell-line derivatives that stably express hNS1 and/or hNS2 were successfully generated to allow RSV NS1 and NS2 to be subjected to HTS. In particular, cell-line characterization showed that the A549.pr(ISRE)GFP-RSV/hNS2 reporter cell-line was more suitable for HTS, mainly because hNS2 expression was less toxic than hNS1, and also due to the fact that hNS2 had a more prevailing function in regards to STAT2 antagonism. Furthermore, we demonstrated partial restoration of GFP expression in the A549.pr(ISRE)GFP-RSV/NS2 cell-line upon NS2 siRNA knockdown, lending support to our hypothesis that small molecules inhibitors of NS2 could be identified based on GFP restoration in the A549.pr(ISRE)GFP-RSV/NS2 cell-line.

# Chapter 5: Assay development and performance of a HTS targeting RSV NS2

## 5.1 Introduction

In order to utilize our cell-based reporter assay to conduct a HTS targeting RSV NS2, our assay had to be first adapted to a HTS format. Prior to this study, one of the parental reporter cell-lines, the A549.pr(IFN-β)GFP has been validated for HTS in collaboration with the Dundee Discovery Unit (DDU), as part of Mrs Zoe's Gage PhD research project. The adaptation of A549.pr(IFN-β)GFP to a HTS setting was successful and was followed by a screen against 15,667 compounds, which led to the identification of small molecules that inhibit the IFN-induction pathway (unpublished Gage *et al.,*). In this study, we applied the statistical validation performed for the A549.pr(IFN-β)GFP reporter cell-line to our assay, in order to verify its quality and robustness. Once the quality of the assay's performance was verified, a HTS approach was performed in-house for the identification of small molecules that inhibit the function of RSV NS2 against the IFN-signalling pathway.

## 5.2 Results

### 5.2.1 Development of a robust 96- and 384-well format cell-based HTS assay

To adapt our assay to a HTS format, we first identified parameters in the assay procedure that acted as potential sources of variation. Key sources of variation were identified, such as (i) TECAN plate reader-induced artifacts, (ii) incubator related plate

patterns, (iii) edge effects attributed to evaporation or cell adhesion, and lastly (iv) liquid handling irregularities. Various practical steps were implemented to minimize exogenous sources of variation to adapt the assay to a HTS format, and further miniaturize it from a 96-well to a 384-well plate HTS format. The performance of the assay in both 96- and 384-well format has been validated according to the DDU quality control (QC) guidelines, based on which a GFP cell-based reporter assay is suitable for HTS when: (i) fold increase (S/B) > 2.5, (ii) % CV < 10 and (iii) Z' factor > 0.5. Both % CV and Z' factor are widely used for evaluation of assay quality; % CV measures the signal variation within a single treatment (e.g. high or low signal controls), whereas the Z' factor is reflective of both assay signal dynamic range and the variation associated with high and low signal control measurements (Zhang 1999).

We initially verified the parental reporter cell-line, A549.pr(ISRE)GFP reporter cell-line, because it produces high GFP signal in response to IFN-α, hence it allows a more thorough evaluation of signal variation compared to A549.pr(ISRE)GFP-RSV/hNS2 cell-line. The robustness of the A549.pr(ISRE)GFP reporter cell-line has been successfully demonstrated though S/B, %CV and Z' factor statistical analyses in a 96- and 384-well format (Figure 5.1 and 5.2). These analyses were performed on ten separate plates to allow us assess the reproducibility and consistency of the assay. The statistical verification of the A549.pr(ISRE)GFP reporter cell-line is summarized on Table 5.1. Specifically, in a 96-well plate format, the A549.pr(ISRE)GFP reporter cell-line had an average fold increase equal to 3.1, an average % CV for the high and low signal control equal to 3.74 and 3.70, respectively and an average Z' factor equal to 0.77 (Figure 5.1; Table 5.1). The quality of the assay was also validated in a 384-well format (Figure 5.2); our data indicated a robust 384-well format HTS assay, which had an

average fold increase of 2.5, an average % CV for the high and low signal control equal

to 5.04 and 4.25, respectively and an average Z' factor equal to 0.65 (Figure 5.2; Table

5.1).
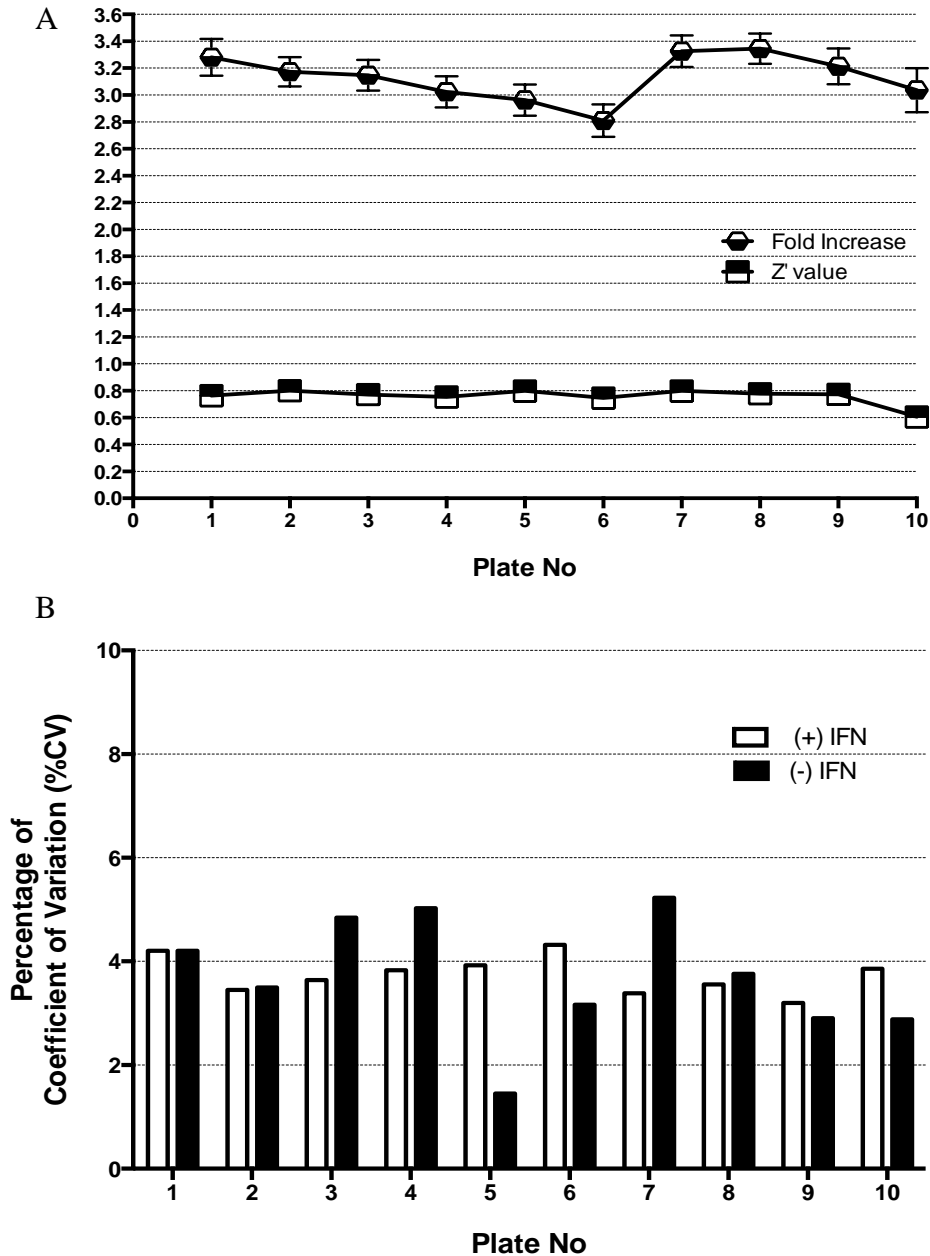


**Figure 5.1 Statistical validation of the A549.pr(ISRE)GFP cell-line in a 96-well plate format.** **(A)** Fold increase in GFP signal (n=80, error bars=SD) and Z' factor for ten separate plates. **(B)** %CV for the high (+ IFN) and low (-IFN) signal controls for the same plates.

A



B
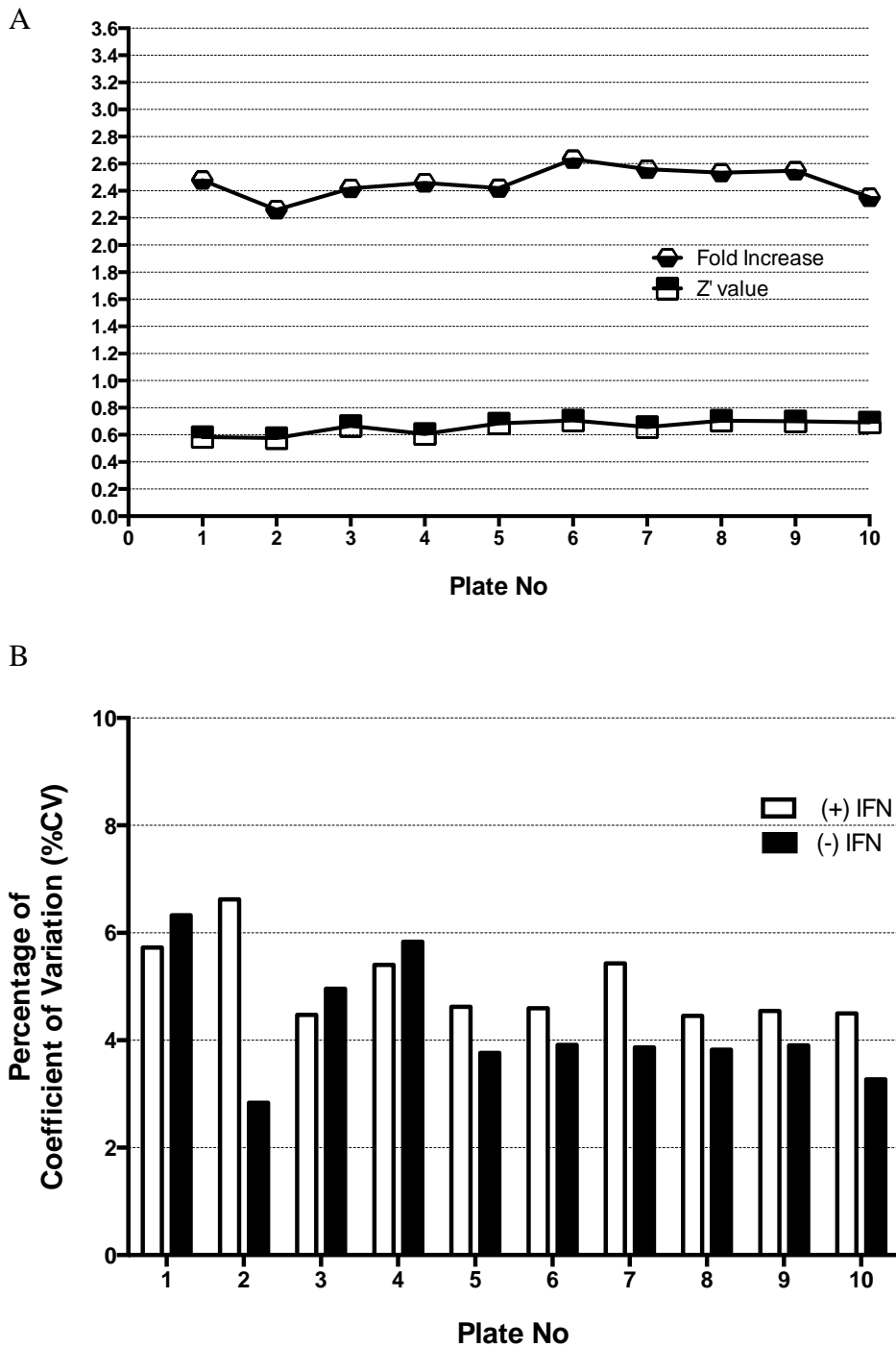


**Figure 5.2 Statistical validation of the A549.pr(ISRE)GFP cell-line in a 384-well plate format.** (**A**) Fold increase in GFP signal (n=32, error bars=SD) and Z' factor for ten separate plates and (**B**) %CV for the high (+ IFN) and low (-IFN) signal controls for the same plates.

**Table 5.1 The robustness of our in-house HTS platform was statistically validated using the A549.pr(ISRE)GFP reporter cell-line.**

| Statistical Parameter | | DDU QC requirements | 96-well format | 384-well format |
|---|---|---|---|---|
| Fold increase or S/B | | $\geq 2.5$ | 3.1 | 2.5 |
| % CV | +IFN | < 10% | 3.70 % | 5.04 % |
| | -IFN | | 3.74 % | 4.25 % |
| Z' factor (> 0.5) | | > 0.5 | 0.77 | 0.65 |

Although the quality of our HTS assay was successfully evaluated based on the statistical analyses performed in the A549.pr(ISRE)GFP reporter cell-line (Table 5.1), we also tested variation in the A549.pr(ISRE)GFP-RSV/hNS2 cell-line (Figure 5.3). The statistical validation of the A549.pr(ISRE)GFP-RSV/hNS2 cell-line was limited to one statistical parameter; %CV, in both a 96- and 384-well format (Figure 5.3). The A549.pr(ISRE)GFP-RSV/hNS2 cell-line had an average %CV for the high (+IFN) and low (-IFN) signal control equal to 2.71 and 3.96, in a 96-well plate format (Figure 5.3/A) and 4.76 and 4.06, in a 384-well plate format (Figure 5.3/B). The Z' factor was not an applicable statistical parameter for the A549.pr(ISRE)GFP-RSV/hNS2 cell-line, as it depends on signal window (GFP signal$_{+IFN}$ - GFP signal$_{-IFN}$). More specifically, hNS2 expression suppresses the IFN-induced ISRE activation, hence low GFP signal is produced by the A549.pr(ISRE)GFP-RSV/hNS2 cell-line, which makes the signal window narrow in this cell-line. Z' factor would be a suitable statistical parameter only in the presence of a NS2 small molecule inhibitor, which could be used as a positive control to restore GFP expression in the A549.pr(ISRE)GFP-RSV/hNS2 cell-line, and hence widen signal window. Due to the lack of NS2 small molecule inhibitors, signal variation and consistency in the A549.pr(ISRE)GFP-RSV/hNS2 was verified only

based on the %CV, which measures signal variation in high and low signal controls

separately, without taking into consideration the signal window (Figure 5.3).

Overall, this data shows that the tested statistical parameters met the DDU QC

guidelines (S/B ratio $\geq$ 2.5, %CV < 10% and Z' factor > 0.5), indicating successful

development of a reproducible and robust assay that allows us to perform HTS in a 384-

well format using in-house liquid handling screening equipment.
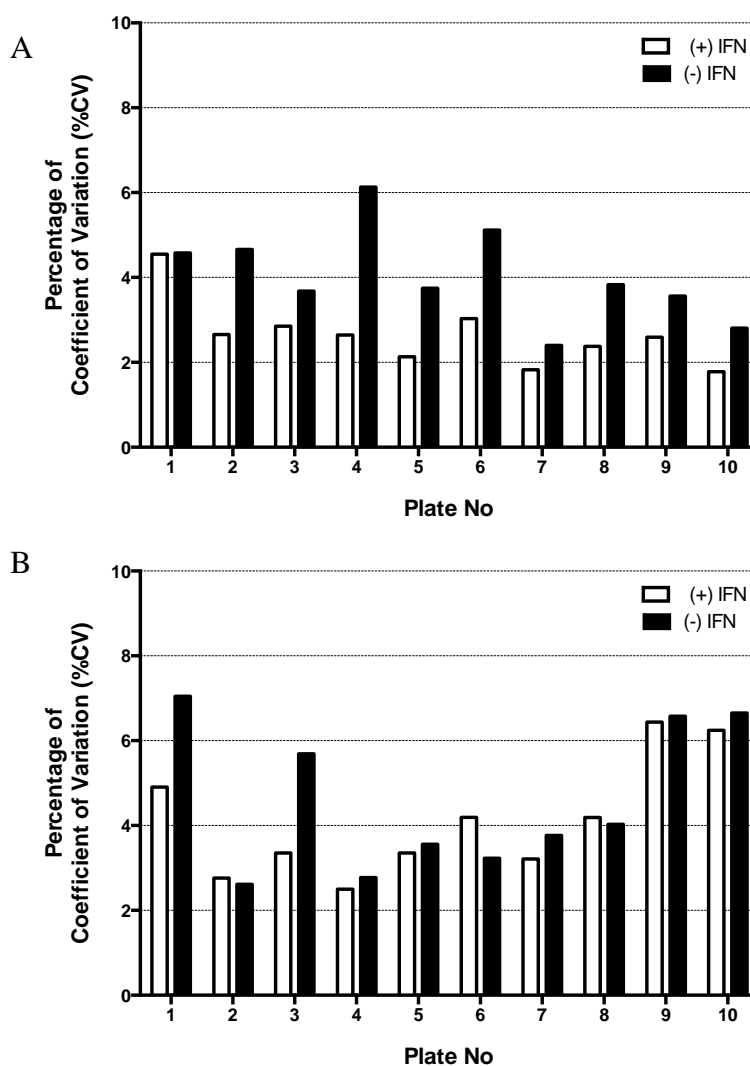


**Figure 5.3 Statistical validation of the A549.pr(ISRE)GFP-RSV/hNS2 cell-line.** % CV for
the high (+ IFN) and low (-IFN) signal controls was measured in ten separate plates in a 96-well
(A) and 384-well (B) plate HTS format (n=32).

## 5.2.2 Primary HTS to identify small molecules that inhibit RSV NS2 function

A primary HTS was conducted against the A549.pr(ISRE)GFP-RSV/hNS2 cell-line to identify small molecules that suppress the NS2 function against the IFN-signalling pathway via restoration of GFP expression. The library screened derived from the Maybridge[1] screening collection, which was kindly provided by Professor Nicholas Westwood (University of St Andrews, UK). The library consists of 16,000 small molecules with drug-like properties that obey the Lipinski's 'rule of 5', according to which, a drug-like molecule should have; (i) no more than five hydrogen bond donors, (ii) no more than ten hydrogen bond acceptors, (iii) a partition of coefficient (log*P*) lower then 5 and (iv) a molecular mass not greater than 500 daltons (Lipinski *et al.,* 2001). The compounds were arrayed in fifty 384-well plates as single compounds at 10 mM in DMSO. In order to make it practicable and minimize handling errors, the screen was performed in five batches of ten 384-well plates. Once the primary screen was completed, we combined the data from all assay plates and calculated the percentage (%) effect of the 16,000 screened compounds to identify the compounds that restored GFP expression in the A549.pr(ISRE)GFP-RSV/hNS2 cell-line (Figure 5.4). A normal distribution curve centred around zero point was formed when the frequencies of the 16,000 screened compounds were plotted against their percentage effect (% of inhibition), indicating that no systemic errors were accosiated with the screen performace (Figure 5.4). Selection of hit compounds is discussed in Section 5.2.3.

The assay quality was monitored during the screen to ensure that no instrumental and/or biological factors were affecting the performance of our assay in the

---

[1] Supplementary information about the Maybridge library:
http://www.maybridge.com/portal/alias__Rainbow/lang__en/tabID__146/DesktopDefault.aspx

HT setting. To determine if the data collected from each plate met the minimum quality requirements, and if any patterns existed before and after data normalization, the distribution of control and test sample data were examined at experiment-, plate- and well-level. The quality of screening data on each plate was assessed using heat maps, which allow the identification of abnormal patterns that are usually related to plate patterns (data not shown). For the quantitative assessment of the screen's performance, we used two statistical parameters; the fold increase (S/B) and the %CV (Figure 5.5). The average fold increase (S/B) of all the assay plates (n=50) was equal to 1.37 (Figure 5.5/A). The average %CV was equal to 4.58 and 6.02 for +IFN controls and -IFN controls, respectively (Figure 5.5/B). Seven assay plates did not meet the QC requirements (%CV > 10%) (Figure 5.5/B). These plates were excluded from the statistical analyses that followed the primary screen for the identification of potential hits that inhibit the function(s) of NS2. Overall, the primary screen fulfilled the statistical requirements for a valid HTS assay, and therefore further statistical analyses followed for hit compound selection.
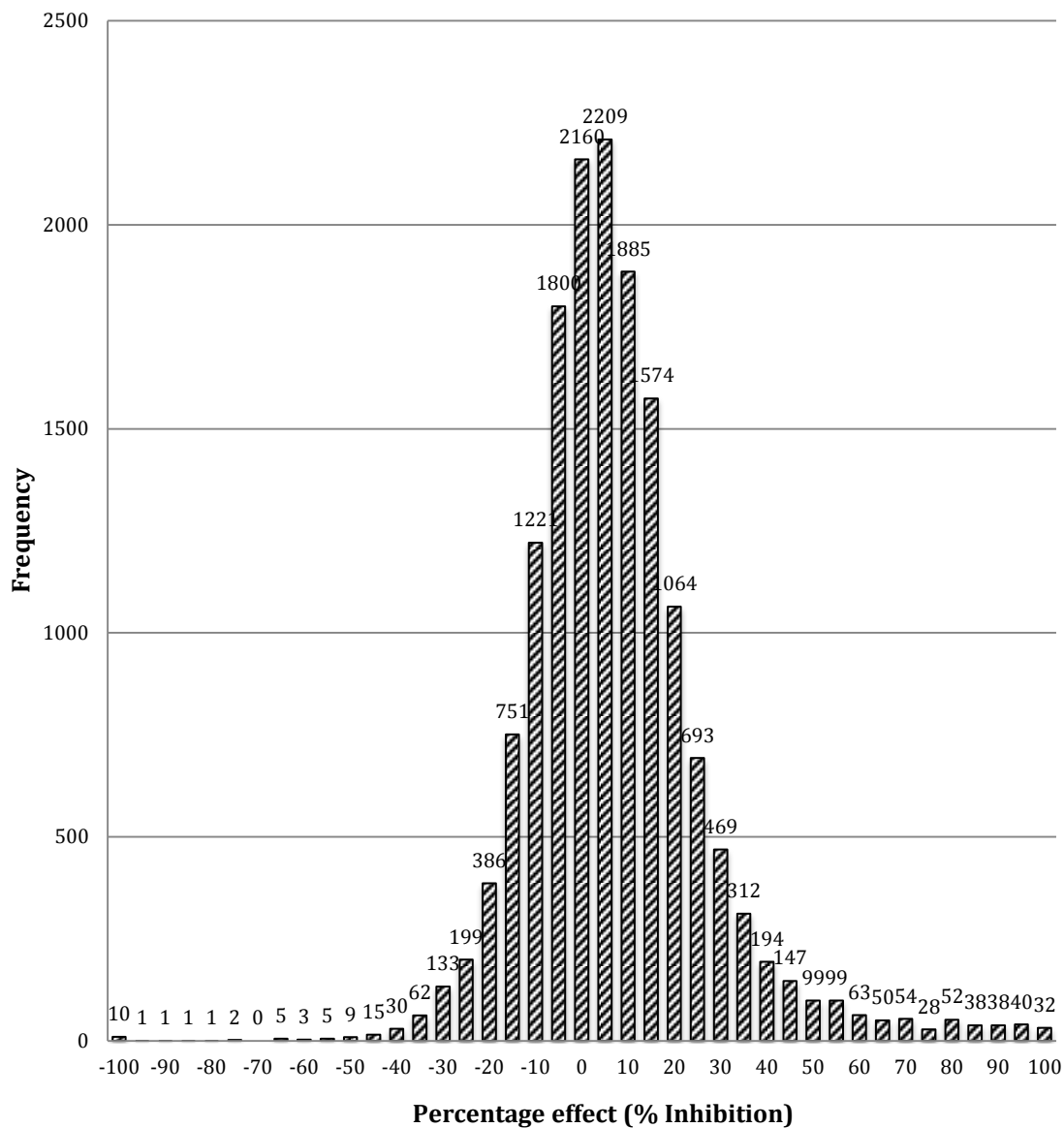
**Figure 5.4 Primary HTS against A549.pr(ISRE)GFP-RSV/hNS2.** Frequency distribution of the 16,000 screened compounds (Maybridge library) plotted against their percentage effect (% inhibition of GFP signal). % Effect = $100 - [100 \times (\text{experimental value} - \text{AVG}_{-IFN}) / (\text{AVG}_{+IFN} - \text{AVG}_{-IFN})]$, where AVG stands for average value of the +IFN controls ($\text{AVG}_{+IFN}$) or -IFN controls ($\text{AVG}_{-IFN}$)
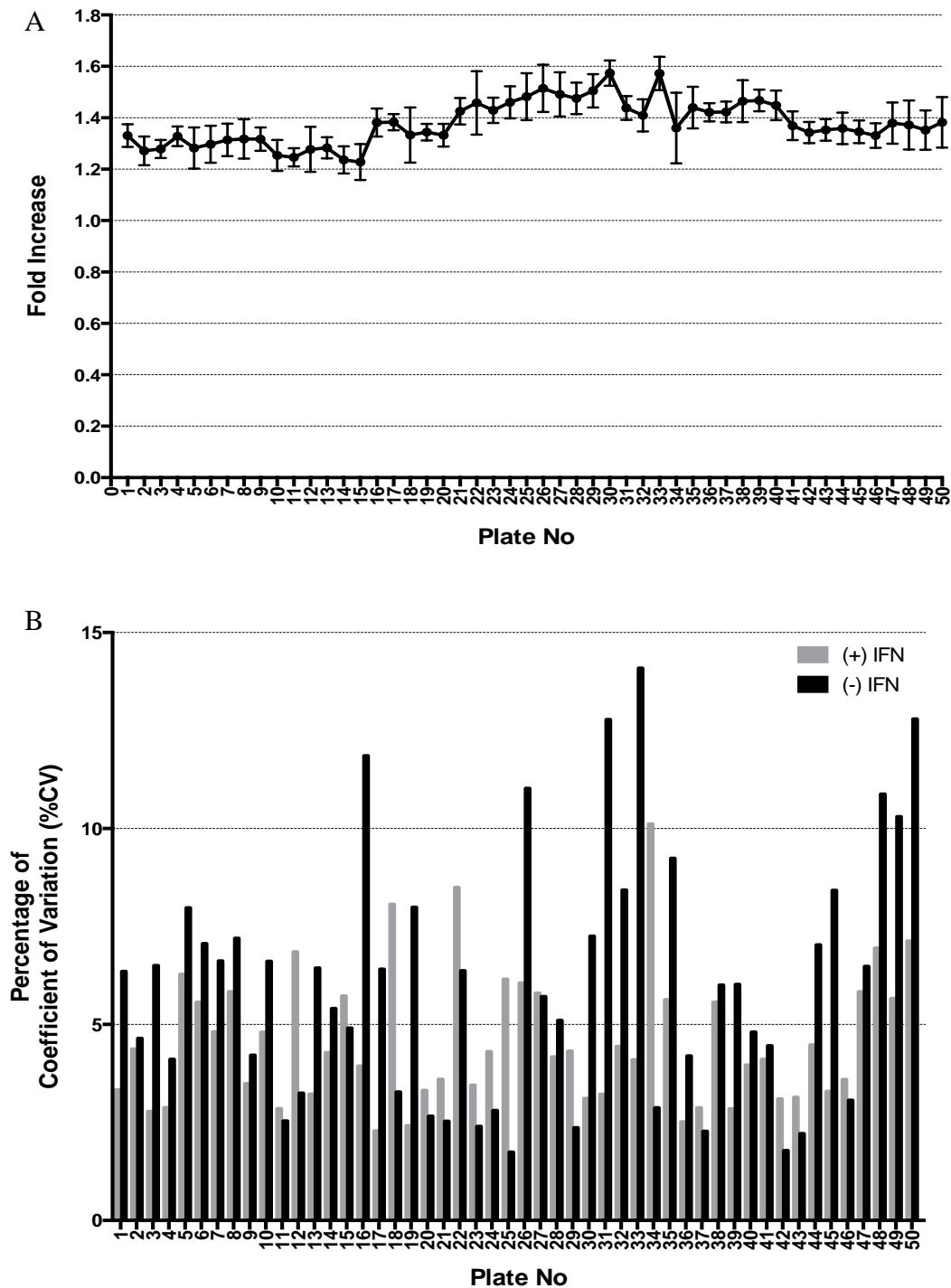
**Figure 5.5 Statistical analysis of the primary screen.** The A549.pr(ISRE)GFP-RSV/hNS2 cell-line was subjected to HTS using a library of 16,000 compounds. The screen was conducted in 5 batches of ten plates **(A)** Fold Increase in GFP expression (n=32, error bars=SD). **(B)** %CV for the +IFN and -IFN controls. The statistical analysis was carried out separately for each assay plate (n=50).

## 5.2.3 Selection of compounds via restoration in GFP expression

The hit selection process was carried out into two steps; hits were initially selected from the primary screen and then, a confirmatory screen analysis was performed to increase the likelihood of obtaining a set of small molecules that have a specific inhibitory activity against RSV NS2.

### 5.2.3/1 Hit selection from the primary screen

The first selection of potential hits was based on the % effect of the compounds. Specifically, compounds that restored GFP expression at 50% above the background levels (GFP signal of IFN-treated controls) were selected for further analysis (Figure 5.6). Based on the percentage effect cut-off (-50% inhibition), the primary screen led to the identification of thirty-eight small molecules, which restored fluorescent signal in the A549.pr(ISRE)GFP-RSV/hNS2 cell-line (Figure 5.6). In addition to the % effect, hits were selected using the Z-Score parameter (also known as standard score), which indicates how many standard deviations (SD) a particular compound is above or below the signal mean of the plate (Goktug *et al.,* 2013).  In our study, hits were designated as molecules that had Z-Score of 3, hence restored GFP expression ≥ three standard deviations above the sample signal mean (mean + 3SD). From the thirty-eight compounds that scored ≥ 50% GFP restoration (Figure 5.6), ten did not pass the 'mean + 3SD' cut-off, and therefore they were excluded from further analyses (data not shown). This led to the identification of 28 potential hits, which increased fluorescent signal 50% above the IFN-treated control in the A549.pr(ISRE)GFP-RSV/hNS2 cell-line, and had Z-Score equal to 3.
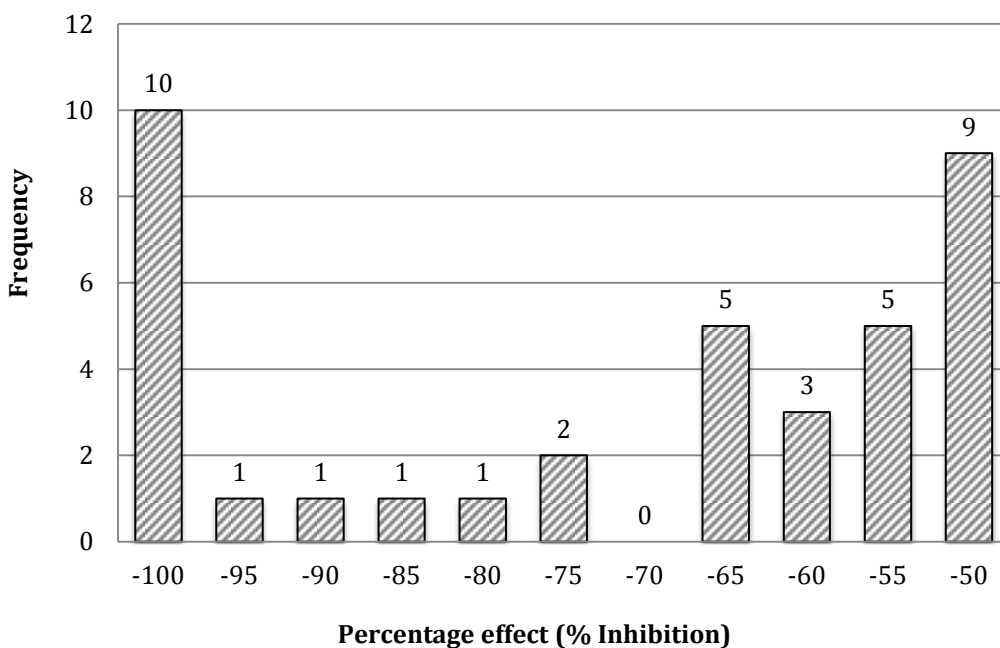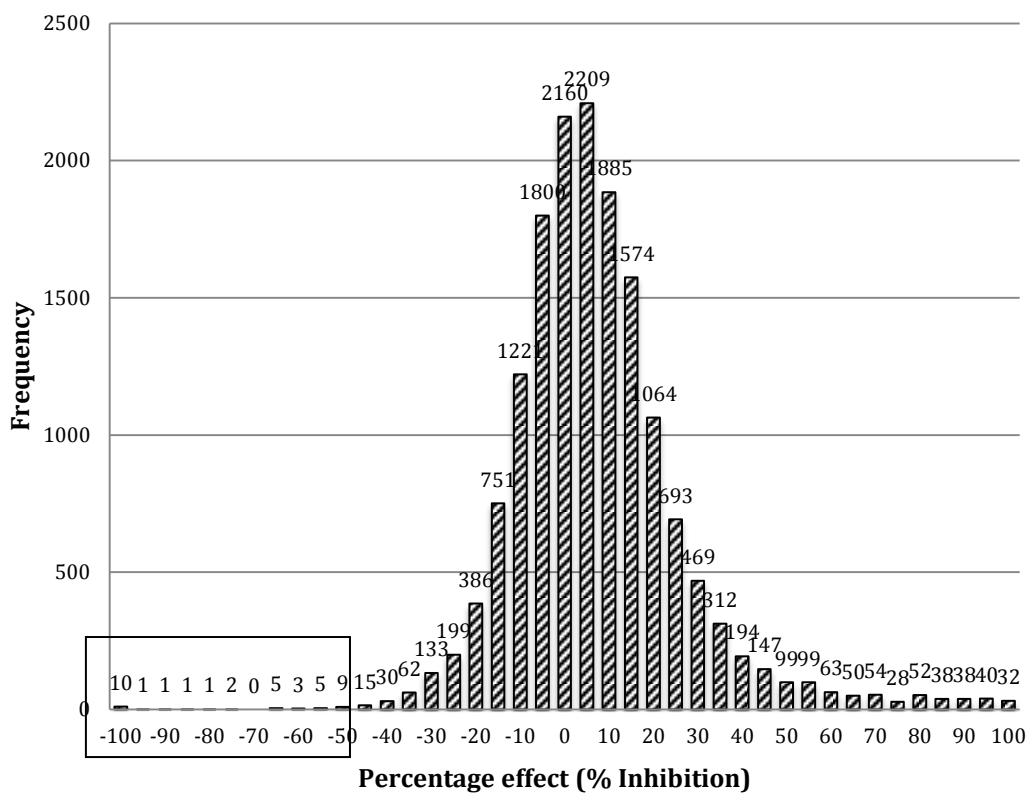
**Figure 5.6 Hit compound selection from primary screen.** Percentage (%) effect shows the level of restoration in GFP expression in the A549.pr(ISRE)GFP-RSV/hNS2 cell-line.The % effect cut-off of our assay was 50% and 38 compounds had increased the GFP signal 50% above the high signal control (IFN-treated control).

In order to analyze these hits further, we measured their fold increase in fluorescent signal (Figure 5.7). HIT-6 and HIT-13 had a fold increase equal to 5.5 and 6.8, respectively, which is higher than the maximum fold increase in GFP expression ever observed in the parental GFP reporter cell line, A549.pr(ISRE)GFP (Figure 5.7). Therefore, these compounds were eliminated, as they were highly likely to be auto-fluorescent compounds. The fold increase of the HIT-5 was at the borderline, and therefore it was not eliminated at this stage (Figure 5.7). Overall, the primary screen against RSV NS2 was successfully performed, leading to the identification of twenty-six compounds, which significantly restored fluorescent signal in the A549.pr(ISRE)GFP-RSV/hNS2 reporter cell-line.
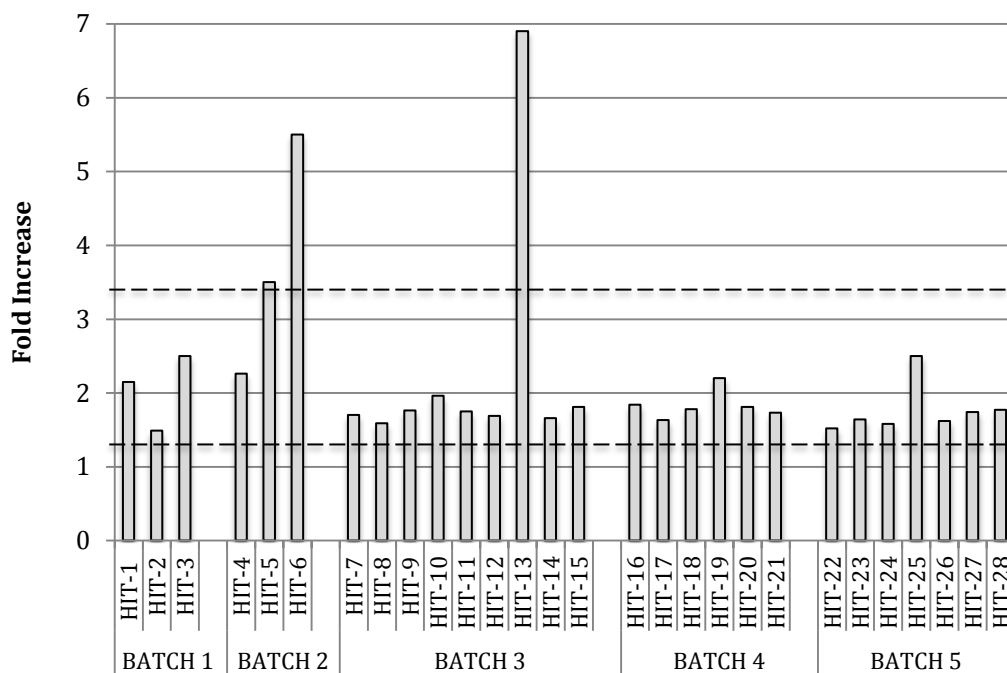


**Primary Screen**

**Figure 5.7 Fold increase in fluorescent signal of the identified twenty-eight hits.** The bottom line shows the fold increase in GFP expression after IFN treatment of the A549.pr(ISRE)GFP-RSV/hNS2 cell-line, the average of which was equal to 1.37 during the primary screen. The top line marks the maximum fold increase of the A549.pr(ISRE)GFP cell-line, which is equal to 3.4.

## 5.2.3/2 Hit selection from the confirmatory screen

The twenty-six selected hits were further validated with a confirmatory screen, during which the activity of the compounds was tested more thoroughly and any other auto-fluorescent compounds were dismissed. The primary screen was conducted at a single concentration (11.42 μM), whereas during the confirmatory screen the selected compounds were tested at various concentrations ranging from 0.1 μM to 50 μM and plotted against their GFP signal to assess whether they form dose-response curves. Specifically, the compounds were cherry-picked from the library plates and tested against: (i) the A549.pr(ISRE)GFP-RSV/hNS2 to confirm their ability to restore GFP expression in our assay, and (ii) growth media to test whether the observed increase in GFP signal was due to auto-fluorescence (Figures 5.8 - 5.10). At this stage, the twenty-six selected compounds were renamed using an AV prefix (AV-1 – AV-26).

The confirmatory screen showed that fourteen of the identified hits produced fluorescent signal when serially diluted in A549.pr(ISRE)GFP-RSV/hNS2 reporter cell-line and also in growth media (Figure 5.8). Most of the compounds were only slightly auto-fluorescent at concentrations around 10 μM (Log10=1) (Figure 5.8), explaining why we did not detect such a high increase in fluorescent signal during the primary screen. Hit compounds, including AV-5, AV-9 and AV-20, were highly auto-fluorescent at concentrations above 10 μM (Log10=1), causing saturation of fluorescent signal in both conditions tested (Figure 5.8). Hit compounds AV-2, AV-7 and AV-15 were less auto-fluorescent, as they produced less fluorescent signal and only at high concentrations (Figure 5.8). Regardless their differences in auto-fluorescence, all fourteen compounds that produced fluorescent signal in growth media were disregarded.

Overall, 57% of the hits were false-positives, since sixteen compounds (including HIT-6 and HIT-13) were found to be auto-fluorescent.
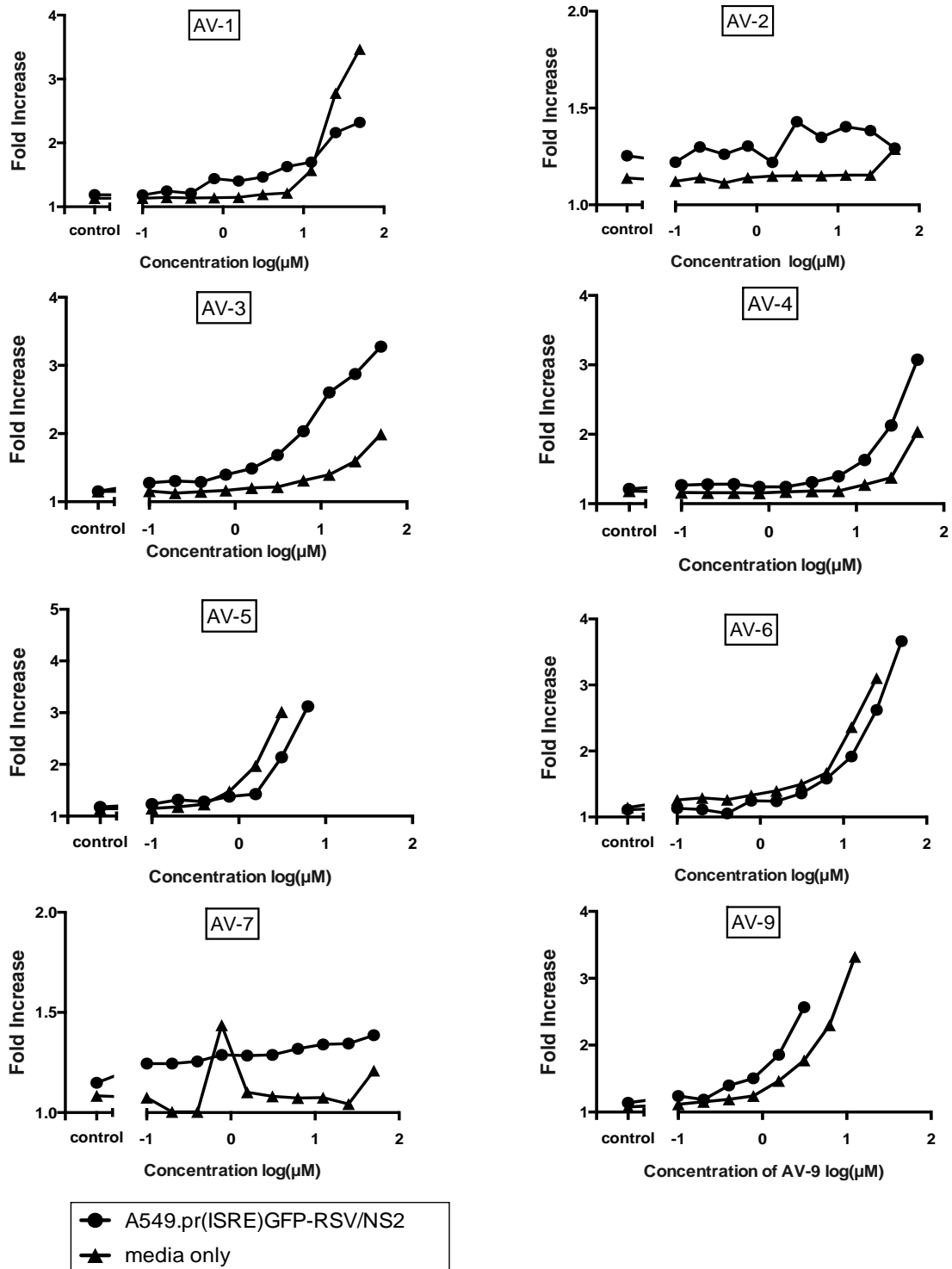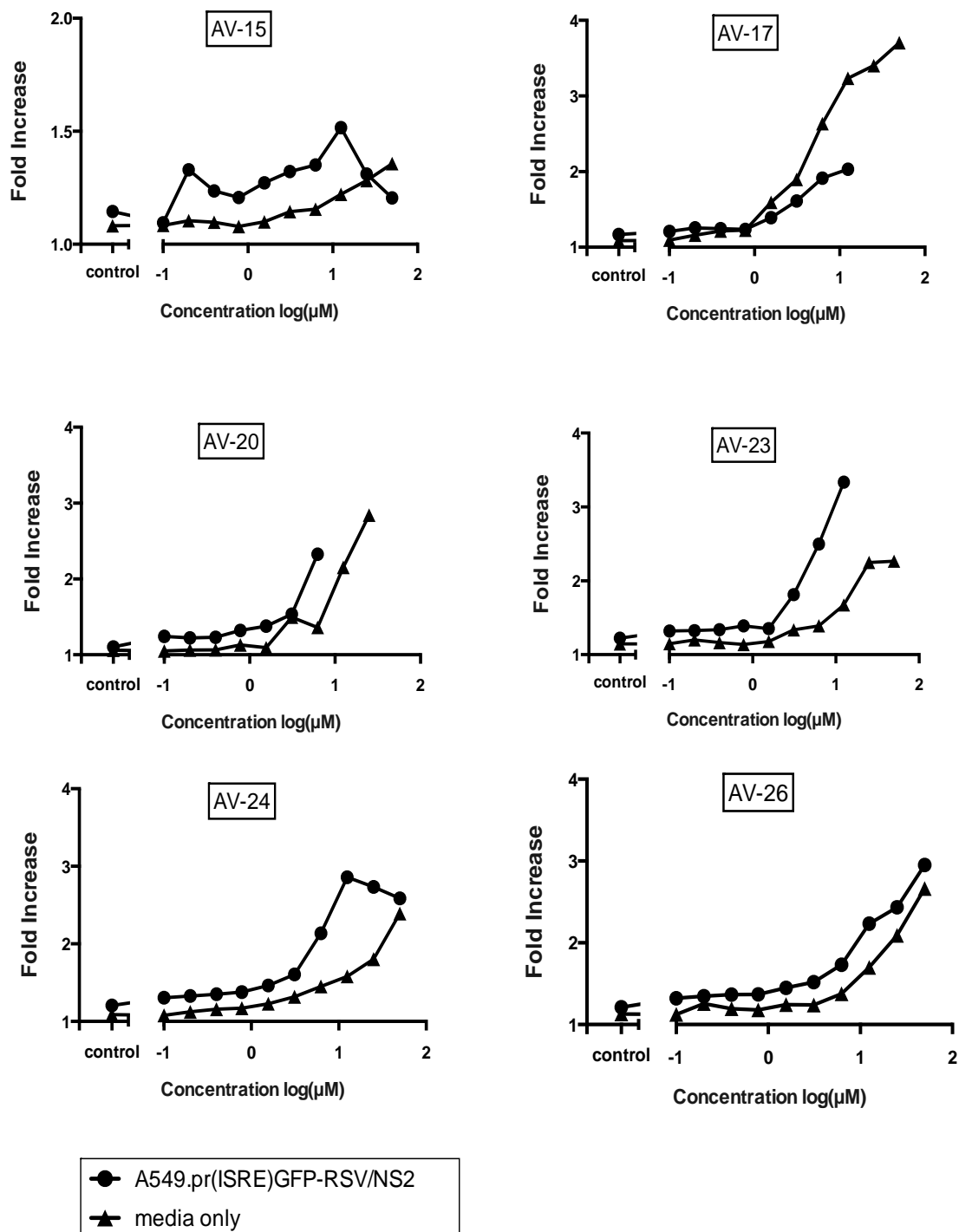
**Figure 5.8 Confirmatory Screen: Auto-fluorescent hit compounds.** Graphs are presented as a fold increase in fluorescent signal. Compounds were serially diluted in A549.pr(ISRE)GFP-RSV/hNS2 cell-line and growth media. The serial dilutions of the compounds range from 0.10 μM (log10= -1) to 50 μM (log10= 1.69). The control values show the fluorescent signal in the + IFN ($10^4$ U/ml), + DMSO control. The discontinued lines are due to 'overflow' values, which had fluroscent signal higher to the reading capacity of TECAN plate reader.

In addition to the auto-fluorescent compounds, another three hit compounds (AV-12, AV-21 and AV-22) were eliminated, as they had no activity during the confirmatory screen (Figure 5.9). These compounds produce no fluorescent signal in the A549.pr(ISRE)GFP-RSV/hNS2 reporter cell-line and neither did in growth media (Figure 5.9). Another hit, AV-25, was eliminated mainly due to toxicity. Although hit AV-25 restored GFP signal in the A549.pr(ISRE)GFP-RSV/hNS2 reporter cell-line without being auto-fluorescent, we observed that fluorescent signal was declining at concentrations higher than 10 μM (Log10=1), indicating that AV-25 was perhaps toxic at higher concentrations (Figure 5.9). Due to the nature of our assay, toxicity was not a major concern, because the compounds were selected based on GFP restoration. For instance, a toxic compound is less likely to be selected from our screen, because the reduction is cell numbers would also reduce GFP signal. Supporting our hypothesis, the identified toxic compound AV-25 showed toxicity only at concentrations higher than the screening concentration (11.42 μM) (Figure 5.9). Although toxicity could be simply identified by a decline in GFP signal, as observed for AV-25 (Figure 5.9), cell densities were also monitored during the primary and confirmatory screens by crystal violet staining (data not shown).

Interestingly, eight compounds (AV-8, AV-10, AV-11, AV-13 AV-14, AV-16, AV-18, AV-19) increased fluorescent signal in the A549.pr(ISRE)GFP-RSV/hNS2 without being auto-fluorescent, as they did not produce any signal in growth media (Figure 5.10). More precisely, the compounds AV-8, AV-14, AV-16, AV-18, AV-19 caused higher GFP restoration than the AV-10, AV-11, AV-13 compounds; AV-8, AV-14, AV-16, AV-18 and AV-19 had a maximum fold increase around 1.6, whereas AV-10, AV-11 and AV-13 had a maximum fold increase ranging from 1.4 to 1.5 (Figure

5.10). Regardless their differences in fold increase, all of these compounds increased

GFP signal in the A549.pr(ISRE)GFP-RSV/hNS2 reporter cell-line without being auto-

fluorescent, hence showing promising activity.
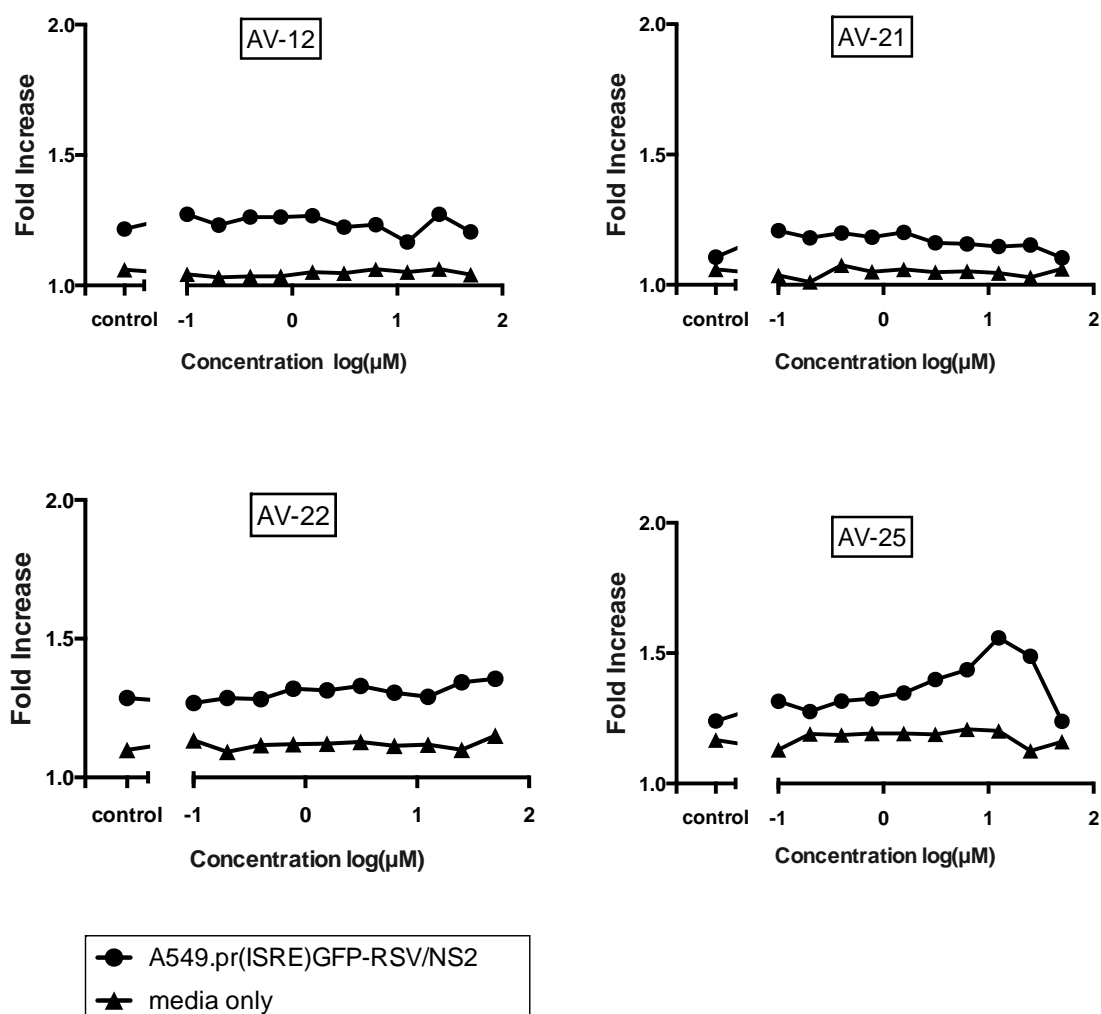


**Figure 5.9 Confirmatory screen: False-positives and a toxic compound.** Graphs are presented as a fold increase in fluorescent signal. Compounds were serially diluted in A549.pr(ISRE)GFP-RSV/hNS2 cell-line and growth media. The serial dilutions of the compounds range from 0.10 μM (log10= -1) to 50 μM (log10= 1.69). The compounds AV-12, AV-21 and AV-22 showed no activity, whereas compound AV-25 showed toxicity at higher concentrations. The control values show the fluorescent signal in the + IFN ($10^4$ U/ml), + DMSO control.
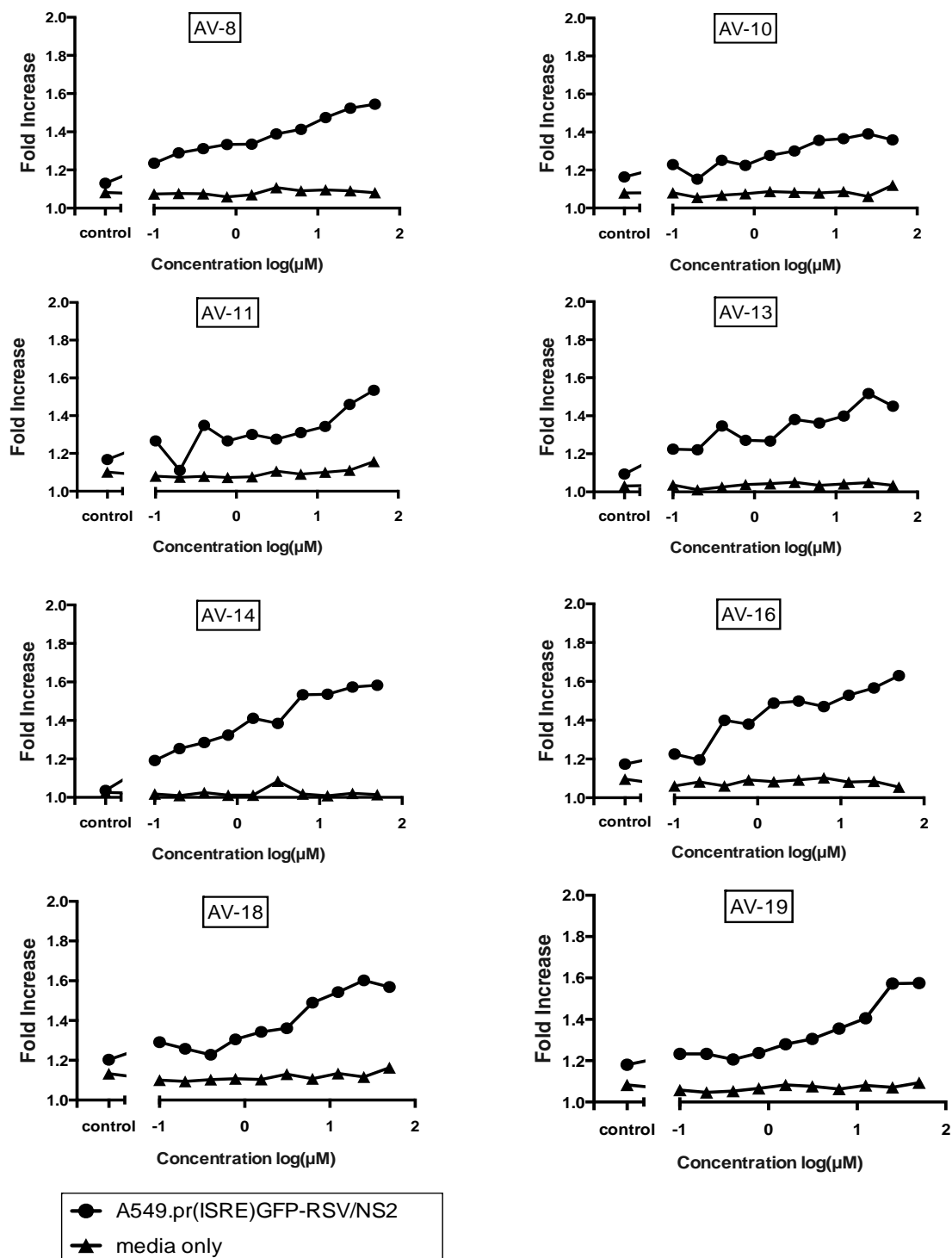
**Figure 5.10 Confirmatory screen: Hit compounds.** Graphs are presented as a fold increase in fluorescent signal. Compounds were serially diluted in A549.pr(ISRE)GFP-RSV/hNS2 cell-line and growth media. The serial dilutions of the compounds range from 0.10 μM (log10= -1) to 50 μM (log10= 1.69). Compounds with prosing activity did not fluorescent in growth media, and showed GFP restoration in the NS2-expressing cell-line. The control values show the fluorescent signal in the + IFN ($10^4$ U/ml), + DMSO control.

These eight hit compounds did not produce fluorescent signal in growth media, however this does not exclude the possibly that they could produce fluorescent byproducts when metabolized in the cellular environment, hence increasing fluorescent signal in the A549.pr(ISRE)GFP-RSV/hNS2 cell-line. To assess this possibility, the eight hit compounds were tested in naïve A549 cells and the A549.pr(ISRE)GFP-RSV/hNS2 reporter cell-line in the absence or presence of IFN-α treatment and fluorescent signal was observed with fluorescent microscopy (Figure 5.11). Interestingly, none of the compounds produced fluorescent signal in the A549 cells in the absence or presence of IFN-α, confirming that the compounds are not auto-fluorescent and do not produce fluorescent metabolic byproducts in cells (Figure 5.11). Likewise, no fluorescent signal was detected in the A549.pr(ISRE)GFP-RSV/hNS2 following compound treatment in the absence of IFN-α (Figure 5.11). In agreement with our previous observations (Figure 5.10), all compounds restored GFP expresion in the A549.pr(ISRE)GFP-RSV/hNS2 in the presence of IFN-α (Figure 5.11). In conclusion, this data confirms that compounds AV-8, AV-10, AV-11, AV-13 AV-14, AV-16, AV-18 and AV-19 are not auto-fluorescent and shows that the observed increase in fluorescent signal is due to restoration in GFP expression in the A549.pr(ISRE)GFP-RSV/hNS2 cell-line.

The identified compounds are minimally substituted heterocyclic building blocks, especially designed for drug discovery by Maybrigde (Table 5.2). As designated by Lipinski's 'Rule of 5', all of these compounds have molecular weight less than 500 Da (Table 5.2). Their minimal substitution allows easier interpretation of structure-activity relationship (SAR), and subsequently more straightforward lead optimization.
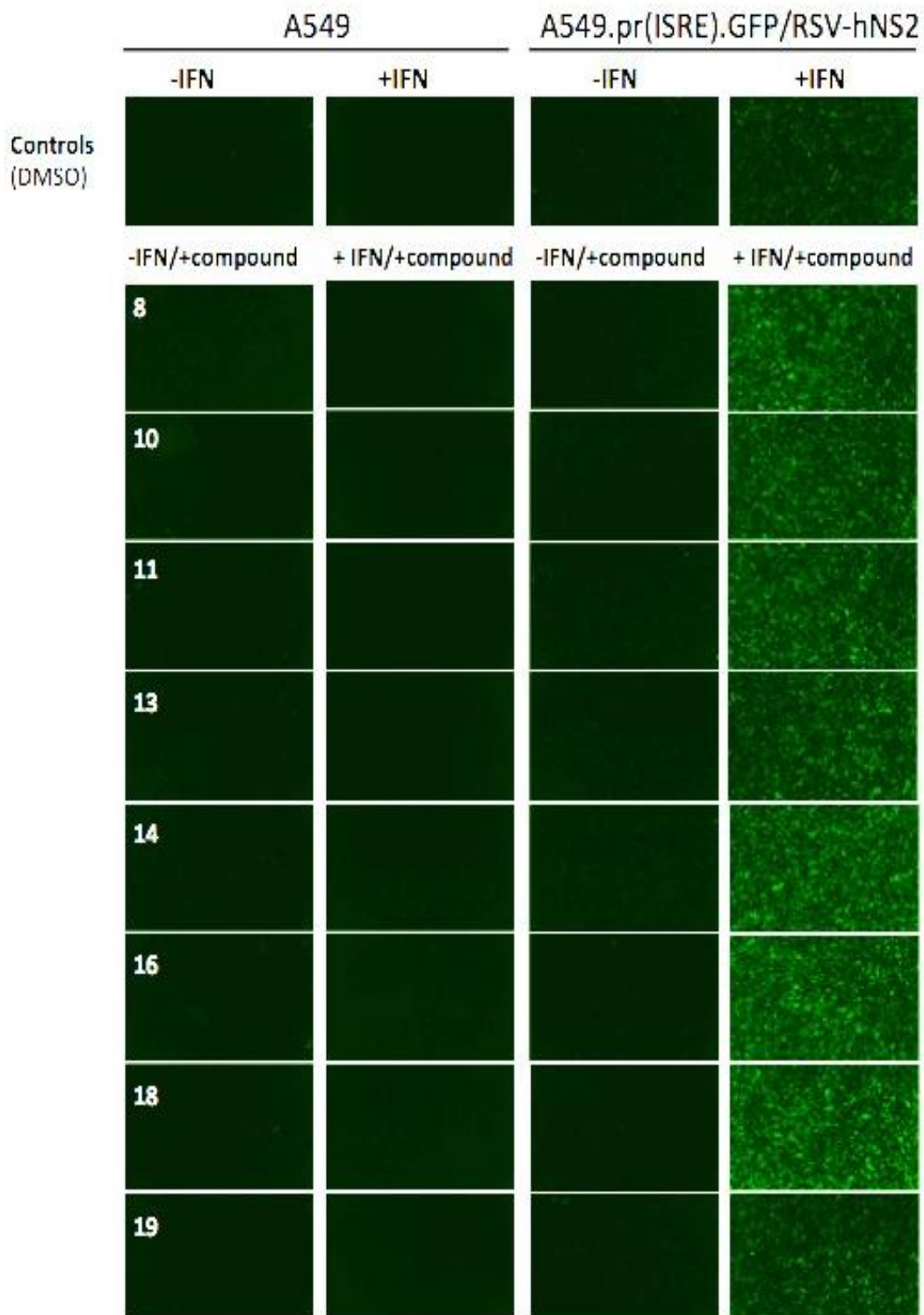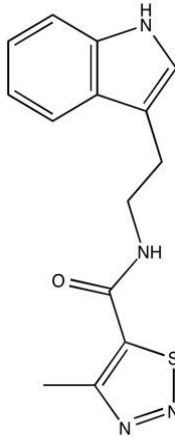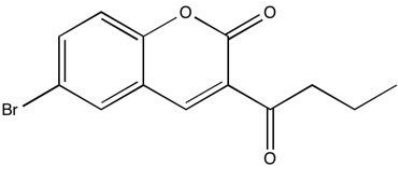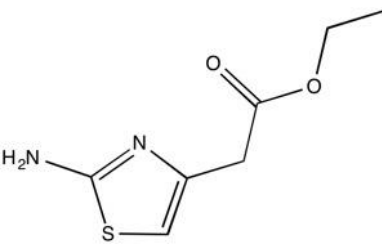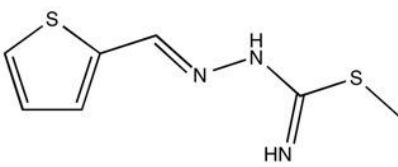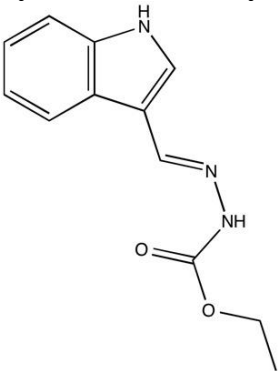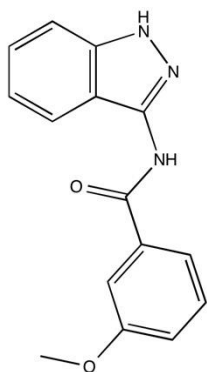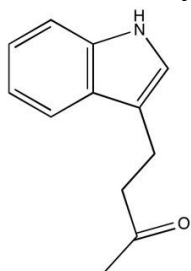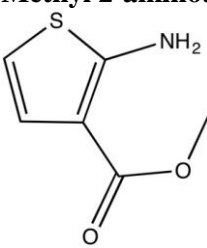
**Figure 5.11 The eight hit compounds restored GFP expression in A549.pr(ISRE)GFP-RSV/hNS2 cell-line, without producing fluorescent signal in A549 naïve cells.** Cells were treated with 25 μM of each compound for 2 hours and then treated with IFN-α ($10^4$ U/ml) for 48 hours. Fluorescent images were taken with IncuCyte cell imager at 10X magnification.

**Table 5.2 Compounds' CAS number, molecular weight (MW), chemical name and chemical structures.** The chemical structures were drawn using the ChemBioDraw software.

| | CAS Number Maybrigde Code | MW(Da) | Chemical Structure |
|---|---|---|---|
| AV-8 | **661475-55-4/** CD06524 | 286.358 | **N-[2-(1H-indol-3-yl)ethyl]-4-methyl-1,2,3-thiadiazole-5-carboxamide** |
| AV-10 | **2199-83-9/** BTB06399 | 295.13 | **6-bromo-3-butyryl-2H-chromen-2-one** |
| AV-11 | **53266-94-7/** SB00646 | 186.234 | **Ethyl 2-(2-amino-1,3-thiazol-4-yl)acetate** |
| AV-13 | **92635-79-5/** BTB05216 | 199.301 | Methyl N-(2-thienylmethylidene)-aminomethanehydrazonothioate |

| | GAS Number/ Maybrigde Code | MW (Da) | Chemical Name and Structure |
|---|---|---|---|
| AV-14 | **15641-27-7/** ML00232 | 231.254 | **Ethyl2-(1H-indol-3 ylmethylidene) hydrazine-1-carboxylate**  |
| AV-16 | **883054-87-3/** SP01362 | 267.287 | **N-(1H-indazol-3-yl)-3-methoxybenzamide**  |
| AV-18 | **5541-89-9/** NRB02761 | 187.2407 | **4-(1H-indol-3-yl)butan-2-one**  |
| AV-19 | **4651-81-4/** GK02784 | 157.1923 | **Methyl 2-aminothiophene-3-carboxylate**  |

## 5.3 Summary

The robustness and reproducibility of our 384-well format HTS assay was successfully demonstrated through statistical assessment. The assay fulfilled the DDU QC requirements, as it had a fold increase (S/B) = 2.5, %CV < 6 and Z' factor > 0.65. Once the quality of the assay was shown to be suitable for HTS, a primary screen was conducted in-house for the identification of small molecule inhibitors of RSV NS2. The A549.pr(ISRE)GFP-RSV/hNS2 was subjected to HTS using a chemical library of 16,000 small molecules. The primary screen was performed using in-house liquid handling equipment, and screen's consistency and validity was demonstrated through statistical analysis (fold increase = 1.37, %CV < 7). The frequencies of the 16,000 screened compounds were normally distributed against their percentage effect (% inhibition), and compounds were selected based on two criteria; compounds were classified as hits when GFP expression was 50% above the background levels and were characterized by a Z-Score of 3. This led to the selection of twenty-eight hits that significantly increased fluorescent signal in the A549.pr(ISRE)GFP-RSV/hNS2 cell-line. Hence, the hit rate of our screen was 0.175% (28 hits out of 16,000), however hit rates typically observed in antagonist or inhibitor format assays are usually around 2-3% (Hughes *et al.,* 2011). This is due to the fact that although we are searching for NS2 inhibitors, our assay is based on restoration in GFP signal and hit rates tend to be lower (<0.5%) in assays that compound selection is based on an increase in assay signal rather than a decrease in signal (Hughes *et al.,* 2011).

Following the primary screen, the twenty-eight selected hits were further characterized based on their ability to generate dose-response curves in the A549.pr(ISRE)GFP-RSV/hNS2 cell-line. The confirmatory screen also allowed us to

eliminate false-positives. Overall, from the twenty-eight initially identified hits, 57% were auto-fluorescent (sixteen compounds), 11% were eliminated because they showed no activity (three compounds) and 3% due to toxicity (one compound), and lastly 29% of the selected hits showed promising activity (eight compounds). The eight hit compounds mediated a significant increase in GFP signal without being auto-fluorescent, and particularly, the AV-8, AV-14, AV-16, AV-18, AV-19 compounds resulted into a higher fold increase in GFP expression than the AV-10, AV-11, AV-13 compounds. The rest of this thesis will focus on the characterization and validation of these eight candidate compounds that significantly restored GFP expression in the A549.pr(ISRE)GFP-RSV/hNS2 cell-line.

# Chapter 6: Hit compound characterization to demonstrate their activity against RSV NS2 function

## 6.1 Introduction

The primary HTS against RSV NS2 led to the identification of eight compounds namely AV-8, AV-10, AV-11, AV-13, AV-14, AV-16, AV-18 and AV-19 that restored GFP expression in the A549.pr(ISRE)GFP-RSV/hNS2 cell-line in a reproducible manner. These compounds were purchased from the Maybridge Company and further characterized, in order to (i) confirm their ability to restore GFP fluorescence signal in the NS2-expressing cell-line and determine their $EC_{50}$ values, (ii) test the stability of their activity and their cytotoxicity, (iii) assess their specificity against NS2, (v) evaluate their mechanism of action with respect to inhibition of NS2-mediated STAT2 degradation, and finally (v) test their ability to restrict RSV replication.

## 6.2 Results

### 6.2.1 Verification of hit compounds ability to restore GFP expression in the A549.pr(ISRE)GFP-RSV/hNS2 cell-line

The activity of the purchased compounds was reassessed with two-fold dose-response curves ranging from 0.01 μM to 50 μM (Figure 6.1). In the absence of compounds, the A549.pr(ISRE)GFP-RSV/hNS2 cell-line had an average fold increase in GFP expression around 1.32, when treated with IFN-α (Figure 6.1). This is in

agreement with our previous data, as during primary screen the cell-line had a fold increase of 1.37. As anticipated, all compounds restored GFP expression but at different levels, with compounds AV-14, -16, -18 and -19 resulting in a higher fold increase in GFP expression (Figure 6.1). The fold increase was significantly increased, ranging from 1.83 to 1.96, in the presence of compounds AV-14, -16, -18 and -19 (Figure 6.1; Table 6.1). The rest of the compounds, AV-8, -10, -11 and -13, were less effective, and led to a lower GFP restoration in the A549.pr(ISRE)GFP-RSV/hNS2 cell-line, ranging from 1.44 to 1.69 (Figure 6.1; Table 6.1). This data confirms the results of the primary screen (Figure 5.10), and indicates that hit compounds can be categorized into two groups based on their activity; group A composed of AV-14, -16, -18 and -19 compounds, which were more potent, and group B composed of AV-8, -10, -11 and -13 compounds, which had a weaker activity (Table 6.1).

In addition to the fold increase in GFP expression, the activity of the compounds was further characterized regarding their $EC_{50}$ values, which determines the concentration of compound that provokes a response halfway between the lowest and higher response (Goktug *et al.,* 2013). The identified compounds had different $EC_{50}$ values; AV-10, -13, and -19 had $EC_{50}$ values within a single μM range (1-2 μM), whereas the $EC_{50}$ values of AV-8, -14, -16 and -18 lay within low μM range (0.2-0.8 μM) (Figure 6.1; Table 6.1). AV-11 had the highest $EC_{50}$ value (419.4 μM) of all the compounds (Figure 6.1). Although some of the compounds had good $EC_{50}$, they had very weak activity, as indicated by their low fold increase (Table 6.1). Hence, the rest of this chapter will focus on the compounds of Group A, which had a fold increase in GFP expression above 1.8 and reproducible $EC_{50}$ values in the single μM range or lower (Table 6.1).
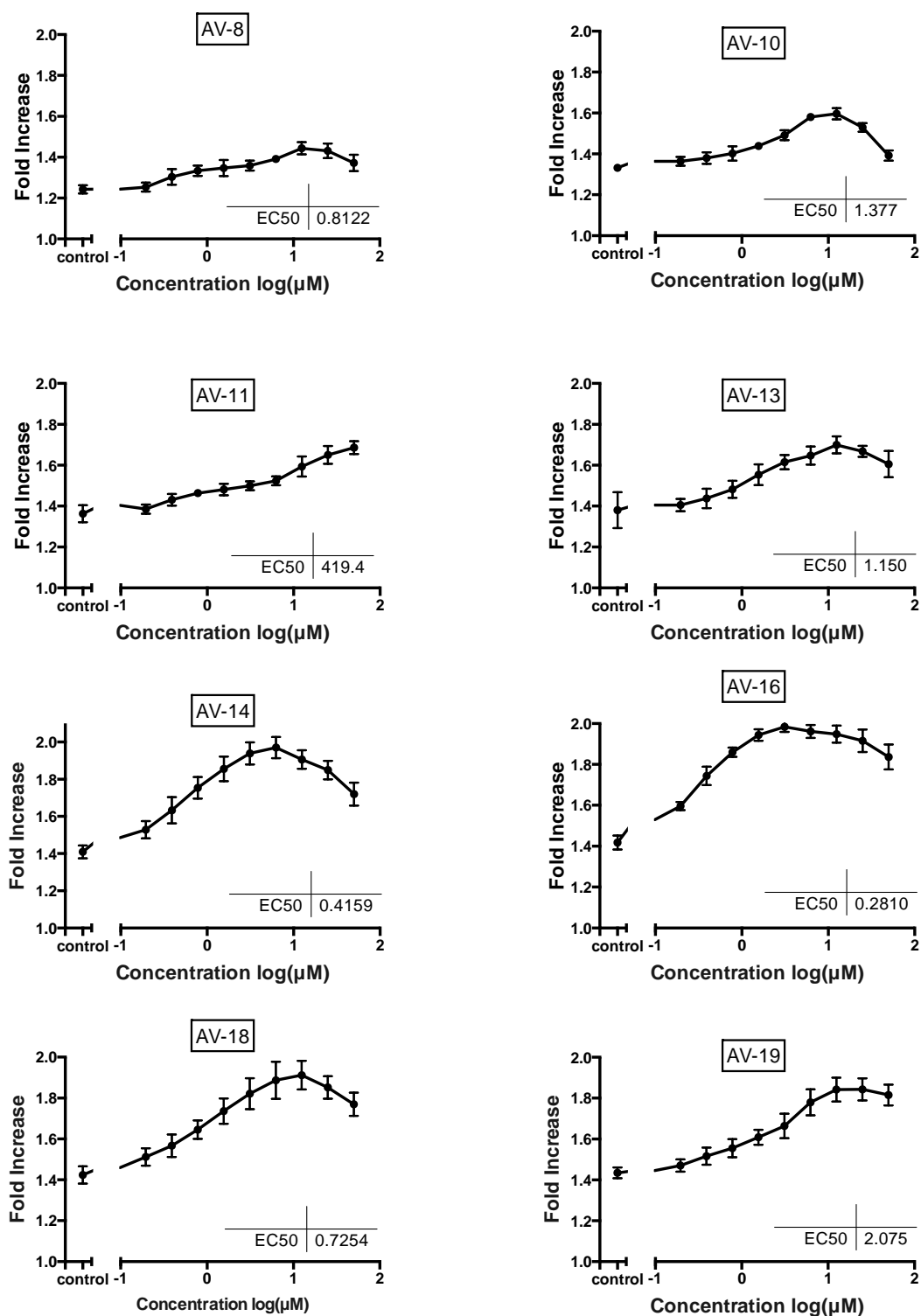
**Figure 6.1. Dose-response curves demonstrating restoration of GFP expression in the A549.pr(ISRE)GFP-RSV/hNS2 cell-line, in the presence of selected compounds.** Dose-response curves range from 0.10 μM (log10= -1) to 50 μM (log10= 1.69). The control values show the fluorescent signal in the +IFN ($10^4$ U/ml), +0.05% [v/v] DMSO control. The $EC_{50}$ (μM) values were calculated using Prism (GraphPad) software. Curves represent mean values (n=8), error bars=SD.

**Table 6.1 Hit Ranking based on fold increase in GFP expression.**

|  |  | HIT | Fold increase | EC$_{50}$ (µM) |
|---|---|---|---|---|
| **Group A** | 1 | AV-16 | 1.96 | 0.28 |
|  | 2 | AV-14 | 1.94 | 0.42 |
|  | 3 | AV-18 | 1.90 | 0.73 |
|  | 4 | AV-19 | 1.83 | 2.08 |
| **Group B** | 5 | AV-13 | 1.69 | 1.15 |
|  | 6 | AV-11 | 1.67 | 419.4 |
|  | 7 | AV-10 | 1.61 | 1.37 |
|  | 8 | AV-8 | 1.44 | 0.81 |

## 6.2.2 Exploring the properties of hit compounds regarding stability, cytotoxicity and chemical structure

6.2.2/1 Hit compounds activity remained stable over a six day period

In order to evaluate compounds stability over time, compounds were incubated with A549 naïve cells or growth media for up to six days, and then tested for their ability to restore GFP expression in the A549.pr(ISRE)GFP-RSV/hNS2 cell-line. Interestingly, the same level of GFP restoration was observed for all the samples tested, regardless of incubation time, with the exception of compound AV-14, which showed a small reduction in activity at later time points (Figure 6.2). Specifically, AV-14 activity was 27% reduced, after a 6-day incubation with A549 cells. Incubating the compounds in the presence of A549 naïve cells or plain growth media had no effect on compounds' activity, as restoration of GFP expression was the same between the samples taken from cells or growth media (Figure 6.2). Overall, this data suggests that the activity of all eight compounds was stable over a period of six days, with only exception being AV-14, which showed a slight reduction in activity at later time points.
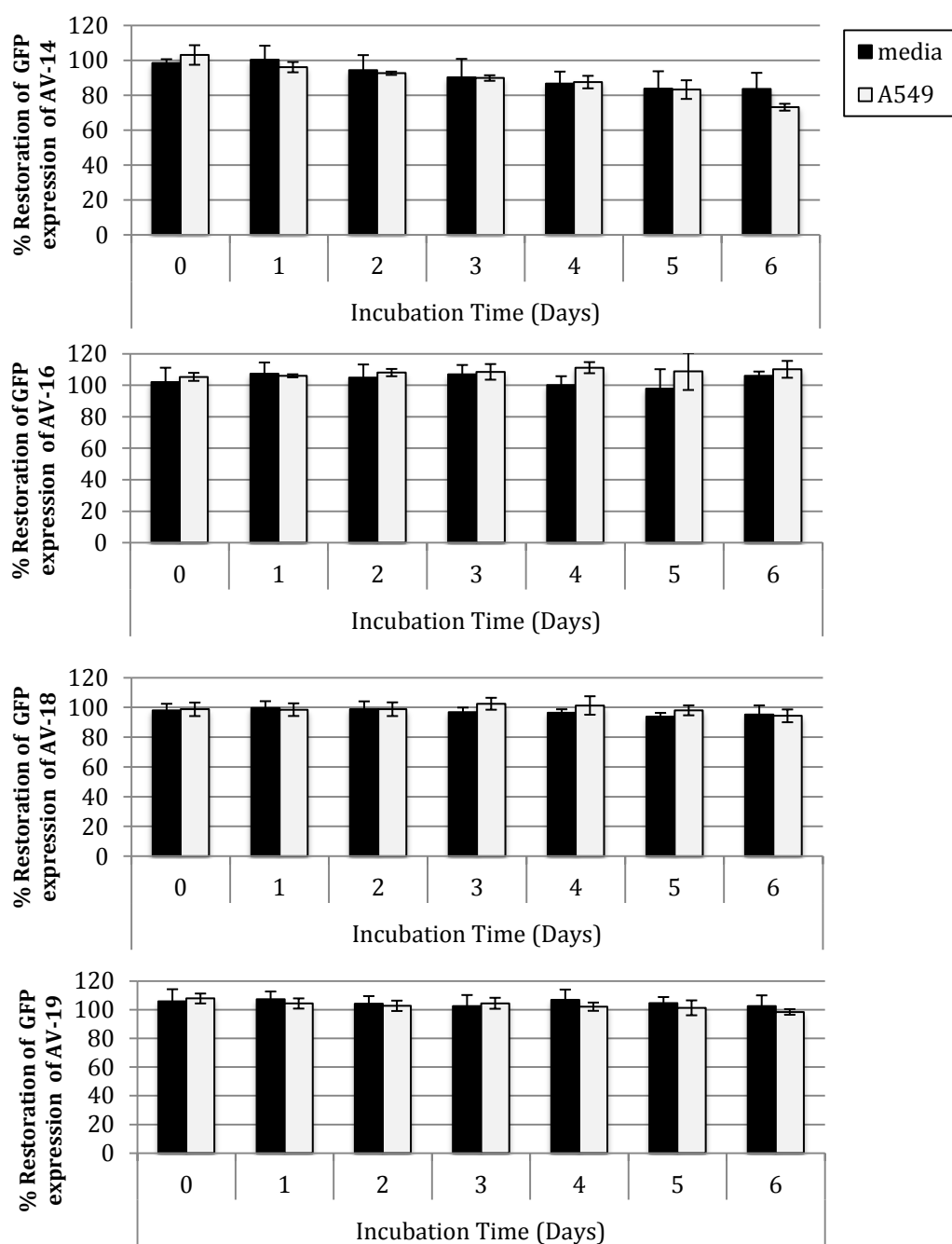
**Figure 6.2 Testing the stability of compounds activity.** 10 μM of each compound was incubated over A549 naïve cells or growth media only, and a sample was collected from each flask for six days. At the end of the assay, samples were added to A549.pr(ISRE)GFP-RSV/hNS2 cell-line, and compounds ability to restore GFP was measured and compared to fresh compound. The graphs are presented as percentage (%) of restoration in GFP expression relative to fresh compounds, which was set as 100%. Absorbance of crystal violet (A650 nm) was used for normalizing the GFP signal to cell density. Bars show mean values (n=3), error bars=SD.

## 6.2.2/2 Compounds showed no cytotoxicity in the A549.pr(ISRE)GFP-RSV/hNS2 cell-line

The compounds' effect on cell viability was monitored throughout the primary and confirmatory screen using crystal violet staining. Crystal violet dye penetrates cell membranes and allows detection of cell density, however it does not show if the compounds have any effect on the cell's metabolism. In contrast, AlamarBlue[TM] is a more sensitive assay, which assesses the viability of mammalian cells based on their ability to metabolically process the oxidized form of AlamarBlue reagent (resazurin) to the reduced form of AlamarBlue reagent, which is the highly red fluorescent resofurin (Hamid *et al.,* 2004). Therefore, the level of AlamarBlue reagent reduction is a quantitative measure, which shows cell viability based on metabolic activity. Our results demonstrated that A549.pr(ISRE)GFP-RSV/hNS2 cell-line was capable of almost fully reducing (80% reduction) the AlamarBlue reagent (Figure 6.3). The ability of the cells to reduce AlamarBlue was not affected by the presence of hit compounds, indicating that none of the compounds is cytotoxic (Figure 6.3). In agreement with the crystal violet staining, this data confirms that the identified compounds do not induce toxicity effects.
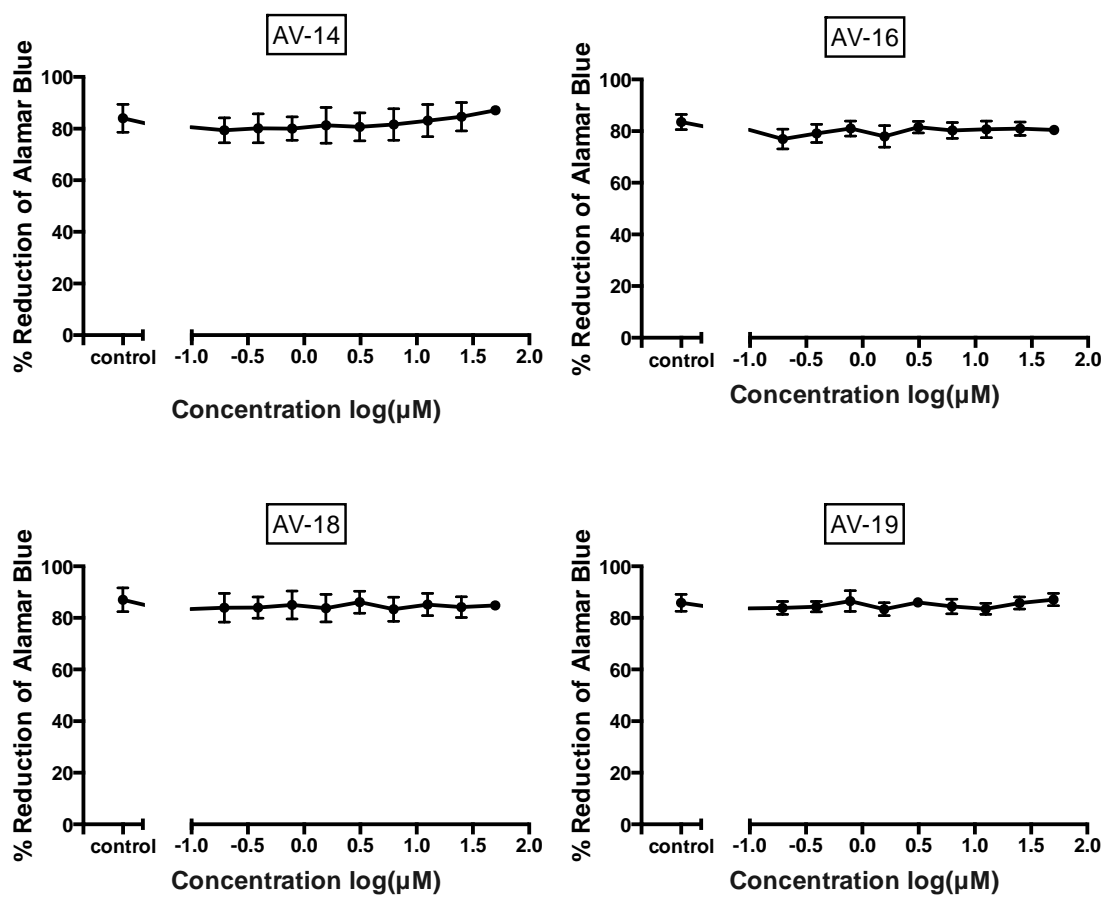
**Figure 6.3 Compounds showed no cytotoxicity by AlamarBlue cell viability assay.**
Compounds was serially diluted in concentrations ranging from 0.10 μM (log10= -1) to 50 μM (log10= 1.69) on A549.pr(ISRE)GFP-RSV/hNS2 cells for 48 hours. The level of AlamarBlue reduction was measured based on fluorescence using the TECAN plate reader. Graphs show mean values (n=6), error bars=SD.

## 6.2.2/3 Compounds AV-14, AV-16, AV-18 represent chemically related series with an indole structure

Hit compounds belong to the Maybridge chemical library, which consists of heterocyclic compounds that are well-known for their good pharmacological properties (Biswal *et al.,* 2012). The identified compounds represent minimally substituted building blocks for drug discovery, with ring structures that are

functionalized with a selection of synthetically useful reactive groups[2] (Table 5.2).

Interestingly, three of the compounds of Group A (AV-14, -16 and -18) shared

structural similarity, as they contained an indole ring (Figure 6.4/A). Indole is an

aromatic heterocyclic organic compound, which consists of a six-membered benzene

ring fused to a five-membered nitrogen-containing pyrrole ring (Figure 6.4/A) (Biswal

*et al.,* 2012).

To assess the importance of the indole ring in NS2 inhibition, the indole

compound (Sigma) was tested against the A549.pr(ISRE)GFP-RSV/hNS2 cell-line,

and GFP fluorescent signal was quantified (Figure 6.4/B). Our results showed that

high concentration of indole (25 μM/ log10=1.39) slightly increased GFP levels in the

A549.pr(ISRE)GFP-RSV/hNS2 cell-line (Figure 6.4). Specifically, indole mediated a

fold increase in GFP expression equal to 1.45, whereas the indole-containing

compounds AV-14, -16 and -18 had a maximum fold increase of 2 (Figure 6.4).

Overall, our results showed that the indole compound alone was not enough to

sufficiently block NS2-mediated suppression of GFP in the A549.pr(ISRE)GFP-

RSV/hNS2 cell-line. This suggests that the indole ring might have a role in NS2

inhibition, but the observed restoration of GFP expression is not strictly linked to this

structure. Hence, structure-activity relationship (SAR) experiments are required to

define the relative importance of the indole ring and molecules' side chains in NS2

inhibition.

---

[2] Supplementary information about the chemical structures of the Maybridge library:
http://www.maybridge.com/portal/alias__Rainbow/lang__en/tabID__23/DesktopDefault.aspx

A



B
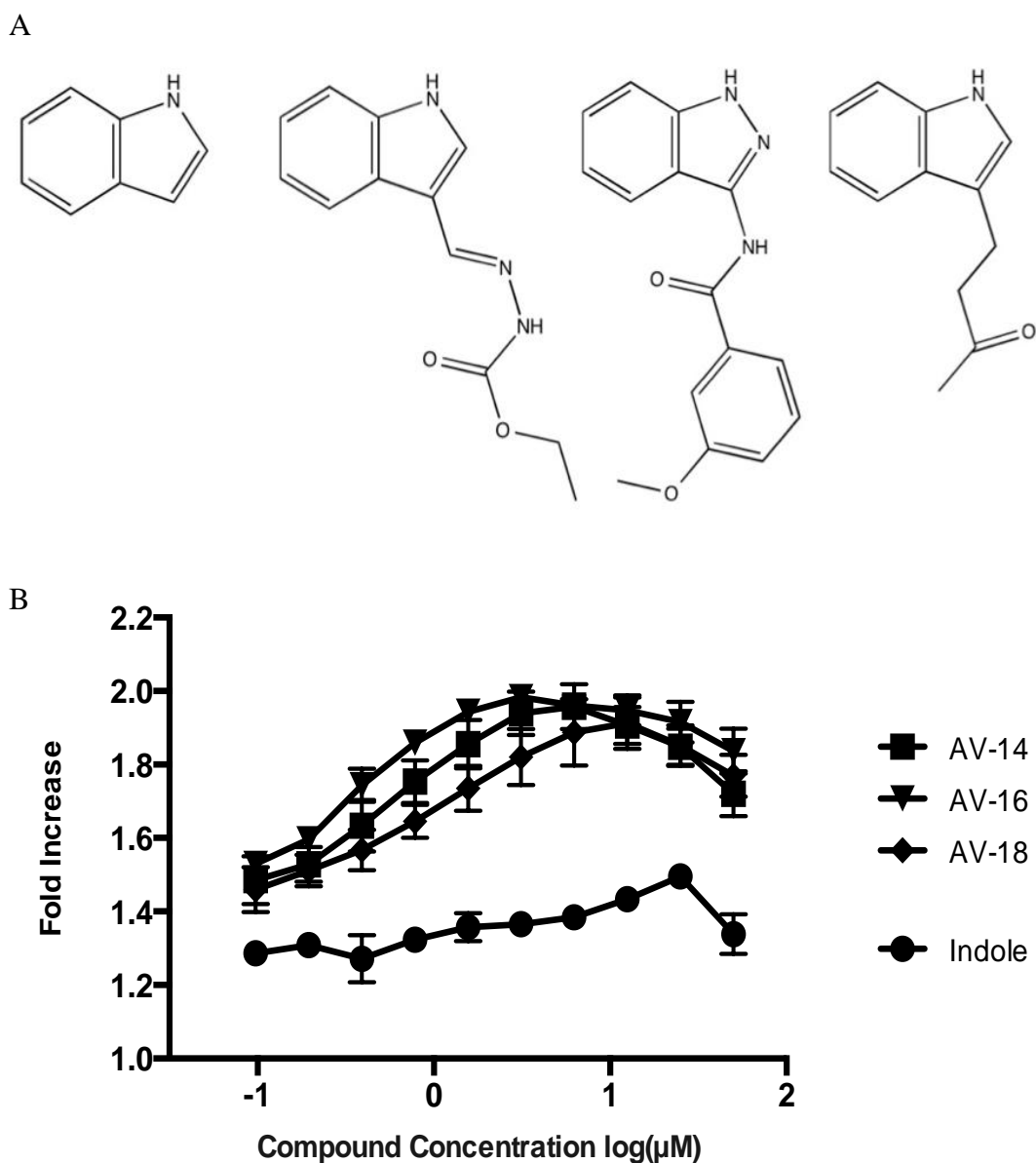


**Figure 6.4 Effect of indole ring on restoration of GFP expression in the A549.pr(ISRE)GFP-RSV/hNS2 cell-line.** (**A**) Chemical structures of indole, AV-14, AV-16 and AV-18 (from left to right). (**B**) Indole and indole-containing compounds AV-14, -16, -18 were serially diluted against A549.pr(ISRE)GFP-RSV/hNS2 cell-line and incubated for 2 hours, before adding IFN-α ($10^4$ U/ml). Dose-response curves range from 0.10 μM (log10= -1) to 50 μM (log10= 1.69). Graphs show mean values (n=6), error bars=SD.

## 6.2.3 Demonstrating compounds specificity to RSV NS2

### 6.2.3/1 Compounds activity is specific to cell-lines expressing RSV hNS2 and not other viral IFN antagonists

In order to demonstrate compounds specificity to RSV NS2, the compounds activity (restoration of GFP expression) was tested against a panel of cell-lines, some of which constitutively expressed other viral IFN antagonists. These were A549 naïve cells, the naïve A549.pr(ISRE)GFP reporter cell-line, and also A549.pr(ISRE)GFP derivatives that expressed: (i) RSV hNS1 protein (A549.pr(ISRE)GFP-RSV/hNS1), which is known to counteract the cellular IFN response using independent, as well as joint mechanisms with NS2 (Lo *et al.,* 2005; Swedan *et al.,* 2009; Swedan *et al.,* 2011), (ii) RSV hNS1 and hNS2 protein together (A549.pr(ISRE)GFP-RSV/hNS1.hNS2) and (iii) PIV5 V protein (A549.pr(ISRE)GFP-PIV5/V), a very potent antagonist of the IFN-signalling pathway, which degrades STAT1 through the proteasome (Didcock *et al.,* 1999).

Compounds AV-14, AV-16, AV-18 and AV-19 were serially diluted two-fold from 0.10 μM to 50 μM in the five cell-lines mentioned above (Figure 6.5). As anticipated, none of the compounds produced fluorescent signal in the A549 naïve cells, which again excludes the possibility of auto-fluorescence (Figure 6.5). The compounds had no impact on the ability of the A549.pr(ISRE)GFP reporter cell-line to produce GFP at concentrations below 10 μM (log10=1), however at concentrations above 10 μM, a small reduction in GFP expresssion was observed (Figure 6.5). Crystal violet staining showed that GFP reduction at higher concentrations was not due to cytotoxicity (data not shown), which is also confirmed by our previous data obtained with AlamarBlue assay (Figure 6.3). Despite the reduction observed at high compound

concentrations, this observation shows that none of the compounds induced GFP expression in any unspecific way.

In agreement with our previous data, all of the compounds induced GFP restoration in the A549.pr(ISRE)GFP-RSV/hNS2 reporter cell-line, mediating approximately a two fold increase in GFP expression (Figure 6.5). Interestingly, all the compounds also restored GFP expression in the NS1.NS2-expressing cell-line but only up to the GFP levels observed in the NS1-expressing cell-line (Figure 6.5). This demonstrates that compounds blocked NS2 function in the hNS1.hNS2-expressing cell-line without affecting NS1 function against the IFN-signalling pathway (Figure 6.5). This agreed with the observation that the compounds had no effect on GFP expression in the A549.pr(ISRE)GFP-RSV/hNS1 cell-line (Figure 6.5). In the PIV5/V-expressing cell-line, GFP expression levels remained stable to background levels (fold increase = 1) after compound treatment (Figure 6.5), showing that hit compounds had no effect on the ability of PIV5 V to antagonize the IFN-signalling pathway. Overall, GFP restoration was only observed in NS2-expressing cell-lines, A549.pr(ISRE)GFP-RSV/hNS2 and A549.pr(ISRE)GFP-RSV/hNS1.hNS2, indicating that identified small molecules are highly likely to be acting specifically against the anti-IFN functions of RSV NS2.
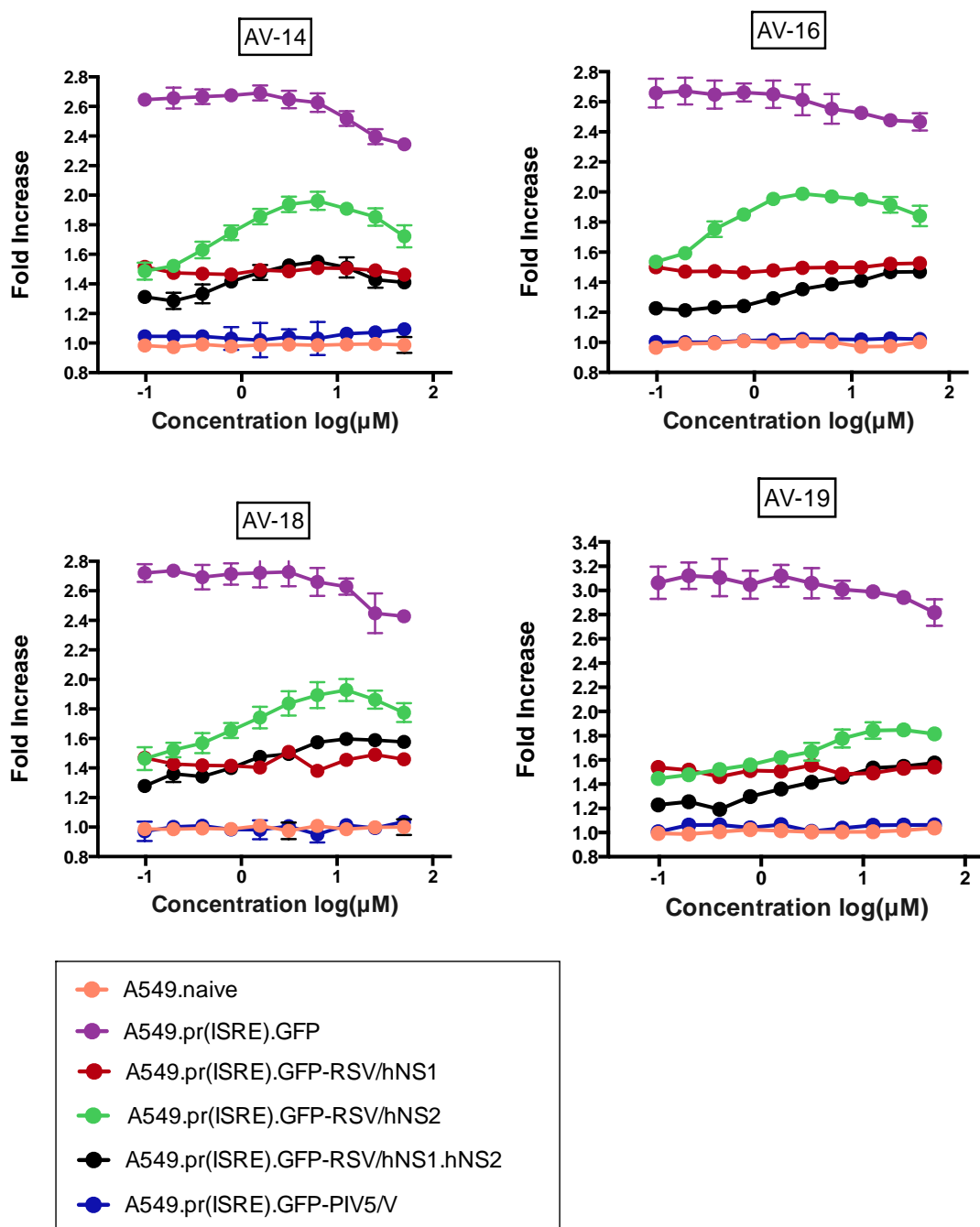
**Figure 6.5 Restoration of GFP expression was observed only in NS2-expressing cell-lines.** Group A compounds diluted on A549 naïve cells (orange), A549.pr(ISRE)GFP reporter cell-line (purple), A549.pr(ISRE)GFP derivatives that RSV/hNS1 (red), RSV/hNS2 (green) and RSV/hNS1.hNS2 (black), and PIV5/V (blue). Dose-response curves range from 0.10 µM (log10= -1) to 50 µM (log10= 1.69). Cells were treated with compound for 2 hours and then treated with IFN-$\alpha$ ($10^4$ U/ml) for 48 hours (n=3, error bars =SD).

154

## 6.2.3/2 Biological activity of the compounds was demonstrated via their ability to block NS2-mediated STAT2 degradation.

The most documented function of RSV NS2 against the IFN-signalling pathway is its ability to degrade STAT2 through the proteasome (Lo *et al.,* 2005; Ramaswamy *et al.,* 2004). As shown in Chapter 4, constitutive expression of RSV NS2 mediates STAT2 degradation in the A549.pr(ISRE)GFP-RSV/hNS2 cell-line. In order to demonstrate biological activity of the selected compounds, we tested their ability to block the NS2-mediated STAT2 degradation, in the A549.pr(ISRE)GFP-RSV/hNS2 cell-line (Figure 6.6). As expected, IFN-α treatment upregulated STAT2 in the A549.pr(ISRE)GFP cell-line and this was not affected by the presence of the hit compounds (Figure 6.6). In agreement with our previous observations, STAT2 expression was considerably reduced in the A549.pr(ISRE)GFP-RSV/hNS2 cell-line, even after IFN-α treatment (Figure 6.6). Specifically, quantification of STAT2 expression showed an 88% reduction in STAT2 levels in the A549.pr(ISRE)GFP-RSV/hNS2 cell-line after IFN-α treatment, compared to the naïve A549.pr(ISRE)GFP cell-line (Figure 6.6). Interestingly, STAT2 expression was increased in the A549.pr(ISRE)GFP-RSV/hNS2 cell-line in the presence of the hit compounds (Figure 6.6). All tested compounds caused approximately 30% increase in STAT2 expression, which is in agreement with our previous observations that demonstrated partial restoration of GFP expression by hit compounds.
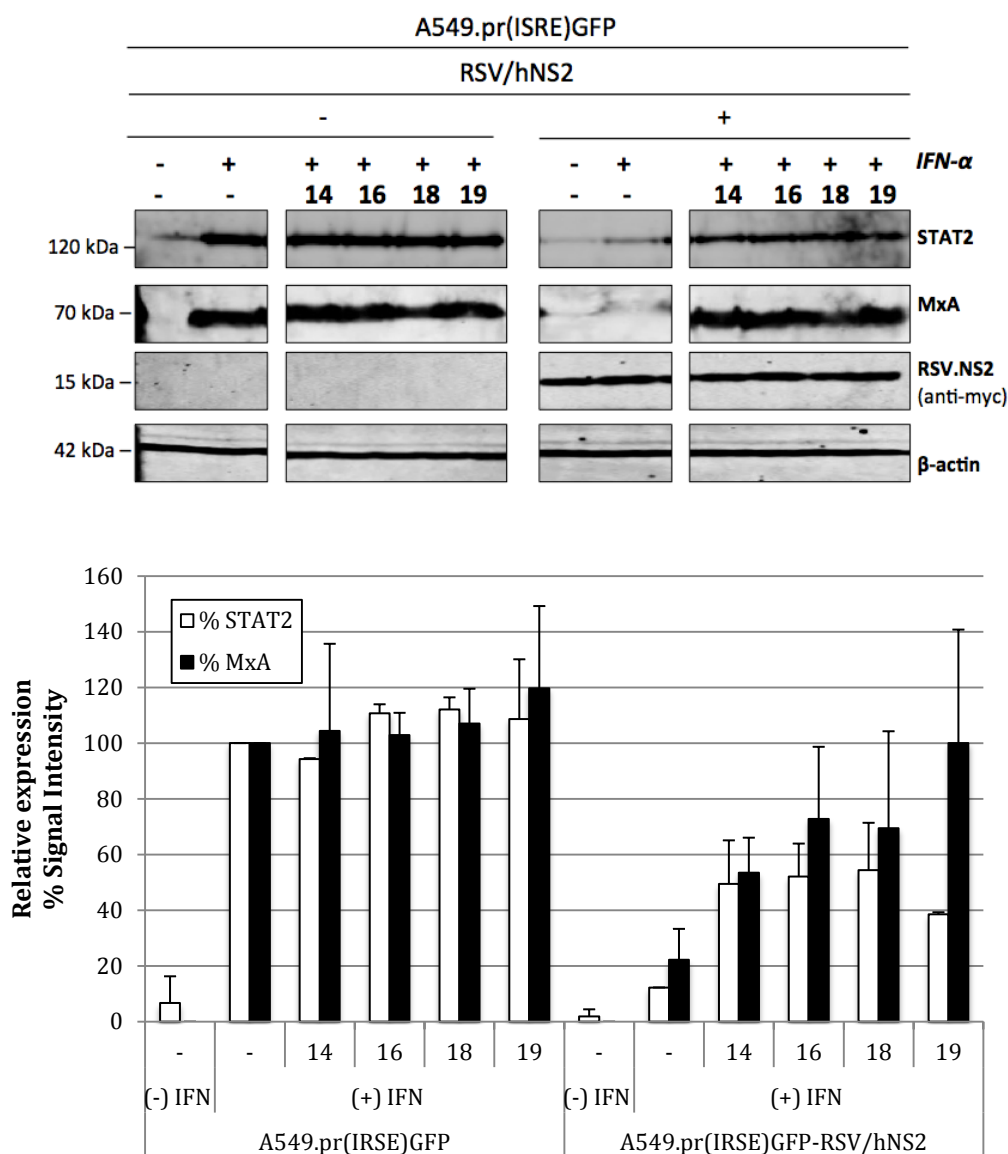
**Figure 6.6 STAT2 and MxA expression is increased after compound treatment in the A549.pr(ISRE)GFP-RSV/hNS2 reporter cell-lines.** A549.pr(ISRE)GFP and A549.pr(ISRE)GFP-RSV/hNS2 cell-lines were treated with 10 μM of compound or 0.05% [v/v] DMSO for 2 hours and then treated with IFN-α (2000 U/ml) for 24 hours, in the presence of the compound. STAT2 and MxA expression was observed with infrared fluorescent western blot analysis (Odyssey CLx imager) and quantified using the Image Studio™ software. Control and test samples run on the same gel to allow quantification. Stable NS2 expression was confirmed in the A549.pr(ISRE)GFP-RSV/hNS2 reporter cell-line. Graphs are presented as percentage (%) of relative STAT2 and MxA expression relative to DMSO/+IFN A549.pr(ISRE)GFP control, which was set as 100%. Mean values (n=3), error bars=SD.

In addition to STAT2 expression, we also tested the effect of the compounds on MxA expression in the A549.pr(ISRE)GFP and A549.pr(ISRE)GFP-RSV/hNS2 cell-lines (Figure 6.6). In the A549.pr(ISRE)GFP cell-line, MxA expression was highly upregulated after IFN-α treatment, in the absence or presence of hit compounds (Figure 6.6). As observed previously, MxA expression is reduced in the A549.pr(ISRE)GFP-RSV/hNS2 cell-lines due to the NS2 antagonism against the IFN-signalling pathway (Figure 6.6). Specifically, MxA expression was 87% reduced in the A549.pr(ISRE)GFP-RSV/hNS2 cell-line compared to the A549.pr(ISRE)GFP cell-line. Similar to STAT2 expression, MxA levels were increased after treatment with hit compounds (Figure 6.6). Specifically, all compounds increased MxA expression more than 50% compared to the DMSO control in the A549.pr(ISRE)GFP-RSV/hNS2 cell-line (Figure 6.6). Overall, this data demonstrates that hit compounds inhibited NS2-mediated STAT2 degradation, and subsequently increased MxA expression in the A549.pr(ISRE)GFP-RSV/hNS2 cells, which correlates with the ability of the hit compounds to mediate restoration of GFP expression.

To further explore compounds specificity, we tested whether the hit compounds are capable of blocking other viral IFN antagonists from degrading STAT2. To investigate this, the activity of compound AV-16 was tested against the PIV2 V protein. The PIV2 V protein circumvents the IFN-signalling pathway in a similar manner to RSV NS2 protein, as PIV2 V also mediates degradation of STAT2 and this proteolytic activity was found to be partially alleviated by proteasome inhibition (Parisien *et al.,* 2001). As anticipated, IFN-α treatment highly upregulated STAT2 in the A549.pr(ISRE)GFP cell-line and Hep2 naïve cells, whereas STAT2 expression was hardly detectable in their derivatives that expressed RSV hNS2 and PIV2 V,

respectively (Figure 6.7). As observed previously, AV-16 partially blocked the RSV/hNS2-mediated STAT2 degradation, but interestingly, had no effect on the PIV2/V-mediated degradation of STAT2 (Figure 6.7). We could not test differences in MxA expression, because Hep2 cells are MxA-deficient. Overall, the ability of the hit compound to inhibit STAT2 degradation appears to be specific to RSV NS2 protein, as AV-16 had no effect on the PIV2/V-mediated STAT2 degradation.
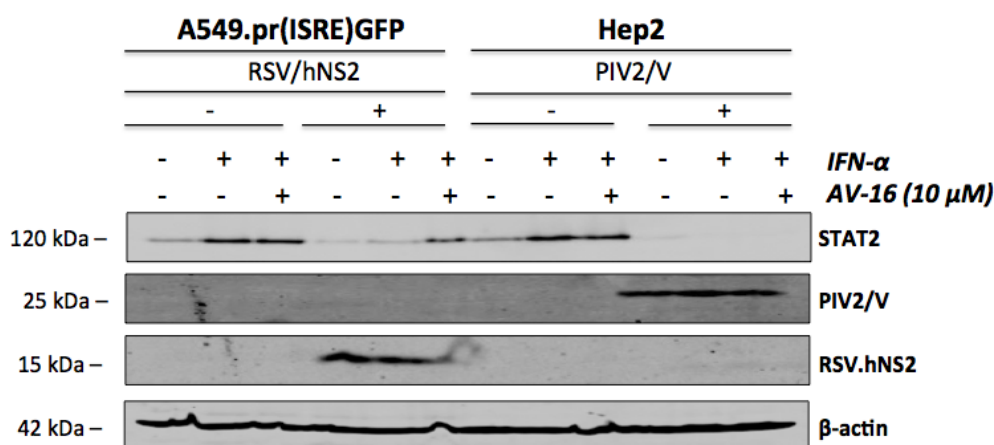


**Figure 6.7 Compound AV-16 had no effect on PIV5/V-mediated STAT2 degradation.** STAT2 levels were tested in cell-lines expressing the RSV/hNS2 and PIV2/V IFN antagonists, namely A549.pr(ISRE)GFP-RSV/hNS2 and Hep2-PIV2/V, respectively. Cells were treated with 10 μM of compound AV-16 for 2 hours and then treated with IFN (1000 U/ml) for 16 hours, in the presence of the compound. RSV.NS2 (anti-myc) and PIV2.V (anti-V5) proteins are also shown on the gel to confirm stable expression of the proteins.

To further explore the biological activity of the compounds, we tested their ability to inhibit the NS2-mediated STAT2 degradation in the context of virus infection *in vitro*. To achieve this, A549 naïve cells were infected with wtRSV, and then treated with AV-16, in the absence or presence of IFN-α (Figure 6.8). In agreement with published work (Ramaswamy *et al.*, 2006), our data showed that RSV infection

effectively blocked most of IFN response, which was activated in response to virus stimulus, as STAT2 levels were marginally increased (18% increase) following RSV infections compared to the mock control (Figure 6.8). Interestingly, when AV-16 compound was added following RSV infection, STAT2 expression was 30% higher, indicating that compound AV-16 partially inhibited the RSV-mediated STAT2 decrease (Figure 6.8). In addition, the virus suppressed STAT2 levels up to 50% in the presence of IFN-α treatment, when compared the -RSV/ +IFN control (Figure 6.8). The ability of the virus to reduce the IFN-mediated STAT2 upregulation was blocked by compound AV-16, leading to a 40% increase in STAT2 levels compared to +RSV/ +IFN control (Figure 6.8). In conclusion, this data indicates that the AV-16 partially inhibits the STAT2 degradation function of RSV, which is in agreement with observations made in our reporter assay.

In order to determine if the increase in STAT2 levels was enough to augment activation of the ISRE element, we tested MxA expression, which represents an end point of the IFN-signalling pathway. Consistent with previous obervations, RSV infection only partially blocked MxA expression, causing a 60% increase in MxA levels in the absence or precence of IFN-α treatment (Figure 6.8). Addition of compound AV-16 increased MxA levels; MxA levels were increased up to 80% in the absence of IFN-α and up to 95% in the presence of IFN-α (Figure 6.8). Taken together, the AV-16-mediated partial inhibition of RSV function against STAT2 increased MxA expression in reponse to RSV infection, demonstrating that the activity of the ISRE element is restored after compound treatment in the A549.pr(ISRE)GFP-RSV/hNS2 cell-line.
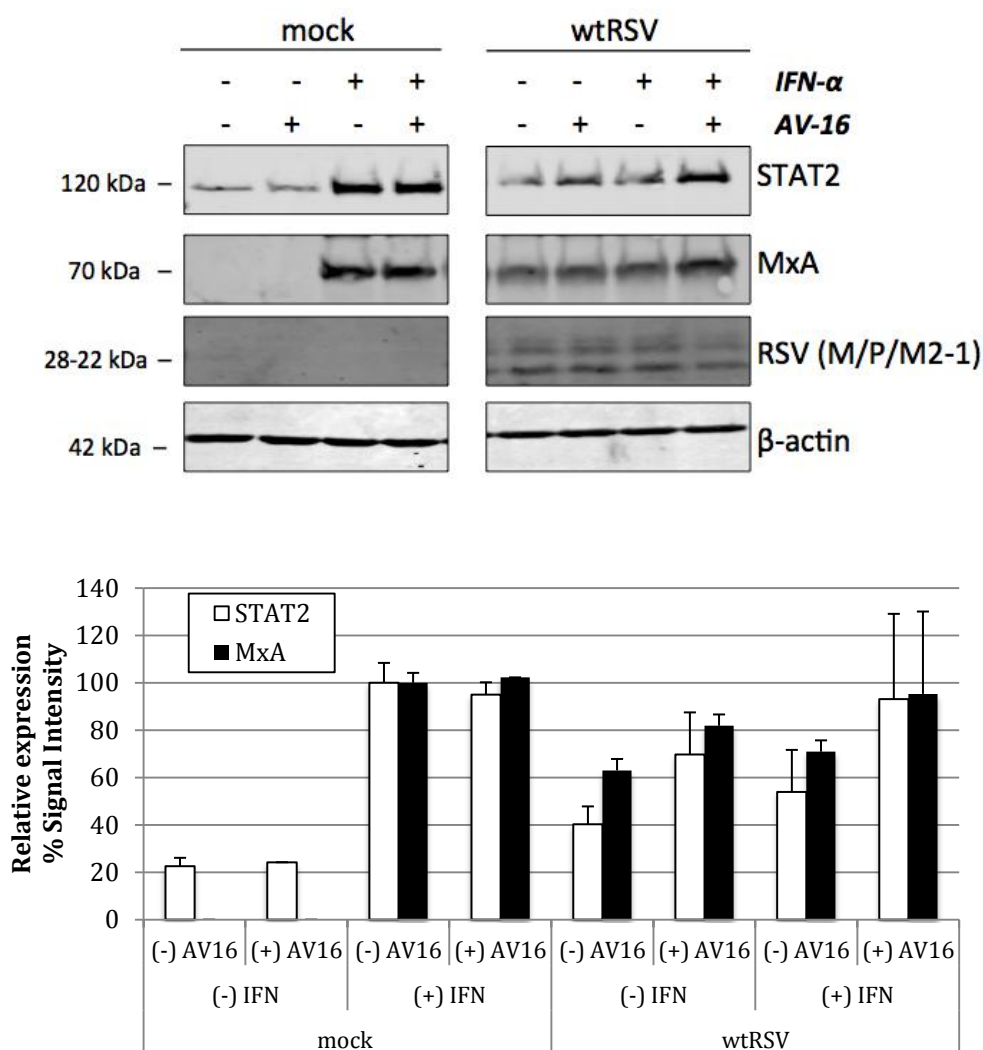
**Figure 6.8 Compound AV-16 partially inhibited STAT2 degradation during RSV infection *in vitro*.** A549 naïve cells were infected with RSV A2 strain (MOI of 5) for 1 hour and then, without removing the inoculum, AV-16 compound (10 μM) was added for 24 hours. The next day, the cells were treated with IFN-α (1000 U/ml) for 16 hours. STAT2 and MxA levels were observed using Odyssey CLx imager and quantified using ImageStudio software. Lanes 1-4 show STAT2 expression in mock infected cells; -/+ IFN treatment and -/+ compound AV-16. Lanes 5-8 show STAT2 expression in RSV infected cells; -/+ IFN treatment and -/+ compound AV-16. Control and test samples run on the same gel to allow quantification. Signal intensity is a relative measure of STAT2 and MxA expression, which was normalised to β-actin expression, and then presented as a % in relation to STAT2/MxA expression in the (-) RSV/ (+) IFN control (lane 3), which was set as 100%. Mean values (n=3), error bars=SD.

## 6.2.4 Hit compounds did not inhibit RSV replication *in vitro*

Our previous observations strongly suggest that our HTS approach successfully led to the identification of compounds that have specific inhibitory activity against the RSV NS2 protein, as they were shown to specifically inhibit the NS2-mediated STAT2 degradation. In order to determine whether inhibiting NS2-mediated STAT2 degradation is enough to restrict RSV growth, we tested the effect of the hit compounds on RSV replication kinetics on A549 naïve cells (Figure 6.9 and 6.10). In particular, the ability of the hit compounds (AV-14, -16, -18, -19) to restrict RSV replication was tested against two RSV strains (A2 and the Long strain), and the virus titers were quantified at various times points post infection. In the absence of AV-14 and AV-18, RSV/A2 peaked 48 hours post infection, reaching its maximum titer, which was approximately $3x10^4$ Pfu/ml (Figure 6.9/A), whereas RSV/Long peaked 72 hours post infection, reaching a maximum titer of $9x10^5$ Pfu/ml (Figure 6.9/B). The presence of compounds AV-14 and AV-18 had no effect on the titer of either RSV/A2 or RSV/Long, as viruses reached same titers in the presence of the compounds (Figure 6.10). Likewise, in the absence of AV-16 and AV-19, RSV/A2 peaked at 48 hours post infection, whereas RSV/Long peaked at 72 hours post infection, reaching maximum titers of $3x10^5$ Pfu/ml and $1x10^7$ Pfu/ml, respectively (Figure 6.10). Similar to compounds AV-14 and AV-18, neither AV-16 nor AV-19 had any inhibitory effect against RSV growth, as both RSV strains grew up to the same titers in the absence or presence of the compounds (Figure 6.10).
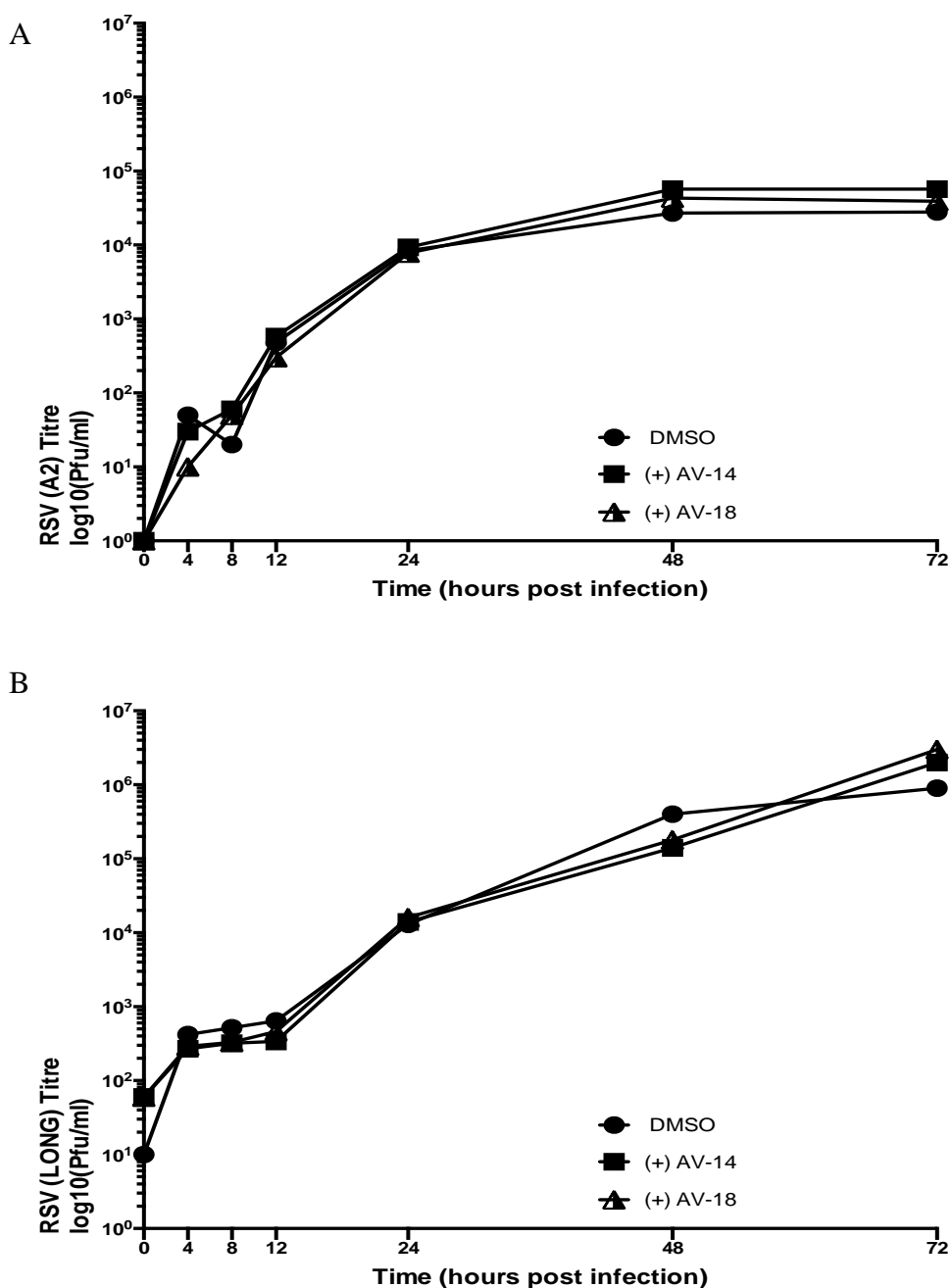
**Figure 6.9 Effect of the AV-14 and AV-18 compounds on RSV growth on A549 naive cells.** The growth of RSV A2 **(A)** and RSV Long **(B)** was monitored in the presence of the AV-16 and AV-19 compounds or 0.05% [v/v] DMSO. A549 cells were infected with RSV viruses at a low MOI (0.01) for 3 hours, and then the inoculum was replaced by fresh media containing 10 μM of compounds or the equivalent volume of DMSO. The virus titers were tested at various time points, as indicated on the growth curves.
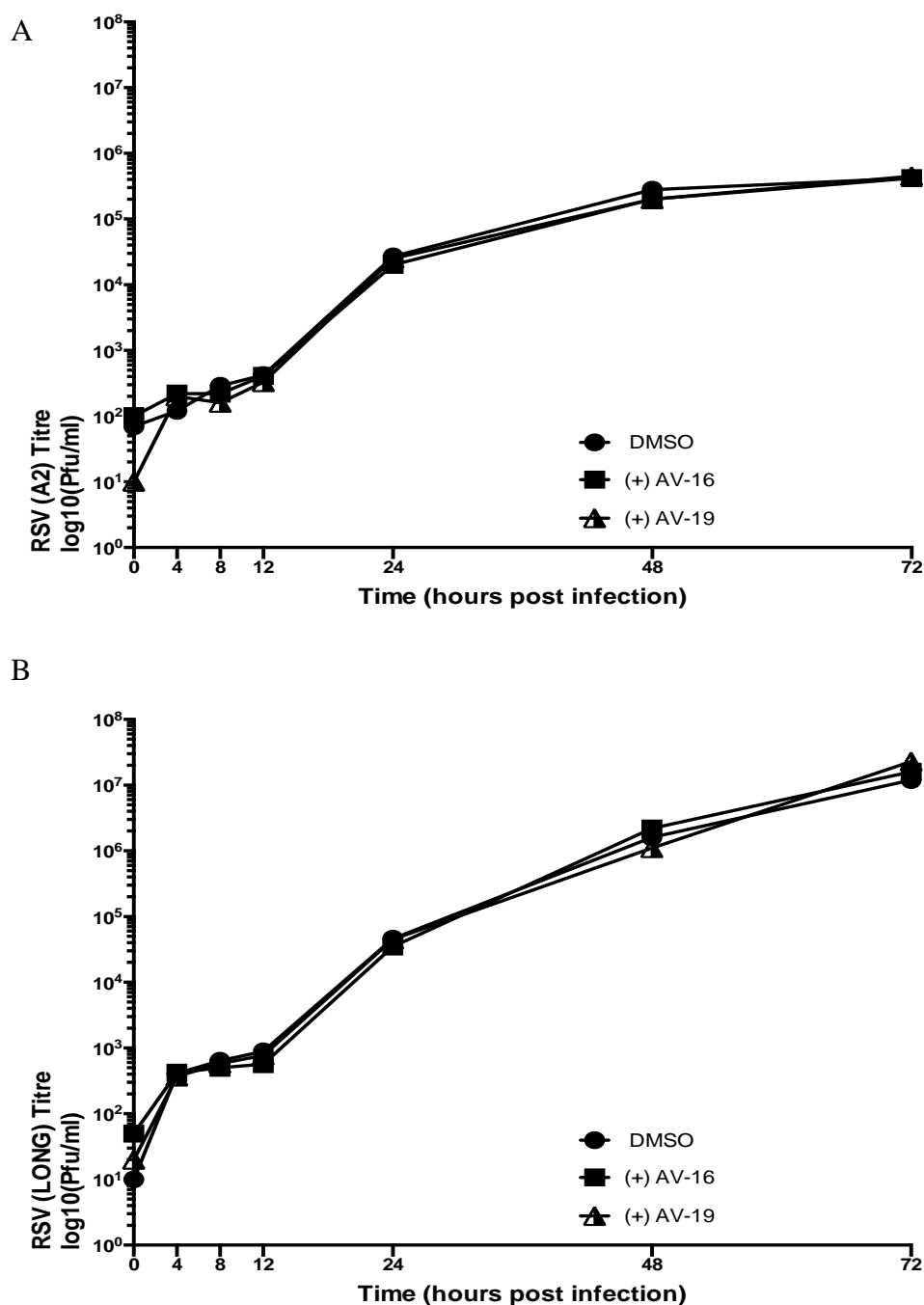
**Figure 6.10 Effect of the AV-16 and AV-19 compounds on RSV growth on A549 naive cells.** The growth of RSV A2 **(A)** and RSV Long **(B)** was monitored in the presence of the AV-16 and AV-19 compounds, as described previously. A549 cells were infected with an MOI (0.01) for 3 hours, and then the inoculum was replaced by fresh media containing 10 μM of compounds or the equivalent volume of DMSO. Virus samples were collected and titrated at various time points, as indicated on the growth curves.

Although hit compounds had no effect on RSV replication kinetics, we also tested whether they have an impact on RSV plaque number and size. RSV plaques were studied on human dermal fibroblasts (Hambleton *et al.,* 2013) and Hep2 cells. Specifically, RSV plaques were observed in the presence of hit compounds or DMSO at 4 days post infection in both cell-lines (Figure 6.11). Although RSV can form plaques on human fibroblasts, plaques are very small and better visualised under the microscope, therefore only virus titers are presented here. According to RSV titration, the virus titre was equal to $1.9 \times 10^6$ Pfu/ml in the absence or presence of the hit compounds, indicating that none of them had an effect on RSV replication on human fibroblasts (Figure 6.11/A). RSV plaque formation was also observed on Hep-2 naïve cells, as RSV forms bigger plaques on this cell-line and it was easier to determine if hit compounds have any effect on virus plaque size. In agreement with the previous observation, RSV titer was estimated to be approximately $3 \times 10^6$ Pfu/ml, both in the absence or presence of the compounds (Figure 6.11). In addition, no obvious difference was observed on RSV plaque size when AV-16 and AV-18 were added (Figure 6.11/B). Overall, RSV replication was quantified after monitoring RSV growth on A549 naïve cells and also observed with plaque assays on human fibroblasts and Hep2 naïve cells. Unfortunately, both approaches indicated that the hit compounds had no apparent effect on RSV replication.

Given that hit compounds work by inhibiting RSV NS2 protein from antagonizing STAT2, we hypothesized that the compounds might have an effect on RSV replication in the presence of IFN-α. To address this, A549 naïve cells were pre-treated with IFN-α, and then infected with RSV/Long before adding AV-16 compound. The virus growth was monitored for two days post infection (Figure 6.12).

A



B
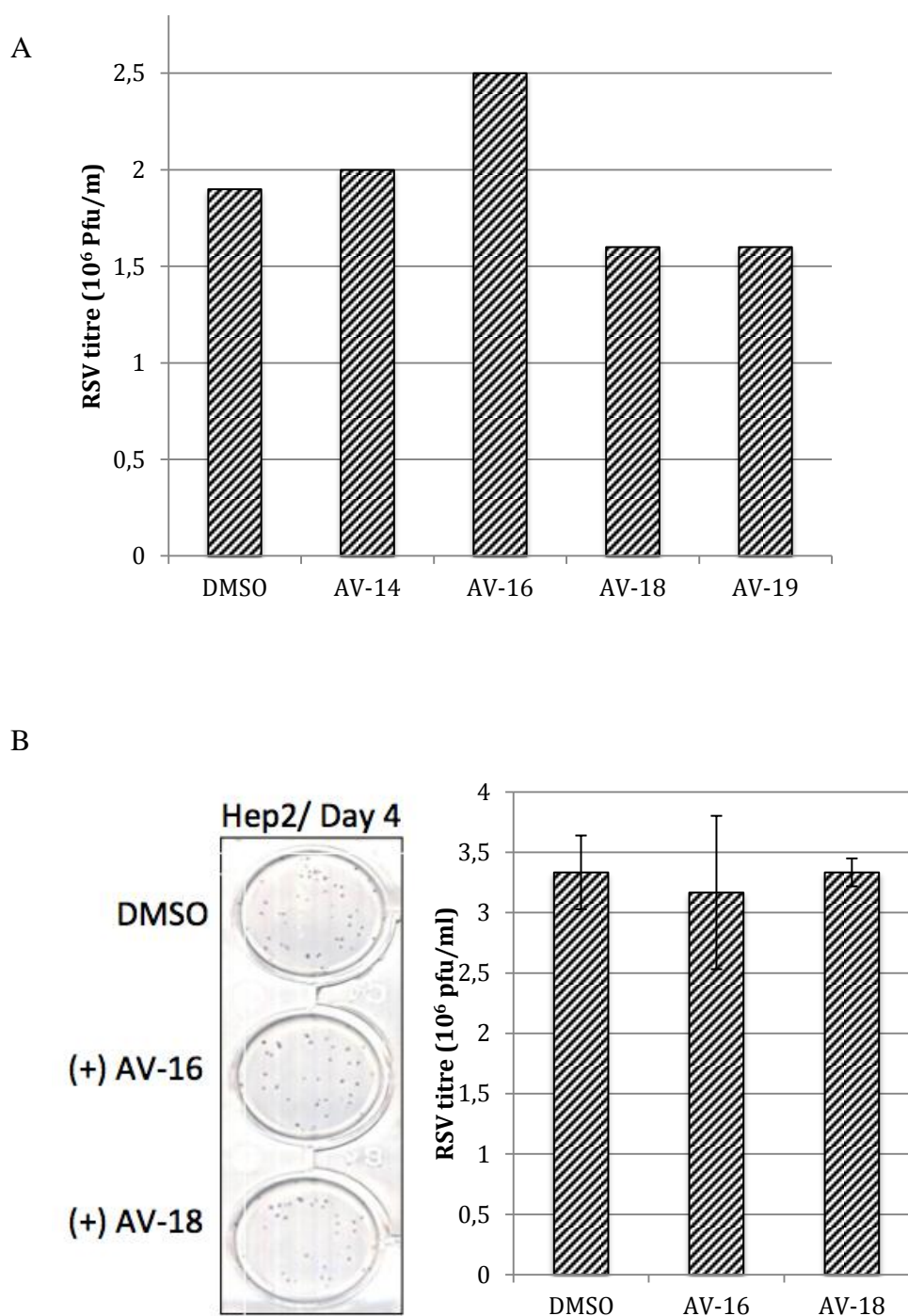


**Figure 6.11 Hit compounds had no effect on RSV plaque size and number.**
**(A)** wtRSV(Long) was added to human fibroblasts at MOI of 0.01 for 1 hour and after removing the inoculum, 10 μM of compounds or 0.05% [v/v] DMSO was added to the 0.5 % methylcellulose overlay. **(B)** wtRSV(A2) was added to Hep2 naive cells, as described above and then 10 μM of AV-16 and AV-18 or DMSO was added to the overlay. In both experiments plaques were fixed four days post-infection and visualized after immunostaining using an anti-RSV/F antibody. Mean values (n=3), error bars=SD.

In the absence of IFN-α treatment and 24 hours post infection, RSV/Long reached a titer of $3x10^4$ Pfu/ml, whereas in the presence of IFN the virus titer was $7x10^2$ Pfu/ml (Figure 6.12). At 48 hours post infection, the IFN's effect on virus replication was less intense, as the virus-IFN balance started shifting in the favor of the virus, resulting into a smaller difference in titers. In particular, the virus reached a titer of $5x10^5$ Pfu/ml in the absence of IFN-α, and had a titer of $5x10^4$ Pfu/ml in the presence of IFN (Figure 6.12). Unfortunately, treatment with AV-16 had no impact on RSV growth neither in the presence nor in the absence of IFN-α (Figure 6.12). This result negated our hypothesis, as it shows that the inhibitory effect of AV-16 is not sufficient enough to restrict RSV replication, not even in the presence of IFN.

Considering that RSV encodes for two IFN antagonists (NS1 and NS2) that are known to work synergistically or independently to antagonize the cellular IFN response (Lo *et al.,* 2005; Swedan *et al.,* 2011; Swedan *et al.,* 2009), we reasoned that the compounds had no effect on RSV replication, perhaps because NS1 compensates for the lost of NS2 function against STAT2. To test this hypothesis, we measured the effect of AV-16 on RSV.ΔNS1 replication, which is a recombinant RSV virus that lacks the ORF that encodes for NS1 protein (Figure 6.13). The replication of RSV.ΔNS1 peaked at 3 days post infection, and had a titer of $3x10^5$ Pfu/ml (Figure 6.13). Virus replication was monitored for 5 days, and no changes observed in regards to virus titer at latter time points (Figure 6.13). In contrast to our hypothesis, treatment with AV-16 had no effect on the replication RSV.ΔNS1, as the virus reached same titers in the presence of the compound (Figure 6.13). Taken together, compound AV-16 had no impact on RSV.ΔNS1 replication; therefore the incapability of the compound to restrict wtRSV replication cannot be attributed to NS1 compensation.
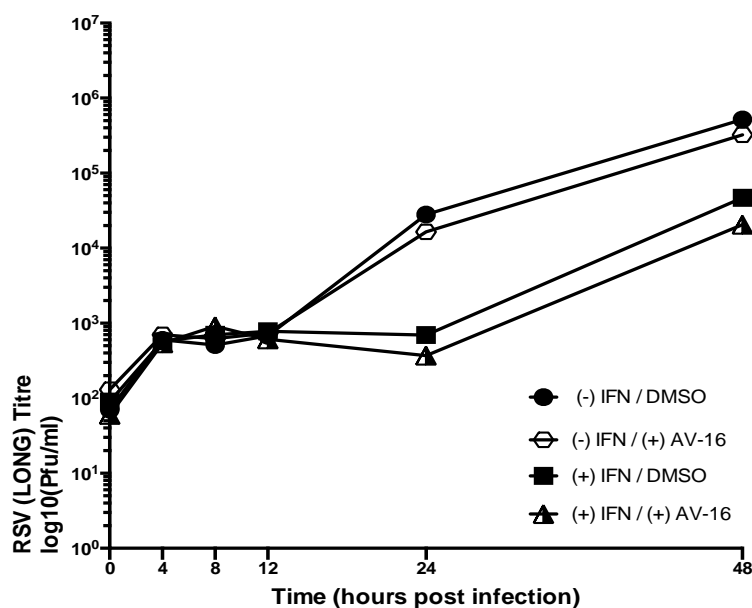
**Figure 6.12 AV-16 had no effect on RSV growth in the presence of IFN-α treatment.** A549 naïve cells were pre-treated with IFN-α (2000 U/ml) for 16 hours and then infected with RSV (Long) at an MOI of 0.01 for 3 hours. Then, the inoculum was removed and replaced by fresh media containing either 10 μM of AV-16 compound or the equivalent volume of DMSO. The virus titers were tested at various time points, as indicated on the growth curve.
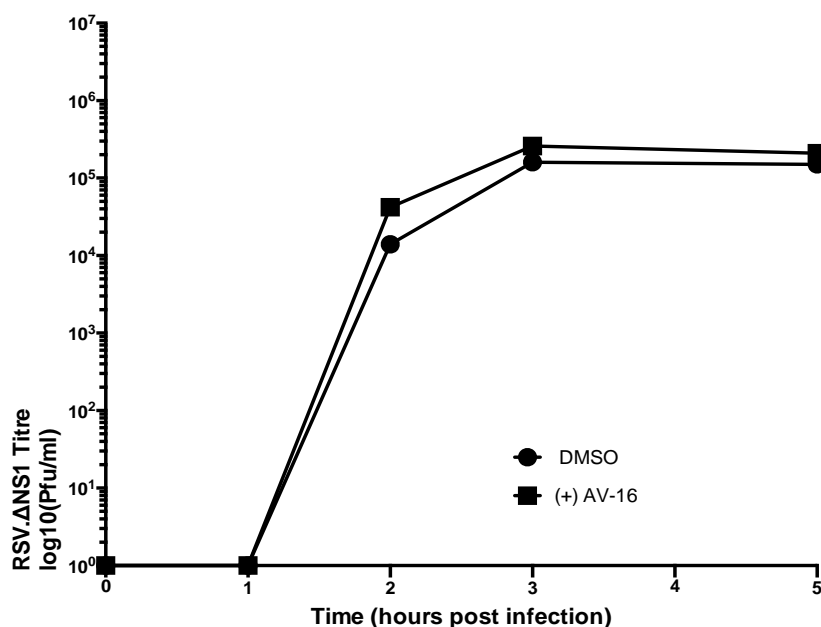


**Figure 6.13 AV-16 had no effect on the replication of RSV.ΔNS1.** Hep2 naïve cells were infected with RSV.ΔNS1 virus at a low MOI (0.01) for 3 hours, and then the inoculum was replaced by fresh media containing 10 μM of AV-16 or the equivalent volume of DMSO. The virus titer were tested at various time points, as indicated on the growth curves.

# 6.3 Summary

A primary HTS targeting RSV NS2 led to the identification of eight compounds, which were further characterized to demonstrate their specificity against RSV NS2 and also determine their biological activity. Hit compound characterization showed that compounds fall into two groups based on their ability to restore GFP expression in the A549.pr(ISRE)GFP-RSV/hNS2 cell-line. The compounds of Group A (AV-14, -16, -18 and -19) had more promising activity, as they mediated a higher fold increase in GFP expression (up to 1.96), compared to the compounds of Group B (AV-8, -10, -11 and -13). Hence, further hit characterization focused primarily on compounds AV-14, AV-16, AV-18 and AV-19. Hit compounds appeared to act specifically against RSV NS2, as they restored GFP expression only in NS2-expresssing reporter cell-lines. Our data demonstrated that the biological activity of the compounds is related to inhibition of NS2-mediated STAT2 degradation. Interestingly, all compounds partially suppressed NS2-mediated STAT2 degradation in the A549.pr(ISRE)GFP-RSV/hNS2 cell-line and also in the context of RSV infection *in vitro*. Supporting compounds specificity to NS2, our data showed that AV-16 did not inhibit STAT2 proteasomal degradation when mediated by another viral IFN antagonist, the PIV2 V protein. Unfortunately, although the compounds showed sufficient inhibition of the NS2-mediated STAT2 degradation, none of the compounds affected RSV replication *in vitro*. The inhibitory effect of the compounds was not enough to restrict RSV replication neither in the presence or absence of IFN-α, as the compounds did not block RSV growth any further than IFN-α. In addition, our data showed that AV-16 had no effect on RSV.ΔNS1 replication. This observation ruled out the possibility that NS1 might compensate for the loss of NS2

functions during wtRSV infection, suggesting that our NS2 inhibitors are not potent enough to restrict RSV growth.

In conclusion, we successfully identified eight compounds, four of which (AV-14, -16, -18 and -19) are certainly more efficient in inhibiting the NS2 degradation function against STAT2. To date, these are the only known small molecules that impose an inhibitory effect against RSV NS2, which underlines the novelty of these compounds. These inhibitors could be used in primary research to improve our understanding in regards to the role of NS2 in IFN antagonism, and dissect its multiple functions during RSV replication. Although at the current time our NS2 inhibitors do not restrict RSV growth, the activity of the hit compounds will be optimized by medicinal chemistry to potentially improve their potency and efficacy against RSV infection.

# Chapter 7: Discussion

Type I IFNs form the first line of defense against virus infections that dampen initial virus replication and ensure survival of the host until specialized adaptive immune responses are developed. However, viruses have evolved a great number of intricate strategies to circumvent the cellular IFN response, including the expression of viral IFN antagonists. The expanding understanding of viral IFN antagonism illustrates that viral interactions with the IFN system form a central host-pathogen interface in determining the outcome of viral infections. Several studies have demonstrated that viruses lacking a fully functional viral IFN antagonist experience attenuated replication *in vivo* due to a potent IFN response, which successively contributes to the establishment of long-lasting immune memory. For instance, Influenza A/B virus NS1 deletion mutants were found to induce IFN and, as a consequence, were attenuated *in vitro* and *in vivo*, while conferring protection against challenge with wild type virus (Donelan *et al.,* 2003; Hai *et al.,* 2008). Moreover, severe acute respiratory syndrome (SARS)-coronavirus nsp1, human PIV1 P/C and Japanese encephalitis virus (JEV) E deletion mutants were also greatly attenuated *in vivo*, while retaining immunogenicity, and therefore are considered good vaccine candidates (Züst *et al.,* 2007; Liang *et al.,* 2009). Since viruses unable to counteract the cellular IFN response are highly attenuated, targeting viral IFN antagonists represents a promising antiviral strategy. Our interest is to investigate whether a novel class of virus-specific drugs that work by inhibiting viral interferon antagonist function could be developed.

This study led to the development of a modular cell-based HTS approach that allows viral IFN antagonists of clinically important viruses to be subjected to HTS for the identification of candidate antiviral molecules, which would allow us to validate

viral IFN antagonists as drug targets. Our cell-based HTS assay is based on two A549 reporter cell-lines, namely A549.pr(IFN-β)GFP (Chen *et al.,* 2010) and A549.pr(ISRE)GFP, which provide a straightforward method for monitoring IFN-induction and IFN-signalling pathways by GFP expression under the control of the IFN-β promoter or the ISRE element. We successfully utilized these validated reporter cell-lines to underpin a novel screening platform for targeting viral IFN antagonists. This screening approach allows small molecule inhibitors of viral IFN antagonists to be identified via GFP restoration, in reporter cell-line derivatives that express viral IFN antagonists. We adapted this assay to a 384-well format and its robustness has been demonstrated though statistical analyses, which validated the assay as being suitable for HTS by consistently achieving Z'-factor scores of 0.65 to 0.77 (Figure 5.2).

## 7.1 Identification of small molecules that suppress RSV NS2 function against STAT2

To the best of our knowledge, this is the first time small molecule inhibitors of RSV NS2 have been identified. RSV is the most frequent viral pathogen causing ALRI, the leading cause of global child mortality (Nair *et al.,* 2010). Despite decades of research and antiviral drug endeavor, no efficacious RSV treatment or vaccine is available, highlighting the urgent need for novel therapeutic approaches. Therefore, there is a compelling case for research to further understand RSV biology and explore novel therapeutic targets. Although a number of small molecule anti-RSV compounds have been described, the majority of them target the F protein (Cianci *et al.,* 2004; Roymans *et al.,* 2010; DeVincenzo *et al.,* 2014), some of them target N or L (Sudo *et al.,* 2005; Chapman *et al.,* 2007), but no small molecules have been previously

identified against either NS2 or NS1. The importance of NS1 and NS2 for viral replication and virulence have been demonstrated through genetic analyses in cell culture and animal studies (Spann *et al.,* 2003; Spann *et al.,* 2004; Teng *et al.,* 2000; Jin *et al.,* 2000; Whitehead *et al.,* 1999). Hence, recombinant viruses lacking NS1 and/or NS2 have been extensively studied as potential RSV vaccine candidates, as their deletion results in highly attenuated RSV replication and diminished pathogenicity *in vivo* (Teng *et al.,* 2000; Whitehead *et al.,* 1999; Wright *et al.,* 2006; Luongo *et al.,* 2013). Since RSV mutants lacking IFN antagonists are severely attenuated, we reasoned that inhibitors of RSV NS1 and NS2 could represent promising direct-acting antiviral drugs.

The use of RSV NS1 and NS2 inhibitors represents a promising strategy for inhibiting RSV, especially in combination with other antiviral agents, such as fusion or polymerase inhibitors. The current RSV antiviral research leans towards F inhibitors; Targeting viral entry has always been a promising therapeutic approach, however another reason for this prevalence may be that F inhibitors do not need to cross the membrane barrier as fusion of the viral and cellular membranes occurs outside the cell. This negates limitations such as lipophilicity and molecular weight, allowing more flexibility in drug design. The most promising antiviral compound currently in clinical trials is the recently discovered F inhibitor, GS-5809 (Mackman *et al.,* 2015; DeVincenzo *et al.,* 2014). Although current evidence suggests that it is possible to restrict RSV replication *in vivo* via small-molecule antiviral agents, treatment with a single antiviral agent would increase the likelihood of the emergence of resistance. As with other viruses (e.g. HIV and HCV), combination therapies with drugs targeted to other RSV proteins, such as NS1 and NS2, should avoid selection of resistant viruses.

One obstacle to the therapeutic use of antivirals against RSV is the narrow window for intervention. Similar to influenza viruses, RSV causes acute respiratory infections with symptoms occurring in the upper respiratory tract before reaching the lungs (Collins & Graham 2008). Therefore, there is a delay of approximately four days between the first symptoms and hospitalization, which emphasizes the need for rapid diagnostics, in order to increase the efficacy of future antiviral treatments (Collins & Melero 2011). Nonetheless, the current use of neuraminidase inhibitors (e.g. Oseltamivir) as a prophylaxis against influenza viruses could serve as a model for an RSV antiviral (Aoki *et al.,* 2013). Although the narrow treatment window is limiting the effectiveness of an antiviral therapy, RSV antiviral drugs represent a promising therapeutic approach, especially given the challenges encountered during the clinical trials of the FI-RSV vaccine.

Although this is the first HTS assay to identify small molecule inhibitors of RSV NS2, small molecules that inhibit other viral IFN antagonists, such as NS1 of Influenza A viruses and Ebola virus VP35, have been previously identified by other screening approaches. A small molecule that inhibited the NS1 function against IFN mRNA expression recently showed potent antiviral activity *in vitro*, however the potential of such a compound to inhibit virus replication *in vivo* remains undetermined (Patnaik *et al.,* 2013). Furthermore, a targeted screening approach has demonstrated that small molecules that target the IFN inhibitory domain of Ebola VP35 also block its polymerase cofactor ability, resulting to reduced virus replication *in vitro* (Brown *et al.,* 2014). Similar to NS1 inhibitors, the efficacy of these compounds *in vivo* remains to be demonstrated.

To date, HCV NS3.4A PIs are the only clinically approved antivirals that function against a viral IFN antagonist. Following the discovery of NS3.4A PIs, great advances have been made in HCV antiviral therapy, as Telaprevir and Boceprevir were the first direct-acting antiviral agents introduced for treatment of genotype 1 HCV in 2011 (Gentile *et al.,* 2009; Hézode *et al.,* 2014). Simeprevir is a more recently approved NS3/4A inhibitor, which has improved pharmacological properties, compared to Telaprevir and Boceprevir (Nagino *et al.,* 2015). In 2013, the U.S. Food and Drug Administration (FDA) approved Simeprevir in combination with Sofosbuvir (polymerase inhibitor) as the first IFN- and ribavirin-free treatment option for genotype 1 chronic hepatitis C infection (Gogela *et al.,* 2015). The advances made in HCV antiviral therapy provide a sense of optimism that inhibitors of viral IFN antagonists could be effective virus-specific antiviral agents, which can improve the effectiveness of combinational antiviral therapies.

## 7.1.1 Potential mechanisms of action of RSV NS2 inhibitors

To be able to screen for small molecules that target RSV NS2, we first created a reporter cell-line derivative that constitutively expressed RSV hNS2, namely A549.pr(ISRE)GFP-RSV/hNS2. Using this cell-line, we screened a library of 16,000 small compounds, among which we found four molecules (AV-14, AV-16, AV-18 and AV-19) capable of inhibiting the NS2 function against the IFN-signalling pathway. Excitingly, we demonstrated that hit compounds specifically inhibited the NS2-mediated STAT2 degradation in the A549.pr(ISRE)GFP-RSV/hNS2 cell-line and also in the context of RSV infections *in vitro* (Figure 6.6 and 6.8). Indeed, none of the compounds inhibited the ability of other viral IFN antagonists, such as RSV NS1, PIV5

V and PIV2 V, to circumvent the cellular IFN-signalling pathway (Figure 6.5), emphasizing the specificity of these compounds towards RSV NS2.

Understanding the compounds mechanism of action could improve our understanding regarding RSV antagonism against STAT2. Published work has shown that RSV modulates the JAK/STAT signalling pathway through proteasome-dependent degradation of STAT2 (Spann *et al.,* 2004; Lo *et al.,* 2005; Goswami *et al.,* 2013). However, the relative importance of NS1 and NS2 in suppressing the cellular IFN response and the precise mechanism by which STAT2 degradation occurs during RSV infections remains undetermined. In agreement with previous studies (Lo *et al.,* 2005; Spann *et al.,* 2004; Ramaswamy *et al.,* 2006; Goswami *et al.,* 2013), our data demonstrates that RSV hNS2 can independently mediate STAT2 degradation and block the IFN-signalling pathway, however NS1 and NS2 co-expression leads to a maximal inhibitory effect (Figure 4.6). In contrast, independent NS1 had little to no effect on STAT2 degradation but does impose a moderate block to IFN-signalling (Figure 4.5). To date, only one study proposed a STAT2 degradation mechanism that does not support a NS2-independent function against STAT2. This study showed that components of the Cul2-RING E3 ligase (CRL2) complex mediate STAT2 degradation via a direct interaction with NS1 but not NS2 (Elliott *et al.,* 2007). However, mutation of the putative NS1 Cul2 binding motif (BC box) did not inhibit STAT2 degradation or any other NS1 function, therefore the ability of NS1 to interact with Cul2 is still questionable (Swedan e*t al.,* 2011). Consequently, the role of NS1 and NS2 in RSV-mediated STAT2 antagonism remains inconclusive and controversial; hence, the identified NS2 inhibitors could be used as research tools to improve our understanding about RSV-mediated STAT2 degradation.

One possible mechanism of action could be that hit compounds suppress NS2 function against STAT2 by binding directly to NS2. This could subsequently block essential interactions of NS2 with cellular factors, such as ubiquitin factors or cellular proteases, which are important for the formation of the NS-degradasome. Swedan *et al.,* (2011) have showed that NS2 C-terminal tetrapeptide DNLP is important for the ability of NS2 to bind the MAP1B, and this interaction was shown to be indispensable for the NS2 degradation function against STAT2. While the mechanistic role of MAP1B is unrevealed, it is possible that MAP1B serves as an adaptor that recruits other host proteins that are essential for STAT2 degradation. Therefore, it is tempting to speculate that hit compounds could inhibit STAT2 antagonism by binding to the NS2 DNLP peptide, hence blocking its interaction with the host factor MAP1B. Moreover, the compounds could bind elsewhere in NS2, and still prevent MAP1B from binding to NS2 DNLP. It is also possible that the compounds do not interfere with NS2-MAP1B interaction but instead block NS2-mediated STAT2 degradation by impeding NS2 from interacting with another cellular factor(s), which is also crucial for this NS2 function. In collaboration with Dr Uli Schwarz-Linek (University of St Andrews, UK), we endeavored to purify RSV NS2 to enable us perform drug-protein binding studies using nuclear magnetic resonance (NMR). Unfortunately, consistent with previous work (Evans *et al.,* 1996), the highly unstable nature of the RSV NS2 protein did not allow us to proceed any further with the structural studies and hindered our attempt to investigate the hypothesis of direct binding.

It is also probable that the hit compounds inhibit STAT2 degradation by blocking the interaction of the NS-degradasome with mitochondria. A recent study has proposed that a stable NS-degradasome requires recruitment of mitochondrial MAVS,

suggesting that mitochondria and MAVS facilitate the function(s) of NS-degradasome, and consecutively assist RSV suppression of innate immunity (Goswami *et al.,* 2013). Supporting the association of NS-degradasome with mitochondria, another study has recently shown that NS1 co-localizes with mitochondria during RSV infection and co-immunoprecipitates with MAVS in NS1 transfected A549 cells (Boyapalle *et al.,* 2012). However, NS2 is capable of degrading STAT2 in the absence of NS1 (Ramaswamy *et al.,* 2006; Lo *et al.,* 2005), therefore if mitochondrial localization is crucial for the STAT2 degradation function, other interactions must be responsible for locating NS2 to mitochondria. In fact, NS2 was found to co-localize with mitochondria when constitutively expressed in A549 cells, however there is no evidence yet to suggest that it directly interacts with MAVS or any other mitochondrial protein (Swedan *et al.,* 2011). Knowing that RIG-I CARD domain binds to MAVS CARD domain during RLR-mediated activation IFN-induction pathway (Seth *et al.,* 2005; Kawai *et al.,* 2005), and given that NS2 was found to interact with RIG-I by direct binding to its CARD domain (Ling *et al.,* 2009), it is conceivable that tethering of RIG-I might facilitate the translocation of NS2 to mitochondria. The effect of hit compounds on NS2 localization can be demonstrated by cellular localization studies in the context of RSV infection. If hit compounds inhibit NS2 by obstructing its localization to mitochondria, it would be also noteworthy to explore whether NS2 ability to bind RIG-I diminishes in the presence of the compounds. It is also feasible that our NS2 inhibitors do not affect NS2 localization, but instead act by blocking NS2 interaction with other mitochondrial factors, which are involved in RSV-mediated STAT2 antagonism, hence interfering with the assemblage of the NS degradation complex. In conclusion, several studies support the association of NS1 and NS2 with mitochondria and mitochondrial MAVS,

however their role in STAT2 degradation needs to be further investigated. If the association with mitochondria is crucial for stabilizing the NS degradation complex, it is possible that our NS2 inhibitors interfere with this process.

The mechanism of action of NS2 inhibitors might not involve direct binding to NS2, but instead these molecules could inhibit host factors involved in RSV-mediated STAT2 degradation. Our results showed that hit compounds were capable of inhibiting NS2-medated STAT2 degradation but they did not block STAT2 degradation when mediated by PIV2 V, and also had no impact on PIV5/V-mediated STAT1 degradation. This data demonstrates that these molecules act specifically against the STAT2 degradation function of NS2, and suggests that these viruses perhaps utilize different host factors to mediate degradation of STATs. Similar to RSV, PIV2 and PIV5 mediate STAT2 or STAT1 degradation, respectively, through the proteasome (Parisien *et al.,* 2001; Didcock *et al.,* 1999). Although these viruses utilize a proteasome-dependent mechanism, they recruit different ubiquitin factors to achieve this. Specifically, the PIV2- and PIV5-mediated STAT degradation requires the formation of a V-dependent degradation complex, which comprises of STAT1 and STAT2 and also involves host-encoded factors like DDB1 (a UV-damage DNA binding protein), and members of the cullin family like Cul4A (Andrejeva *et al.,* 2002; Ulane & Horvath 2002; Precious *et al.,* 2007). Although the mechanism for RSV-mediated STAT2 degradation remains unknown, a previous study suggested that it requires Cul2 and Rbx1 ubiquitin factors (Elliott *et al.,* 2007), which are not known to be related to PIV2 or PIV5 degradation activity. For instance, if the hit compounds do not inhibit NS2 function by direct binding to NS2, they could bind and hence inhibit the function of ubiquitin ligases, which are essential for NS2-mediated degradation but are not involved in the V-

dependent degradation complex. This could explain why our inhibitors suppressed NS2 function against STAT2 but had no effect against PIV2 V or PIV5 V degradation function against STATs. Since Elliot *et al.,* (2007) demonstrated that RSV-mediated STAT2 degradation requires Cul2, we tested whether hit compounds interfere with Cul2 in the A549.pr(ISRE)GFP-RSV/hNS2 cell-line. However, none of the compounds had an effect on Cul2 expression levels in the A549.pr(ISRE)GFP-RSV/hNS2 cell-line (Appendix 4). Furthermore, the compounds are not likely to inhibit STAT2 degradation by blocking Cul2 activation. Specifically, the cullin-RING ubiquitin ligases are activated by NEDD8, a process known as neddylation (Merlet *et al.,* 2009). Both neddylated and uneddylated forms of Cul2 were detected in NS2-expressing cells in the presence of the hit compounds (Appendix 4), suggesting the compounds are not likely to suppress Cul2 activation to inhibit NS2-mediated STAT2 degradation. However, these observations do not exclude the possibility that the compounds could interact with Cul2 in a different manner. On the other hand, it is possible that Cul2 activity is only related to RSV NS1 degradation functions and it is not important for the NS2-mediated STAT2 degradation function. Hence, other members of the cullin-RING ubiquitin ligase family might associate with NS2 and are possibly targeted by the hit compounds. Exploring this hypothesis will allow us gain more insight into the degradation activity of RSV NS2, and perhaps NS1.

Another possibility is that compounds might interact with host factors that bring STAT2 into close proximity to the NS degradation complex. There is no evidence to suggest that NS1 or NS2 directly bind to STAT2, therefore it remains undermined which cellular or viral factors are involved in this process. Furthermore, although NS1 has been reporter to degrade other host factors, such as RIG-I and IRF7 (Goswami *et*

*al.,* 2013), it still remains unknown whether NS2 degrades other cellular factor(s) except from STAT2. It is possible that NS2 targets additional factors for degradation; these might be either innate immune proteins or host factors involved in other signalling cascades, such as apoptosis. If more proteins were targeted by NS2 for proteasomal degradation, we could investigate whether our NS2 inhibitors are also capable of blocking this function. This would allow us to assess whether our NS2 inhibitors can block multiple interactions of NS2 with the host cell.

Our results exclude the possibility that hit compounds interfere with the proteolytic activity of the 20S core subunit of the 26S proteasome. In brief, the 26S proteasome is a multi-protein complex, which comprises of one or two 19S regulatory particles, which are capable of binding the polyubiquitin chain and cleaving it from the protein substrate, and a core 20S core particle, which proteolytically processes the denatured proteins (Da Fonseca *et al.,* 2012). Previously described proteasome inhibitors, such as MG132 and TMC-95A interfere directly with the active sites in the core particle and block its proteolytic activity (Adams *et al.,* 1998; Koguchi *et al.,* 2000; Goldberg 2012). The identified small molecules do not impose a similar function against the proteasome, because they did not block STATs degradation when mediated by PIV2 or PIV5. Furthermore, the compound-mediated increase in STAT2 levels in the NS2-expressing cell-line is less likely to be due to STAT2 stabilization, because no STAT2 increase was observed in the PIV2/V-expressing cell-line. Undoubtedly, further investigations are required to provide mechanistic insight into the compound-mediated NS2 inhibition.

In summary, our NS2 inhibitors are likely to counteract the STAT2 degradation function of NS2 through a number of possible mechanisms (Figure 7.1). First, they

could possibly bind NS2 to block its interaction with cellular host factors, such as MAP1B or other host proteins, including mitochondrial factors, ubiquitin factors or cellular proteases that might be essential for STAT2 degradation. Second, hit compounds might not bind NS2 but instead bind to host factors involved in STAT2 degradation. For instance, they might sequester host factors that bring STAT2 into close proximity to NS-degradasome. Third, they could interfere with the activation of ubiquitin factors, which are crucial for the assembly of the NS degradation complex.
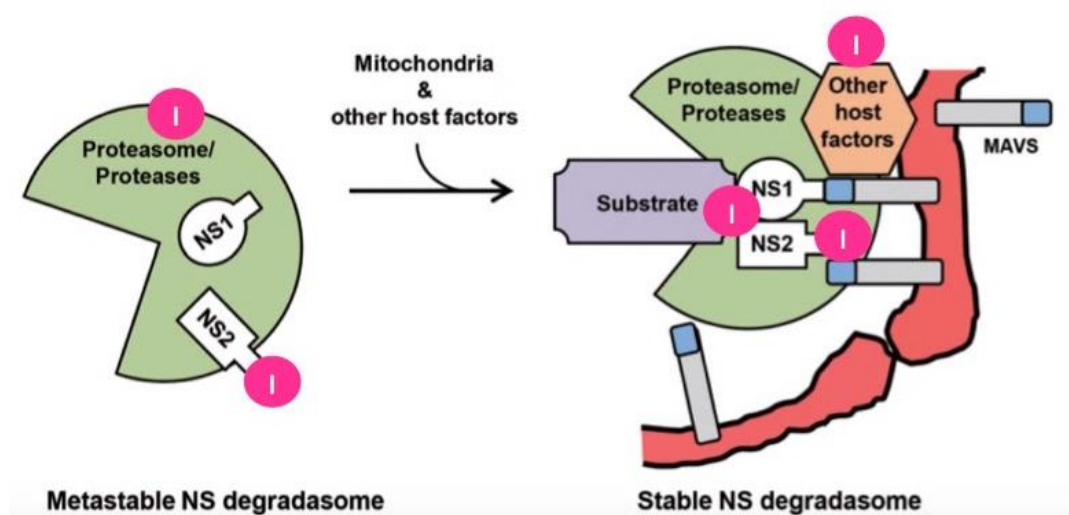


**Figure 7.1 Potential mechanisms of action of hit compounds against NS2 STAT2 degradation function.** According to Goswami *et al.,* (2013), the metastable NS-degradasome comprises of NS1, NS2 and other cellular factors, which loosely interact with each other. NS-degradasome is stabilized by recruitment to MAVS on motile mitochondria, perhaps allowing recruitment of other host factors, such as chaperones and ubiquitination pathway proteins. NS2 inhibitors (I) could block STAT2 degradation function by interacting with the formation of the metastable NS degradasome by either binding to NS2 or cellular factors, such as proteasome components or proteases essential for STAT2 degradation. Furthermore, the small molecules might inhibit NS2 by blocking its interaction with mitochondria, hence disrupting stabilization of the degradation complex. It could be also possible that the compounds interfere with cellular factors that bring STAT2 in close proximity to the degradation complex. Modified by Goswami *et al.,* (2013)

To investigate their mechanism of action, the compounds can be used in immunoprecipitation studies to reveal specific protein-protein interactions involved in the NS-degradasome formation. Biotinylation of hit compounds could facilitate such studies and could also allow the development of fluorescent assays using biotin conjugates. The limited knowledge about RSV-mediated STAT2 degradation function makes it difficult to explore the compounds mechanism of action. However, understanding how the compounds inhibit NS2 will enable us to gain more insight into the proteasome-mediated degradation of STAT2.

## 7.1.2 The impact of our NS2 inhibitors on RSV growth

Unfortunately, although hit compounds had an inhibitory effect against NS2 function, none of the compounds restricted RSV replication *in vitro*. The inhibitory effect of compound AV-16 was not strong enough to inhibit RSV growth either in the presence or absence of IFN-α, suggesting that the compound did not block the anti-IFN properties of RSV, which facilitate virus replication in the presence of IFN. Our first speculation was that hit compounds did not have an effect against RSV replication *in vitro*, because RSV also encodes for NS1 that also antagonizes the cellular IFN response (Lo *et al.,* 2005; J Ren *et al.,* 2011; Goswami *et al.,* 2013; Swedan *et al.,* 2009; Swedan *et al.,* 2011). Negating our hypothesis, compound AV-16 had no effect against a mutant RSV that lacks NS1, therefore the idea that NS1 compensates for the NS2 lost cannot explain the incapability of hit compounds to inhibit RSV.

Consequently, another possible reason for the compounds' ineffectiveness against RSV could be that the compounds are not potent enough to restrict virus replication. Indeed, none of the compounds restored GFP expression up to 100%, as the

maximum fold increase observed was 1.96 as opposed to 3.4, which was previously

obtained in the A549.pr(ISRE)GFP reporter cell-line when no viral IFN antagonist is

expressed. Consistent with this observation, hit compounds partially inhibited STAT2

degradation in the A549.pr(ISRE)GFP-RSV/hNS2 cell-line and also during RSV

infection on A549 cells, causing a 30% increase in STAT2 levels (Figure 6.6 and 6.8).

Using the hit compounds in combination or extending incubation time did not increase

compounds' inhibitory effect against NS2 function (Appendices 5 and 6). Hence, a

reasonable explanation could be that this level of inhibition is not sufficient enough to

restrict virus replication *in vitro*.

To improve the compounds potency and perhaps their ability to restrict virus

growth, structure-activity relationship (SAR) studies are required. Interestingly, three of

the hit compounds AV-14, AV-16, AV-18 share structural similarity as they all contain

an indole ring (Table 5.3). Although indole moiety is very small, it is an interesting

chemical structure, because of its diverse biological activities, which are imposed not

only by indole but its various substituted derivatives as well. Indole ring containing

marketed drugs show various biological activities, including anticancer, antimicrobial,

anti-diabetic, antidepressant and also antiviral activity (Biswal *et al.,* 2012).

Specifically, Arbidol (Umifemovir) is an indole-containing small molecule that blocks

virus fusion, and therefore has an antiviral activity against many viruses, including

influenza A viruses (Liu *et al.,* 2013). Our results demonstrated that indole weakly

restored GFP expression in the A549.pr(ISRE)GFP-RSV/hNS2 reporter cell-line

(Figure 6.4), indicating that the indole ring on its own does not account for the ability of

the hit compounds to mediate NS2 inhibition. Furthermore, all the identified molecules

have different side chains, however they share structural similarity with other molecules

of the screened library, which did not appear to have an inhibitory effect against NS2. This observation suggests that both functionalities (indole ring and side chains) are important for compounds activity. Hence, the relative importance of these moieties in NS2 inhibition needs to be further explored using more thorough SAR investigations.

The incapability of the NS2 inhibitors to counteract RSV replication could also indicate that targeting the STAT2 degradation function of NS2 may not be enough to restrict RSV. It was previously shown that the C-terminal NS2 tetrapeptide DNLP is indispensable for the STAT2 degradation function of NS2 (Swedan *et al.,* 2011), though the effect of NS2 DNLP on RSV replication has not been studied. Therefore, studying the replication kinetics of a RSV mutant that lacks NS2 DNLP would allow us to determine if targeting STAT2 degradation function is a promising antiviral strategy.

Another factor that could contribute to the compounds' inability to inhibit RSV growth is perhaps the multifunctional nature of NS2. For instance, hit compounds are inhibiting the NS2 function against STAT2, however a few studies suggested that NS2 has other functions important for IFN antagonism and virus pathogenicity that might not be inhibited by our hit compounds (Spann *et al.,* 2005; Swedan *et al.,* 2009; Ling *et al.,* 2009; Liesman *et al.,* 2014). It remains unknown whether these functions are related to the same or different molecular mechanisms. Due to their multifunctional nature of NS2, our NS2 inhibitors could possibly work as a double-edged sword. For example, if NS2 was operating as an E3 ligase to degrade STAT2 and used the same activity to degrade other cellular factors, then a molecule that inhibited NS2 ability to degrade STAT2 could possibly inhibit other degradation functions of this protein. This is essentially the reason behind the effectiveness of the PIs of HCV NS3.4A. More precisely, HCV NS3/4A protease has a crucial role for virus replication, which is the

processing of viral polypeptide. In addition, HCV NS3/4A protease is a potent antagonist of the type I IFN-induction pathway, as it interferes with the pathogen recognition RLR- and TLR3-mediated signalling pathways by cleaving TRIF and MAVS signalling adaptors (Li *et al.,* 2005; Meylan *et al.,* 2005; Horner *et al.,* 2011). NS3/4A protease inhibitors suppress HCV replication by simultaneously disrupting two processes critical to the survival of the virus; the enzymatic cleavage of HCV C-terminal polyprotein into discrete nonstructural proteins and evasion of early innate immunity (Gogela *et al.,* 2015). The fact that no other NS2 function is as well defined as the STAT2 degradation function prevented us from determining if hit compounds target any other NS2 function.

It is also tempting to speculate that NS2 inhibitors are more likely to have a significant impact on RSV replication *in vivo*, since RSV NS2 seems to be a virulence factor that is more important for the establishment of lower respiratory tract infections, which are associated with severe respiratory disease. Evidence suggests that RSV NS2 is an important virulence determinant of RSV infections in humans, as deletion of the NS2 gene severely attenuated RSV in children and adults (Wright *et al.,* 2006). A recent study have also shown that RSV NS2 could be a contributing factor for enhanced propensity of RSV to cause severe airway disease in young children (Liesman *et al.,* 2014). Specifically, using a human cartilaginous airway epithelium (HAE) and a hamster model, they have shown NS2 promotes epithelial cell shedding, which accelerates viral clearance but also contributes to acute obstruction of the distal airways (Liesman *et al.,* 2014). Moreover, a chimpanzee model showed RSV/ΔNS2 replication was moderately attenuated in the upper respiratory tract, however 10,000-fold reduction was observed in the lower respiratory tract (Whitehead *et al.,* 1999). Hence *in vivo*

studies might be more appropriate for testing the impact of the identified compounds against RSV replication. Several animal species are used for experimental modeling of RSV disease, including chimpanzees, cattle, sheep, cotton rats and mice, however none of them completely reproduces all the characteristic features of RSV disease in humans (Simões *et al.,* 2015; Bem *et al.,* 2011). The newborn lamb RSV model is an attractive model for testing the efficacy of NS2 inhibitors *in vivo*, mainly because (i) airway structure and function of newborn lambs are more similar to those in infants compared to mice and (ii) RSV pathology, including anti-viral and anti-inflammatory responses observed in new-born lambs was similar to humans (Sow *et al.,* 2011; Scheerlinck *et al.,* 2008). Due to the ethical and economic constrains related to such animal models, BALB/c mice are extensively used for studying RSV infections *in vivo*, clearly because of their relatively low cost and the extensive experience and molecular tools available (Prince *et al.,* 1979). Although the efficacy of this animal model is limited due to important genetic and structural differences with humans, neonatal mice represent a more suitable animal model than adult mice for testing the antiviral effect of NS2 inhibitors, because they can develop asthma-like disease, including increased airway hypersensitivity (Cormier *et al.,* 2010). Hence, it would be interesting to investigate whether hit compounds impose an inhibitory effect against RSV disease in these animal models.

In order to target the majority of RSV functions against the cellular IFN response, the ideal scenario would be to target both RSV NS1 and NS2, since they are the two primary IFN antagonists encoded by RSV. RSV NS1 represents a promising target for drug discovery, as in addition to its primary role as an IFN antagonist, it also performs other important functions for virus replication, which are unrelated to IFN

modification (Evans *et al.,* 1996; Hengst & Kiefer 2000; Atreya *et al.,* 1998; Bitko *et al.,* 2008; Wu *et al.,* 2012). Although we developed reporter cell-line derivatives that constitutively expressed NS1, we noted that constitutive expression of NS1 was toxic to the cells hence slowing down their growth rate. It is possible that NS1 had only a moderate effect on the activation of the IFN-β promoter and ISRE element due to the fact that cells perhaps cannot sustain high NS1 expression. This limitation could be overcome by the development of an inducible expression system. Specifically, a tetracycline-dependent induction (Tet-on) system has been previously validated using human cytomegalovirus (CMV) immediate-early 1 (IE1) protein and it represents a powerful system for inducible protein expression (Knoblach *et al.,* 2011). Future work will be to incorporate this inducible system into our A549 reporter assay and determine if an inducible HTS assay can be developed. If successful, this would allow us to target RSV NS1 for the identification for small molecules that inhibit NS1 function against the IFN-induction and/or IFN-signalling pathway and test whether a combination of NS1 and NS2 small molecule inhibitors could restrict RSV replication. Antiviral drugs that target NS1 and NS2 could potentially restrict RSV infection due to impair replication and virulence but also due to increased IFN responses and enhanced immunogenicity against the virus.

A major concern for targeting RSV IFN antagonists is the fact that evidence suggests that host immune responses could contribute to viral disease. Hence targeting IFN antagonists could increase the risk of developing more potent immune responses to RSV infections, which could subsequently lead to disease exacerbation. For instance, RSV-mediated bronchiolitis in children was shown to be associated with a Th2-predominant immune response and a number of other cytokines (e.g. IFN-γ, TNF-α)

and chemokines (e.g. CXC) that are related to innate and adaptive immunity (Bermejo-Martin *et al.,* 2007). However, RSV NS1 protein is thought to enhance RSV disease by promoting proliferation and activation of Th2 cells, emphasizing the fact that targeting RSV IFN antagonists is more likely to restrain RSV virulence rather than enhancing RSV disease (Munir *et al.,* 2011). In addition, a recent study has shown that RSV NS1 and NS2 suppress the activation of glucocorticoids, one of the most powerful anti-inflammatory agents, by suppressing the transactivation of the glucocorticoid receptor (Webster Marketon *et al.,* 2014). Hence, inhibitors of RSV NS1 and NS2 could enhance glucocorticoid responsiveness, and subsequently limit RSV pathogenicity by preventing inflammatory responses, which worsen the outcome of RSV infections.

Despite that immune and inflammatory responses to RSV can contribute to disease exacerbation, early innate immunity is crucial for controlling RSV infection. Hence, small molecules that inhibit RSV IFN antagonists and restore early innate immunity against RSV are more likely to contribute towards RSV control rather than supplementing RSV virulence. Specifically, effector molecules of the cellular IFN system such as STAT1 and STAT2 were shown to be important for preventing severe RSV infection *in vivo*. RSV infection in STAT1-/- or STAT2-/- mice was 100-fold higher in the lower respiratory tract, indicating that STATs are required for RSV control *in vivo* (Cline *et al.,* 2009*)*. In agreement with these findings, an earlier study have shown that RSV infection in STAT1 knockout mice was characterized by airway dysfunction, airway mucus and airway hyperresponsiveness, related to augmented IL-17 levels (Hashimoto *et al.,* 2005). Notably, it was also shown that activation of STAT1 by both type I and type II IFNs plays an important role in establishing a protective Th1-biased immune response to RSV, supporting the role early innate immunity in

controlling RSV infection (Durbin *et al.,* 2002). *In vitro* studies have demonstrated that

RSV NS2 and NS1 target STAT2 for degradation, which successively interferes with

the type I IFN-mediated activation of STAT1 (Ramaswamy *et al.,* 2004; Goswami *et*

*al.,* 2013). Therefore, small molecules that suppress RSV NS1 and NS2 function against

STATs could allow the establishment of enhanced innate immunity against RSV

infection and prevent the development of ALRI. Taken together, although immune and

inflammatory responses to RSV contribute to virus pathogenicity, evidence suggests

that early innate immunity, especially the JAK/STAT signalling cascade, plays a crucial

role in controlling the outcome of RSV infection, supporting that NS1 and NS2 could

represent promising therapeutic targets. Hence, a therapy that combines antiviral and

anti-inflammatory drugs, which are more specific and less toxic, is likely to represent a

promising strategy for RSV prevention and control.

## 7.2 The advantages of our HTS approach and future applications

This study led to the development of a cell-based HTS assay, which allows the

identification of small molecules that inhibit targeted viral IFN antagonists. This HTS

assay offers several advantages over other drug discovery approaches. First, it negates

challenging downstream target identification required for non-targeted phenotypic

approaches. For example, a recent study has used a phenotypic cell-based reporter

assay, where the expression of firefly luciferase was under the control of IFN-β

promoter and identified molecules that inhibited the ability of Dengue virus to replicate

and hence induce activation of the IFN-β promoter (Guo *et al.,* 2014). Although this

study successfully identified small molecules that inhibit the replication of several

viruses of the family *Flaviviridae,* further investigations were required to reveal the antiviral mechanism of these compounds, which seems to be related to viral entry (Guo *et al.,* 2014). In contrast, our assay allows direct selection of compounds that inhibit targeted viral IFN antagonists.

Second, our HTS assay avoids lengthy *de novo* assay development required by traditional targeted approaches, as it allows the identification of small molecules that inhibit viral IFN antagonists from screened chemical libraries. In addition, targeted approaches are applicable only when structural information is available for the targeted protein. In this context, another advantage of this HTS approach is that it allows us to target viral IFN antagonists, which might not be completely characterized, and therefore cannot be used in a biochemical or structure-based assays. For instance, although the molecular structure of HCV NS5A protein is yet not fully elucidated, cell-based HTS assays led to the discovery of small molecules that inhibit the function(s) of this viral protein (Gao *et al.,* 2010; Lemm *et al.,* 2010). One of these inhibitors, Daclatasvir (BMS-790052) is currently in advanced stages of clinical trials and expected to get approval soon (Belema *et al.,* 2014). Previous work supports that cell-based HTS assays could outcompete limitations imposed by the lack of molecular structure and allow the discovery of inhibitors of not fully characterized viral proteins.

Targeting individual viral proteins also represents a promising screening approach for viruses that cause intense cytopathology in cell culture, such as RSV. Previous HTS screening efforts for identification of RSV inhibitors using CPE as endpoint have been hampered due to the inherent virus instability. More specifically, RSV causes cell-cell fusion and death in cell culture, which interferes with the consistency and robustness of cell-based HTS approaches against RSV. To overcome

the virus instability problem, a recent study has proposed the use of cryopreserved RSV-infected cells as the source of infectious material, and developed a cell-based HTS assay that allows identification of inhibitors of RSV-induced CPE (Rasmussen *et al.,* 2011). Additional studies have demonstrated that cryopreserved RSV-replicon-infected cells are a more promising alternative to RSV CPE assays for HTS (Plant *et al.,* 2015; Tiong-Yip *et al.,* 2014). In particular, RSV replicon HTS assays are more consistent than RSV CPE assays, as RSV replicon lacks all three glycoproteins (F, G, SH), and hence cannot cause syncytia cytopathology or virus spread, which are key sources of assay variation (Malykhina *et al.,* 2011). In conclusion, although virus replicon or virus CPE-based HTS assays require target identification, one major advantage these assays have is the capability to simultaneously target several virus mechanisms. On the other hand, targeting isolated viral proteins allows the development of screening approaches that (i) are not affected by RSV cytotoxicity and instability, (ii) are readily amendable to scale and (iii) do not pose biological safety hazards associated with live viral assays.

In addition to virus instability and cytotoxicity, virus pathogenicity is also a major obstacle for HTS approaches. Indeed, drug discovery for highly pathogenic viruses (e.g. Ebola and Nipah viruses) is hindered due to requirement for biosafety level 4 containment facilities. Overcoming this limitation, this screening platform allows the discovery of direct-acting antiviral agents by targeting their viral IFN antagonists in lower containment facilities. Screening at lower containment level provides more flexibility in experimental design, allowing for a more effective HTS method, and considerably reduces the screening costs. Overall, the suitability and effectiveness of a HTS approach depends on the virus itself, the current knowledge about virus replication and the available information regarding the biochemistry of viral proteins.

## 7.2.1 A global strategy for targeting viral IFN antagonists

The conservation of IFN antagonism within certain virus families and its importance in viral replication makes viral IFN antagonists attractive targets for drug discovery. As most viruses express at least one viral IFN antagonist, this provides a wide variety of targets for the discovery of novel antiviral drugs. The effectiveness of this screening platform has been validated after the successful identification of RSV NS2 inhibitors. This technology can be expanded to a number of different viral IFN antagonists expressed by other clinically important viruses, which cause different type of infections such as chronic, zoonotic or emerging infections.

One of the viral IFN antagonists that we are interested in targeting is the rabies virus (RABV) phosphoprotein (P) protein. Although there is an effective rabies vaccine, rabies still remains a devastating zoonotic disease as it causes 40,000 to 70,000 human deaths per year worldwide and has a case-fatality rate of almost 100% in non-vaccinated individuals (Schnell *et al.,* 2010). The primary focus in rabies therapeutics is to reduce cost and complexity, and also improve effectiveness of postexposure prophylaxis (PEP). The only available PEP treatment for individuals with category III exposures to rabies (bites, scratches, and mucosal contacts) is active immunization with multiple doses of rabies vaccine, and passive immunization with human rabies immune globulin (Smith *et al.,* 2011; WHO 2015). The objective of PEP is to prevent rabies from gaining access to the nervous system, hence PEP's eficacy is limited once clinical signs of rabies develop. Antiviral molecules are highly likely to increase the effectiveness of the current PEP therapy, as they could more rapidly restrict virus replication; however penetration through the blood-brain barrier is essential for their therapeutic efficacy in the central nervous system (Appolinario & Jackson 2015).

RABV is a poor inducer of type I IFNs, indicating the existence of viral mechanisms preventing the cellular IFN response to virus infection. The ability of rabies virusto escape the antiviral response induced by IFNs is attributed to its P protein, which is considered the major IFN antagonist of lyssaviruses (Rieder & Conzelmann 2011). Similar to all the viruses in the order *Mononegavirales*, RABV P protein is also critical for virus replication, as together with nucleoprotein (N) and RNA polymerase (L) forms the viral ribonucleoprotein, which is essential for transcription and replication of the viral RNA genome (Conzelmann 1998).

Targeting RABV P represents a promising target for drug discovery, especially due to the well-defined interaction of P protein with the IFN-signalling pathway. Previous studies have shown that RABV P prevents IFNα/β- and IFNγ-stimulated JAK/STAT signalling as it binds to tyrosine-phosphoryalted STATs in the cytoplasm, and thereby blocks ISGF3 formation and the subsequent activation of the ISRE elements (Brzózka *et al.,* 2006; Lieu *et al.,* 2013). Specifically, a hydrophobic pocket in the P protein CTD was found to be critical for STAT antagonism (Wiltzer *et al.,* 2014; Brzózka *et al.,* 2006). The interaction of Rabies P with STATs is critical to lethal rabies disease, as mutant rabies viruses that lacked STAT-antagonism function were highly attenuated in mice (Wiltzer *et al.,* 2014). Notably, the unique mechanism of selective targeting of IFN-activated STAT proteins by RABV P protein is conserved between the most distantly related lyssaviruses, indicating a conserved immune evasion strategy between the *Lyssavirus* genus (Wiltzer *et al.,* 2012). Hence the current insights into the conserved mechanisms by which lyssaviruses coordinate distinct functions in IFN antagonism, highlight the potential of targeting P for the development of virus-specific antivirals with broad activity against the lyssaviruses.

In order to target RABV P using HTS, we developed an A549.pr(ISRE)GFP derivative that constitutively expresses RABV P (Figure 7.2/A). Once RABV expression was confirmed, the functionality of RABV P in the A549.pr(ISRE)GFP-RABV/P cell-line was tested by measuring the effect of P expression on the IFN-signalling pathway (Figure 7.2/B). In agreement with previous work (Brzózka *et al.,* 2005; Brzózka *et al.,* 2006; Lieu *et al.,* 2013), RABV P completely blocked the IFN-induced activation of the ISRE element, hence no GFP positive cells were detected in the P-expressing A549.pr(ISRE)GFP reporter cell-line (Figure 7.2/B). Likewise, GFP quantification showed that GFP expression was reduced to background levels in the A549.pr(ISRE)GFP-RABV/P reporter cell-line (Figure 7.2/B). The clear cut reduction in MxA expression also confirmed the inhibitory effect of RABV P against the IFN-signalling  pathway (Figure 7.2/C). Overall, our data shows that we successfully generated a derivate of the A549.pr(ISRE)GFP reporter cell-line that constitutively expresses RABV P protein, which completely blocks activation of the IFN-signalling, hence no GFP expression was observed in the A549.pr(ISRE)GFP-RABV/P reporter cell-line.

Future work will be to perform HTS using the A549.pr(ISRE)GFP-RABV/P to identify small molecules that inhibit RABV P function against the IFN-signalling pathway. Evidence suggests that the hydrophobic pocket in the P CTD is indispensable for STATs antagonism and virus replication; hence it signifies a promising therapeutic target.

A

A549.pr(ISRE)GFP

RABV/P

| - | + |

RABV/P (anti-V5)

β-actin

B

| - IFN | + IFN |

A549.pr(ISRE)GFP

RABV/P

-

+



v

C

A549.pr(ISRE)GFP

RABV/P

| - | + |

| - | + | + | - | + | + | *IFN-α* |
| 48 | 16 | 48 | 48 | 16 | 48 | hours post treatment |

72kDa — MxA

42kDa — β-actin
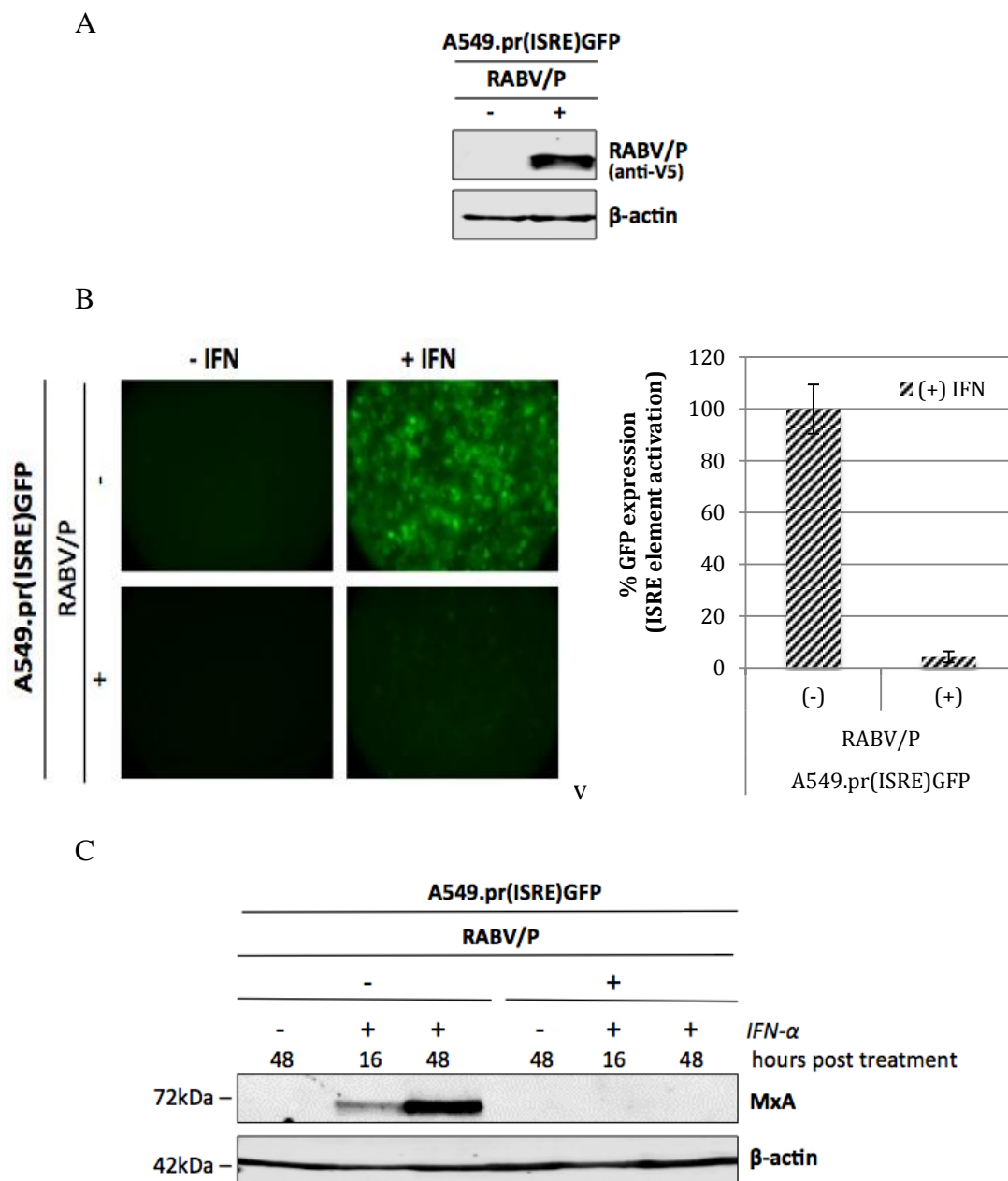
**Figure 7.2 Generation of a cell-based reporter assay for targeting RABV P. (A)** Expression of RABV P in the A549.pr(ISRE)GFP cell-line, as determined by western blot analysis. RABV P expression was detected using an anti-V5 antibody, which recognizes the V5 peptide tag that is fused to the N-terminus of the protein. **(B-C)** The effect of RABV P against the IFN-α activation of the ISRE element was monitored by measuring GFP expression (B) and MxA expression (C). GFP expression was observed with fluorescent microscopy and quantified using TECAN plate reader. Graph is presented as percentage (%) of GFP expression relative to naïve A549.pr(ISRE)GFP, which was set as 100% control. Bars present mean values (n=12) and error bars show SD. MxA expression levels were observed at 16h and 48h post IFN-α (2000 U/ml) treatment using Odyssey CLx imager.

## 7.3 Conclusion

This study led to the development of a modular cell-based screening platform, which could enable the discovery of novel direct-acting antivirals by the identification of small molecules that inhibit targeted viral IFN antagonists of clinically important viruses. Our HTS approach has been validated and its effectiveness has been demonstrated though the successful identification of four small molecules that specifically inhibit the STAT2 degradation function of RSV NS2, a crucial function for RSV antagonism against type I IFNs. The compounds' activity will be further optimized using medicinal chemistry and subsequently, these compounds will be used as chemical tools to determine the unknown mechanism by which NS2 mediates STAT2 degradation and also to determine if NS2 is a suitable drug target. Future work will target IFN antagonists from other viruses for which there is a clinical need for new antiviral drugs, such as Rabies P, PIV3 C and Dengue NS5 proteins. In conclusion, this HTS approach provides a global strategy for the identification of virus-specific antiviral compounds that inhibit viral IFN antagonists. This allows us to validate viral IFN antagonists as drug targets and determine whether inhibitors of viral IFN antagonist could represent a novel class of virus specific antivirals.

# References

Abu-Harb, M., Bell, F., Finn, A., Rao, W.H., Nixon, L., Shale, D. & Everard, M.L., (1999). IL-8 and neutrophil elastase levels in the respiratory tract of infants with RSV bronchiolitis. *European Respiratory Journal*, **14**(1), pp.139–143.

Adams, J., Behnke, M., Chen, S., Cruickshank, A.A., Dick, L.R., Grenier, L., Klunder, J.M., Ma, Y.T., Plamondon, L. & Stein, R.L., (1998). Potent and selective inhibitors of the proteasome: dipeptidyl boronic acids. *Bioorganic & medicinal chemistry letters*, **8**(4), pp.333–8.

Adkins, B., Leclerc, C. & Marshall-Clarke, S., (2004). Neonatal adaptive immunity comes of age. *Nat Rev Immunol*, **4**(7), pp.553–564.

Agoti, C.N., Otieno, J.R., Munywoki, P.K., Mwihuri, A.G., Cane, P.A., Nokes, D.J., Kellam, P. & Cotten, M., (2015). Local Evolutionary Patterns of Human Respiratory Syncytial Virus Derived from Whole-Genome Sequencing. *Journal of Virology*, **89**(7), pp.3444–3454.

Alansari, H. & Potgieter, L.N., (1994). Nucleotide and predicted amino acid sequence analysis of the ovine respiratory syncytial virus non-structural 1C and 1B genes and the small hydrophobic protein gene. *J Gen Virol*, **75**, pp.401–404.

Alexopoulou, L., Holt, C., Medzhitov, R. & Flavell, R., (2001). Recognition of double-stranded RNA and activation of NF-kappaB by Toll-like receptor 3. *Nature*, **413**(1985), pp.732–738.

Anderson, L.J., Hierholzer, J.C., Tsou, C., Hendry, R.M., Fernie, B.F., Stone, Y. & McIntosh, K., (1985). Antigenic characterization of respiratory syncytial virus strains with monoclonal antibodies. *The Journal of infectious diseases*, **151**(4), pp.626–633.

Andrejeva, J., Childs, K.S., Young, D.F., Carlos, T.S., Stock, N., Goodbourn, S. & Randall, R.E., (2004). The V proteins of paramyxoviruses bind the IFN-inducible RNA helicase, mda-5, and inhibit its activation of the IFN-beta promoter. *Proceedings of the National Academy of Sciences of the United States of America*, **101**(49), pp.17264–17269.

Andrejeva, J., Norsted, H., Habjan, M., Thiel, V., Goodbourn, S. & Randall, R.E., (2013). ISG56/IFIT1 is primarily responsible for interferoninduced changes to patterns of parainfluenza virus type 5 transcription and protein synthesis. *Journal of General Virology*, **94**, pp.59–60.

Andrejeva, J., Poole, E., Young, D.F., Goodbourn, S. & Randall, R.E., (2002). The p127 subunit (DDB1) of the UV-DNA damage repair binding protein is essential for the targeted degradation of STAT1 by the V protein of the paramyxovirus simian virus 5. *Journal of virology*, **76**(22), pp.11379–11386.

Anon, (2006). Diagnosis and management of bronchiolitis. *Pediatrics*, **118**(4), pp.1774–93.

Aoki, F.Y., Allen, U.D., Stiver, H.G. & Evans, G. a., (2013). The use of antiviral drugs for influenza: A foundation document for practitioners. *Canadian Journal of Infectious Diseases and Medical Microbiology*, **24**(3), pp.1–15.

Appolinario, C.M. & Jackson, A.C., (2015). Antiviral therapy for human rabies. *Antiviral therapy*, **20**(1), pp.1–10.

Asenjo, A., Calvo, E. & Villanueva, N., (2006). Phosphorylation of human respiratory syncytial virus P protein at threonine 108 controls its interaction with the M2-1 protein in the viral RNA polymerase complex. *The Journal of general virology*, **87**, pp.3637–42.

Atreya, P.L., Peeples, M.E. & Collins, P.L., (1998). The NS1 protein of human respiratory syncytial virus is a potent inhibitor of minigenome transcription and RNA replication. *Journal of virology*, **72**(2), pp.1452–61.

Audsley, M.D. & Moseley, G.W., (2013). Paramyxovirus evasion of innate immunity: Diverse strategies for common targets. *World journal of virology*, **2**(2), pp.57–70.

Barik, S., (2013). Respiratory Syncytial Virus Mechanisms to Interfere with Type 1 Interferons. In L. J. Anderson & B. S. Graham, eds. *Challenges and Opportunities for Respiratory Syncytial Virus Vaccines*. Springer Berlin Heidelberg, pp. 173–191.

Barik, S. & Lu, P., (2015). Therapy of respiratory viral infections with intranasal siRNAs. *Methods in molecular biology*, **1218**, pp.251–62.

Basagoudanavar, S.H., Thapa, R.J., Nogusa, S., Wang, J., Beg, A. a & Balachandran, S., (2011). Distinct roles for the NF-kappa B RelA subunit during antiviral innate immune responses. *Journal of virology*, **85**(6), pp.2599–2610.

Bawage, S.S., Tiwari, P.M., Pillai, S., Dennis, V. & Singh, S.R., (2013). Recent advances in diagnosis, prevention, and treatment of human respiratory syncytial virus. *Advances in virology*, **2013**, p.595768.

Belema, M., Nguyen, V.N., Bachand, C., Deon, D.H., Goodrich, J.T., James, C.A., Lavoie, R., Lopez, O.D., Martel, A., Romine, J.L., Ruediger, E.H., Snyder, L.B., St Laurent, D.R., Yang, F., Zhu, J., Wong, H.S., Langley, D.R., Adams, S.P., Cantor, G.H., Chimalakonda, A., Fura, A., Johnson, B.M., Knipe, J.O., Parker, D.D., Santone, K.S., Fridell, R.A., Lemm, J.A., O'Boyle, D.R., Colonno, R.J., Gao, M., Meanwell, N.A. & Hamann, L.G., (2014). Hepatitis C virus NS5A replication complex inhibitors: the discovery of daclatasvir. *Journal of medicinal chemistry*, **57**(5), pp.2013–32.

Bem, R.A., Domachowske, J.B. & Rosenberg, H.F., (2011). Animal models of human

respiratory syncytial virus disease. *American journal of physiology. Lung cellular and molecular physiology*, **301**(2), pp.L148–56.

Bermejo-Martin, J.F., Garcia-Arevalo, M.C., De Lejarazu, R.O., Ardura, J., Eiros, J.M., Alonso, A., Matías, V., Pino, M., Bernardo, D., Arranz, E. & Blanco-Quiros, A., (2007). Predominance of Th2 cytokines, CXC chemokines and innate immunity mediators at the mucosal level during severe respiratory syncytial virus infection in children. *European cytokine network*, **18**(3), pp.162–7.

Bermingham, A. & Collins, P.L., (1999). The M2-2 protein of human respiratory syncytial virus is a regulatory factor involved in the balance between RNA replication and transcription. *Proceedings of the National Academy of Sciences of the United States of America*, **96**(20), pp.11259–64.

Biswal, S., Sahoo, U., Sethy, S., Kumar, H.K.S., Banerjee, M. & Hooker, J., (2012). Asian Journal of Pharmaceutical and clinical Research. *Asian Journal of Pharmaceutical and Clinical Research*, **5**(1), pp.1–6.

Bitko, V., Musiyenko, A., Bayfield, M. a, Maraia, R.J. & Barik, S., (2008). Cellular La protein shields nonsegmented negative-strand RNA viral leader RNA from RIG-I and enhances virus growth by diverse mechanisms. *Journal of virology*, **82**, pp.7977–7987.

Bitko, V., Musiyenko, A., Shulyayeva, O. & Barik, S., (2005). Inhibition of respiratory viruses by nasally administered siRNA. *Nature medicine*, **11**(1), pp.50–55.

Blount, R.E., Morris, J.A. & Savage, R.E., (1956). Recovery of Cytopathogenic Agent from Chimpanzees with Goryza. *Experimental Biology and Medicine*, **92**(3), pp.544–549.

Le Bon, A. & Tough, D.F., (2002). Links between innate and adaptive immunity via type I interferon. *Current Opinion in Immunology*, **14**(4), pp.432–436.

Bossert, B., Marozin, S. & Conzelmann, K., (2003). Nonstructural Proteins NS1 and NS2 of Bovine Respiratory Syncytial Virus Block Activation of Interferon Regulatory Factor 3. *Journal of Virology*, **77**(16), pp.8661–8668.

van Boxel-Dezaire, A.H.H., Rani, M.R.S. & Stark, G.R., (2006). Complex modulation of cell type-specific signaling in response to type I interferons. *Immunity*, **25**(3), pp.361–72.

Boyapalle, S., Wong, T., Garay, J., Teng, M., San Juan-Vergara, H., Mohapatra, S. & Mohapatra, S., (2012). Respiratory syncytial virus NS1 protein colocalizes with mitochondrial antiviral signaling protein MAVS following infection. *PLoS ONE*, **7**(2), p.e29386.

Brierley, M.M., Marchington, K.L., Jurisica, I. & Fish, E.N., (2006). Identification of GAS-dependent interferon-sensitive target genes whose transcription is STAT2-

dependent but ISGF3-independent. *The FEBS journal*, **273**(7), pp.1569–81.

Brock, S.C., Goldenring, J.R. & Crowe, J.E., (2003). Apical recycling systems regulate directional budding of respiratory syncytial virus from polarized epithelial cells. *Proceedings of the National Academy of Sciences of the United States of America*, **100**(25), pp.15143–8.

Brown, C.S., Lee, M.S., Leung, D.W., Wang, T., Xu, W., Luthra, P., Anantpadma, M., Shabman, R.S., Melito, L.M., MacMillan, K.S., Borek, D.M., Otwinowski, Z., Ramanan, P., Stubbs, A.J., Peterson, D.S., Binning, J.M., Tonelli, M., Olson, M.A., Davey, R.A., Ready, J.M., Basler, C.F. & Amarasinghe, G.K., (2014). In silico derived small molecules bind the filovirus VP35 protein and inhibit its polymerase cofactor activity. *Journal of molecular biology*, **426**(10), pp.2045–58.

Broz, P. & Monack, D.M., (2013). Newly described pattern recognition receptors team up against intracellular pathogens. *Nature reviews. Immunology*, **13**(8), pp.551–65.

Brzózka, K., Finke, S. & Brzo, K., (2005). Identification of the Rabies Virus Alpha / Beta Interferon Antagonist : Phosphoprotein P Interferes with Phosphorylation of Interferon Regulatory Factor 3 Identification of the Rabies Virus Alpha / Beta Interferon Antagonist : Phosphoprotein P Interferes. *Journal*, **79**(12), pp.7673–81.

Brzózka, K., Finke, S. & Conzelmann, K.-K., (2006). Inhibition of interferon signaling by rabies virus phosphoprotein P: activation-dependent binding of STAT1 and STAT2. *Journal of virology*, **80**(6), pp.2675–2683.

Caraglia, M., Dicitore, A., Marra, M., Castiglioni, S., Persani, L., Sperlongano, P., Tagliaferri, P., Abbruzzese, A. & Vitale, G., (2013). Type I interferons: ancient peptides with still under-discovered anti-cancer properties. *Protein and peptide letters*, **20**(4), pp.412–23.

Carlos, T.S., Young, D., Stertz, S., Kochs, G. & Randall, R.E., (2007). Interferon-induced inhibition of parainfluenza virus type 5; the roles of MxA, PKR and oligo A synthetase/RNase L. *Virology*, **363**(1), pp.166–73.

Carnero, E., (2006). High throughput screening in drug discovery. *Clinical & translational oncology : official publication of the Federation of Spanish Oncology Societies and of the National Cancer Institute of Mexico*, **8**, pp.482–490.

Chambers, R. & Takimoto, T., (2009). Antagonism of innate immunity by Paramyxovirus accessory proteins. *Viruses*, **1**, pp.574–593.

Chang, S., Dolganiuc, A. & Szabo, G., (2007). Toll-like receptors 1 and 6 are involved in TLR2-mediated macrophage activation by hepatitis C virus core and NS3 proteins. *Journal of leukocyte biology*, **82**(3), pp.479–87.

Chanock, R.M., Roizman B & Myers R, (1956). Recovery from infants with respiratory illness of a virus related to chimpanzee coryza agent (CCA). II. Epidemiologic

aspects of infection in infants and young children. *American Journal of Epidemiology*, **92**, pp.544–9.

Chapman, J., Abbott, E., Alber, D.G., Baxter, R.C., Bithell, S.K., Henderson, E. a., Carter, M.C., Chambers, P., Chubb, A., Cockerill, G.S., Collins, P.L., Dowdell, V.C.L., Keegan, S.J., Kelsey, R.D., Lockyer, M.J., Luongo, C., Najarro, P., Pickles, R.J., Simmonds, M., Taylor, D., Tyms, S., Wilson, L.J. & Powell, K.L., (2007). RSV604, a novel inhibitor of respiratory syncytial virus replication. *Antimicrobial Agents and Chemotherapy*, **51**(9), pp.3346–3353.

Chen, J., Ng, M.M.-L. & Chu, J.J.H., (2015). Activation of TLR2 and TLR6 by Dengue NS1 Protein and Its Implications in the Immunopathogenesis of Dengue Virus Infection. *PLoS pathogens*, **11**(7), p.e1005053.

Chen, S., Short, J. a L., Young, D.F., Killip, M.J., Schneider, M., Goodbourn, S. & Randall, R.E., (2010). Heterocellular induction of interferon by negative-sense RNA viruses. *Virology*, **407**(2), pp.247–255.

Childs, K., Stock, N., Ross, C., Andrejeva, J., Hilton, L., Skinner, M., Randall, R., Goodbourn, S. & Virology, (2007). mda-5, but not RIG-I, is a common target for paramyxovirus V proteins. *Virology*, **359**(1), pp.190–200.

Chirkova, T., Boyoglu-Barnum, S., Gaston, K. a, Malik, F.M., Trau, S.P., Oomens, A.G.P. & Anderson, L.J., (2013). Respiratory Syncytial Virus G Protein CX3C Motif Impairs Human Airway Epithelial and Immune Cell Responses. *Journal of Virology*, **87**(24), pp.13466–79.

Chu, H.Y. & Englund, J.A., (2013). Respiratory syncytial virus disease: prevention and treatment. *Current topics in microbiology and immunology*, **372**, pp.235–58.

Cianci, C., Langley, D.R., Dischino, D.D., Sun, Y., Yu, K.-L., Stanley, A., Roach, J., Li, Z., Dalterio, R., Colonno, R., Meanwell, N. a & Krystal, M., (2004). Targeting a binding pocket within the trimer-of-hairpins: small-molecule inhibition of viral fusion. *Proceedings of the National Academy of Sciences of the United States of America*, **101**(42), pp.15046–15051.

Cline, T., Jewell, N., Mertz, S., Kotenko, S., Schindler, C., Durbin, R. & Durbin, J., (2009). STAT1 and STAT2 are required for control of RSV replication in vivo. *The Journal of Immunology*, **182**, p.44.7.

Collins, P.L., (1991). *Paramyxoviruses; The Molecular Biology of Human Respiratory Syncytial Virus (RSV) of the Genus Pneumovirus* D. W. Kingsbury, ed., Boston, MA: Springer US.

Collins, P.L. & Crowe J., (2007). *Respiratory Syncytial Virus and Metapneumovirus.* 5th ed. H. P. In Fields Virology Knipe DM, ed., Philadelphia: Wolters Kluwer and Lippincott Williams & Wilkins.

Collins, P.L., Fearns, R. & Graham, B.S., (2013). Respiratory syncytial virus: virology, reverse genetics, and pathogenesis of disease. *Current topics in microbiology and immunology*, **372**, pp.3–38.

Collins, P.L. & Graham, B.S., (2008). Viral and host factors in human respiratory syncytial virus pathogenesis. *Journal of virology*, **82**(5), pp.2040–55.

Collins, P.L., Huang, Y.T. & Wertz, G.W., (1984). Nucleotide sequence of the gene encoding the fusion (F) glycoprotein of human respiratory syncytial virus. *Proceedings of the National Academy of Sciences of the United States of America*, **81**(24), pp.7683–7.

Collins, P.L. & Melero, J. a., (2011). Progress in understanding and controlling respiratory syncytial virus: Still crazy after all these years. *Virus Research*, **162**(1-2), pp.80–99.

Collins, P.L. & Murphy, B.R., (2002). Respiratory syncytial virus: reverse genetics and vaccine strategies. *Virology*, **296**(2), pp.204–211.

Collins, P.L., Olmsted, R. a, Spriggs, M.K., Johnson, P.R. & Buckler-White, a J., (1987). Gene overlap and site-specific attenuation of transcription of the viral polymerase L gene of human respiratory syncytial virus. *Proceedings of the National Academy of Sciences of the United States of America*, **84**(15), pp.5134–5138.

Conzelmann, K.K., (1998). Nonsegmented negative-strand RNA viruses: genetics and manipulation of viral genomes. *Annual review of genetics*, **32**, pp.123–62.

Cordano, P., Gillan, V., Bratlie, S., Bouvard, V., Banks, L., Tommasino, M. & Campo, M.S., (2008). The E6E7 oncoproteins of cutaneous human papillomavirus type 38 interfere with the interferon pathway. *Virology*, **377**(2), pp.408–418.

Cormier, S.A., You, D. & Honnegowda, S., (2010). The use of a neonatal mouse model to study respiratory syncytial virus infections. *Expert review of anti-infective therapy*, **8**(12), pp.1371–80.

De Corte, B.L., (2005). From 4,5,6,7-tetrahydro-5-methylimidazo[4,5,1-jk](1,4)benzodiazepin-2(1H)-one (TIBO) to etravirine (TMC125): fifteen years of research on non-nucleoside inhibitors of HIV-1 reverse transcriptase. *Journal of medicinal chemistry*, **48**(6), pp.1689–96.

Decker, T., Lew, D.J. & Darnell, J.E., (1991). Two distinct alpha-interferon-dependent signal transduction pathways may contribute to activation of transcription of the guanylate-binding protein gene. *Molecular and cellular biology*, **11**(10), pp.5147–53.

DeVincenzo, J., Lambkin-Williams, R., Wilkinson, T., Cehelsky, J., Nochur, S., Walsh, E., Meyers, R., Gollob, J. & Vaishnaw, A., (2010). A randomized, double-blind,

placebo-controlled study of an RNAi-based therapy directed against respiratory syncytial virus. *Proceedings of the National Academy of Sciences of the United States of America*, **107**(19), pp.8800–8805.

DeVincenzo, J.P., Whitley, R.J., Mackman, R.L., Scaglioni-Weinlich, C., Harrison, L., Farrell, E., McBride, S., Lambkin-Williams, R., Jordan, R., Xin, Y., Ramanathan, S., O'Riordan, T., Lewis, S. a, Li, X., Toback, S.L., Lin, S.-L. & Chien, J.W., (2014). Oral GS-5806 Activity in a Respiratory Syncytial Virus Challenge Study. *The New England journal of medicine*, **371**, pp.711–722.

Dhar, J., Cuevas, R.A., Goswami, R., Zhu, J., Sarkar, S.N. & Barik, S., (2015). 2' -5' - Oligoadenylate Synthetase-Like Inhibits Respiratory Syncytial Virus Replication and is Targeted by the Viral Nonstructural Protein 1. *Journal of virology*, **89**(19), pp.10115–9.

Diamond, M.S. & Farzan, M., (2013). The broad-spectrum antiviral functions of IFIT and IFITM proteins. *Nature reviews. Immunology*, **13**(1), pp.46–57.

Didcock, L., Young, D.F., Goodbourn, S. & Randall, R.E., (1999). The V protein of simian virus 5 inhibits interferon signalling by targeting STAT1 for proteasome-mediated degradation. *Journal of virology*, **73**(12), pp.9928–33.

Dinwiddie, D.L. & Harrod, K.S., (2008). Human metapneumovirus inhibits IFN-alpha signaling through inhibition of STAT1 phosphorylation. *American Journal of Respiratory Cell and Molecular Biology*, **38**(6), pp.661–670.

Donelan, N.R., Basler, C.F. & García-Sastre, A., (2003). A recombinant influenza A virus expressing an RNA-binding-defective NS1 protein induces high levels of beta interferon and is attenuated in mice. *Journal of virology*, **77**(24), pp.13257–66.

Donnelly, M.L., Hughes, L.E., Luke, G., Mendoza, H., ten Dam, E., Gani, D. & Ryan, M.D., (2001). The "cleavage" activities of foot-and-mouth disease virus 2A site-directed mutants and naturally occurring "2A-like" sequences. *The Journal of general virology*, **82**(Pt 5), pp.1027–41.

Van Drunen Littel-Van Den Hurk, S. & Watkiss, E.R., (2012). Pathogenesis of respiratory syncytial virus. *Current Opinion in Virology*, **2**(3), pp.300–305.

Duffy, K.J., Darcy, M.G., Delorme, E., Dillon, S.B., Eppley, D.F., Erickson-Miller, C., Giampa, L., Hopson, C.B., Huang, Y., Keenan, R.M., Lamb, P., Leong, L., Liu, N., Miller, S.G., Price, A.T., Rosen, J., Shah, R., Shaw, T.N., Smith, H., Stark, K.C., Tian, S.S., Tyree, C., Wiggall, K.J., Zhang, L. & Luengo, J.I., (2001). Hydrazinonaphthalene and azonaphthalene thrombopoietin mimics are nonpeptidyl promoters of megakaryocytopoiesis. *Journal of medicinal chemistry*, **44**(22), pp.3730–45.

Durbin, J.E., Johnson, T.R., Durbin, R.K., Mertz, S.E., Morotti, R. a, Peebles, R.S. &

Graham, B.S., (2002). The role of IFN in respiratory syncytial virus pathogenesis. *Journal of immunology*, **168**(6), pp.2944–2952.

Egli, A., Santer, D.M., O'Shea, D., Tyrrell, D.L. & Houghton, M., (2014). The impact of the interferon-lambda family on the innate and adaptive immune response to viral infections. *Emerging Microbes & Infections*, **3**(7), p.e51.

Elliott, J., Lynch, O.T., Suessmuth, Y., Qian, P., Boyd, C.R., Burrows, J.F., Buick, R., Stevenson, N.J., Touzelet, O., Gadina, M., Power, U.F. & Johnston, J.A., (2007). Respiratory syncytial virus NS1 protein degrades STAT2 by using the Elongin-Cullin E3 ligase. *Journal of virology*, **81**, pp.3428–3436.

Evans, J.E., Cane, P.A. & Pringle, C.R., (1996). Expression and characterisation of the NS1 and NS2 proteins of respiratory syncytial virus. *Virus research*, **43**(2), pp.155–61.

Everett, R.D. & Chelbi-Alix, M.K., (2007). PML and PML nuclear bodies: Implications in antiviral defence. *Biochimie*, **89**(2001), pp.819–830.

Falsey, A., Walsh, E. & Clin Microbiol, R., (2000). Respiratory syncytial virus infection in adults. *Clinical Microbiology Reviews* , **13**(3), pp.371–384.

Fearns, R. & Collins, P.L., (1999). Role of the M2-1 transcription antitermination protein of respiratory syncytial virus in sequential transcription. *Journal of virology*, **73**(7), pp.5852–64.

Ferrantini, M., Capone, I. & Belardelli, F., Interferon-alpha and cancer: mechanisms of action and new perspectives of clinical use. *Biochimie*, **89**(6-7), pp.884–93.

Da Fonseca, P.C., He, J. & Morris, E.P., (2012). Molecular Model of the Human 26S Proteasome. *Molecular Cell*, **46**(1), pp.54–66.

Fry, D.W., Kraker, A.J., McMichael, A., Ambroso, L.A., Nelson, J.M., Leopold, W.R., Connors, R.W. & Bridges, A.J., (1994). A specific inhibitor of the epidermal growth factor receptor tyrosine kinase. *Science*, **265**(5175), pp.1093–5.

Gack, M.U., Albrecht, R.A., Urano, T., Inn, K.S., Huang, I.C., Carnero, E., Farzan, M., Inoue, S., Jung, J.U. & Garcia-Sastre, A., (2009). Influenza A virus NS1 targets the ubiquitin ligase TRIM25 to evade recognition by the host viral RNA sensor RIG-I. *Cell host & microbe*, **5**(5), pp.439–449.

Gago, S., Elena, S.F., Flores, R. & Sanjuán, R., (2009). Extremely high mutation rate of a hammerhead viroid. *Science*, **323**(5919), p.1308.

Gao, M., Nettles, R.E., Belema, M., Snyder, L.B., Nguyen, V.N., Fridell, R.A., Serrano-Wu, M.H., Langley, D.R., Sun, J.-H., O'Boyle, D.R., Lemm, J.A., Wang, C., Knipe, J.O., Chien, C., Colonno, R.J., Grasela, D.M., Meanwell, N.A. & Hamann, L.G., (2010). Chemical genetics strategy identifies an HCV NS5A inhibitor with a

potent clinical effect. *Nature*, **465**(7294), pp.96–100.

García-Barreno, B., Delgado, T. & Melero, J.A., (1996). Identification of protein regions involved in the interaction of human respiratory syncytial virus phosphoprotein and nucleoprotein: significance for nucleocapsid assembly and formation of cytoplasmic inclusions. *Journal of virology*, **70**(2), pp.801–8.

Garcin, D., Marq, J.-B., Strahle, L., le Mercier, P. & Kolakofsky, D., (2002). All four Sendai Virus C proteins bind Stat1, but only the larger forms also induce its mono-ubiquitination and degradation. *Virology*, **295**(2), pp.256–65.

Gauzzi, M.C., Velazquez, L., McKendry, R., Mogensen, K.E., Fellous, M. & Pellegrini, S., (1996). Interferon-alpha-dependent activation of Tyk2 requires phosphorylation of positive regulatory tyrosines by another kinase. *The Journal of biological chemistry*, **271**(34), pp.20494–500.

Gentile, I., Viola, C., Borgia, F., Castaldo, G. & Borgia, G., (2009). Telaprevir: a promising protease inhibitor for the treatment of hepatitis C virus infection. *Current medicinal chemistry*, **16**(9), pp.1115–21.

Georgel, P., Jiang, Z., Kunz, S., Janssen, E., Mols, J., Hoebe, K., Bahram, S., Oldstone, M.B.A. & Beutler, B., (2007). Vesicular stomatitis virus glycoprotein G activates a specific antiviral Toll-like receptor 4-dependent pathway. *Virology*, **362**(2), pp.304–13.

Ghildyal, R., Baulch-Brown, C., Mills, J. & Meanger, J., (2003). The matrix protein of Human respiratory syncytial virus localises to the nucleus of infected cells and inhibits transcription. *Archives of virology*, **148**(7), pp.1419–29.

Gibbs, J.D., Ornoff, D.M., Igo, H.A., Zeng, J.Y. & Imani, F., (2009). Cell cycle arrest by transforming growth factor beta1 enhances replication of respiratory syncytial virus in lung epithelial cells. *Journal of virology*, **83**(23), pp.12424–31.

Gogela, N.A., Lin, M. V, Wisocky, J.L. & Chung, R.T., (2015). Enhancing Our Understanding of Current Therapies for Hepatitis C Virus (HCV). *Current HIV/AIDS reports*, **12**(1), pp.68–78.

Goktug, A.N., Chai, S.C. & Chen, T., (2013). Drug Discovery - Data analysis approaches in high throughput screening. In *Intech*. pp. 201–226.

Goldberg, A.L., (2012). Development of proteasome inhibitors as research tools and cancer drugs. *The Journal of cell biology*, **199**(4), pp.583–8.

Gomez, D. & Reich, N.C., (2003). Stimulation of primary human endothelial cell proliferation by IFN. *Journal of immunology*, **170**(11), pp.5373–81.

Gonzalez, M.E. & Carrasco, L., (2003). Viroporins. *FEBS letters*, **552**(1), pp.28–34.

González-Navajas, J.M., Lee, J., David, M. & Raz, E., (2012). Immunomodulatory functions of type I interferons. *Nature reviews. Immunology*, **12**(2), pp.125–35.

González-Reyes, L., Ruiz-Argüello, M.B., García-Barreno, B., Calder, L., López, J.A., Albar, J.P., Skehel, J.J., Wiley, D.C. & Melero, J.A., (2001). Cleavage of the human respiratory syncytial virus fusion protein at two distinct sites is required for activation of membrane fusion. *Proceedings of the National Academy of Sciences of the United States of America*, **98**(17), pp.9859–64.

Goodbourn, S. & Randall, R.E., (2009). The regulation of type I interferon production by paramyxoviruses. *Journal of interferon & cytokine research : the official journal of the International Society for Interferon and Cytokine Research*, **29**(9), pp.539–547.

Goswami, R., Majumdar, T., Dhar, J., Chattopadhyay, S., Bandyopadhyay, S.K., Verbovetskaya, V., Sen, G.C. & Barik, S., (2013). Viral degradasome hijacks mitochondria to suppress innate immunity. *Cell research*, **23**(8), pp.1025–42.

Gotoh, B., Takeuchi, K., Komatsu, T., Yokoo, J., Kimura, Y., Kurotani, A., Kato, A. & Nagai, Y., (1999). Knockout of the Sendai virus C gene eliminates the viral ability to prevent the interferon-alpha/beta-mediated responses. *FEBS letters*, **459**(2), pp.205–10.

Goubau, D., Deddouche, S. & Reis e Sousa, C., (2013). Cytosolic Sensing of Viruses. *Immunity*, **38**(5), pp.855–869.

Graham, B.S., Bunton, L. a, Wright, P.F. & Karzon, D.T., (1991). Role of T lymphocyte subsets in the pathogenesis of primary infection and rechallenge with respiratory syncytial virus in mice. *The Journal of clinical investigation*, **88**(9), pp.1026–1033.

Groskreutz, D.J., Babor, E.C., Monick, M.M., Varga, S.M. & Hunninghake, G.W., (2010). Respiratory syncytial virus limits alpha subunit of eukaryotic translation initiation factor 2 (eIF2alpha) phosphorylation to maintain translation and viral replication. *The Journal of biological chemistry*, **285**(31), pp.24023–31.

Guo, F., Zhao, X., Gill, T., Zhou, Y., Campagna, M., Wang, L., Liu, F., Zhang, P., DiPaolo, L., Du, Y., Xu, X., Jiang, D., Wei, L., Cuconati, A., Block, T.M., Guo, J.-T. & Chang, J., (2014). An interferon-beta promoter reporter assay for high throughput identification of compounds against multiple RNA viruses. *Antiviral Research*, **107**, pp.56–65.

Gupta, S., Jiang, M. & Pernis, A.B., (1999). IFN-alpha activates Stat6 and leads to the formation of Stat2:Stat6 complexes in B cells. *Journal of immunology*, **163**(7), pp.3834–41.

Hai, R., Martínez-Sobrido, L., Fraser, K.A., Ayllon, J., García-Sastre, A. & Palese, P., (2008). Influenza B virus NS1-truncated mutants: live-attenuated vaccine

approach. *Journal of virology*, **82**(21), pp.10580–90.

Hale, B.G., Randall, R.E., Ortin, J. & Jackson, D., (2008). The multifunctional NS1 protein of influenza A viruses. *The Journal of general virology*, **89**(Pt 10), pp.2359–2376.

Hall, C.B., Weinberg, G.A., Iwane, M.K., Blumkin, A.K., Edwards, K.M., Staat, M.A., Auinger, P., Griffin, M.R., Poehling, K.A., Erdman, D., Grijalva, C.G., Zhu, Y. & Szilagyi, P., (2009). The Burden of Respiratory Syncytial Virus Infection in Young Children. *New England Journal of Medicine*, **360**(6), pp.588–598.

Hallak, L.K., Collins, P.L., Knudson, W. & Peeples, M.E., (2000). Iduronic acid-containing glycosaminoglycans on target cells are required for efficient respiratory syncytial virus infection. *Virology*, **271**(2), pp.264–75.

Hallak, L.K., Kwilas, S.A. & Peeples, M.E., (2007). Interaction between respiratory syncytial virus and glycosaminoglycans, including heparan sulfate. *Methods in molecular biology (Clifton, N.J.)*, **379**, pp.15–34.

Haller, O. & Kochs, G., (2011). Human MxA protein: an interferon-induced dynamin-like GTPase with broad antiviral activity. *Journal of interferon & cytokine research : the official journal of the International Society for Interferon and Cytokine Research*, **31**(1), pp.79–87.

Hambleton, S., Goodbourn, S., Young, D.F., Dickinson, P., Mohamad, S.M.B., Valappil, M., McGovern, N., Cant, A.J., Hackett, S.J., Ghazal, P., Morgan, N. V & Randall, R.E., (2013). STAT2 deficiency and susceptibility to viral illness in humans. *Proceedings of the National Academy of Sciences of the United States of America*, **110**(8), pp.3053–8.

Hamid, R., Rotshteyn, Y., Rabadi, L., Parikh, R. & Bullock, P., (2004). Comparison of alamar blue and MTT assays for high through-put screening. *Toxicology in vitro : an international journal published in association with BIBRA*, **18**(5), pp.703–10.

Hardy, R.W. & Wertz, G.W., (1998). The product of the respiratory syncytial virus M2 gene ORF1 enhances readthrough of intergenic junctions during viral transcription. *Journal of virology*, **72**(1), pp.520–6.

Harrison, M.S., Sakaguchi, T. & Schmitt, A.P., (2010). Paramyxovirus assembly and budding: building particles that transmit infections. *The international journal of biochemistry & cell biology*, **42**(9), pp.1416–29.

Hashimoto, K., Durbin, J.E., Zhou, W., Collins, R.D., Ho, S.B., Kolls, J.K., Dubin, P.J., Sheller, J.R., Goleniewska, K., O'Neal, J.F., Olson, S.J., Mitchell, D., Graham, B.S. & Peebles, R.S., (2005). Respiratory syncytial virus infection in the absence of STAT 1 results in airway dysfunction, airway mucus, and augmented IL-17 levels. *The Journal of allergy and clinical immunology*, **116**(3), pp.550–7.

Hastie, M.L., Headlam, M.J., Patel, N.B., Bukreyev, A.A., Buchholz, U.J., Dave, K.A., Norris, E.L., Wright, C.L., Spann, K.M., Collins, P.L. & Gorman, J.J., (2012). The human respiratory syncytial virus nonstructural protein 1 regulates type I and type II interferon pathways. *Molecular & cellular proteomics : MCP*, **11**(5), pp.108–27.

He, B., Paterson, R.G., Stock, N., Durbin, J.E., Durbin, R.K., Goodbourn, S., Randall, R.E. & Lamb, R.A., (2002). Recovery of paramyxovirus simian virus 5 with a V protein lacking the conserved cysteine-rich domain: the multifunctional V protein blocks both interferon-beta induction and interferon signaling. *Virology*, **303**(1), pp.15–32.

Heil, F., Hemmi, H., Hochrein, H., Ampenberger, F., Kirschning, C., Akira, S., Lipford, G., Wagner, H. & Bauer, S., (2004). Species-specific recognition of single-stranded RNA via toll-like receptor 7 and 8. *Science*, **303**(2004), pp.1526–1529.

Helbig, K.J. & Beard, M.R., (2014). The role of viperin in the innate antiviral response. *Journal of molecular biology*, **426**(6), pp.1210–9.

Hengst, U. & Kiefer, P., (2000). Domains of human respiratory syncytial virus P protein essential for homodimerization and for binding to N and NS1 protein. *Virus genes*, **20**(3), pp.221–5.

Hertzog, P.J., (2012). Overview. Type I interferons as primers, activators and inhibitors of innate and adaptive immune responses. *Immunology and cell biology*, **90**(5), pp.471–3.

Hertzog, P.J. & Williams, B.R.G., (2013). Fine tuning type I interferon responses. *Cytokine & growth factor reviews*, **24**(3), pp.217–25.

Hézode, C., Fontaine, H., Dorival, C., Zoulim, F., Larrey, D., Canva, V., De Ledinghen, V., Poynard, T., Samuel, D., Bourliere, M., Alric, L., Raabe, J., Zarski, J., Marcellin, P., Riachi, G., Bernard, P., Loustaud–Ratti, V., Chazouilleres, O., Abergel, A., Guyader, D., Metivier, S., Tran, A., Di Martino, V., Causse, X., Dao, T., Lucidarme, D., Portal, I., Cacoub, P., Gournay, J., Grando–Lemaire, V., Hillon, P., Attali, P., Fontanges, T., Rosa, I., Petrov–Sanchez, V., Barthe, Y., Pawlotsky, J., Pol, S., Carrat, F. & Bronowicki, J., (2014). Effectiveness of Telaprevir or Boceprevir in Treatment-Experienced Patients With HCV Genotype 1 Infection and Cirrhosis. *Gastroenterology*, **147**(1), pp.132–142.e4.

Hilton, L., Moganeradj, K., Zhang, G., Chen, Y.-H., Randall, R.E., McCauley, J.W. & Goodbourn, S., (2006). The NPro product of bovine viral diarrhea virus inhibits DNA binding by interferon regulatory factor 3 and targets it for proteasomal degradation. *Journal of virology*, **80**, pp.11723–11732.

Hoesel, B. & Schmid, J. a, (2013). The complexity of NF-κB signaling in inflammation and cancer. *Molecular cancer*, **12**(1), p.86.

Horner, S.M., Liu, H.M., Park, H.S., Briley, J. & Gale, M., (2011). Mitochondrial-

associated endoplasmic reticulum membranes (MAM) form innate immune synapses and are targeted by hepatitis C virus. *Proceedings of the National Academy of Sciences of the United States of America*, **108**(35), pp.14590–5.

Houben, M.L., Coenjaerts, F.E.J., Rossen, J.W.A., Belderbos, M.E., Hofland, R.W., Kimpen, J.L.L. & Bont, L., (2010). Disease severity and viral load are correlated in infants with primary respiratory syncytial virus infection in the community. *Journal of medical virology*, **82**(7), pp.1266–71.

Hughes, D.J., Wood, J.J., Jackson, B.R., Baquero-Pérez, B. & Whitehouse, A., (2015). NEDDylation is essential for Kaposi's sarcoma-associated herpesvirus latency and lytic reactivation and represents a novel anti-KSHV target. *PLoS pathogens*, **11**(3), p.e1004771.

Hughes, J.P., Rees, S.S., Kalindjian, S.B. & Philpott, K.L., (2011). Principles of early drug discovery. *British Journal of Pharmacology*, **162**(6), pp.1239–1249.

Ibsen, M.S., Gad, H.H., Andersen, L.L., Hornung, V., Julkunen, I., Sarkar, S.N. & Hartmann, R., (2015). Structural and functional analysis reveals that human OASL binds dsRNA to enhance RIG-I signaling. *Nucleic acids research*, **43**(10), pp.5236–48.

Isaacs, A. & Lindenmann, J., (1957). Virus Interference. I. The Interferon. *Proceedings of the Royal Society of London. Series B - Biological Sciences*, **147**(927), pp.258–267.

Ishii, K.J., Coban, C., Kato, H., Takahashi, K., Torii, Y., Takeshita, F., Ludwig, H., Sutter, G., Suzuki, K., Hemmi, H., Sato, S., Yamamoto, M., Uematsu, S., Kawai, T., Takeuchi, O. & Akira, S., (2006). A Toll-like receptor-independent antiviral response induced by double-stranded B-form DNA. *Nature immunology*, **7**(1), pp.40–48.

Israël, A., (2010). The IKK complex, a central regulator of NF-kappaB activation. *Cold Spring Harbor perspectives in biology*, **2**(3), p.a000158.

Ivashkiv, L.B. & Donlin, L.T., (2014). Regulation of type I interferon responses. *Nature reviews. Immunology*, **14**(1), pp.36–49.

Iwasaki, A., (2012). A Virological View of Innate Immune Recognition. *Annual Review of Microbiology*, **66**(1), pp.177–196.

Janssen, R., Pennings, J., Hodemaekers, H., Buisman, A., van Oosten, M., de Rond, L., Oztürk, K., Dormans, J., Kimman, T. & Hoebee, B., (2007). Host transcription profiles upon primary respiratory syncytial virus infection. *Journal of virology*, **81**(11), pp.5958–67.

Jiang, X. & Chen, Z.J., (2011). The role of ubiquitylation in immune defence and pathogen evasion. *Nature Reviews Immunology*, **12**(1), pp.35–48.

Jin, H., Zhou, H., Cheng, X., Tang, R., Munoz, M., Nguyen, N. & Virology, (2000). Recombinant respiratory syncytial viruses with deletions in the NS1, NS2, SH, and M2-2 genes are attenuated in vitro and in vivo. *Virology*, **273**(1), pp.210–218.

Johnson, P.R. & Collins, P.L., (1989). The 1B (NS2), 1C (NS1) and N proteins of human respiratory syncytial virus (RSV) of antigenic subgroups A and B: sequence conservation and divergence within RSV genomic RNA. *The Journal of general virology*, **70**, pp.1539–47.

Karron, R.A., Buchholz, U.J. & Collins, P.L., (2013). Live-attenuated respiratory syncytial virus vaccines. *Current topics in microbiology and immunology*, **372**, pp.259–84.

Kato, H., Takeuchi, O., Mikamo-Satoh, E., Hirai, R., Kawai, T., Matsushita, K., Hiiragi, A., Dermody, T.S., Fujita, T. & Akira, S., (2008). Length-dependent recognition of double-stranded ribonucleic acids by retinoic acid-inducible gene-I and melanoma differentiation-associated gene 5. *The Journal of experimental medicine*, **205**(7), pp.1601–1610.

Katze, M.G., He, Y. & Gale, M., (2002). Viruses and interferon: a fight for supremacy. *Nature reviews. Immunology*, **2**, pp.675–687.

Kawai, T. & Akira, S., (2006). TLR signaling. *Cell death and differentiation*, **13**, pp.816–825.

Kawai, T., Takahashi, K., Sato, S., Coban, C., Kumar, H., Kato, H., Ishii, K.J., Takeuchi, O. & Akira, S., (2005). IPS-1, an adaptor triggering RIG-I- and Mda5-mediated type I interferon induction. *Nature immunology*, **6**(10), pp.981–8.

Khattar, S.K., Yunus, A.S., Collins, P.L. & Samal, S.K., (2001). Deletion and substitution analysis defines regions and residues within the phosphoprotein of bovine respiratory syncytial virus that affect transcription, RNA replication, and interaction with the nucleoprotein. *Virology*, **285**(2), pp.253–69.

Kim, H.W., Chanock, R.M., Jensen, K. & Parrott, R.H., (1969). Respiratory Syncytial Virus Disease in Infants. , **89**(4), pp.422–434.

Kim, S.H., Cohen, B., Novick, D. & Rubinstein, M., (1997). Mammalian type I interferon receptors consists of two subunits: IFNaR1 and IFNaR2. *Gene*, **196**(1-2), pp.279–286.

Kneyber, M.C., Brandenburg, a H., de Groot, R., Joosten, K.F., Rothbarth, P.H., Ott, A. & Moll, H., (1998). Risk factors for respiratory syncytial virus associated apnoea. *European journal of pediatrics*, **157**(4), pp.331–335.

Knoblach, T., Grandel, B., Seiler, J., Nevels, M. & Paulus, C., (2011). Human cytomegalovirus IE1 protein elicits a type II interferon-like host cell response that depends on activated STAT1 but not interferon-γ. *PLoS pathogens*, **7**(4),

p.e1002016.

Kochs, G., Garcia-Sastre, A. & Martinez-Sobrido, L., (2007). Multiple anti-interferon actions of the influenza A virus NS1 protein. *Journal of virology*, **81**(13), pp.7011–7021.

Koguchi, Y., Kohno, J., Nishio, M., Takahashi, K., Okuda, T., Ohnuki, T. & Komatsubara, S., (2000). TMC-95A, B, C, and D, novel proteasome inhibitors produced by Apiospora montagnei Sacc. TC 1093. Taxonomy, production, isolation, and biological activities. *The Journal of antibiotics*, **53**(2), pp.105–9.

Kotenko, S. V, Gallagher, G., Baurin, V. V, Lewis-Antes, A., Shen, M., Shah, N.K., Langer, J.A., Sheikh, F., Dickensheets, H. & Donnelly, R.P., (2003). IFN-lambdas mediate antiviral protection through a distinct class II cytokine receptor complex. *Nature immunology*, **4**(1), pp.69–77.

Krilov, L.R., (2011). Respiratory syncytial virus disease: update on treatment and prevention. *Expert review of anti-infective therapy*, **9**(1), pp.27–32.

Kurai, D., Saraya, T., Ishii, H. & Takizawa, H., (2013). Virus-induced exacerbations in asthma and COPD. *Frontiers in microbiology*, **4**, p.293.

Lay, M.A., Ce, P.F., Lay, M.K., Gonza, P.A., Bueno, S.M., Riedel, C.A. & Kalergis, A.M., (2013). Advances in understanding respiratory syncytial virus infection in airway epithelial cells and consequential effects on the immune response. *Microbes and Infection*, **15**(3), pp.230–242.

Lazear, H.M., Nice, T.J. & Diamond, M.S., (2015). Review Interferon- 1: Immune Functions at Barrier Surfaces and Beyond. *Immunity*, **43**(1), pp.15–28.

Lemaire, P.A., Anderson, E., Lary, J. & Cole, J.L., (2008). Mechanism of PKR Activation by dsRNA. *Journal of molecular biology*, **381**(2), pp.351–60.

Lemm, J.A., O'Boyle, D., Liu, M., Nower, P.T., Colonno, R., Deshpande, M.S., Snyder, L.B., Martin, S.W., St Laurent, D.R., Serrano-Wu, M.H., Romine, J.L., Meanwell, N.A. & Gao, M., (2010). Identification of hepatitis C virus NS5A inhibitors. *Journal of virology*, **84**(1), pp.482–91.

Lenschow, D.J., (2010). Antiviral Properties of ISG15. *Viruses*, **2**(10), pp.2154–68.

Li, K., Foy, E., Ferreon, J.C., Nakamura, M., Ferreon, A.C.M., Ikeda, M., Ray, S.C., Gale, M. & Lemon, S.M., (2005). Immune evasion by hepatitis C virus NS3/4A protease-mediated cleavage of the Toll-like receptor 3 adaptor protein TRIF. *Proceedings of the National Academy of Sciences of the United States of America*, **102**(8), pp.2992–2997.

Li, X., Leung, S., Kerr, I.M. & Stark, G.R., (1997). Functional subdomains of STAT2 required for preassociation with the alpha interferon receptor and for signaling.

*Molecular and cellular biology*, **17**(4), pp.2048–56.

Liang, J.-J., Liao, C.-L., Liao, J.-T., Lee, Y.-L. & Lin, Y.-L., (2009). A Japanese encephalitis virus vaccine candidate strain is attenuated by decreasing its interferon antagonistic ability. *Vaccine*, **27**(21), pp.2746–54.

Liesman, R.M., Buchholz, U.J., Luongo, C.L., Yang, L., Proia, A.D., DeVincenzo, J.P., Collins, P.L. & Pickles, R.J., (2014). RSV-encoded NS2 promotes epithelial cell shedding and distal airway obstruction. *Journal of Clinical Investigation*, **124**(5), pp.2219–2233.

Lieu, K.G., Brice, A., Wiltzer, L., Hirst, B., Jans, D. a, Blondel, D. & Moseley, G.W., (2013). The rabies virus interferon antagonist P protein interacts with activated STAT3 and inhibits Gp130 receptor signaling. *Journal of virology*, **87**(14), pp.8261–5.

Lifland, a. W., Jung, J., Alonas, E., Zurla, C., Crowe, J.E. & Santangelo, P.J., (2012). Human Respiratory Syncytial Virus Nucleoprotein and Inclusion Bodies Antagonize the Innate Immune Response Mediated by MDA5 and MAVS. *Journal of Virology*, **86**(15), pp.8245–8258.

Lin, R., Lacoste, J., Nakhaei, P., Sun, Q., Yang, L., Paz, S., Wilkinson, P., Julkunen, I., Vitour, D., Meurs, E. & Hiscott, J., (2006). Dissociation of a MAVS/IPS-1/VISA/Cardif-IKKepsilon molecular complex from the mitochondrial outer membrane by hepatitis C virus NS3-4A proteolytic cleavage. *Journal of virology*, **80**(12), pp.6072–6083.

Ling, Z., Tran, K.C. & Teng, M.N., (2009). Human respiratory syncytial virus nonstructural protein NS2 antagonizes the activation of beta interferon transcription by interacting with RIG-I. *Journal of virology*, **83**(8), pp.3734–3742.

Lipinski, C.A., Lombardo, F., Dominy, B.W. & Feeney, P.J., (2001). Experimental and computational approaches to estimate solubility and permeability in drug discovery and development settings. *Advanced drug delivery reviews*, **46**(1-3), pp.3–26.

Liu, Q., Xiong, H., Lu, L., Liu, Y., Luo, F., Hou, W. & Yang, Z., (2013). Antiviral and anti-inflammatory activity of arbidol hydrochloride in influenza A (H1N1) virus infection. *Acta pharmacologica Sinica*, **34**(8), pp.1075–83.

Lo, M.S., Brazas, R.M. & Holtzman, M.J., (2005). Respiratory Syncytial Virus Nonstructural Proteins NS1 and NS2 Mediate Inhibition of Stat2 Expression and Alpha / Beta Interferon Responsiveness. *Journal of virology*, **79**(14), pp.9315–9319.

Luongo, C., Winter, C.C., Collins, P.L. & Buchholz, U.J., (2013). Respiratory syncytial virus modified by deletions of the NS2 gene and amino acid S1313 of the L polymerase protein is a temperature-sensitive, live-attenuated vaccine candidate that is phenotypically stable at physiological temperature. *Journal of virology*,

**87**(4), pp.1985–96.

Macarron, R., Banks, M.N., Bojanic, D., Burns, D.J., Cirovic, D. a, Garyantes, T., Green, D.V.S., Hertzberg, R.P., Janzen, W.P., Paslay, J.W., Schopfer, U. & Sittampalam, G.S., (2011). Impact of high-throughput screening in biomedical research. *Nature reviews. Drug discovery*, **10**, pp.188–195.

MacArthur, R.D. & Novak, R.M., (2008). Reviews of anti-infective agents: maraviroc: the first of a new class of antiretroviral agents. *Clinical infectious diseases : an official publication of the Infectious Diseases Society of America*, **47**(2), pp.236–41.

Mackman, R.L., Sangi, M., Sperandio, D., Parrish, J.P., Eisenberg, E., Perron, M., Hui, H., Zhang, L., Siegel, D., Yang, H., Saunders, O., Boojamra, C., Lee, G., Samuel, D., Babaoglu, K., Carey, A., Gilbert, B.E., Piedra, P. a, Strickley, R., Iwata, Q., Hayes, J., Stray, K., Kinkade, A., Theodore, D., Jordan, R., Desai, M. & Cihlar, T., (2015). Discovery of an Oral Respiratory Syncytial Virus (RSV) Fusion Inhibitor (GS-5806) and Clinical Proof of Concept in a Human RSV Challenge Study. *Journal of Medicinal Chemistry*, **58**(4), pp.1630–1643.

Maher, S.G., Romero-Weaver, A.L., Scarzello, A.J. & Gamero, A.M., (2007). Interferon: cellular executioner or white knight? *Current medicinal chemistry*, **14**(12), pp.1279–89.

Malur, A.G., Chattopadhyay, S., Maitra, R.K. & Banerjee, A.K., (2005). Inhibition of STAT 1 phosphorylation by human parainfluenza virus type 3 C protein. *Journal of virology*, **79**(12), pp.7877–82.

Malykhina, O., Yednak, M. a, Collins, P.L., Olivo, P.D. & Peeples, M.E., (2011). A respiratory syncytial virus replicon that is noncytotoxic and capable of long-term foreign gene expression. *Journal of virology*, **85**(10), pp.4792–4801.

Marr, N. & Turvey, S.E., (2012). Role of human TLR4 in respiratory syncytial virus-induced NF-κB activation, viral entry and replication. *Innate immunity*, **18**(6), pp.856–65.

McLellan, J.S., Yang, Y., Graham, B.S. & Kwong, P.D., (2011). Structure of respiratory syncytial virus fusion glycoprotein in the postfusion conformation reveals preservation of neutralizing epitopes. *Journal of virology*, **85**(15), pp.7788–96.

Meanwell, N. a, Cianci, C. & Krystal, M., (2011). *Antiviral Drugs* W. M. Kazmierski, ed., Hoboken, NJ, USA: John Wiley & Sons, Inc.

Mehta, J., Walsh, E.E., Mahadevia, P.J. & Falsey, A.R., (2013). Risk factors for respiratory syncytial virus illness among patients with chronic obstructive pulmonary disease. *COPD*, **10**(3), pp.293–9.

Merlet, J., Burger, J., Gomes, J.-E. & Pintard, L., (2009). Regulation of cullin-RING E3 ubiquitin-ligases by neddylation and dimerization. *Cellular and molecular life sciences : CMLS*, **66**(11-12), pp.1924–38.

Meylan, E., Curran, J., Hofmann, K., Moradpour, D., Binder, M., Bartenschlager, R. & Tschopp, J., (2005). Cardif is an adaptor protein in the RIG-I antiviral pathway and is targeted by hepatitis C virus. *Nature*, **437**(7062), pp.1167–1172.

Minor, R.A.C., Limmon, G. V, Miller-DeGraff, L., Dixon, D., Andrews, D.M.K., Kaufman, R.J. & Imani, F., (2010). Double-stranded RNA-activated protein kinase regulates early innate immune responses during respiratory syncytial virus infection. *Journal of interferon & cytokine research : the official journal of the International Society for Interferon and Cytokine Research*, **30**(4), pp.263–72.

Mitra, R., Baviskar, P., Duncan-Decocq, R.R., Patel, D. & Oomens, A.G.P., (2012). The human respiratory syncytial virus matrix protein is required for maturation of viral filaments. *Journal of virology*, **86**(8), pp.4432–43.

Munday, D.C., Howell, G., Barr, J.N. & Hiscox, J. a., (2015). Proteomic analysis of mitochondria in respiratory epithelial cells infected with human respiratory syncytial virus and functional implications for virus and cell biology. *Journal of Pharmacy and Pharmacology*, **67**(3), pp.300–318.

Munir, S., Hillyer, P., le Nouën, C., Buchholz, U.J., Rabin, R.L., Collins, P.L. & Bukreyev, A., (2011). Respiratory syncytial virus interferon antagonist NS1 protein suppresses and skews the human T lymphocyte response. *PLoS Pathogens*, **7**(4), p.e1001336.

Murawski, M.R., Bowen, G.N., Cerny, A.M., Anderson, L.J., Haynes, L.M., Tripp, R.A., Kurt-Jones, E.A. & Finberg, R.W., (2009). Respiratory syncytial virus activates innate immunity through Toll-like receptor 2. *Journal of virology*, **83**(3), pp.1492–500.

Nagino, K., Tsutsumi, K., Ishido, M. & Harada, Y., (2015). Pharmacological properties of simeprevir (SOVRIAD® capsules 100 mg), a new drug for the treatment of hepatitis C, and results of its clinical studies. *Folia Pharmacologica Japonica*, **145**(2), pp.92–99.

Nair, H., Nokes, D., Gessner, B., Dherani, M., Madhi, S., Singleton, R., O'Brien, K., Roca, A., Wright, P., Bruce, N., Chandran, A., Theodoratou, E., Sutanto, A., Sedyaningsih, E., Ngama, M., Munywoki, P., Kartasasmita, C., Simoes, E., Rudan, I., Weber, M., Campbell, H. & Lancet, (2010). Global burden of acute lower respiratory infections due to respiratory syncytial virus in young children: a systematic review and meta-analysis. *Lancet*, **375**(9725), pp.1545–1555.

Nakayama, Y., Plisch, E.H., Sullivan, J., Thomas, C., Czuprynski, C.J., Williams, B.R.G. & Suresh, M., (2010). Role of PKR and Type I IFNs in viral control during primary and secondary infection. *PLoS pathogens*, **6**(6), p.e1000966.

Ng, S.-L., Friedman, B.A., Schmid, S., Gertz, J., Myers, R.M., Tenoever, B.R. & Maniatis, T., (2011). IκB kinase epsilon (IKK(epsilon)) regulates the balance between type I and type II interferon responses. *Proceedings of the National Academy of Sciences of the United States of America*, **108**(52), pp.21170–5.

Okabayashi, T., Kojima, T., Masaki, T., Yokota, S.I., Imaizumi, T., Tsutsumi, H., Himi, T., Fujii, N. & Sawada, N., (2011). Type-III interferon, not type-I, is the predominant interferon induced by respiratory viruses in nasal epithelial cells. *Virus Research*, **160**(1-2), pp.360–366.

Onoguchi, K., Yoneyama, M., Takemura, A., Akira, S., Taniguchi, T., Namiki, H. & Fujita, T., (2007). Viral infections activate types I and III interferon genes through a common mechanism. *Journal of Biological Chemistry*, **282**(10), pp.7576–7581.

Oshansky, C.M., Krunkosky, T.M., Barber, J., Jones, L.P. & Tripp, R.A., (2009). Respiratory syncytial virus proteins modulate suppressors of cytokine signaling 1 and 3 and the type I interferon response to infection by a toll-like receptor pathway. *Viral immunology*, **22**(3), pp.147–61.

Paes, B. a., Mitchell, I., Banerji, A., Lanctôt, K.L. & Langley, J.M., (2011). A decade of respiratory syncytial virus epidemiology and prophylaxis: Translating evidence into everyday clinical practice. *Canadian Respiratory Journal*, **18**(2), pp.10–19.

Parisien, J.P., Lau, J.F., Rodriguez, J.J., Sullivan, B.M., Moscona, a, Parks, G.D., Lamb, R. a & Horvath, C.M., (2001). The V protein of human parainfluenza virus 2 antagonizes type I interferon responses by destabilizing signal transducer and activator of transcription 2. *Virology*, **283**(2), pp.230–239.

Parks, G.D. & Alexander-Miller, M. a., (2013). Paramyxovirus activation and inhibition of innate immune responses. *Journal of Molecular Biology*, **425**(24), pp.4872–4892.

Pastey, M.K. & Samal, S.K., (1995). Nucleotide sequence analysis of the non-structural NS1 (1C) and NS2 (1B) protein genes of bovine respiratory syncytial virus. *J Gen Virol*, **76 ( Pt 1**)(1995), pp.193–197.

Patnaik, S., Basu, D., Dehdashti, S., Zheng, W., Ferrer, M., Southall, N., Taylor, M., Engel, D.A. & Marugan, J.J., (2013). Discovery of Small Molecule Influenza Virus NS1 Antagonist. *Probe Reports from the NIH Molecular Libraries Program*. Available at: http://www.ncbi.nlm.nih.gov/books/NBK169451/ [Accessed August 26, 2015].

Paul, S.M., Mytelka, D.S., Dunwiddie, C.T., Persinger, C.C., Munos, B.H., Lindborg, S.R. & Schacht, A.L., (2010). How to improve R&D productivity: the pharmaceutical industry's grand challenge. *Nat Rev Drug Discov*, **9**(3), pp.203–214.

Paz, S., Vilasco, M., Werden, S.J., Arguello, M., Joseph-Pillai, D., Zhao, T., Nguyen,

T.L.-A., Sun, Q., Meurs, E.F., Lin, R. & Hiscott, J., (2011). A functional C-terminal TRAF3-binding site in MAVS participates in positive and negative regulation of the IFN antiviral response. *Cell research*, **21**(6), pp.895–910.

Perola, E., (2010). An Analysis of the Binding Efficiencies of Drugs and Their Leads in Successful Drug Discovery Programs. *Journal of Medicinal Chemistry*, **53**(7), pp.2986–2997.

Perry, A.K., Chen, G., Zheng, D., Tang, H. & Cheng, G., (2005). The host type I interferon response to viral and bacterial infections. *Cell research*, **15**(6), pp.407–22.

Plant, H., Stacey, C., Tiong-Yip, C.-L., Walsh, J., Yu, Q. & Rich, K., (2015). High-Throughput Hit Screening Cascade to Identify Respiratory Syncytial Virus (RSV) Inhibitors. *Journal of biomolecular screening*, **20**, pp.597–605.

Platanias, L.C., (2005). Mechanisms of type-I- and type-II-interferon-mediated signalling. *Nature reviews. Immunology*, **5**(5), pp.375–386.

Precious, B.L., Carlos, T.S., Goodbourn, S. & Randall, R.E., (2007). Catalytic turnover of STAT1 allows PIV5 to dismantle the interferon-induced anti-viral state of cells. *Virology*, **368**(1), pp.114–21.

Prince, G.A., Horswood, R.L., Berndt, J., Suffin, S.C. & Chanock, R.M., (1979). Respiratory syncytial virus infection in inbred mice. *Infection and immunity*, **26**(2), pp.764–6.

Ramaswamy, M., Shi, L., Monick, M.M., Hunninghake, G.W. & Look, D.C., (2004). Specific inhibition of type I interferon signal transduction by respiratory syncytial virus. *American Journal of Respiratory Cell and Molecular Biology*, **30**(6), pp.893–900.

Ramaswamy, M., Shi, L., Varga, S.M., Barik, S., Behlke, M. a. & Look, D.C., (2006). Respiratory syncytial virus nonstructural protein 2 specifically inhibits type I interferon signal transduction. *Virology*, **344**(2), pp.328–339.

Rameix-Welti, M.-A., Le Goffic, R., Hervé, P.-L., Sourimant, J., Rémot, A., Riffault, S., Yu, Q., Galloux, M., Gault, E. & Eléouët, J.-F., (2014). Visualizing the replication of respiratory syncytial virus in cells and in living mice. *Nature Communications*, **5**, p.5104.

Randall, R.E. & Goodbourn, S., (2008). Interferons and viruses: An interplay between induction, signalling, antiviral responses and virus countermeasures. *Journal of General Virology*, **89**, pp.1–47.

Randall, R.E., Young, D.F., Goswami, K.K. & Russell, W.C., (1987). Isolation and characterization of monoclonal antibodies to simian virus 5 and their use in revealing antigenic differences between human, canine and simian isolates.

*Journal of General Virology*, **68**, pp.2769–80.

Rasmussen, L., Maddox, C., Moore, B.P., Severson, W. & White, E.L., (2011). A high-throughput screening strategy to overcome virus instability. *Assay and drug development technologies*, **9**(2), pp.184–190.

Rebuffo-Scheer, C., Bose, M., He, J., Khaja, S., Ulatowski, M., Beck, E.T., Fan, J., Kumar, S., Nelson, M.I. & Henrickson, K.J., (2011). Whole genome sequencing and evolutionary analysis of human respiratory syncytial virus A and B from Milwaukee, WI 1998-2010. *PloS one*, **6**(10), p.e25468.

Ren, J., Kolli, D., Liu, T., Xu, R., Garofalo, R.P., Casola, A. & Bao, X., (2011). Human metapneumovirus inhibits IFN-β signaling by downregulating Jak1 and Tyk2 cellular levels. *PloS one*, **6**(9), p.e24496.

Ren, J., Liu, T., Pang, L., Li, K., Garofalo, R.P., Casola, A. & Bao, X., (2011). A novel mechanism for the inhibition of interferon regulatory factor-3-dependent gene expression by human respiratory syncytial virus NS1 protein. *The Journal of general virology*, **92**, pp.2153–2159.

Rieder, M. & Conzelmann, K.-K., (2011). *Interferon in rabies virus infection.* 1st ed., Elsevier Inc.

Rodriguez, J.J., Parisien, J., Curt, M. & Horvath, C.M., (2002). Nipah Virus V Protein Evades Alpha and Gamma Interferons by Preventing STAT1 and STAT2 Activation and Nuclear Accumulation Nipah Virus V Protein Evades Alpha and Gamma Interferons by Preventing STAT1 and STAT2 Activation and Nuclear Accumulation. *Society*, **76**(22), pp.11476–11483.

Roymans, D., De Bondt, H.L., Arnoult, E., Geluykens, P., Gevers, T., Van Ginderen, M., Verheyen, N., Kim, H., Willebrords, R., Bonfanti, J.-F., Bruinzeel, W., Cummings, M.D., van Vlijmen, H. & Andries, K., (2010). Binding of a potent small-molecule inhibitor of six-helix bundle formation requires interactions with both heptad-repeats of the RSV fusion protein. *Proceedings of the National Academy of Sciences of the United States of America*, **107**(1), pp.308–313.

Sanjuán, R., Nebot, M.R., Chirico, N., Mansky, L.M. & Belshaw, R., (2010). Viral mutation rates. *Journal of virology*, **84**(19), pp.9733–48.

Scheerlinck, J.-P.Y., Snibson, K.J., Bowles, V.M. & Sutton, P., (2008). Biomedical applications of sheep models: from asthma to vaccines. *Trends in biotechnology*, **26**(5), pp.259–66.

Schlender, J., Bossert, B., Buchholz, U., Conzelmann, K.K. & Virol, J., (2000). Bovine respiratory syncytial virus nonstructural proteins NS1 and NS2 cooperatively antagonize alpha/beta interferon-induced antiviral response. *Journal of virology*, **74**(18), pp.8234–8242.

Schnell, M.J., McGettigan, J.P., Wirblich, C. & Papaneri, A., (2010). The cell biology of rabies virus: using stealth to reach the brain. *Nature reviews. Microbiology*, **8**(1), pp.51–61.

Schoggins, J.W. & Rice, C.M., (2011). Interferon-stimulated genes and their antiviral effector functions. *Current opinion in virology*, **1**(6), pp.519–25.

Schroder, K., Hertzog, P.J., Ravasi, T. & Hume, D.A., (2004). Interferon-gamma: an overview of signals, mechanisms and functions. *Journal of leukocyte biology*, **75**(2), pp.163–89.

Schulz, O., Diebold, S.S., Chen, M., Näslund, T.I., Nolte, M.A., Alexopoulou, L., Azuma, Y.-T., Flavell, R.A., Liljeström, P. & Reis e Sousa, C., (2005). Toll-like receptor 3 promotes cross-priming to virus-infected cells. *Nature*, **433**(7028), pp.887–92.

Seet, B.T., McCaughan, C.A., Handel, T.M., Mercer, A., Brunetti, C., McFadden, G. & Fleming, S.B., (2003). Analysis of an orf virus chemokine-binding protein: Shifting ligand specificities among a family of poxvirus viroceptors. *Proceedings of the National Academy of Sciences of the United States of America*, **100**(25), pp.15137–42.

Seth, R.B., Sun, L., Ea, C.-K. & Chen, Z.J., (2005). Identification and characterization of MAVS, a mitochondrial antiviral signaling protein that activates NF-kappaB and IRF 3. *Cell*, **122**(5), pp.669–82.

Shaw, M.L., Cardenas, W.B., Zamarin, D., Palese, P. & Basler, C.F., (2005). Nuclear localization of the Nipah virus W protein allows for inhibition of both virus- and toll-like receptor 3-triggered signaling pathways. *Journal of virology*, **79**(10), pp.6078–6088.

Silverman, R.H., (2007). Viral encounters with 2',5'-oligoadenylate synthetase and RNase L during the interferon antiviral response. *Journal of virology*, **81**(23), pp.12720–12729.

Simoes, E., Carbonell-Estrany, X. & Pediatr Infect Dis, J., (2003). Impact of severe disease caused by respiratory syncytial virus in children living in developed countries. *The Pediatric Infectious Disease Journal*, **22**(2 Suppl), pp.S13–S20.

Simões, E.A.F., DeVincenzo, J.P., Boeckh, M., Bont, L., Crowe, J.E., Griffiths, P., Hayden, F.G., Hodinka, R.L., Smyth, R.L., Spencer, K., Thirstrup, S., Walsh, E.E. & Whitley, R.J., (2015). Challenges and opportunities in developing respiratory syncytial virus therapeutics. *The Journal of infectious diseases*, **211**(1 Suppl), pp.S1–S20.

Smith, T.G., Wu, X., Franka, R. & E. Rupprecht, C., (2011). Design of Future Rabies Biologics and Antiviral Drugs. *Advances in Virus Research*, **79**, pp.345–363.

Sow, F.B., Gallup, J.M., Olivier, A., Krishnan, S., Patera, A.C., Suzich, J. & Ackermann, M.R., (2011). Respiratory syncytial virus is associated with an inflammatory response in lungs and architectural remodeling of lung-draining lymph nodes of newborn lambs. *American journal of physiology. Lung cellular and molecular physiology*, **300**(1), pp.L12–24.

Spann, K., Collins, P.L., Teng, M.N. & Virol, J., (2003). Genetic recombination during coinfection of two mutants of human respiratory syncytial virus. *Journal of virology*, **77**(20), pp.11201–11211.

Spann, K.M., Tran, K.C., Chi, B., Rabin, R.L. & Collins, P.L., (2004). Suppression of the Induction of Alpha, Beta, and Gamma Interferons by the NS1 and NS2 Proteins of Human Respiratory Syncytial Virus in Human Epithelial Cells and Macrophages. *Journal of virology*, **78**(8), pp.4363–4369.

Spann, K.M., Tran, K.C. & Collins, P.L., (2005). Effects of Nonstructural Proteins NS1 and NS2 of Human Respiratory Syncytial Virus on Interferon Regulatory Factor 3, NF- κ B, and Proinflammatory Cytokines. *Journal of virology*, **79**(9), pp.5353–5362.

Stancato, L.F., David, M., Carter-Su, C., Larner, A.C. & Pratt, W.B., (1996). Preassociation of STAT1 with STAT2 and STAT3 in separate signalling complexes prior to cytokine stimulation. *The Journal of biological chemistry*, **271**(8), pp.4134–7.

Stark, G.R., Kerr, I.M., Williams, B.R., Silverman, R.H. & Schreiber, R.D., (1998). How cells respond to interferons. *Annual review of biochemistry*, **67**, pp.227–64.

Stewart, C.E., Randall, R.E. & Adamson, C.S., (2014). Inhibitors of the Interferon Response Enhance Virus Replication In Vitro. *PLoS ONE*, **9**(11), p.e112014.

Sudo, K., Miyazaki, Y., Kojima, N., Kobayashi, M., Suzuki, H., Shintani, M. & Shimizu, Y., (2005). YM-53403, a unique anti-respiratory syncytial virus agent with a novel mechanism of action. *Antiviral Research*, **65**(2), pp.125–131.

Sun, L., Wu, J., Du, F., Chen, X. & Chen, Z.J., (2013). Cyclic GMP-AMP synthase is a cytosolic DNA sensor that activates the type I interferon pathway. *Science*, **339**(6121), pp.786–91.

Swedan, S., Andrews, J., Majumdar, T., Musiyenko, A. & Barik, S., (2011). Multiple functional domains and complexes of the two nonstructural proteins of human respiratory syncytial virus contribute to interferon suppression and cellular location. *Journal of virology*, **85**(19), pp.10090–10100.

Swedan, S., Musiyenko, A. & Barik, S., (2009). Respiratory syncytial virus nonstructural proteins decrease levels of multiple members of the cellular interferon pathways. *Journal of virology*, **83**(19), pp.9682–9693.

Tabeta, K., Georgel, P., Janssen, E., Du, X., Hoebe, K., Crozat, K., Mudd, S., Shamel, L., Sovath, S., Goode, J., Alexopoulou, L., Flavell, R. a & Beutler, B., (2004). Toll-like receptors 9 and 3 as essential components of innate immune defense against mouse cytomegalovirus infection. *Proceedings of the National Academy of Sciences of the United States of America*, **101**(10), pp.3516–3521.

Takeda, K. & Akira, S., (2004). TLR signaling pathways. *Seminars in Immunology*, **16**(1), pp.3–9.

Takeuchi, O. & Akira, S., (2009). Innate immunity to virus infection. *Immunological Reviews*, **227**(1), pp.75–86.

Tanaka, Y. & Chen, Z.J., (2012). STING specifies IRF3 phosphorylation by TBK1 in the cytosolic DNA signaling pathway. *Science signaling*, **5**(214), p.ra20.

Temesgen, Z. & Feinberg, J., (2007). Tipranavir: a new option for the treatment of drug-resistant HIV infection. *Clinical infectious diseases : an official publication of the Infectious Diseases Society of America*, **45**(6), pp.761–9.

Teng, M.N. & Collins, P.L., (1998). Identification of the respiratory syncytial virus proteins required for formation and passage of helper-dependent infectious particles. *Journal of virology*, **72**(7), pp.5707–16.

Teng, M.N., Whitehead, S.S., Bermingham, A., St Claire, M., Elkins, W.R., Murphy, B.R. & Collins, P.L., (2000). Recombinant respiratory syncytial virus that does not express the NS1 or M2-2 protein is highly attenuated and immunogenic in chimpanzees. *Journal of virology*, **74**(19), pp.9317–9321.

Thornburg, N., Hayward, S. & Crowe, J., (2012). Respiratory Syncytial Virus Regulates Human MicroRNAs by Using Mechanisms Involving Beta Interferon and NF-κB. *mBio*, **3**(6), pp.1–9.

Tiong-Yip, C.L., Plant, H., Sharpe, P., Fan, J., Rich, K., Gorseth, E. & Yu, Q., (2014). Development of a high-throughput replicon assay for the identification of respiratory syncytial virus inhibitors. *Antiviral Research*, **101**, pp.75–81.

Torpey, N., Maher, S.E., Bothwell, A.L.M. & Pober, J.S., (2004). Interferon alpha but not interleukin 12 activates STAT4 signaling in human vascular endothelial cells. *The Journal of biological chemistry*, **279**(25), pp.26789–96.

Tran, K.C., He, B. & Teng, M.N., (2007). Replacement of the respiratory syncytial virus nonstructural proteins NS1 and NS2 by the V protein of parainfluenza virus 5. *Virology*, **368**, pp.73–82.

Trinchieri, G., (2010). Type I interferon: friend or foe? *The Journal of experimental medicine*, **207**(10), pp.2053–63.

Uddin, S., Sassano, A., Deb, D.K., Verma, A., Majchrzak, B., Rahman, A., Malik, A.B.,

Fish, E.N. & Platanias, L.C., (2002). Protein kinase C-delta (PKC-delta ) is activated by type I interferons and mediates phosphorylation of Stat1 on serine 727. *The Journal of biological chemistry*, **277**(17), pp.14408–16.

Ulane, C.M. & Horvath, C.M., (2002). Paramyxoviruses SV5 and HPIV2 assemble STAT protein ubiquitin ligase complexes from cellular components. *Virology*, **304**(2), pp.160–166.

Unterholzner, L., Keating, S.E., Baran, M., Horan, K.A., Jensen, S.B., Sharma, S., Sirois, C.M., Jin, T., Latz, E., Xiao, T.S., Fitzgerald, K.A., Paludan, S.R. & Bowie, A.G., (2010). IFI16 is an innate immune sensor for intracellular DNA. *Nature immunology*, **11**(11), pp.997–1004.

Venkatesh, M.P. & Weisman, L.E., (2006). Prevention and treatment of respiratory syncytial virus infection in infants: an update. *Expert Review of Vaccines*, **5**(2), pp.261–268.

Versteeg, G. & Garcia-Sastre, A., (2010). Viral tricks to grid-lock the type I interferon system. *Current opinion in microbiology*, **13**(4), pp.508–516.

Vissers, M., Remijn, T., Oosting, M., de Jong, D.J., Diavatopoulos, D.A., Hermans, P.W.M. & Ferwerda, G., (2012). Respiratory syncytial virus infection augments NOD2 signaling in an IFN-β-dependent manner in human primary cells. *European journal of immunology*, **42**(10), pp.2727–35.

Wack, A., Terczyńska-Dyla, E. & Hartmann, R., (2015). Guarding the frontiers: the biology of type III interferons. *Nature Immunology*, **16**(8), pp.802–809.

Wang, L.F., Harcourt, B.H., Yu, M., Tamin, A., Rota, P. a., Bellini, W.J. & Eaton, B.T., (2001). Molecular biology of Hendra and Nipah viruses. *Microbes and Infection*, **3**(4), pp.279–287.

Weber, F. & Haller, O., (2007). Viral suppression of the interferon system. *Biochimie*, **89**(6-7), pp.836–842.

Webster Marketon, J., I, J., Corry, J. & Teng, M.N., (2014). The respiratory syncytial virus (RSV) nonstructural proteins mediate RSV suppression of glucocorticoid receptor transactivation. *Virology*, **449**, pp.62–9.

Welliver, T.P., Garofalo, R.P., Hosakote, Y., Hintz, K.H., Avendano, L., Sanchez, K., Velozo, L., Jafri, H., Chavez-Bueno, S., Ogra, P.L., McKinney, L., Reed, J.L. & Welliver, R.C., (2007). Severe human lower respiratory tract illness caused by respiratory syncytial virus and influenza virus is characterized by the absence of pulmonary cytotoxic lymphocyte responses. *The Journal of infectious diseases*, **195**(8), pp.1126–36.

Whitehead, S.S., Bukreyev, a, Teng, M.N., Firestone, C.Y., St Claire, M., Elkins, W.R., Collins, P.L. & Murphy, B.R., (1999). Recombinant respiratory syncytial virus

bearing a deletion of either the NS2 or SH gene is attenuated in chimpanzees. *Journal of virology*, **73**, pp.3438–3442.

Whitehouse, D., (2014). *Molecular Biology and Biotechnology*, Royal Society of Chemistry.

WHO, (2015). WHO | Guide for Rabies post-exposure prophylaxis. Available at: http://www.who.int/rabies/human/postexp/en/ [Accessed June 22, 2015].

Wiltzer, L., Larrous, F., Oksayan, S., Ito, N., Marsh, G. a., Wang, L.F., Blondel, D., Bourhy, H., Jans, D. a. & Moseley, G.W., (2012). Conservation of a Unique Mechanism of Immune Evasion across the Lyssavirus Genus. *Journal of Virology*, **86**(18), pp.10194–10199.

Wiltzer, L., Okada, K., Yamaoka, S., Larrous, F., Kuusisto, H.V., Sugiyama, M., Blondel, D., Bourhy, H., Jans, D.A., Ito, N. & Moseley, G.W., (2014). Interaction of Rabies virus P-protein with STAT proteins is critical to lethal rabies disease. *Journal of Infectious Diseases*, **209**(11), pp.1744–1753.

Wright, M. & Piedimonte, G., (2011). Respiratory syncytial virus prevention and therapy: Past, present, and future. *Pediatric Pulmonology*, **46**(8), pp.324–347.

Wright, P.F., (2014). Progress in the prevention and treatment of RSV infection. *The New England journal of medicine*, **371**(8), pp.776–7.

Wright, P.F., Karron, R.A., Madhi, S.A., Treanor, J.J., King, J.C., O'Shea, A., Ikizler, M.R., Zhu, Y., Collins, P.L., Cutland, C., Randolph, V.B., Deatly, A.M., Hackell, J.G., Gruber, W.C. & Murphy, B.R., (2006). The interferon antagonist NS2 protein of respiratory syncytial virus is an important virulence determinant for humans. *The Journal of infectious diseases*, **193**(4), pp.573–81.

Wu, H., Pfarr, D.S., Johnson, S., Brewah, Y. a., Woods, R.M., Patel, N.K., White, W.I., Young, J.F. & Kiener, P. a., (2007). Development of Motavizumab, an Ultra-potent Antibody for the Prevention of Respiratory Syncytial Virus Infection in the Upper and Lower Respiratory Tract. *Journal of Molecular Biology*, **368**, pp.652–665.

Wu, W., Tran, K.C., Teng, M.N., Heesom, K.J., Matthews, D. a., Barr, J.N. & Hiscox, J. a., (2012). The Interactome of the Human Respiratory Syncytial Virus NS1 Protein Highlights Multiple Effects on Host Cell Biology. *Journal of Virology*, **86**(15), pp.7777–7789.

Xu, X., Zheng, J., Zheng, K., Hou, Y., Zhao, F. & Zhao, D., (2014). Respiratory syncytial virus NS1 protein degrades STAT2 by inducing SOCS1 expression. *Intervirology*, **57**(2), pp.65–73.

Yamamoto, M., Sato, S., Mori, K., Hoshino, K., Takeuchi, O., Takeda, K. & Akira, S., (2002). Cutting edge: a novel Toll/IL-1 receptor domain-containing adapter that

preferentially activates the IFN-beta promoter in the Toll-like receptor signaling. *Journal of immunology*, **169**(12), pp.6668–72.

Yan, H., Krishnan, K., Greenlund, A.C., Gupta, S., Lim, J.T., Schreiber, R.D., Schindler, C.W. & Krolewski, J.J., (1996). Phosphorylated interferon-alpha receptor 1 subunit (IFNaR1) acts as a docking site for the latent form of the 113 kDa STAT2 protein. *The EMBO journal*, **15**(5), pp.1064–74.

Yap, M.W. & Stoye, J.P., (2012). TRIM proteins and the innate immune response to viruses. *Advances in experimental medicine and biology*, **770**, pp.93–104.

Yarilina, A., Park-Min, K.-H., Antoniv, T., Hu, X. & Ivashkiv, L.B., (2008). TNF activates an IRF1-dependent autocrine loop leading to sustained expression of chemokines and STAT1-dependent type I interferon-response genes. *Nature immunology*, **9**(4), pp.378–87.

Yoshimura, A., Naka, T. & Kubo, M., (2007). SOCS proteins, cytokine signalling and immune regulation. *Nature reviews. Immunology*, **7**(6), pp.454–65.

Young, D.F., Andrejeva, L., Livingstone,  a, Goodbourn, S., Lamb, R. a, Collins, P.L., Elliott, R.M. & Randall, R.E., (2003). Virus Replication in Engineered Human Cells That Do Not Respond to Interferons. *Society*, **77**(3), pp.2174–2181.

Zandi, E., Rothwarf, D.M., Delhase, M., Hayakawa, M. & Karin, M., (1997). The IκB Kinase Complex (IKK) Contains Two Kinase Subunits, IKKα and IKKβ, Necessary for IκB Phosphorylation and NF-κB Activation. *Cell*, **91**(2), pp.243–252.

Zang, R., Li, D., Tang, I.-C., Wang, J. & Yang, S.-T., (2012). Cell-Based Assays in High-Throughput Screening for Drug Discovery. *International Journal of Biotechnology for Wellness Industries*, **1**(1), pp.31–51.

Zhang, J.-H., (1999). A Simple Statistical Parameter for Use in Evaluation and Validation of High Throughput Screening Assays. *Journal of Biomolecular Screening*, **4**(2), pp.67–73.

Zhang, L., Peeples, M.E., Boucher, R.C., Collins, P.L. & Pickles, R.J., (2002). Respiratory Syncytial Virus Infection of Human Airway Epithelial Cells Is Polarized , Specific to Ciliated Cells , and without Obvious Cytopathology. *Journal of virology*, **76**(11), pp.5654–5666.

Zhang, W., Yang, H., Kong, X., Mohapatra, S., San Juan-Vergara, H., Hellermann, G., Behera, S., Singam, R., Lockey, R.F. & Mohapatra, S.S., (2005). Inhibition of respiratory syncytial virus infection with intranasal siRNA nanoparticles targeting the viral NS1 gene. *Nature medicine*, **11**(1), pp.56–62.

Zhang, Z., Yuan, B., Bao, M., Lu, N., Kim, T. & Liu, Y.-J., (2011). The helicase DDX41 senses intracellular DNA mediated by the adaptor STING in dendritic

cells. *Nature immunology*, **12**(10), pp.959–65.

Züst, R., Cervantes-Barragán, L., Kuri, T., Blakqori, G., Weber, F., Ludewig, B. & Thiel, V., (2007). Coronavirus non-structural protein 1 is a major pathogenicity factor: implications for the rational design of coronavirus vaccines. *PLoS pathogens*, **3**(8), p.e109.

# Appendices

## Appendix 1: DNA and amino-acid sequences

**A) RSV/hNS1 DNA and amino-acid sequence:** Codon-optimized, 'humanized' version of the RSV genes for NS1 (GenBank accession no. AY904040.1). The RSV/hNS1 sequence derived from RSV Long strain, and had a V5-tag fused to its N-terminus. In order to clone to the gene into the pdl.SV5V'IB vector, the BamH1 and NdeI restriction sites were added to the 5' and 3' end of the DNA sequence, respectively.

```
BamHI
|
gga tcc atg GGA AAG CCG ATC CCA AAC CCT CTA TTA GGT CTG GAC TCC ACC ggc a   < 55
G   S   M   G   K   P   I   P   N   P   L   L   G   L   D   S   T   G   S
cct agg tac CCT TTC GGC TAG GGT TTG GGA GAT AAT CCA GAC CTG AGG TGG ccg t


gc aac tcc ctg agc atg atc aaa gtg cgg ctg cag aac ctg ttc gac aac gac ga   < 110
   N   S   L   S   M   I   K   V   R   L   Q   N   L   F   D   N   D   E
cg ttg agg gac tcg tac tag ttt cac gcc gac gtc ttg gac aag ctg ttg ctg ct


a gtc gca ctg ctc aag atc aca tgc tac acc gac aag ctc atc cac ctg acc aac   < 165
  V   A   L   L   K   I   T   C   Y   T   D   K   L   I   H   L   T   N
t cag cgt gac gag ttc tag tgt acg atg tgg ctg ttc gag tag gtg gac tgg ttg


gcc ctg gca aag gca gtg atc cac act atc aaa ctg aac ggt atc gtg ttc gtg c   < 220
A   L   A   K   A   V   I   H   T   I   K   L   N   G   I   V   F   V   H
cgg gac cgt ttc cgt cac tag gtg tga tag ttt gac ttg cca tag cac aag cac g


ac gtc atc acc agc agc gac atc tgc cct aac aac aac atc gtc gtc aag tcc aa   < 275
   V   I   T   S   S   D   I   C   P   N   N   N   I   V   V   K   S   N
tg cag tag tgg tcg tcg ctg tag acg gga ttg ttg ttg tag cag cag ttc agg tt


c ttc aca aca atg ccc gtg ctg cag aac ggc ggc tac atc tgg gag atg atg gag   < 330
  F   T   T   M   P   V   L   Q   N   G   G   Y   I   W   E   M   M   E
g aag tgt tgt tac ggg cac gac gtc ttg ccg ccg atg tag acc ctc tac tac ctc


ctc aca cac tgc tcc cag ccc aac gga ctg atc gac gac aac tgc gag atc aag t   < 385
L   T   H   C   S   Q   P   N   G   L   I   D   D   N   C   E   I   K   F
gag tgt gtg acg agg gtc ggg ttg cct gac tag ctg ctg ttg acg ctc tag ttc a


tc tcc aag aag ctg agc gac tcc acc atg acc aac tac atg aac cag ctc tcc ga   < 440
   S   K   K   L   S   D   S   T   M   T   N   Y   M   N   Q   L   S   E
ag agg ttc ttc gac tcg ctg agg tgg tac tgg ttg atg tac ttg gtc gag agg ct


                                  NdeI
                                  |
g ctg ctg gga ttc gac ctc aac cct taa cat atg   < 474
  L   L   G   F   D   L   N   P   *   H   M
c gac gac cct aag ctg gag ttg gga att gta tac
```

**B) RSV/hNS2 DNA and amino-acid sequence:** Codon-optimized, 'humanized' version of the RSV genes for NS2 (GenBank accession no. AY904041.1): The RSV/hNS2 sequence derived from RSV Long strain, had a myc-tag fused to its N-terminus. In order to clone to the gene into the pdl.Not'I.IRES.puro vector, the BamH1 and NotI restriction sites were added to the 5' and 3' end of the DNA sequence, respectively.

```
BamHI
|
gga tcc atg GAA CAG AAA CTG ATC TCT GAA GAA GAC CTG gac acc acc cac aac g  < 55
 G   S   M   E   Q   K   L   I   S   E   E   D   L   D   T   T   H   N   D
cct agg tac CTT GTC TTT GAC TAG AGA CTT CTT CTG GAC ctg tgg tgg gtg ttg c


ac acc act cca cag cgg ctg atg atc acc gac atg cgg cca ctg tcc ctg gag ac  < 110
    T   T   P   Q   R   L   M   I   T   D   M   R   P   L   S   L   E   T
tg tgg tga ggt gtc gcc gac tac tag tgg ctg tac gcc ggt gac agg gac ctc tg


c acc atc acc tcc ctg acc cgc gac atc atc acc cac cgg ttc atc tac ctg atc  < 165
   T   I   T   S   L   T   R   D   I   I   T   H   R   F   I   Y   L   I
g tgg tag tgg agg gac tgg gcg ctg tag tag tgg gtg gcc aag tag atg gac tag


aac cac gag tgc atc gtg cgg aag ctg gac gag cgg cag gcc acc ttc acc ttc c  < 220
 N   H   E   C   I   V   R   K   L   D   E   R   Q   A   T   F   T   F   L
ttg gtg ctc acg tag cac gcc ttc gac ctg ctc gcc gtc cgg tgg aag tgg aag g


tg gtg aac tac gag atg aag ctg ctg cac aaa gtc ggc agc acc aag tac aag aa  < 275
    V   N   Y   E   M   K   L   L   H   K   V   G   S   T   K   Y   K   K
ac cac ttg atg ctc tac ttc gac gac gtg ttt cag ccg tcg tgg ttc atg ttc tt


g tac act gag tac aac acc aaa tac ggc acc ttc cca atg ccc atc ttc atc aac  < 330
   Y   T   E   Y   N   T   K   Y   G   T   F   P   M   P   I   F   I   N
c atg tga ctc atg ttg tgg ttt atg ccg tgg aag ggt tac ggg tag aag tag ttg


cac gac ggc ttc ctg gag tgc atc ggc atc aag ccc aca aag cac act ccc atc a  < 385
 H   D   G   F   L   E   C   I   G   I   K   P   T   K   H   T   P   I   I
gtg ctg ccg aag gac ctc acg tag ccg tag ttc ggg tgt ttc gtg tga ggg tag t
                                  NotI
                                   |
tc tac aaa tac gac ctc aac cct tga gcg gcc gc  < 419
   Y   K   Y   D   L   N   P   *   A   A   X
ag atg ttt atg ctg gag ttg gga act cgc cgg cg
```

**C) Rabies virus P (RV/P) DNA and amino-acid sequence:** The RV/P sequence derived from challenge virus standard (CVS)- 11 strain (GenBank accession no. ADJ29909.1) and had a V5-tag fused to its N-terminus. In order to clone to the gene into the pdl.Not'I.IRES.puro vector, the BamH1 and NotI restriction sites were added to the 5' and 3' end of the DNA sequence, respectively.

```
BamHI
 |
gga tcc atg GGA AAG CCG ATC CCA AAC CCT CTA TTA GGT CTG GAC TCC ACC agc a   < 55
G   S   M   G   K   P   I   P   N   P   L   L   G   L   D   S   T   S   K
cct agg tac CCT TTC GGC TAG GGT TTG GGA GAT AAT CCA GAC CTG AGG TGG tcg t


ag atc ttc gtg aac ccc agc gcc atc aga gcc ggc ctg gcc gac ctg gag atg gc   < 110
   I   F   V   N   P   S   A   I   R   A   G   L   A   D   L   E   M   A
tc tag aag cac ttg ggg tcg cgg tag tct cgg ccg gac cgg ctg gac ctc tac cg


c gag gag acc gtg gac ctg atc aac aga aac atc gag gac aac cag gcc cac ctg   < 165
  E   E   T   V   D   L   I   N   R   N   I   E   D   N   Q   A   H   L
g ctc ctc tgg cac ctg gac tag ttg tct ttg tag ctc ctg ttg gtc cgg gtg gac


cag ggc gag ccc atc gag gtg gac aac ctg ccc gag gac atg aag aga ctg cac c   < 220
Q   G   E   P   I   E   V   D   N   L   P   E   D   M   K   R   L   H   L
gtc ccg ctc ggg tag ctc cac ctg ttg gac ggg ctc ctg tac ttc tct gac gtg g


tg gac gac gag aag agc agc aac ctg ggc gag atg gtg aga gtg ggc gag ggc aa   < 275
   D   D   E   K   S   S   N   L   G   E   M   V   R   V   G   E   G   K
ac ctg ctg ctc ttc tcg tcg ttg gac ccg ctc tac cac tct cac ccg ctc ccg tt


g tac aga gag gac ttc cag atg gac gag ggc gag gac ccc aac ctg ctg ttc cag   < 330
  Y   R   E   D   F   Q   M   D   E   G   E   D   P   N   L   L   F   Q
c atg tct ctc ctg aag gtc tac ctg ctc ccg ctc ctg ggg ttg gac gac aag gtc


agc tac ctg gac aac gtg ggc gtg cag atc gtg aga cag atg aga agc ggc gag a   < 385
S   Y   L   D   N   V   G   V   Q   I   V   R   Q   M   R   S   G   E   R
tcg atg gac ctg ttg cac ccg cac gtc tag cac tct gtc tac tct tcg ccg ctc t


ga ttc ctg aag atc tgg agc cag acc gtg gag gag atc gtg agc tac gtg acc gt   < 440
   F   L   K   I   W   S   Q   T   V   E   E   I   V   S   Y   V   T   V
ct aag gac ttc tag acc tcg gtc tgg cac ctc ctc tag cac tcg atg cac tgg ca


g aac ttc ccc aac ccc ccc aga aga agc agc gag gac aag agc acc cag acc acc   < 495
  N   F   P   N   P   P   R   R   S   S   E   D   K   S   T   Q   T   T
c ttg aag ggg ttg ggg ggg tct tct tcg tcg ctc ctg ttc tcg tgg gtc tgg tgg


ggc aga gag ctg aag aag gag acc acc agc gcc ttc agc cag aga gag agc cag c   < 550
G   R   E   L   K   K   E   T   T   S   A   F   S   Q   R   E   S   Q   P
ccg tct ctc gac ttc ttc ctc tgg tgg tcg cgg aag tcg gtc tct ctc tcg gtc g


cc agc aag gcc aga atg gtg gcc cag gtg gcc ccc ggc ccc ccc gcc ctg gag tg   < 605
   S   K   A   R   M   V   A   Q   V   A   P   G   P   P   A   L   E   W
gg tcg ttc cgg tct tac cac cgg gtc cac cgg ggg ccg ggg ggg cgg gac ctc ac


g agc gcc acc aac gag gag gac gac ctg agc gtg gag gcc gag atc gcc cac cag   < 660
  S   A   T   N   E   E   D   D   L   S   V   E   A   E   I   A   H   Q
c tcg cgg tgg ttg ctc ctc ctg ctg gac tcg cac ctc cgg ctc tag cgg gtg gtc


atc gcc gag agc ttc agc aag aag tac aag ttc ccc agc aga agc agc ggc atc t   < 715
I   A   E   S   F   S   K   K   Y   K   F   P   S   R   S   S   G   I   F
tag cgg ctc tcg aag tcg ttc ttc atg ttc aag ggg tcg tct tcg tcg ccg tag a
```

227

```
tc ctg tac aac ttc gag cag ctg aag atg aac ctg gac gac atc gtg aag gag gc  < 770
   L   Y   N   F   E   Q   L   K   M   N   L   D   D   I   V   K   E   A
ag gac atg ttg aag ctc gtc gac ttc tac ttg gac ctg ctg tag cac ttc ctc cg

c aag aac gtg ccc ggc gtg acc aga ctg gcc cac gac ggc agc aag atc ccc ctg  < 825
   K   N   V   P   G   V   T   R   L   A   H   D   G   S   K   I   P   L
g ttc ttg cac ggg ccg cac tgg tct gac cgg gtg ctg ccg tcg ttc tag ggg gac

aga tgc gtg ctg ggc tgg gtg gcc ctg gcc aac agc aag aag ttc cag ctg ctg g  < 880
 R   C   V   L   G   W   V   A   L   A   N   S   K   K   F   Q   L   L   V
tct acg cac gac ccg acc cac cgg gac cgg ttg tcg ttc ttc aag gtc gac gac c

tg gag gcc gac aag ctg agc aag atc atg cag gac gac ctg aac aga tac acc ag  < 935
  E   A   D   K   L   S   K   I   M   Q   D   D   L   N   R   Y   T   S
ac ctc cgg ctg ttc gac tcg ttc tag tac gtc ctg ctg gac ttg tct atg tgg tc

            NotI
             |
c tgc tga gcg gcc gc  < 950
  C   *   A   A   X
g acg act cgc cgg cg
```

Note:

V5-tag: GGAAAGCCGATCCCAAACCCTCTATTAGGTCTGGACTCCACC

myc-tag: GAACAGAAACTGATCTCTGAAGAAGACCTG

ggatcc: BamH1 restriction site

gcggccgc: NotI restriction site

catatg: NdeI restriction site

## Appendix 2: Lentiviral Vectors

The pdl.SV5V'IB vector contains the gene for blasticidin-S deaminase confers blasticidin resistance The pdl.Not'I.IRES.puro vector contains the Pac gene encoding a puromycin N-acetyl-transferase (PAC), which confers resistance to puromycin. Both vectors were previously made by Dr Hsiang Chen.
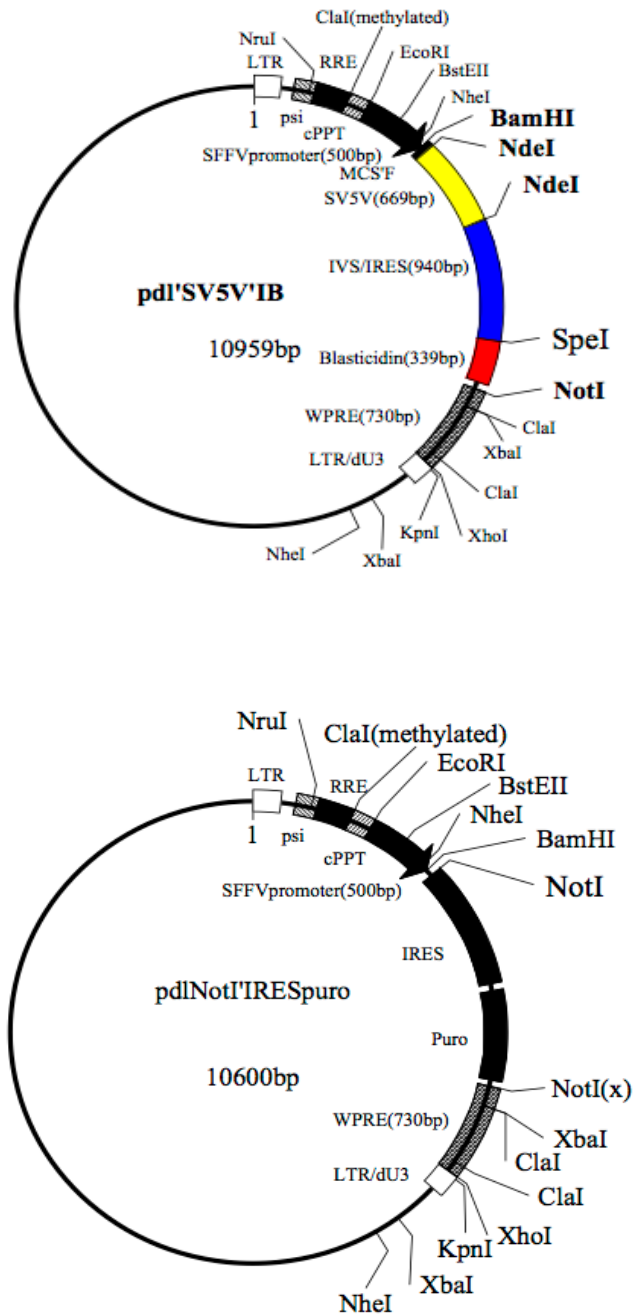
## Appendix 3: A549.pr(ISRE)GFP-2A-RSV/hNS2 reporter cell-line

Generation of a A549.pr(ISRE)GFP derivative that expresses mcherry and RSV NS2 protein from a single ORF, using 2A technology.RSV hNS2 expression was observed with immunofluorescence using a mouse anti-myc primary antibody and an anti-mouse FITC secondary antibody
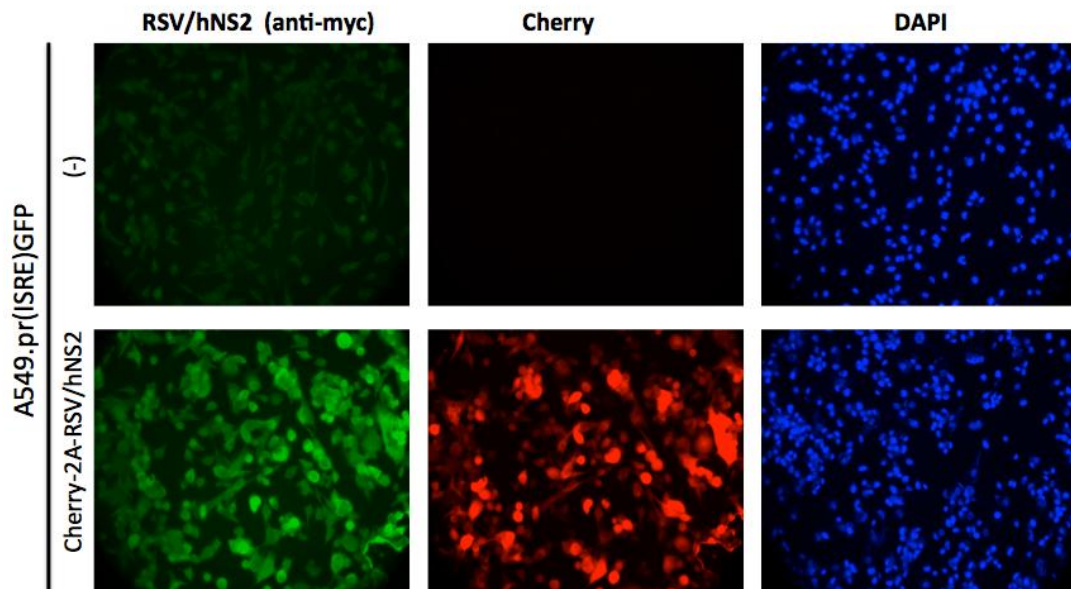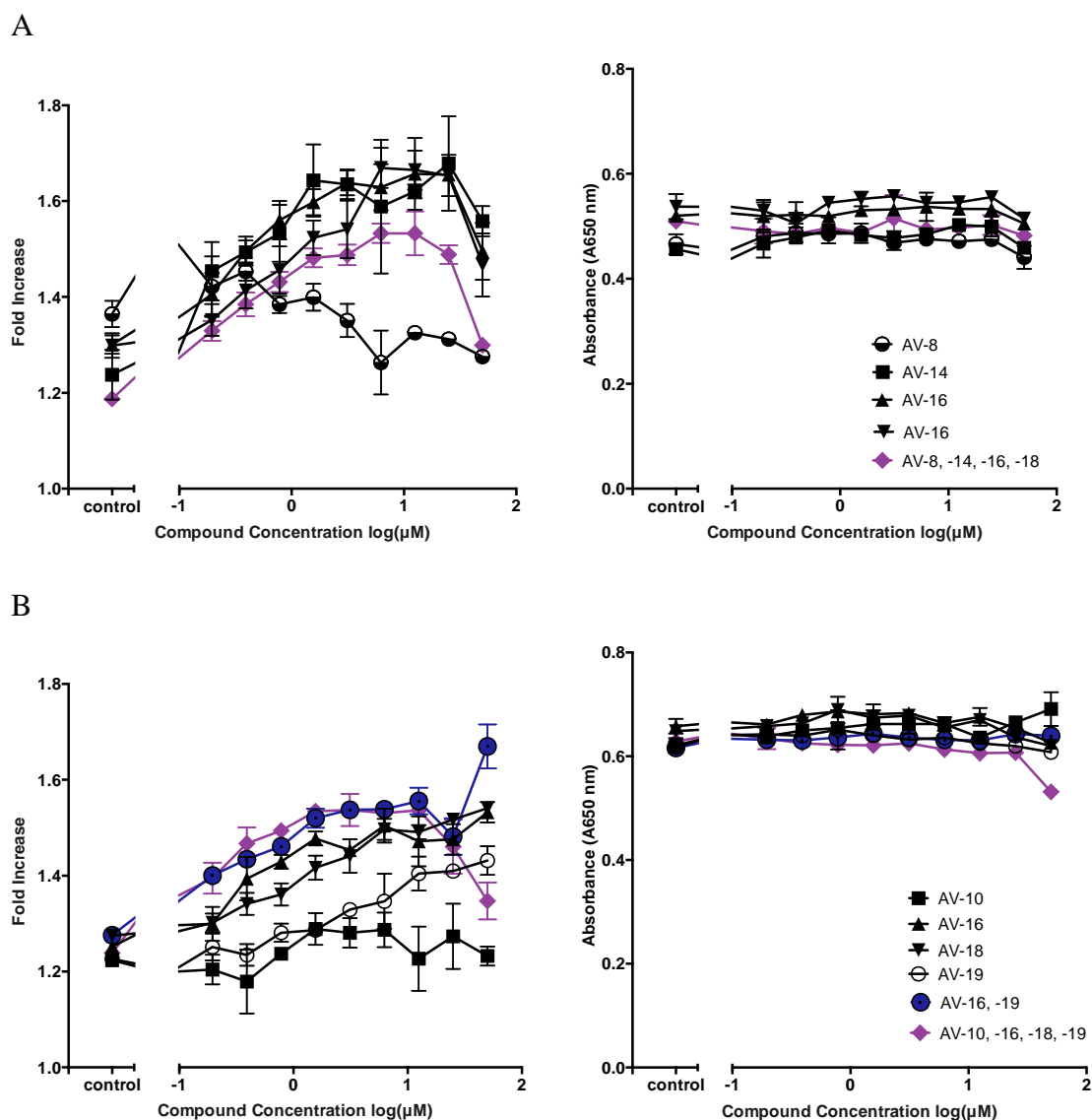
Appendix 4: Cullin-2 expression in A549.pr(ISRE)GFP-RSV/hNS2
reporter cell-line in the presence of compounds AV-8, -14, -16, -18 and -19

A549.pr(ISRE)GFP and A549.pr(ISRE)GFP-RSV/hNS2 cell-lines were treated with 10 μM of compound or 0.05% [v/v] DMSO for 24 hours, and STAT2 and Cullin-2 (Cul2) expression was observed with near-infrared fluorescent western blot analysis (Odyssey CLx imager). Cul2 was detected using rabbit anti-Cullin 2 monoclonal antibody (1:1000 dilution; Life Technology). This antibody detects two Cul2 species; the top band presents the neddylated form (addition of NEDD8) of Cul2, whereas the lower band is the uneddylated form of Cull2.
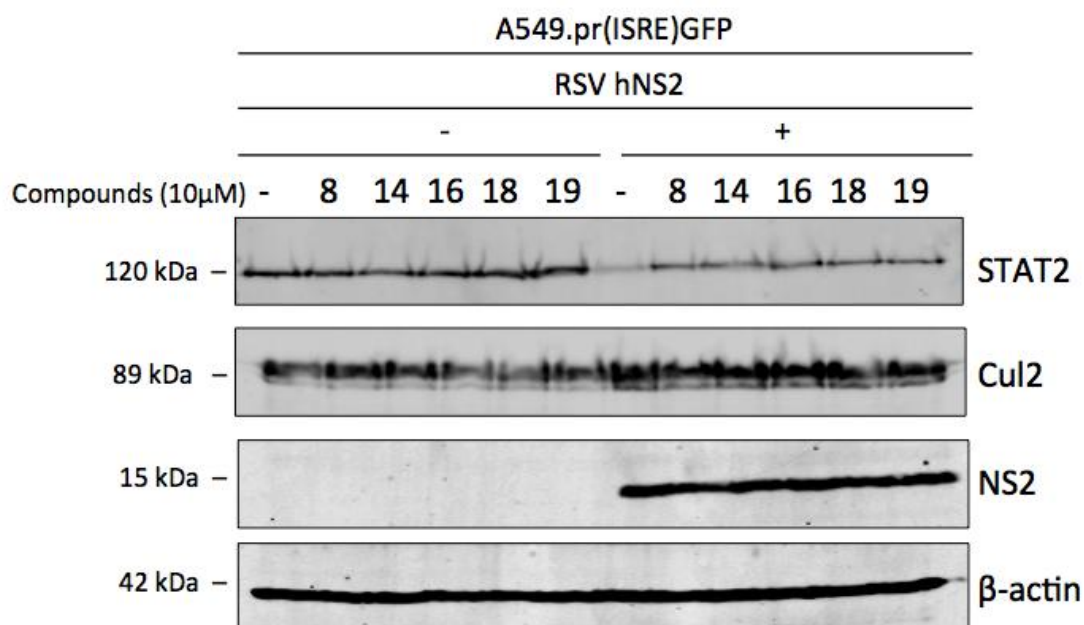
## Appendix 5: Addition of different compound combinations did not increase fold increase in GFP expression in A549.pr(ISRE)GFP-RSV/hNS2 cell-line

**(A)** A549.pr(ISRE)GFP-RSV/hNS2 cell-line was treated with 10 μM of compound AV-18, AV-14, AV-16, AV-18 or all compounds together for 2 hours and then treated with $10^4$ (Units/ml) IFN-α for 48 hours. **(B)** A549.pr(ISRE)GFP-RSV/hNS2 cell-line was treated with 10 μM of compound AV-10, AV-16, AV-18, AV-19, AV-16 and AV-19 together or all compounds together for 2 hours and then treated with $10^4$ IFN-α for 48 hours. GFP expression (fold increase) was measured using TECAN plate reader. Crystal violet staining (A650 nm) was also measured with TECAN and shows cell density after treatment with different compounds.

Appendix 6: Increasing the incubation period of compound AV-14, -16, -18 and -19 decreases the fold increase in GFP expression in A549.pr(ISRE)GFP-RSV/hNS2 cell-line

A549.pr(ISRE)GFP-RSV/hNS2 cell-line was treated with 10 µM of compound AV-14, -16, -18 and -19 or 0.05% [v/v] DMSO for 2, 8, 18 or 26 hours and then treated with $10^4$ (Units/ml) IFN-α for 48 hours. GFP expression was measured using TECAN plate reader.